

***In Vitro* Studies of the Hepatotoxic and
Hepatoprotective Potential and Metabolism of
Chalcones and a Tacrine-Silibinin Codrug**



Dissertation

**zur Erlangung des Doktorgrades der Naturwissenschaften (Dr. rer. nat.)
der Naturwissenschaftlichen Fakultät IV – Chemie und Pharmazie –
der Universität Regensburg**

vorgelegt von
Katharina Zenger
aus Duggendorf

2013

Die vorliegende Arbeit wurde im Zeitraum März 2009 bis März 2013 unter Anleitung von Prof. Dr. Jörg Heilmann am Lehrstuhl Pharmazeutische Biologie der Universität Regensburg angefertigt.

Das Promotionsgesuch wurde eingereicht am: 12.07.2013

Tag der mündlichen Prüfung: 30.08.2013

Prüfungsausschuss: Prof. Dr. Achim Göpferich (Vorsitzender)
Prof. Dr. Jörg Heilmann (Erstgutachter)
Prof. Dr. Michael Decker (Zweitgutachter)
Prof. Dr. Joachim Wegener (dritter Prüfer)

Für meine Eltern Ingrid und Josef

Danksagung

Die letzten vier Jahre waren für mich in vielerlei Hinsicht eine Herausforderung. An dieser Stelle möchte ich mich bei all den Menschen bedanken, die durch ihren Rückhalt, ihre Zuversicht und fachliche sowie persönliche Unterstützung wesentlich zum Gelingen dieser Arbeit beigetragen haben:

Prof. Dr. Jörg Heilmann danke ich vielmals für die Vergabe und Betreuung des Promotionsthemas, seine stetige Unterstützung, die fachlichen Anregungen und Diskussionen und sein Vertrauen in meine Arbeitsweise.

Prof. Dr. Michael Decker danke ich für die erfolgreiche Zusammenarbeit, seine hohe Einsatzbereitschaft, Unterstützung und kompetenten Ratschläge.

Vielen Dank an Dr. Birgit Kraus für die wissenschaftliche Betreuung meiner Promotionsarbeit, die fachlichen Gespräche, ihre Unterstützung in allen Fragestellungen der Zellkultur und die Möglichkeit, meine Arbeit selbständig gestalten zu können. Des Weiteren möchte ich ihr für die kritische Durchsicht dieser Arbeit danken. Dr. Horst Wolff danke ich für die Einführung in die Fluoreszenzmikroskopie und Bildauswertung und seine wertvollen Hilfestellungen bezüglich aller Fragen zum Cell Observer.

Dr. Guido Jürgenliemk möchte ich für die kollegiale Unterstützung, sein Engagement und die schöne Zeit im Praktikum und auf Exkursion in Südtirol danken.

Ein herzliches Dankeschön an alle meine Kollegen der Pharmazeutischen Biologie für das sehr angenehme Arbeitsklima, die große Hilfsbereitschaft und den Zusammenhalt. Ganz besonderen Dank schulde ich Dr. Anne Freischmidt, Dr. Magdalena Motyl und Rosmarie Scherübl. Vielen Dank, Mädels, für die schöne Zeit und die lustigen Abende, die vielen interessanten Gespräche, euren Rückhalt und Zuspruch und den vielen gemeinsamen Spaß! Ihr ward mir eine große Stütze und seid einfach toll! Gabriele Brunner danke ich für ihre Hilfsbereitschaft im Laboralltag und ihr Organisationstalent. Anne Grashuber danke ich für die Zusammenarbeit im Praktikum und unsere netten Gespräche im Glaskasten.

Meinen Wahlpflichtstudenten Lisa, Janina, Andreas, Nikola und Alex möchte ich für die schöne Zusammenarbeit danken.

Vielen Dank an die Mitarbeiter der „Masse“ für die Vermessung meiner vielen Metaboliten-Proben und die Unterstützung bei der Auswertung. Dr. Xinyu Chen, Petr Jirásek und Dr. Susanne Vogel danke ich für die Synthese der Testsubstanzen, Rosmarie Scherübl für die Hilfe bei der HPTLC Analytik und Dr. Magdalena Motyl für die HPLC Reinheitsprüfungen. Der Firma Martin Bauer sei gedankt für die kostenlose Zurverfügungstellung des Drogenmaterials. Dr. Bernd Schneider vom Max Planck Institut Jena danke vielmals ich für die Möglichkeit der LC–NMR Messung und Dr. Sara Agnolet für die Probenaufarbeitung, Vermessung und die nette Korrespondenz.

Meinen lieben Freunden danke ich für die vielen Gespräche und ihre Unterstützung in allen Lebenslagen. Vor allem dir, liebe Martina, vielen Dank, für deine Freundschaft, deine optimistische und weltoffene Art und dass du - auch wenn du oft unterwegs bist - im richtigen Moment immer für mich da warst und bist!

Ganz besonders möchte ich mich bei meiner ganzen Familie bedanken. Danke, danke, danke für eure Kraft, Motivation, Unterstützung und Fürsorge und dass ihr immer an mich glaubt!

Table of Contents

| | | |
|------------|--|-----------|
| 1 | General Introduction | 1 |
| 1.1 | The liver | 1 |
| 1.1.1 | Anatomy and physiology | 1 |
| 1.1.2 | Liver function tests | 4 |
| 1.1.3 | Liver diseases | 4 |
| 1.2 | Herbal hepatoprotectives | 6 |
| 1.2.1 | Silymarin | 7 |
| 1.2.2 | Glycyrrhizin | 8 |
| 1.2.3 | Curcumin..... | 9 |
| 1.2.4 | <i>Phyllanthus</i> | 9 |
| 1.2.5 | Other herbal hepatoprotectives | 10 |
| 1.3 | Herbal hepatotoxicity | 11 |
| 1.3.1 | Pyrrolizidine alkaloids..... | 11 |
| 1.3.2 | Germander..... | 12 |
| 1.3.3 | Kava..... | 12 |
| 1.3.4 | Chaparral | 13 |
| 1.3.5 | <i>Atractylis gummifera, Callilepis laureola</i> | 13 |
| 1.3.6 | Greater Celandine | 14 |
| 1.3.7 | Other hepatotoxic herbs and natural compounds | 14 |
| 1.4 | Aims | 15 |
| | | |
| 2 | Materials and Methods..... | 17 |
| 2.1 | Phytochemical and analytical methods | 17 |
| 2.1.1 | Plant material and extraction | 17 |
| 2.1.2 | Fractionation and isolation of kavalactones | 17 |
| 2.1.2.1 | Flash chromatography..... | 17 |
| 2.1.2.2 | Semi preparative high pressure liquid chromatography | 19 |
| 2.1.2.3 | Recrystallization | 19 |

| | | |
|------------|--|-----------|
| 2.1.3 | Analytical methods | 19 |
| 2.1.3.1 | Thin layer chromatography / High performance thin layer chromatography | 19 |
| 2.1.3.2 | Nuclear magnetic resonance spectroscopy | 20 |
| 2.1.3.3 | Analytical high pressure liquid chromatography..... | 20 |
| 2.2 | Cell culture..... | 21 |
| 2.2.1 | Chemicals, reagents, supplements..... | 21 |
| 2.2.2 | Culture media, cell lines | 21 |
| 2.2.2.1 | Heat inactivation of fetal calf serum..... | 21 |
| 2.2.2.2 | Culture media..... | 22 |
| 2.2.2.3 | Cell line data | 22 |
| 2.2.3 | Laboratory expendables..... | 23 |
| 2.2.4 | Cultivation, handling, treatment | 23 |
| 2.2.4.1 | Cultivation of cells | 23 |
| 2.2.4.2 | Determination of cell number, seeding of cells | 23 |
| 2.2.4.3 | Cell treatment..... | 24 |
| 2.2.4.4 | Cryopreservation and thawing of cell lines..... | 24 |
| 2.2.5 | Viability and proliferation assays | 25 |
| 2.2.5.1 | MTT assay | 25 |
| 2.2.5.2 | Crystal violet assay | 25 |
| 2.2.6 | Fluorescence microscopic assays | 26 |
| 2.2.6.1 | High content analysis | 26 |
| 2.2.6.2 | Cytochrome c assay..... | 28 |
| 2.2.6.3 | DNA content..... | 29 |
| 2.3 | <i>In vitro</i> stability and metabolism..... | 30 |
| 2.3.1 | Human liver microsomes | 30 |
| 2.3.2 | Chemicals, reagents..... | 30 |
| 2.3.3 | Microsomal metabolism of chalcones and identification of phase I and phase II metabolites..... | 31 |
| 2.3.3.1 | Incubation systems..... | 31 |
| 2.3.3.2 | Analytical high pressure liquid chromatography..... | 32 |
| 2.3.3.3 | Liquid chromatography–high resolution electrospray ionization mass spectrometry | 33 |
| 2.3.3.4 | High pressure liquid chromatography–nuclear magnetic resonance spectroscopy | 33 |

| | | |
|------------|--|-----------|
| 2.3.4 | <i>In vitro</i> degradation stability and microsomal metabolism of the tacrine-silibinin codrug..... | 35 |
| 2.3.4.1 | Analytical methods..... | 35 |
| 2.3.4.2 | Stability of the codrug under <i>in vitro</i> assay conditions..... | 36 |
| 2.3.4.3 | Microsomal metabolism and metabolic stability in microsomal incubation systems | 36 |
| 2.4 | Test compounds, solvents, and other chemicals | 37 |
| 2.5 | Laboratory instruments | 38 |
| 2.6 | Statistical analysis | 40 |
| | | |
| 3 | Isolation of kava constituents and reevaluation of their hepatotoxic potential..... | 41 |
| 3.1 | Introduction | 41 |
| 3.1.1 | Botany..... | 41 |
| 3.1.2 | Chemical constituents | 42 |
| 3.1.3 | Traditional use..... | 44 |
| 3.1.4 | Experimental pharmacology | 44 |
| 3.1.5 | Preclinical studies..... | 46 |
| 3.1.6 | Clinical pharmacology | 47 |
| 3.1.7 | Pharmacokinetic studies..... | 48 |
| 3.1.8 | Adverse reactions and drug interactions..... | 50 |
| 3.1.9 | Kava extracts, approved indication, posology..... | 52 |
| 3.2 | Aim of the study | 52 |
| 3.3 | Results and discussion | 53 |
| 3.3.1 | Fractions and isolated structures..... | 53 |
| 3.3.2 | Analytical characterization of isolated kavalactones | 55 |
| 3.3.3 | <i>In vitro</i> cytotoxicity of kavalactones and chalcones, major and minor constituents in kava rhizome extract | 56 |
| 3.4 | Conclusion..... | 66 |

| | | |
|------------|--|------------|
| 4 | Inhibitory activity of structurally related chalcones on activated human hepatic stellate cells..... | 68 |
| 4.1 | Introduction | 68 |
| 4.1.1 | The role of hepatic stellate cells in liver fibrosis | 68 |
| 4.1.2 | Pharmacological characterization of the test compounds | 69 |
| 4.1.3 | Chalcones with anti-fibrotic effects | 75 |
| 4.2 | Aim of the study | 78 |
| 4.3 | Results and discussion | 78 |
| 4.3.1 | Analytical characterization of test compounds | 78 |
| 4.3.2 | Effects on cell viability and proliferation | 80 |
| 4.3.3 | Effects on cell organelles..... | 85 |
| 4.3.4 | Cytochrome c release | 89 |
| 4.3.5 | DNA content and cell cycle analysis..... | 92 |
| 4.4 | Conclusion..... | 95 |
| | | |
| 5 | <i>In vitro</i> metabolism of chalcones: identification and structure elucidation of microsomal metabolites | 99 |
| 5.1 | Introduction | 99 |
| 5.1.1 | <i>In vitro</i> metabolism systems and their applications | 99 |
| 5.1.2 | Absorption, bioavailability, and metabolism of flavonoids and chalcones..... | 104 |
| 5.2 | Aim of the study | 110 |
| 5.3 | Results and discussion | 110 |
| 5.3.1 | Preliminary experiments..... | 110 |
| 5.3.2 | Identification of microsomal chalcone phase I and II metabolites..... | 112 |
| 5.3.3 | Structure elucidation of major flavokawain metabolites..... | 118 |
| 5.4 | Conclusion..... | 123 |

| | | |
|------------|--|------------|
| 6 | <i>In vitro</i> stability, metabolism, and hepatotoxicity of a tacrine-silibinin codrug | 125 |
| 6.1 | Introduction | 125 |
| 6.2 | Aim of the study | 127 |
| 6.3 | Results and discussion | 127 |
| 6.3.1 | Analytical characterization of the test compounds | 127 |
| 6.3.2 | Degradation stability under <i>in vitro</i> assay conditions | 129 |
| 6.3.3 | Microsomal metabolism and metabolic stability in microsomal incubation systems | 130 |
| 6.3.4 | Comparative evaluation of the <i>in vitro</i> hepatotoxicity of tacrine, an equimolar mixture of tacrine/silibinin, and the codrug | 134 |
| 6.3.5 | <i>In vitro</i> hepatotoxicity of the codrug's primary metabolites | 137 |
| 6.4 | Conclusion..... | 140 |
| | | |
| 7 | Summary | 141 |
| | | |
| 8 | References | 144 |
| | | |
| 9 | Abbreviations..... | 177 |
| | | |
| 10 | Appendix | 183 |
| 10.1 | Supplementary HCA data of the chalcones..... | 183 |
| 10.2 | Mass spectra of chalcone metabolites | 202 |
| 10.3 | Supplementary table of the codrug metabolites | 227 |
| 10.4 | List of publications | 228 |
| 10.5 | Curriculum Vitae..... | 229 |

1 General Introduction

1.1 The liver

1.1.1 Anatomy and physiology

The liver is the largest internal organ of the body with an average weight of 1500 g (~ 2.5% of body weight). The organ is located below the diaphragm in the upper right quadrant of the abdominal cavity, between the organs of the gastrointestinal tract and the heart, linked to portal and general circulation, respectively [1]. The portal vein carries the nutrient-enriched venous blood from the small intestine, stomach, pancreas, and spleen and constitutes the main blood flow entering the liver (~ 75% of blood supply). Additionally, the hepatic artery, branching from the celiac trunk and descending aorta, supplies the liver with oxygen enriched arterial blood (~ 25% of blood supply). Terminal branches of both vessels join in the capillary bed of the liver where the arterial and venous blood is mixed as it enters the sinusoids. The blood leaves the sinusoids via central veins, which coalesce into hepatic veins and finally empty into the inferior vena cava [2] (Figure 1.1).

The falciform ligament divides the liver in the right and left lobe, the right lobe being the larger (Figure 1.1). Each liver lobe is divided by the right and left hepatic veins into anterior and posterior (right lobe) and medial and lateral (left lobe) sections. Finally, the Couinaud classification further subdivides the sections into eight functionally independent segments. The smaller caudate and quadrate lobes are located posteriorly [2] (Figure 1.1).

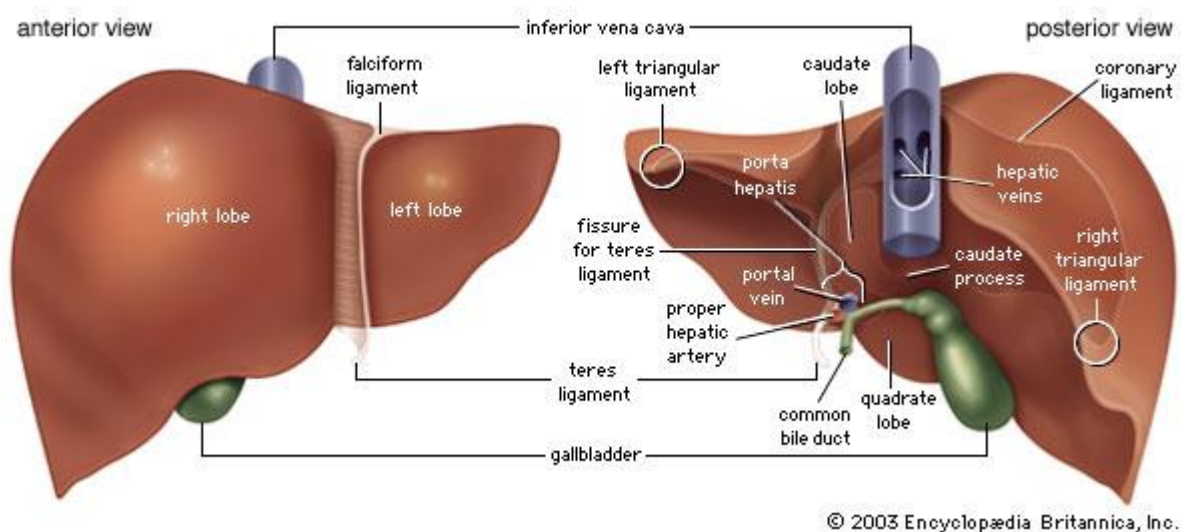


Figure 1.1: Gross anatomy of the liver: anterior and posterior views. Encyclopædia Britannica Online. <http://www.britannica.com/EBchecked/media/68633/Anterior-and-posterior-views-of-the-liver>.

The basic functional unit of the liver is the lobule [3] (Figure 1.2). The hexagonal lobule largely consists of interconnected plates of hepatocytes, which are separated by the sinusoids. At the corner of each lobule, three vessels form the portal triad containing branches of the hepatic artery, portal vein, and bile ducts. From a metabolic point of view, the liver ascinus is the smallest functional unit. Each ascinus consists of hepatocytes aligned around the portal canal and the central veins lying at the corner. Corresponding to the distance from arterial blood supply, the ascinus is divided in three zones: the periportal zone 1 directly around the portal canal, the zone 2 in further distance to the arterial blood supply, and the centrilobular zone 3 nearest to the central veins [4].

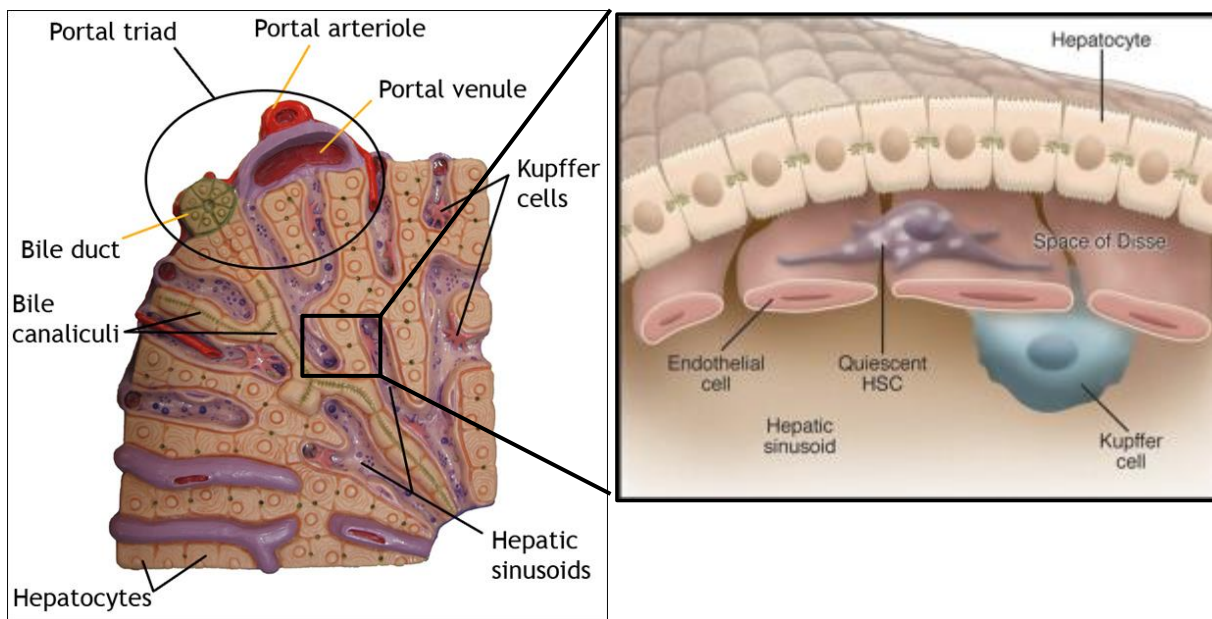


Figure 1.2: Left: The liver lobule with the portal triad, sinusoids, bile canaliculi, and the collecting central vein. <http://www.dnwalcker.com/Laboratory11and12.html>. Right: More detailed view of the liver sinusoidal structure with the involved cell types. <http://www.vetscite.org/publish/articles/000074/index.html>.

Hepatocytes are highly specialized cells, which represent 60% of the liver cells and account for about 80% of the liver's total cell mass [4]. Most of the liver's metabolic and synthetic functions are performed by these cells [5]. They have an average life span of 5 months and the ability to regenerate. The radial orientated plates of hepatocytes are separated by vascular channels (sinusoids), in which the blood from the portal arteriole and venule flows towards the central vein (Figure 1.2). Via the perisinusoidal space of Disse, the surface areas of the hepatocytes get in contact to nutrients and toxins that are transported within the blood. On the opposite site, the hepatocyte plates line the bile canaliculi. Secreted bile is transported back towards the portal canal, drains into a series of bile ducts, and finally empties via the common bile duct into the gallbladder to become available for digestive processes in the intestine [6].

The sinusoidal endothelial cells separate the sinusoids from the space of Disse. The fenestration of these cells allows the exchange of plasma, proteins, nutrients, xenobiotics, and oxygen between both sides [7].

Kupffer cells are resident macrophages in the sinusoids. They have an important function in removing bacteria, virus particles, fibrin-fibrinogen complexes, and damaged erythrocytes from circulation by phagocytosis. They also break down heme into bilirubin, which is the main pigment of the bile [8].

Stellate cells (Ito cells) are located in the perisinusoidal space of Disse. Their major task is to store vitamin A in intracellular lipid droplets [9]. Persistent hepatic inflammation leads to activation of quiescent hepatic stellate cells transforming them into proliferative, fibrinogenic, and contractile myofibroblasts (see chapter 4.1.1). Activated hepatic stellate cells play a central role in the pathological process of hepatic fibrosis [10].

The liver fulfills a multitude of different tasks including synthetic, excretory, metabolic, endocrine, and storage functions [11]. Amongst others, the liver is responsible for bile production and excretion [6]. Via enterohepatic circulation, 95% of the bile acids are regained by recuperation from the terminal ileum, returned to the liver, re-uptaken into hepatocytes and excreted into the bile again. Only 400-500 mg of bile acids are produced per day, balancing the fecal loss [12]. Cholesterol is the starting molecule in the synthesis of bile acids. The formation of bile acids encloses hydroxylation, modification of the sterol ring, shortening of the side chain, and conjugation to glycine or taurine. The amphiphilic properties of bile acids support the digestion of nutritional components and the excretion of lipophilic compounds (such as cholesterol) by the formation of micelles. Therefore, the liver is mainly responsible for the cholesterol homeostasis [13].

Hepatocytes play a crucial role in the metabolism of drugs and xenobiotics [14]. The biotransformation reactions intend to render molecules more hydrophilic and consequently facilitate their excretion. The phases of drug metabolism and involved catalyzing enzymes are introduced in detail in chapter 5.1.1.

The liver is also responsible for the metabolism of carbohydrates, lipids, and proteins. Maintenance of blood glucose levels (~ 70-100 mg/dL) is a main function of the liver [15]. Glycogenesis, glycogenolysis, and gluconeogenesis are hormonally regulated by insulin and glucagon. Glycogen is the main carbohydrate store in the liver. After uptake of glucose by hepatocytes, the enzyme glucokinase catalyzes the phosphorylation of glucose to form glucose-6-phosphate. Depending on the energy requirement, glucose-6-phosphate is further converted and provided for glycogen synthesis or used for energy production by the glycolytic pathway. Also other monosaccharides like fructose and galactose can be enzymatically transformed to join the glycolytic pathway.

Furthermore, metabolism of lipids, lipogenesis and lipoprotein synthesis are regulated by the liver [16]. On the one hand, fatty acids from plasma can be broken down in mitochondria of hepatocytes by β -oxidation to provide energy. On the other hand, synthesis of fatty acids is carried out in the hepatocellular cytosol. The liver is responsible for the synthesis, secretion, and the catabolism of lipoproteins [17]. Most of the circulating proteins are synthesized by hepatocytes including cargo proteins such as albumin, immune-related proteins (components of the complement system, acute-phase proteins), and coagulation factors [6]. The liver is involved in the synthesis and interconversion of nonessential amino acids from essential amino acids and in the formation of ketone bodies.

Moreover, the liver regulates the endocrine function of hormones [11]. As an essential step in hormone activation, the liver is the major site of conversion of vitamin D₃ to 25-hydroxy vitamin D₃, and thyroxine (T₄) to the biologically more active triiodothyronine (T₃). The liver modifies the function of growth hormones and constitutes the major organ for the removal of peptide hormones. Additionally, it is the main storage site for fat-soluble vitamins (vitamin A, vitamin D), vitamin B₁₂, iron, and copper [6].

1.1.2 Liver function tests

Liver function can be determined by means of several blood tests measuring the concentration of a variety of proteins and enzymes that are either produced by liver cells or that are released after liver cell damage [18]. Assessment of liver function includes the determination of prothrombin time (PT) and serum albumin levels. Both prolonged PT and decreased serum albumin may reflect liver dysfunction. Elevated alanine amino transferase (ALT) and aspartate amino transferase (AST) indicate liver cell damage. Increased bilirubin occurs in haemolysis, biliary obstruction, hepatitis, and cirrhosis and becomes apparent in form of jaundice. In biliary obstruction, alkaline phosphatase (ALP) levels may be elevated. Elevated gamma glutamyl transpeptidase (GGT) can be observed in diseases of the liver, biliary system or pancreas, as well as after significant alcohol consumption, and the use of several drugs.

1.1.3 Liver diseases

The term liver disease (hepatic disease) includes all kind of damage or impairment of the liver which leads to restriction or loss of organ function. The duration of liver disorders constitutes one way to classify hepatic diseases. Acute liver disease may be displayed in acute inflammation provoked by different noxae including intoxication or acute infections [19]. Chronic hepatic diseases can be caused by chronic infections with hepatotropic viruses (HBV, HCV), alcohol or drug abuse, autoimmune reactions, and metabolic disorders [19].

Hepatitis (hepatic inflammation) can have several causes, virus infections and alcoholism being the most common. Hepatitis A virus (HAV) infection induces acute liver inflammation, which is usually followed by complete recovery of the organ. Due to improvement of hygiene and sanitation coupled with economic and social advancement, the incidence of hepatitis A is declining in most European countries [20]. Hepatitis B virus (HBV) and hepatitis C virus (HCV) can cause chronic liver infections and constitute main risk factors for the development of hepatocellular carcinoma (HCC). According to a recent review, hepatitis B has a prevalence of 0.5-0.7%, and hepatitis C of 0.13-3.26% in Europe [20]. To date, vaccines are available for HAV and HBV. Interferons (IFN- α_{2a} , INF- α_{2B}) constitute the most established anti-viral treatment in hepatitis B and C infections.

Alcohol is the main cause of liver disease, including liver cirrhosis. In Europe, over 20% of the population aged ≥ 15 years report heavy episodic drinking at least once a week [20]. Alcoholic liver disease can be differentiated by three major histological stages: alcoholic steatosis (fatty liver), acute alcoholic hepatitis, and alcoholic cirrhosis [21]. Steatosis is considered as a reversible condition, which is characterized by the intracytoplasmic accumulation of triglycerides in liver cells. Alcohol abuse can cause acute and chronic hepatitis accompanied by hepatocellular injury, inflammation, and fibrosis. Alcoholic hepatitis can be reversed by strictly abstaining from alcohol. Continuous alcohol abuse leads to chronic inflammation, fibrogenesis, and alcoholic cirrhosis at late stage [22].

Besides of alcohol, other factors such as obesity and insulin resistance can cause fatty liver disease. Non-alcoholic fatty liver disease (NAFLD) is characterized by the accumulation of liver fat exceeding 5% of hepatocytes in the absence of significant alcohol intake, viral infection, or any other defined cause of liver injury [23]. The more severe non-alcoholic steatohepatitis (NASH) is accompanied by hepatocellular damage, inflammation, and fibrosis [24].

Hepatic fibrosis (see chapter 4.1.1) is the most common manifestation of most types of chronic liver injury leading to cirrhosis in progressive stages [25]. According to World Health Organization (WHO) reports, cirrhosis accounts for 1.8% of all deaths in Europe [20]. Complete pictured cirrhosis is considered to be irreversible and is characterized by loss of hepatocyte activity, the excessive formation of fibrous scars, and inhibited blood flow leading to portal hypertension.

Persistent hepatocellular damage and chronic inflammation may finally be responsible for the development of primary liver cancer. However, most of the liver cancers develop secondarily out of metastases from primary tumors of other organs. HCC constitutes the most important type of primary liver cancer, representing 70-90% of all cases [26]. In 80% of the patients, HCC is associated with liver cirrhosis [20]. HCC is one of the most common cancers worldwide with over half a million new cases each year and highest incidence rates in

Southeast Asia and Africa. HBV and HCV infections constitute the most prominent risk factors for the development of HCC; other risk factors include chronic alcohol abuse, metabolic liver disease, aflatoxins, and other cirrhosis-inducing conditions [26]. Liver cancer has a high mortality rate because of the lack of efficient therapies (46 801 deaths per annum in Europe according to WHO mortality database) [20].

Drug-induced liver injury (DILI) is the most common cause of cancelled drug development or withdrawal of already approved drugs [27,28]. DILI can be classified into intrinsic/predictable hepatotoxicity and idiosyncratic/unpredictable hepatotoxicity. The intrinsic form of injury develops in all or most recipients provided adequate up-take of the drug (dose-dependent; e.g. acetaminophen). However, a large percentage of DILI occurs as an idiosyncratic toxicity underlying immunoallergic mechanisms or metabolic aberrations in individual patients. Risk factors, prevalence, and incidence are still only partly known. Gender, age, genetic disposition, pre-existing conditions such as diabetes mellitus, and alcohol use are considered as probable influencing factors [29].

1.2 Herbal hepatoprotectives

Liver diseases (see chapter 1.1.3) like viral hepatitis, alcoholic liver disease, NAFLD, and HCC constitute a major health burden worldwide affecting humans of all ages. Current therapies are often limited in efficacy, connected to adverse effects, and they are often very expensive. Hence, new therapeutic approaches such as the use of herbal medicine are of great common interest. The treatment of liver diseases with medicinal plants or herbal drugs has a long tradition, especially in eastern countries [30]. In scientific literature, the list of herbal constituents and preparations with claimed hepatoprotective properties is continuously getting longer. The mechanisms of hepatoprotection of these compounds include a variety of effects such as anti-oxidant, anti-viral, anti-fibrotic, anti-inflammatory, anti-carcinogenic, and immunomodulatory activities [31]. However, only for a few standardized extracts or herbal compounds, evident data of experimental pharmacology, animal studies or clinical trials are currently available. In particular, for most herbal drugs there is a lack of randomized clinical trials with well-selected end-points, powerful sample size, and comparison to placebo or conventional treatment which proof the efficacy and safety [32,33]. The current status of clinically evaluated hepatoprotective herbal remedies has recently been reviewed [34]. Standardization of herbal medicines and identification of active constituents is a general problem as well. Nevertheless, a number of herbals is quite extensively investigated and shows promising effects *in vitro* and *in vivo* [30–32,35]. The most important hepatoprotective herbal “leads” are shortly presented in the following.

1.2.1 Silymarin

Milk thistle (*Silybum marianum* (L.) GAERTN.) constitutes the most researched plant for the treatment of liver diseases and has been already used in the 16th century for this purpose [30]. Silymarin, the active principle of the drug, is a mixture of different flavonolignans, mainly silibinin (60-70%), silydianin, and silychristin [36] (Figure 1.3). Pharmaceutically used extracts are standardized to silibinin, which constitutes the biologically most active constituent and is a diastereomeric mixture of silybin A and silybin B (Figure 1.3).

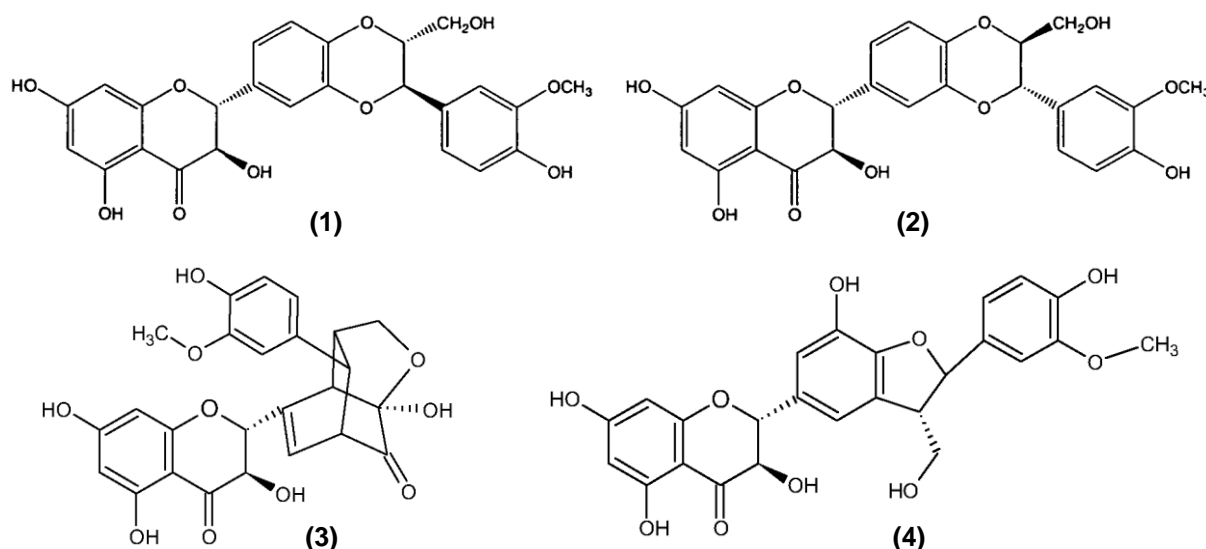


Figure 1.3: Structures of silybin A (1), silybin B (2), silydianin (3), and silychristin (4).

The pharmacological profile of silymarin has been extensively investigated both *in vitro* and *in vivo* [37]. Its biological activities comprise anti-oxidant, radical scavenging, anti-fibrotic, anti-inflammatory, membrane stabilizing, and regenerative effects [38]. In various experimental studies, silymarin has shown protective activity against several hepatotoxins including carbon tetrachloride (CCl₄), acetaminophen, ethanol, and *Amanita phalloides* toxins [33]. Silymarin is clinically used to treat *Amanita* mushroom poisoning, drug-induced liver disease, alcoholic liver disease, and acute and chronic viral hepatitis [39]. The oral dosage form is coated tablets or capsules containing standardized extract. Around 20-40% of silymarin is excreted via bile in form of glucuronides and sulfates. In human, C_{max} is reached after 4-6 h and t_{max} is approximately 6 h [39].

Numerous clinical trials of different outcome and quality have been performed to evaluate the efficacy and safety of milk thistle in treating liver diseases. Several systematic reviews and meta-analyses deal with the evaluation of clinical trial outcomes [40,41]. Treatment with silymarin is considered to be safe and well-tolerated. However, the definition of valuable end points is considered as major problem. Rating previous data, no reduction of mortality could be found with milk thistle treatment. Further randomized, controlled clinical trials with longer duration and bigger sample size are required to finally proof the efficacy of silymarin for treatment of chronic liver diseases.

1.2.2 Glycyrrhizin

Glycyrrhizin (Figure 1.4) is a synonym for a mixture of Ca^{2+} and K^+ salts of glycyrrhizic acid as well as for an aqueous extract of licorice root (*Glycyrrhiza glabra* L.) containing glycyrrhetic acid, flavonoids, hydroxycoumarins, and β -sitosterol. A Japanese preparation, stronger neominophagen C (SNMC), contains glycyrrhizin in combination with cysteine and glycine and is used as a parenteral drug for treatment of chronic hepatitis [33].

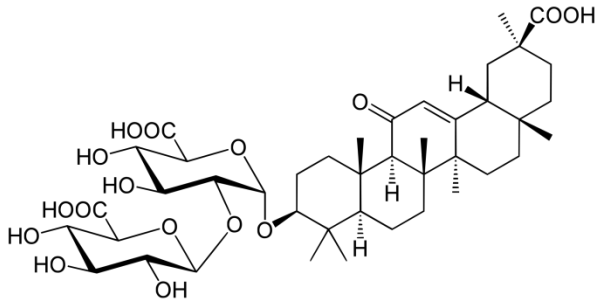


Figure 1.4: Structure of glycyrrhizic acid.

In animal studies, a protective effect against CCl_4 -induced liver injury could be shown [42]. The hepatoprotective activity of glycyrrhizin is mainly attributed to its anti-oxidant, anti-inflammatory, and immunomodulatory activities [31]. *In vitro*, glycyrrhizin inhibited CD^+ -T-cell- and TNF-mediated cytotoxicity [43]. Furthermore, it showed membrane-stabilizing effects and stimulated the endogenous production of interferon (INF) [33]. Glycyrrhizin altered the glycosylation and blocked the sialylation of hepatitis B surface antigen (HBsAg) in cell culture experiments [44]. Anti-inflammatory properties could be mediated by inhibition of 11-beta-hydroxysteroid dehydrogenase activity and prostaglandin E2 (PGE2) production in macrophages [45]. Anti-oxidant properties may be attributed to the induction of glutathione-S-transferase and catalase [45]. Moreover, glycyrrhizin showed anti-fibrotic activities in CCl_4 treated rats by inhibition of NF- κ B pathways [46]. Clinical trials have been performed as well mainly investigating the effects of SNMC on viral hepatitis B and C infections [32]. Taken together, anti-viral activity of glycyrrhizin could not be demonstrated. Beneficial effects regarding biochemical reposes (liver function test) may rather be ascribed to its anti-inflammatory and cytoprotective effects. Other trials evaluated the efficacy of SNMC in treatment of subacute liver failure or cirrhosis. For subacute liver failure, survival rate of the glycyrrhizin-treated group was higher compared to historical control data [47]. In cirrhotic patients, biochemical parameters were mostly improved by glycyrrhizin treatment, however, there was no effect on mortality or HBV or HCV clearance [33]. Glycyrrhizin may cause mineralocorticoid adverse reactions like high blood pressure, water and salt retention, and hypokalemia. To date, treatment of liver diseases with glycyrrhizin is not recommended due to the lack of evident benefit.

1.2.3 Curcumin

The yellow-colored curcumin (Figure 1.5) is a major constituent of turmeric rhizome (*Curcuma* spp.). The hepatoprotective effects of curcumin were addressed in several *in vitro* and in animal studies. Curcumin possesses a wide range of biological activities including potent anti-oxidant, radical scavenging, and anti-inflammatory effects, to mention just the most important ones [31,38,48].

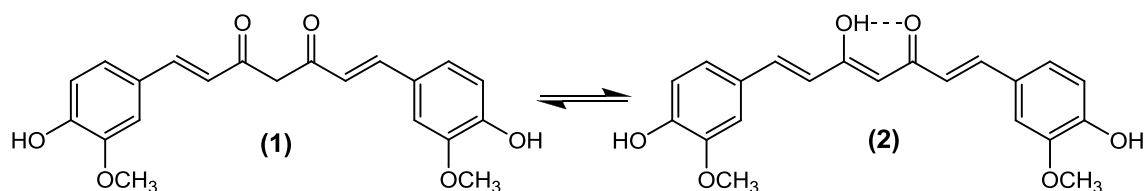


Figure 1.5: The keto- (1) and enol-form (2) of curcumin.

As a potent inhibitor of cytochrome P450 enzymes (CYP450), curcumin can prevent the metabolic activation of toxic chemicals [49]. Curcumin increases the activity of glutathione-S-transferase which may support liver detoxification [48]. By inhibition of NF- κ B signaling pathways, curcumin prevented alcohol-induced liver disease and diet-induced steatohepatitis in animals [48]. Furthermore, curcumin demonstrated hepatoprotective effects against liver damage induced by toxins like CCl₄ [50]. It showed also anti-fibrotic effects by inhibition of hepatic stellate cells (HSC) activation and proliferation [51]. Moreover, it altered the expression of matrix metalloproteinase and decreased the deposition of extracellular matrix (ECM) in hepatocytes [52]. Additionally, curcumin modulated TGF- β signaling and reduced levels of pro-inflammatory cytokines such as INF- α , TNF- α , and IL-6 [53].

After oral administration, curcumin is poorly absorbed. It is conjugated to glucuronic acid and sulfate and is metabolized to tetrahydrocurcumin (active metabolite), hexahydrocurcumin, and hexahydrocurcuminol. Conjugated metabolites of tetrahydrocurcumin are found as well [38]. Safety studies detected no signs of toxicity in human (100 mg/day) and rats (5 g/day) [48]. Curcumin is poorly soluble in water, has a low oral bioavailability, and is sensitive to light and temperature which may lower its pharmaceutical use as single component. The hepatoprotective activities have not been evaluated in controlled clinical trials yet.

1.2.4 *Phyllanthus*

Plants of the genus *Phyllanthus* are found in tropical and subtropical regions and are traditionally used in Ayurvedic and folk medicine to treat liver disorders. Polyphenols and the lignans phyllantin and hypophyllantin are considered as pharmacologically active constituents [31] (Figure 1.6).

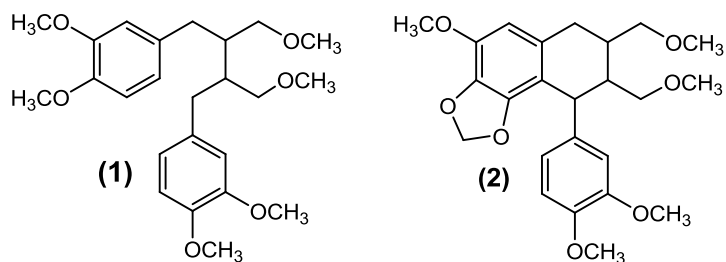


Figure 1.6: Structures of phyllantin (1) and hypophyllantin (2).

Results of experimental pharmacology imply activity against HBV infection by interference with polymerase activity, mRNA transcription and replication [32]. In primary cultured hepatocytes, the lignans showed hepatoprotective effects against CCl₄ and galactosamine-induced toxicity [54]. Several clinical trials have addressed the beneficial effects of *Phyllanthus* extracts in patients with chronic HBV infection. A systematic review including 22 randomized, controlled clinical trials has revealed positive effects on clearance of serum HBsAg compared with placebo or no intervention, while there was no significant difference to interferon treatment [55]. Noteworthy, a combination of *Phyllanthus* and interferon seemed to enhance the effects. However, other clinical trials found no beneficial effects of *Phyllanthus* treatment in HBV carriers. To date, treatment of HBV patients with *Phyllanthus* is not recommended due to the lack of prospective large-scale controlled trials and long-term safety studies. In addition, active ingredients and modes of action have to be further elucidated.

1.2.5 Other herbal hepatoprotectives

Several herbal preparations from Japanese traditional medicine (Kampo) and Chinese traditional medicine (TCM) are used to treat liver diseases [32]. The Kampo-formula TJ-9 (sho saiko-to), a combination of seven herbs, shows anti-fibrotic activity inhibiting the proliferation and transformation of HSC *in vitro* and *in vivo*. A long-term prospective study in HBV carriers found significant lower development of HCC with treatment of 7.5 g/day of an aqueous TJ-9 extract and INF within 5 years [56]. The TCM drug 'compound 861', a mixture of 10 herbs, exhibits anti-fibrotic activity *in vitro* [32]. Controlled trials in HBV positive patients reported beneficial effects on liver fibrosis and liver enzyme levels, but no clearance of HBsAg [32]. The Ayurvedic medicine Liv.52 (combination of herbs) is marketed in India for the therapy of chronic liver diseases, however, most of the claimed activities are not assured by well-planned randomized clinical trials [57]. An alcoholic root extract from *Picrorhiza kurroa* ROYLE EX BENTH ('Picroliv') containing the iridoid glycosides picroside and kutkoside is used in India as a hepatoprotective drug [31]. In experimental studies, *trans*-resveratrol (3,4,5'-*trans*-trihydroxystilbene) has shown promising anti-fibrotic and hepatoprotective effects due to its anti-oxidant and anti-inflammatory properties [38]. The efficacy of resveratrol has not

been evaluated in clinical studies yet. Andrographolide, a labdane diterpene lactone from *Andrographis paniculata* (BURM.F.) WALL. EX NEES, exhibits protective effects against toxin-induced liver damage and choleric activity in rats [31]. For a huge variety of natural compounds and herbal extracts, hepatoprotective effects were demonstrated in hepatocyte cultures or in animal studies. Results were compiled in several reviews [31,48,57,58].

1.3 Herbal hepatotoxicity

Worldwide, the popularity of herbal products is increasing, especially with regard to self-medication, dietary supplements, and life-style products [27,59,60]. In many countries, the use of herbal preparations does not underlie prescription regulations and quality standards may not be fulfilled due to insufficient labeling or missing regulatory requirement. Several herbal drugs have been identified to cause adverse hepatic reactions such as acute and chronic hepatitis, hepatic fibrosis, bile duct injury, venoocclusive disease (VOD), cholestasis, drug-induced autoimmunity, vascular lesion, and even hepatic necrosis and liver failure [61]. Besides direct herbal hepatotoxicity, herb-herb and herb-drug interactions have to be considered for a full assessment of adverse effects [62,63]. The identification of the responsible toxin in herbal remedies often remains a very difficult issue as preparations often contain several ingredients or even represent mixtures of various herbs or herbal extracts. Besides, herbal preparations of doubtful origin may be contaminated with microorganism, fungal toxins, heavy metals, pesticides, and synthetic drugs. In the last decades, several herbal drugs were made responsible for hepatotoxic events [64]. They are shortly presented in the following.

1.3.1 Pyrrolizidine alkaloids

The dose-dependent hepatotoxicity of plants from *Senecio*, *Heliotropium*, *Crotalaria*, and *Symphytum* species containing pyrrolizidine alkaloids (PA) is known for more than 90 years when 'Senecio disease' was first reported in South Africa [65]. PA poisoning of children was reported in Jamaica after the ingestion of 'bush tea' containing *Crotalaria* species [66]. In India [67] and Afghanistan [68] several cases of liver injury were attributed to food contamination (e.g. cereals, wheat flour) with toxic weeds (*Crotalaria* or *Heliotropium* species). PA intoxication was likewise reported in Europe [69] and the US [70,71] (*Senecio* and Comfrey poisoning). The liver injury caused by PA is mainly reflected in the VOD. The acute manifestation of VOD (also called sinusoidal obstruction syndrome) may come along with abdominal pain, ascites, hepatomegaly, elevated ALT, and jaundice [72]. Pathologically, the clinical picture resembles the Budd-Chiari syndrome. Non-thrombolytic obstruction of terminal centrilobular veins leads to a post-sinusoidal block and elevated sinusoidal

pressure. Damage of sinusoidal endothelial cells contributes to partial obstruction of the sinusoids, permitting erythrocytes to enter the space of Disse. Altogether, this results in hepatic congestion and centrilobular necrosis leading either to acute liver failure or liver fibrosis and cirrhosis. The mechanism of hepatotoxicity was assessed in animal studies. The hepatotoxicity of PA probably can be attributed to the biotransformation into reactive pyrrole derivatives which act as alkylating agents and hepatocarcinogens [73]. Indeed, the hepatotoxicity of PA was enhanced by co-administration of phenobarbital, a potent inducer of CYP450 isoenzymes [74]. This further supports the hypotheses that PA's hepatotoxicity is due to metabolic toxification.

1.3.2 Germander

Germander (*Teucrium chamaedrys* L.) has been used as a traditional herbal remedy for its choleric and antiseptic properties for more than 2000 years. Considered as completely safe, Germander preparations were approved in France in 1986 as an adjuvant to treat obesity and mild diarrhea [60]. In 1992, several cases of germander-associated acute, chronic, and even fulminant hepatitis were reported to the French pharmacovigilance authorities, which led to the withdrawal of germander preparations from the drug market [75]. Usually, hepatitis appeared after a daily intake of 600-1600 mg for 2 months [60]. Mostly, signs of acute cytolytic hepatitis were present and reflected in hyperbilirubinemia, elevated aminotransferase levels, and impaired synthetic function. However, some patients developed chronic hepatitis, fibrosis, and cirrhosis. Most of the patients recovered after the discontinuation of germander treatment. Accidental re-exposure caused the recurrence of liver injury. Germander contains saponins, glycosides, flavonoids, and a number of furano neoclerodane diterpenoids [60]. Loeper et al. evaluated the liver toxicity of germander in mice and could show the formation of electrophilic metabolites from furano diterpenoids by cytochrome P450 3A [76]. Furthermore, induction of CYP3A and GSH depletion enhanced the toxicity. *In vitro*, the reactive metabolites induced apoptosis of hepatocytes [77].

A case of fulminant hepatic failure requiring liver transplantation was reported in a 37-year-old female after intake of tea made from the Mediterranean plant *Teucrium polium* L. [78].

1.3.3 Kava

Kava kava (*Piper methysticum* FORST.) is a traditional psychoactive beverage used for socio-ceremonial, spiritual, and medicinal purposes in Hawaii, Polynesia, and the Fiji Islands. Standardized organic kava root extracts and other kava-containing products were marketed for the treatment of anxiety disorders, depression, and as a sleeping aid all over the world. Despite of still inconclusive data on this issue, case reports of severe hepatotoxic side effects (hepatic necrosis, cholestatic hepatitis, liver failure) led to withdrawal of kava-containing

preparations in several countries (for an overview see [64,79,80]). To date, the mechanisms and elicitors of the putative hepatotoxic side effects still remain unclear. Kava's constituents, pharmacology, and toxicity are extensively discussed in chapter 3.1 and 3.3.3.

1.3.4 Chaparral

Chaparral (*Larrea tridentate* (DC.) COVILLE) commonly known as 'creosote bush' or 'greasewood' originates from Southwestern United States and Mexico and is used as a herbal remedy by the Native Americans to treat various conditions like common colds, bone and muscle pain, bronchitis, and snakebites [81]. Commercially, chaparral plant extracts are available as tablets, capsules, and salves for the treatment of skin disorders, as well as for weight-reducing, anti-inflammatory, and 'blood-purifying' properties. Chaparral preparations are even applied in alternative treatment of AIDS [81]. Since 1990, the Food and Drug Administration (FDA) evaluated several reports of chaparral toxicity. Sheikh et al. reviewed the chaparral-associated toxicity in 18 patients [82]. Liver injury was evident in 13 patients ranging from mild hepatitis to cirrhosis and even fulminant liver failure. Mostly, cholestatic hepatitis with elevated serum transaminase and ALP, and hyperbilirubinemia appeared within 3 to 52 weeks of intake. Mechanism of toxicity is not fully understood yet. Chaparral contains flavonoids, volatile oil, amino acids, lignans, and other compounds [59]. Toxicity might be attributed to the active ingredient nordihydroguaiaretic acid, which inhibits cyclooxygenase (COX) and CYP450 enzymes [83]. However, also idiosyncratic/immune-mediated mechanisms are discussed. The causality of chaparral-associated toxicity is quite clearly estimated because of temporal correlation between intake and appearance of liver injury, and because re-exposure leads to relapse of clinical signs.

1.3.5 *Atractylis gummifera*, *Callilepis laureola*

In the Mediterranean region, the whitish gummy fluid secreted by the thistle *Atractylis gummifera* L. is used for its antipyretic, emetic, and diuretic activities and it is also enjoyed by children as a chewing gum [60]. Few hours after ingestion, acute toxicity can become apparent in unspecific symptoms such as nausea, abdominal pain, anxiety, diarrhea, and headache [84]. The clinical picture includes hepatorenal failure and hypoglycemia due to inhibited gluconeogenesis. Two constituents, atractyloside and gummiferin, were identified as fairly toxic compounds impairing mitochondrial functions. In *in vitro* kidney epithelial as well as hepatocyte cultures, the compounds provoked oxidative stress, depleted glutathione levels, and increased lipid peroxidation [85].

Atractyloside is also found in *Callilepis laureola* DC. (Impila), an herbaceous South African plant that is used as a traditional multipurpose remedy by the Zulu people. Several cases of acute hepato- and nephrotoxicity have been reported since the 1970s [59].

1.3.6 Greater Celandine

Greater Celandine (*Chelidonium majus* L.) extracts are used for the treatment of dyspepsia and biliary disorders; however, therapeutic efficacy has never been proven in controlled clinical trials [60]. The plant contains several alkaloids including berberine, coptisine, chelerythrine, and chelidonine. Several cases of acute putative hepatotoxicity were related to the intake of commercially available drug preparations in high doses. In 10 female patients, signs of hepatotoxicity were reflected in elevated ALT and ALP levels, cholestasis, and low titers of antinuclear and smooth muscle antibodies indicating drug-induced autoimmunity [86]. Histologically, lobular and portal inflammation and eosinophilic infiltrates were detected. The mechanism of toxicity is unknown, but immune-mediated mechanisms are discussed. The up-dated recommendation for the daily doses is considered to be safe concerning liver toxicity.

1.3.7 Other hepatotoxic herbs and natural compounds

Teschke et al. recently compiled case reports of herbal hepatotoxicity and identified 60 different herbal drugs and herbal supplements which are linked to hepatotoxicity [64]. In many cases, however, data acquisition, documentation, and presentation were of rather poor quality. Adequate causality assessment was missing in most cases.

The hepatotoxicity of several Chinese herbs/herbal mixtures e.g. Ma-huang (*Ephedra* sp.), Jin Bu Huan (*Lycopodium serratum* THUNB.) is quite clearly estimated [59,61,63]. Black cohosh (*Actaea racemosa*, *Cimicifuga racemosa* (NUTT.) L.) intake was connected to acute hepatitis and liver failure in several reports [87,88] but causality assessment revealed inconsistencies in most cases. Mechanisms of hepatotoxicity remain as well unidentified. The hepatotoxicity of mistletoe (*Viscum album* L.) is controversially discussed as it is based on one single case report although the drug is quite widely used [89]. Noni juice (*Morinda citrifolia* L.) which is rigorously campaigned in European tabloid press for its beneficial health effects has been reported to cause severe hepatitis in a 45-year-old man [90]. Liver damage has been observed after use of herbal laxatives such as Senna (*Cassia angustifolia* VAHL.) [91]. 'Prostata', a combination of herbal ingredients containing *Serenoa serrulata* (W.BARTRAM) SMALL, sold for treatment of benign prostatic hyperplasia, has been reported to cause cholestatic hepatitis in a man [92]. Pennyroyal (*Mentha pulegium* L.) is associated with several cases of hepatic and neurologic injury [93,94]. Toxicity is believed to be mediated by both (+)-pulegone producing oxidative stress and pulegone's primary metabolite menthofuran that is further oxidized by CYP450, increasing its toxicity [95].

1.4 Aims

(1) Drug-induced hepatotoxicity constitutes the main reason for a drug not reaching approval or for withdrawal of drugs from the market. Kava kava is a prominent example for putative herbal hepatotoxicity. For centuries, the plant has been used by the Pacific Islanders for ceremonial and medicinal purpose. In Western countries, standardized organic kava root extracts were approved for the treatment of non-psychotic anxiety disorders. In 2002, German health authorities banned kava-containing products from the market because several cases of severe hepatotoxic side effects have been reported which were putatively linked to kava-intake. Recently, a reevaluation of case reports stirred up the debate of still unknown mechanisms and elicitors of kava-hepatotoxicity. Particularly, there is a lack of studies, which address the putative toxicity of single constituents. For this reason, major and minor constituents were isolated from an acetonic kava root extract and tested towards their hepatotoxic potential *in vitro* (chapter 3). The study was aimed to uncover the hepatotoxic potential of individual constituents and thereby to contribute to the controversial discussion of kava-hepatotoxicity.

(2) The anti-Alzheimer's drug tacrine, an acetylcholinesterase inhibitor, constitutes another example for DILI. Despite its clinical efficacy and high potency, tacrine was withdrawn from the market due to hepatotoxic side effects. In order to face these therapy limiting side effects, a "co-drug" was designed by linking a tacrine-based acetylcholinesterase (AChE)-inhibiting part to the hepatoprotective flavonolignane silibinin via a liable ester bond. At first, the question should be answered whether this chemical connection is related to beneficial pharmacological effects in particular in comparison to a physical mixture of tacrine and silibinin. Therefore, the *in vitro* hepatotoxicity should be evaluated and compared to that of tacrine and an equimolar mixture of tacrine and silibinin (chapter 6). Furthermore, the *in vitro* degradation stability and metabolism of the codrug should be studied in different incubations systems to obtain valuable information about possible degradation products and metabolites of the codrug, which finally may help to identify the active principle of the codrug both *in vitro* and *in vivo*. In the face of toxification of tacrine to protein-reactive metabolites, the *in vitro* hepatotoxicity of the codrug cleavage products, a tacrine hemi succinamide and silibinin, should be addressed as they constitute the primary metabolites and may be rapidly formed *in vivo*. The absence of metabolite toxicity would as well point out the superiority of the codrug in terms of the therapy limiting side effects of tacrine.

(3) Chalcones represent an interesting substance class for treatment of liver diseases such as hepatic fibrosis as they comprise a set of favorable pharmacological properties such as anti-inflammatory, anti-oxidant, pro-apoptotic, and immunomodulatory activity. Several chalcones, among xanthohumol, have already shown anti-fibrotic effects both *in vitro* and *in vivo*. Driven by these positive results, this study comprises the testing of a set of structurally related prenylated and non-prenylated chalcones towards their anti-proliferative and apoptosis-inducing effects against activated human HSC, which have been identified as central cellular mediators in the pathogenesis of hepatic fibrosis (chapter 4). Comparing the inhibitory effects of the test chalcones, the study was also aimed to identify structure elements which enhance or attenuate the inhibitory activity. Chalcones being active may be selected for further pharmacological testing.

(4) As the previous chapters deal with the toxicity and biological activity of chalcones, the *in vitro* metabolism of the pharmacologically active flavokawains and alpinetin chalcone were investigated in different microsomal incubation systems (chapter 5). Apart from alpinetin chalcone, the metabolism of these chalcones has not been studied before. By choosing appropriate liquid chromatography–mass spectrometry techniques, the phase I and phase II metabolites should be identified. Based on these data, a metabolism scheme might be proposed for the test chalcones. Moreover, liquid chromatography–nuclear magnetic resonance spectroscopy is applied for structure elucidation of (major) metabolites. For future *in vitro* and *in vivo* studies, the metabolite profiling might provide helpful information for the identification of *in vivo* metabolites. Moreover, this study might highlight the role of generated metabolites and the importance of comprising (conjugated) metabolites to pharmacological *in vitro* testing.

2 Materials and Methods

2.1 Phytochemical and analytical methods

2.1.1 Plant material and extraction

Dried Kava Kava rhizome (*Piper methysticum* FORST., Piperaceae) was kindly provided by Martin Bauer GmbH (batch no. 10787/09 96117). The plant material (250 g) was powdered and sonicated three times with acetone for 4 h. Due to incompleteness of the extraction, the plant material was transferred to a percolation column (\emptyset 5 cm) and macerated in 500 mL acetone overnight. The next day percolation (3 mL/min) was carried out until complete exhaustion of the plant material. Overall for the extraction, an amount of 4.2 L acetone was used. After rotary evaporation of the acetone, 17.52 g crude extract was obtained.

2.1.2 Fractionation and isolation of kavalactones

2.1.2.1 Flash chromatography

For flash chromatography, the crude extract or the dried fractions were resolved in acetone, adsorbed to a part of the stationary phase (silica gel (Si60) or reversed phase 18 (RP18) material) by rotary evaporation, and filled in a precolumn for chromatography. The fractions (20 mL) were automatically collected and analyzed by ultraviolet/visible spectroscopy at one wavelength ($\lambda = 270$ nm or 340 nm).

Table 2.1 lists the used methods and indicates the chromatographic conditions. Collected fractions were reasonably combined after thin layer chromatography (TLC) analyses on silica plates using solvent system **T1** and derivatization reagent **D1** (see chapter 2.1.3.1).

Table 2.1: Methods for flash chromatography. M method, St stationary phase (column), A and B solvent A and solvent B, t time [min], A/B solvent composition, f flow [mL/min]. EtOAc p.a., MeOH p.a., H₂O ultra-pure.

| M | St | A | B | t | A/B | f |
|-----------|--|--------------------------------|-----------------------|----------|-------------|----------|
| F1 | Precolumn Si60, 20 g SVP D40-Si, 15-40 µm, 90 g | Hexane | EtOAc + 10% MeOH | 0-5 | 100/0 | 30 |
| | | | | 5-110 | 100/0→60/40 | |
| | | | | 110-130 | 60/40→0/100 | |
| | | | | 130-140 | 0/100 | |
| F2 | Precolumn LiChrorep RP18, 25-40 µM, 5 g SVP D40-RP18, 25- 40 µm, 90 g | H ₂ O/MeOH 50/50 | MeOH | 0-5 | 100/0 | 20 |
| | | | | 5-70 | 80/20→50/50 | |
| | | | | 70-85 | 50/50→0/100 | |
| | | | | 85-90 | 0/100 | |
| F3 | Precolumn Si60, 10 g SVP D40-Si, 15-40 µm, 90 g | Hexane | Acetone + 1% EtOAc | 0-5 | 100/0 | 30 |
| | | | | 5-25 | 100/0→80/20 | |
| | | | | 25-55 | 80/20 | |
| | | | | 55-85 | 80/20→70/30 | |
| | | | | 85-90 | 70/30→0/100 | |
| 90-100 | 0/100 | | | | | |
| F4 | Silica Si60 15-40 µm, 30 g | Hexane | Acetone + 1% EtOAc | 0-3 | 100/0 | 10 |
| | | | | 3-23 | 100/0→80/20 | |
| | | | | 23-43 | 80/20 | |
| | | | | 43-53 | 80/20→70/30 | |
| | | | | 53-55 | 70/30→0/100 | |
| | | | | 55-75 | 0/100 | |
| F5 | Silica Si60 15-40 µm, 30 g | Hexane | Acetone + 1% EtOAc | 0-5 | 100/0 | 15 |
| | | | | 5-25 | 100/0→80/20 | |
| | | | | 25-45 | 80/20 | |
| | | | | 45-55 | 80/20→0/100 | |
| | | | | 55-60 | 0/100 | |
| F6 | Silica Si60 15-40 µm, 30 g | Hexane | Acetone + 1% EtOAc | 0-2 | 100/0 | 15 |
| | | | | 2-20 | 100/0→80/20 | |
| | | | | 20-40 | 80/20 | |
| | | | | 40-60 | 80/20→70/30 | |
| F7 | Silica Si60 15-40 µm, 30 g | Hexane | Acetone + 1% EtOAc | 0-15 | 100/0→80/20 | 10 |
| | | | | 15-30 | 80/20 | |
| | | | | 30-50 | 80/20→70/30 | |
| | | | | 50-55 | 70/30→0/100 | |
| | | | | 55-60 | 0/100 | |
| F8 | Silica Si60 15-40 µm, 30 g | Hexane | Acetone + 1% EtOAc | 0-2 | 100/0 | 15 |
| | | | | 2-15 | 100/0→80/20 | |
| | | | | 15-35 | 80/20 | |
| | | | | 35-55 | 80/20→70/30 | |
| | | | | 55-60 | 70/30→0/100 | |
| | | | | 60-65 | 0/100 | |

2.1.2.2 Semi preparative high pressure liquid chromatography

One fraction (G2.6') was further purified by semi preparative high pressure liquid chromatography (HPLC) (**H1**). The sample was dissolved in 50% (v/v) methanol (MeOH) to a concentration of 2.5 mg/mL and a volume of 1 mL was manually injected. For detection, a diode array detector (DAD) was used. HPLC analysis was performed on a Eurosphere-100 column (C18, 7 μ M, 16 x 25 mm, Knauer, Berlin) at ambient temperature with a flow rate of 10 mL/min. The eluents were H₂O and MeOH and following gradient system was used: 0-5 min 50/50, 5 min 40/60, 5-30 min 40/60→30/70, 30-35 min 30/70→0/100, 35-40 min 0/100, 40-45 min 0/100→50/50.

2.1.2.3 Recrystallization

Yangonin, methysticin, and desmethoxyyangonin (G2.8) were recrystallized in MeOH at 4 °C. Kawain (G2.4) was dissolved in MeOH and recrystallized by the addition of water. Precipitates were sucked off and dried in the exsiccator.

2.1.3 Analytical methods

2.1.3.1 Thin layer chromatography / High performance thin layer chromatography

(High performance) thin layer chromatography ((HP)TLC) analyses were performed using aluminum or glass plates coated with silica 60 F₂₅₄ (Merck, Darmstadt, Germany). Substances/fractions were either manually applied or sprayed on plates with a Linomat 5 in case of HPTLC analysis. The dried plates were developed in a saturated chamber. Development of HPTLC plates was performed with an automatic ADC2 Chamber (Twin Trough Chamber) to a distance of 7 mm from bottom to the top. Plates were analyzed under UV light (254 nm and 365 nm) or daylight after derivatization. The images were recorded on a Reprostar 3.

Solvent systems

| | |
|--------------|---|
| T1 | Hexane: EtOAc: MeOH (70: 20: 10) |
| T1+FA | Hexane: EtOAc: MeOH (70: 20: 10) + 0.1% formic acid (FA) |
| T2 | EtOAc: Toluene: MeOH: Diethylamine: NH ₃ (8: 2: 2: 0.5: 1) |

Derivatization reagents

| | |
|-----------------------------------|--|
| D1 Anisaldehyde reagent | 0.5% anisaldehyde, 84.5% MeOH, 10% glacial acid, 5% H ₂ SO ₄ conc., heating at 105 °C for 10 min, daylight |
| D2 Natural product reagent | 1% in MeOH (m/v) / Polyethylene glycol 400 5% in MeOH (m/v), heating at 105 °C for 5 min, UV 365 nm |

2.1.3.2 Nuclear magnetic resonance spectroscopy

For identification and structure confirmation of isolated kavalactones ^1H NMR spectra were recorded in deuterated chloroform (CDCl_3) at ambient temperature using a Bruker Avance spectrometer (300 MHz). Structures of synthesized chalcones were confirmed by Dr. Susanne Vogel [96–98]. Hydrogenation of flavokawain C, dihydroxanthohumol C, and helichrysetin was executed by Petr Jirásek using an established method [99]. Again, molecular structures of hydrogenated compounds were approved by ^1H NMR (CDCl_3 , acetone- d_6 , 400 MHz). Structures of tacrine hemi succinamide (4-oxo-4-(6-(1,2,3,4-tetrahydroacridin-9-ylamino)butanoic acid) and the codrug (((2*S*,3*S*)-3-(4-hydroxy-3-methoxyphenyl)-6-((2*R*,3*R*)-3,5,7-trihydroxy-4-oxochroman-2-yl)-2,3-dihydrobenzo[*b*][1.4]dioxin-2-yl)-methyl 4-oxo-4-(6-(1,2,3,4-tetrahydroacridin-9-ylamino)-hexylamino)butanoate hydrochloride) synthesized by Dr. Xinyu Chen were confirmed by ^1H NMR (CDCl_3 , 300 MHz) and ^{13}C NMR (CDCl_3 , 75 MHz) spectroscopy [100].

2.1.3.3 Analytical high pressure liquid chromatography

Purity of isolated and synthesized test compounds was evaluated by HPLC–DAD (Table 2.2). For **P1**, **P3**, and **P4** the compounds were dissolved in 50% (v/v) MeOH to a concentration of 1 mg/10 mL; for **P2**, compounds were dissolved in 50% (v/v) acetone to a concentration of 10 μM .

The purity was calculated as percentage of total peak area at indicated wavelengths (λ). Purity analysis of method **P2** was performed by Dr. Magdalena Motyl [101]; purity analysis of **P3** and **P4** was conducted by Dr. Xinyu Chen [100].

Table 2.2: Methods for analytical HPLC. M method, C column 1 Purosphere STAR 250-4 RP 18e 5 μm , column 2 Purosphere STAR 125-4 RP 18e 3 μm (Merck, Darmstadt), A and B eluents A and B, t time [min], A/B solvent composition, f flow [mL/min], V injection volume [μL], λ wavelength [nm], T oven temperature [$^\circ\text{C}$]. FA 98% p.a., MeCN for HPLC, TFA p.a.

| M | C | A | B | t | A/B | f | V | λ | T |
|-----------|---|-----------|-------------------------|-------|-------------|-----|----|--------------------------|----|
| P1 | 1 | 0.1% FA | 95% MeCN | 0-15 | 80/20→0/100 | 1 | 10 | UV_{max} | 40 |
| | | | | 15-20 | 0/100 | | | | |
| P2 | 1 | 0.1% FA | 95% MeCN | 0-27 | 45/55→15/85 | 1 | 20 | 368 | 30 |
| | | | | 27-30 | 15/85→45/55 | | | | |
| | | | | 30-40 | 45/55 | | | | |
| P3 | 2 | 0.1% FA | 95% MeCN + 0.1% FA | 0-30 | 80/20→0/100 | 0.4 | 10 | 287 | 40 |
| | | | | 30-40 | 0/100 | | | | |
| | | | | 40-45 | 0/100→80/20 | | | | |
| P4 | 2 | 0.05% TFA | 95% MeCN + 0.05% TFA | 0-30 | 90/10→10/90 | 0.4 | 10 | 247 | 20 |
| | | | | 30-45 | 10/90 | | | | |
| | | | | 45-55 | 10/90→90/10 | | | | |
| | | | | 55-60 | 90/10 | | | | |

2.2 Cell culture

2.2.1 Chemicals, reagents, supplements

| | |
|---|---|
| Alexa Fluor [®] 488 phalloidin | Molecular Probes, Life Technologies, Carlsbad, USA |
| CV | crystal violet, Merck, Darmstadt |
| CV solution | 0.5% (w/v) crystal violet in 20% (v/v) methanol |
| Cytochrome C detection kit | Cellomics [®] , Thermo Fisher Scientific, Waltham, USA |
| FCS | fetal calf serum, Lot.No. 1050L, Biochrom, Berlin |
| L-Glutamine | 200 mM, Biochrom, Berlin |
| Hoechst33342 | bisbenzimidazole H 33342 trihydrochloride, Sigma-Aldrich, Taufkirchen |
| MitoTracker Red CMXRos [®] | Molecular Probes, Life Technologies, Carlsbad, USA |
| MTT | 3-(4,5-dimethylthiazol-2-yl)-2,5-diphenyl tetrazolium bromide, Sigma-Aldrich, Taufkirchen |
| MTT solution | 4 mg/mL MTT in PBS, sterile-filtered |
| NEA | nonessential amino acids, 100x, Biochrom, Berlin |
| Paraformaldehyde solution 10% | phosphate buffered, Applichem, Darmstadt |
| PBS | Dulbecco's Phosphate Buffered Saline (w/o Mg ²⁺ , Ca ²⁺), Sigma-Aldrich, Taufkirchen |
| Permeabilization buffer | Triton [®] X-100, 10x, Cellomics, Pittsburgh, USA |
| SDS | sodium dodecyl sulfate, Sigma-Aldrich, Taufkirchen |
| SDS solution | 10% (w/v) in PBS |
| Sodium citrate | tri-sodium citrate-2-hydrate, Merck, Darmstadt |
| SP | sodium pyruvate, 100 mM, Biochrom, Berlin |
| Trypan blue | Sigma-Aldrich, Taufkirchen |
| Trypan blue solution | 0.4% (w/v) trypan blue in PBS, sterile-filtered |
| Trypsin/EDTA | 10x trypsin/EDTA solution (0.5%/0.2% (w/v)), Biochrom, Berlin |
| Trypsin/EDTA solution | 10% (v/v) in PBS |

2.2.2 Culture media, cell lines

2.2.2.1 Heat inactivation of fetal calf serum

FCS was stored at -20 °C. Initially, 500 mL of FCS were thawed in a water bath at 37 °C. For inactivation, FCS was heated to 56 °C in a water bath for 30 min. Aliquots of heat inactivated FCS (FCS_{hi}, 50 mL) were stored at -20 °C prior to use.

2.2.2.2 Culture media

- 1) Culture medium (CM 1) Dulbecco's Modified Eagle Medium (DMEM GIBCO with phenol red, 2 mM glutamine, 4.5 g/L glucose, Life Technologies, Carlsbad, USA) supplemented with 10% FCS_{hi} (Biochrom, Berlin, Germany).
- 2) Culture medium (CM 2) Dulbecco's Modified Eagle Medium (DMEM with phenol red, 1.0 g/L glucose, Biochrom, Berlin, Germany) supplemented with 10% FCS_{hi}, 1% SP and 1% NEA (v/v).
- 3) Incubation medium Dulbecco's Modified Eagle Medium (DMEM GIBCO without phenol red, 4.5 g/L glucose, Life Technologies, Carlsbad, USA) supplemented with 10% FCS_{hi} and 2 mM L-glutamine.
- 3) Staining medium Dulbecco's Modified Eagle Medium (DMEM GIBCO without phenol red, 4.5 g/L glucose, Life Technologies, Carlsbad, USA) supplemented with 1% FCS_{hi} and 2 mM L-glutamine.
- 4) Freezing medium 70% DMEM, 20% FCS_{hi}, 10% DMSO

2.2.2.3 Cell line data

| Cell name | Tissue | Charact. | Source | Cell Bank | Cell number |
|---------------|--------|----------------|--------|------------------------------|-------------|
| HuH-7 (CM 1) | liver | hepatoma | human | HSRRB | JCRB0403 |
| HepG2 (CM 1) | liver | hepatoma | human | ATCC | HB-8065 |
| HSC (CM 1) | liver | stellate cells | human | Univ. Hospital of Regensburg | |
| Caco-2 (CM 2) | colon | cancer | human | ATCC | HTB-37 |

The human hepatoma cell line HepG2 (ATCC[®]-number HB-8065[™]) was obtained from the American Type Culture Collection (ATCC), USA. The human hepatoma cell line HuH-7 (HSRRB-number JCRB0403) was purchased from the Health Science Research Resources Bank (HSRRB) of the Japan Health Sciences Foundation (JHSF), Japan. The immortalized activated human hepatic stellate cell line (HSC) was provided by the University Hospital of Regensburg, Department of Internal Medicine I [102]. The human colorectal cell line (Caco-2, ATCC[®]-number HTB-37[™]) was obtained from the Institute of Virology, Helmholtz Zentrum München, Germany.

2.2.3 Laboratory expendables

| | |
|-------------------------------------|---|
| Cell culture flasks (various sizes) | TPP, Trasadingen, Switzerland |
| Centrifuge tubes (15 and 50 mL) | TPP, Trasadingen, Switzerland |
| Cryotubes (2 mL) | Greiner, Frickenhausen |
| Eppendorf tubes (1.5 and 2 mL) | Eppendorf, Hamburg |
| Multiwell plates | TPP, Trasadingen, Switzerland |
| Pipette tips | 200 µL/1000 µL, Sarstedt, Nümbrecht 10 µL, Axygen, Union City, USA |
| Serological pipettes | TPP, Trasadingen, Switzerland |
| Syringe filter units | 0.2 µm, Minisart, Sartorius, Göttingen |

2.2.4 Cultivation, handling, treatment

2.2.4.1 Cultivation of cells

Cells were cultivated under standard cell culture conditions at 37 °C in a humidified atmosphere with 5% CO₂ in the appropriate cell culture medium (see chapter 2.2.2.2 and 2.2.2.3). Medium was changed every 3-4 days and cells were splitted 1-2 times a week when about 80% confluence was reached. For this, cells were washed with PBS and detached by incubation with trypsin/ETDA solution at 37 °C for 5 min. The trypsin activity was stopped by the addition of FCS-supplemented medium (fivefold the amount of trypsin/EDTA solution). The cell suspension was transferred to a flacon tube and centrifuged at 700 x g for 5 min. The cell pellet was re-suspended in fresh medium. Cells were reseeded in new cell culture flasks with a split ratio of 1:5, 1:10 or 1:20 as needed. Cell growth, density and morphology were checked periodically using an inverted microscope.

2.2.4.2 Determination of cell number, seeding of cells

For determination of cell number, the cell suspension was diluted 1:10 with trypan blue solution and transferred to a Neubauer hemocytometer (Brand, Wertheim, Germany). Trypan blue only stains cells with impaired cell membranes whereas living cells appear as white spots and therefore can be easily distinguished from dead cells. Only living cells were counted in four big quadrates of the hemocytometer and cell number was calculated according to following equation:

$$\frac{\text{Cell number}}{\text{mL}} = (N \times f \times 10^4) \div 4$$

N: number of counted cells in the four quadrates

f: dilution factor (10)

Depending on the determined cell number, the cell suspension was diluted with medium and adjusted to a defined cell concentration in a centrifuge tube. For the experiments, 100 μL /well of cell suspension were seeded in 96-well plates with a multichannel pipette (Eppendorf, Research); the outer wells were just filled with buffer or medium without cells. The seeding density of the cell lines was maintained throughout different experiments to make the results comparable. In preliminary tests, the optimal seeding density was determined for the different cell lines as shown below:

| | | |
|--------|-----------------------------|-------------------------------|
| HuH-7 | $1.5 \times 10^5/\text{mL}$ | $1.5 \times 10^4/\text{well}$ |
| HepG2 | $1.0 \times 10^5/\text{mL}$ | $1.0 \times 10^4/\text{well}$ |
| HSC | $5.0 \times 10^4/\text{mL}$ | $5.0 \times 10^3/\text{well}$ |
| Caco-2 | $2.0 \times 10^5/\text{mL}$ | $2.0 \times 10^4/\text{well}$ |

Subsequently, the plates were horizontally shaken to evenly distribute the cells inside the wells. Prior to treatment, the cells were cultured for 24 h at 37 °C and 5% CO_2 in a humidified incubator.

2.2.4.3 Cell treatment

Concentrations series of the test compound(s) were prepared by diluting the stock solution (in dimethyl sulfoxide (DMSO) or ethanol (EtOH)) in the incubation medium (see chapter 2.2.2.2). The end concentration of the solvents was kept at a maximum concentration of 0.1% for DMSO and 0.5% for EtOH in the medium as these concentrations lacked significant effects in all performed assays.

Culture medium was carefully aspirated from each well of a plate and cells were treated with 100 μL of the test solutions. For each concentration, at least three parallels were performed. Untreated (pure medium) and solvent-treated (0.1% DMSO or 0.5% EtOH) cells were employed as controls. If not mentioned otherwise, the cells were incubated for another 24 h at 37 °C and 5% CO_2 before cell assays were performed.

2.2.4.4 Cryopreservation and thawing of cell lines

For cryopreservation, the cell number was adjusted to 5.0×10^5 cells/mL in freezing medium (see chapter 2.2.2.2). Afterward, 2 mL of the cell suspension were transferred into a cryotube and immediately frozen at -80 °C. For long-term cryopreservation, the frozen cell suspension was finally stored in a liquid nitrogen storage tank.

Cell thawing was performed quickly in a 37 °C water bath. The cell suspension was mixed with 8 mL of fresh culture medium in a centrifuge tube. After re-suspension, cells were centrifuged for 5 min at 700 x g. Finally, 2 mL culture medium was added to the obtained cell

pellet and the whole cell suspension was transferred to a new culture flask containing already 18 mL culture medium. Medium was exchanged the following day.

2.2.5 Viability and proliferation assays

2.2.5.1 MTT assay

For determination of cell viability, MTT (3-(4,5-dimethylthiazol-2-yl)-2,5-diphenyl tetrazolium bromide) assay was adapted to previously described procedures [103]. After treatment and removal of the incubation medium, cells were incubated with 100 μ L MTT solution (0.4 mg/mL) per well. The yellow tetrazolium salt is reduced by enzymes of the endoplasmic reticulum (ER) of metabolically active cells to a blue insoluble formazan. After 3 h, supernatants were removed and 100 μ L lysis buffer (10% SDS, pH 4.1) was added to each well. The next day the absorbance of the formazan solution was measured with a multiwell plate reader at 560 nm. The absorption directly correlates with the number of viable cells. Untreated cells were set as 100% values and served as controls. Cell viability was calculated using following equation:

$$cell\ viability\ [\%] = \frac{A_x - A_{blank}}{A_{ctl} - A_{blank}} \times 100$$

A_x : absorbance treated well

A_{ctl} : absorbance control well

A_{blank} : absorbance blank well

2.2.5.2 Crystal violet assay

Crystal violet (tris(4-(dimethylamino)phenyl)methyl)ium chloride) also known as Gentian violet primarily used for Gram stain, is a basic dye which stains DNA of cell nuclei. Accordingly, the photometrically measured absorbance directly correlates with the number of cells and is used to determine cell proliferation [104].

The incubation medium was carefully removed, and cells were incubated with 50 μ L CV solution (0.5% in 20% methanol) per well for 10 minutes at room temperature. Staining solution was aspirated, and cells were thoroughly washed three times with ultra-pure water. After drying plates overnight, 100 μ L of sodium citrate buffer (EtOH + 0.1 M sodium citrate (1:1, v/v)) was added to each well and absorbance of the solution was determined at 560 nm using a multiwell plate reader. To gather information of initial cell number, one 96 well plate was already stained 24 h after seeding (before treatment). Untreated cells served as controls and were set as 100% values. A significant deviation from 100% values indicates pro- or anti-proliferative (cytostatic) effects whereas a drop below the initial cell number suggests a cytotoxic effect.

2.2.6 Fluorescence microscopic assays

2.2.6.1 High content analysis

Nowadays, the development of novel cytotoxicity assays proceeds to multiparameter screening methods since conventional cytotoxicity assays often lack sensitivity and only detect endpoints without revealing prelethal effects like organelle impairment or morphological changes. Hence, a high content analysis (HCA) assay for fluorescence microscopy was established applying three different fluorescent dyes staining nuclei, mitochondria, and the actin fibers of cells. The used fluorescent dyes and probes showed different, non-overlapping excitation and emission spectra (Figure 2.1) what made them suitable for multicolor labeling experiments using appropriate filters.

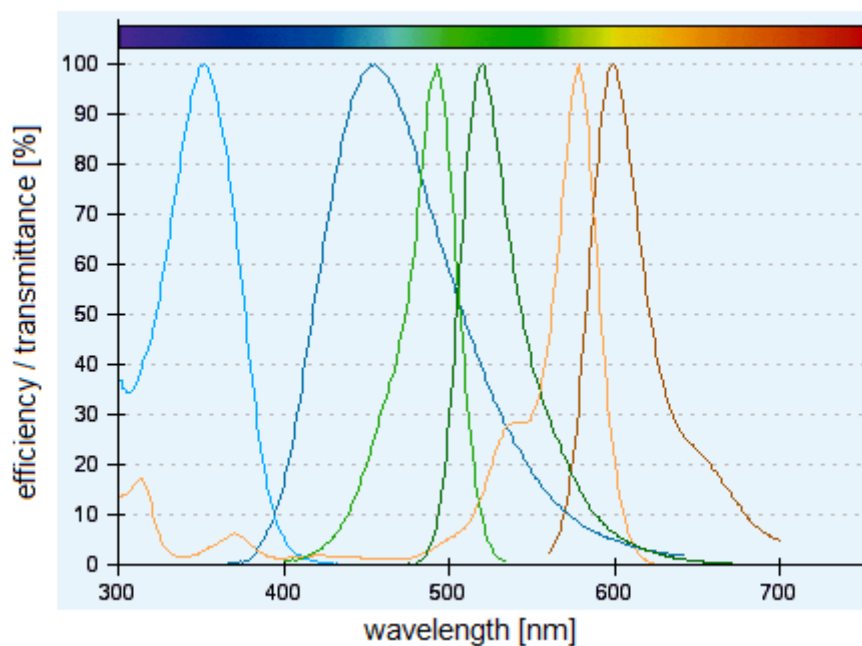


Figure 2.1: Excitation and emission spectra of used fluorescent dyes. Hoechst 33342 (blue) 352/455 nm, Alexa Fluor 488 (green) 485/581 nm, MitoTracker Red (red) 579/599 nm.

The HCA assay was established on human HSC which are suitable for fluorescence microscopy applications due to their smooth morphology.

For the staining procedure, stock solutions of fluorescent dyes were diluted in staining medium (see chapter 2.2.2.2) to applicable concentrations and kept strictly away from light while handling. First, cells were incubated with 50 μ L/well of a 1:2000 dilution of MitoTracker Red CMXRos[®] (1 mM stock solution) for 25 min at 37 °C. This mitochondrion-selective, rosamine-based probe passively diffuses across the plasma membrane and accumulates in active mitochondria. In contrast to tetramethylrosamine and rhodamine 123, the MitoTracker is not washed out after fixation and permeabilization steps according to manufacturer. Subsequently, 25 μ L/well of Hoechst33342 staining solution (bisbenzimidazole H 33342 trihydrochloride, 20 mM, 1:1200) was added to the wells for 5 min. Hoechst33342 is a well-

established intercalating dye for staining cell nuclei. Furthermore, Hoechst33342 staining intensity can be used for determination of cellular DNA content (see chapter 2.2.6.3). Next, the staining solution was aspirated and cells were washed with 100 μL /well of pre-warmed PBS. Afterward, cells were fixed with 100 μL /well of 3% paraformaldehyde (PFA) for 30 min at room temperature. Cells were washed again with PBS and then shortly treated with 50 μL /well of permeabilization buffer (0.1% Triton[®] X-100 in PBS). After a further washing step, the actin skeleton of cells was stained with an Alexa Fluor[®] 488 labeled phalloidin. Bicyclic phallotoxins from *Amanita phalloides* label F-actin at nanomolar concentrations in a stoichiometric ratio, which makes them also suitable to quantify the amount of F-actin in cells. The methanolic stock solution (200 units/mL) was diluted 1:50 with staining medium and 35 μL were added to each well for 20 min at room temperature. The medium was aspirated and cells were washed thoroughly with PBS. At the end, 100 μL of PBS buffer were added to each well for image acquisition.

Automatic image acquisition was carried out using a Carl Zeiss AxioObserver.Z1 (Carl Zeiss, Göttingen, Germany) with an EC Plan-Neofluar 10x objective, appropriate filters (filter sets: 49, 43 HE, 38 HE) for the fluorescent dyes, and Software AxioVision 4.8.1 (Carl Zeiss MicroImaging, Germany).

Other default settings for image acquisition:

- Multichannel: Ch1 Alexa Fluor[®] 488, Ch2 MitoTracker Red, Ch3 Hoechst33342
Fixed exposure times
Ch1 Autofocus, Ch2 Channel position +3 μm , Ch3 Channel position -20 μm
- Positionlist: Three images/well

Image analysis was automatically performed by the ASSAYbuilder Physiology Analyst software. Cell nuclei were identified by the software and used to automatically detect and count the cells. Besides, Hoechst staining was also used to examine the nuclear area. The mean total fluorescence intensity of detected mitochondria spots was measured within a defined ring mask over and around the nucleus. The area of actin spots was investigated over the complete cellular area defining another ring mask.

Other default settings for image analysis:

- Ch1 = Primary Object (nuclei), Ch2 = actin, Ch3 = mitochondria
- Primary Object Identification: Threshold Method Isodata (0)
Separation Method Peak (8)
- Primary Object Selection: Gating: Area 262–2492 pixel^2 , Shape 1.1–1.7 (1= round), reject objects on edge
- Ch2: Detection Method Morphological (25)

Threshold Method Fixed (mean Isodata ctl cells)

Circ 3, Ring Distance -20, Ring Width 80

- Ch3: Detection Method Box (4)

Threshold Method Fixed (mean Isodata ctl cells)

Circ 3, Ring Distance -20, Ring Width 60

2.2.6.2 Cytochrome c assay

For the determination of cytochrome c release from apoptotic mitochondria of HSC, the Cellomics[®] Cytochrome C Detection kit (Thermo Fisher Scientific) was applied followed by fluorescence microscopic analysis.

Kit contents

Cytochrome C Primary Antibody

DyLight[™] 549 Conjugated Goat Anti-Mouse IgG (ex/em 550/568 nm)

Hoechst33342 Dye (ex/em 350/461 nm)

Wash Buffer (10x Dulbecco's PBS)

Wash Buffer II (10x Dulbecco's PBS with Tween[®]-20)

Permeabilization Buffer (10x Dulbecco's PBS with 1% Triton[®] X-100)

Blocking Buffer (10x)

The assay was conducted according to the manufacturer's protocol with slight modifications. After treatment, cells were fixed with 4% PFA (100 μ L/well) for 15 min at room temperature. Fixation solution was aspirated and cells were washed twice with Wash Buffer. Following, cells were incubated with permeabilization buffer (100 μ L/well) for 15 min at room temperature. Again, the buffer was aspirated and cells were washed twice with Wash Buffer. Subsequently, cells were treated with Blocking Buffer (+ 2% FCS, 100 μ L/well) for 15 min at room temperature. The Blocking Buffer was aspirated and cells were incubated with Primary Antibody Solution (1:400 in Blocking Buffer; 50 μ L/well) for 1 h at room temperature. After removal of the antibody solution, the plate was washed twice with Wash Buffer II and Wash Buffer respectively. Staining with Secondary Antibody Solution (1:500 in Blocking Buffer; 50 μ L/well) was performed for 45 min at room temperature under exclusion of light. Finally, the staining solution was aspirated, cells were washed twice with Wash Buffer II, Wash Buffer, and 200 μ L of PBS were added to each well for image acquisition.

Automatic image acquisition was carried out using a Carl Zeiss AxioObserver.Z1 (Carl Zeiss, Göttingen, Germany) with an EC Plan-Neofluar 10x objective, appropriate filters (filter sets: 49, 43 HE) for the fluorescent dyes, and Software AxioVision 4.8.1 (Carl Zeiss MicroImaging, Germany).

Other default settings for image acquisition:

- Multichannel: Ch1 DyLight 549, Ch2 Hoechst33342, Ch3 Phase
Fixed exposure time
Ch1 and Ch2 Autofocus, Ch3 Current Focus Position
- Positionlist: Three images/well

Image analysis was automatically done by the ASSAYbuilder Physiology Analyst software.

In normal cells, cytochrome c is located in the mitochondria, which can be detected as cytoplasmic spots. Upon induction of apoptosis, cytochrome c is released from the mitochondria and can diffuse into the nucleus. Thus, a reallocation of stained cytochrome c is detectable. For image analysis, a circ mask was put over the nucleus area and a ring mask over the cytoplasmic area of a cell. The ring mask measures the fluorescence in the cytoplasm of cells where unreleased cytochrome c within the mitochondria can be found. The circ mask determines the fluorescence in the nucleus area of cells where cytochrome c diffuses when it is released from the mitochondria. To determine the reallocation and therefore the extent of released cytochrome c, the mean average fluorescence intensity between circ and ring mask was analyzed (MEAN_CircRingAvgIntenDiff).

Other default settings for image analysis:

- Ch1 = Primary Object (nuclei), Ch2 = cytochrome c
- Primary Object Identification: Threshold Method Isodata (0)
Separation Method Peak (9)
- Primary Object Selection: Gating: Area 351–2406 pixel², Shape 1.0861–2.065,
reject objects on edge
- Ch2: Detection Method Box (5)
Threshold Method Isodata (0)
Circ 3, Ring Distance 3, Ring Width 40

2.2.6.3 DNA content

DNA content analysis was performed within the HCA assay system (see chapter 2.2.6.1) analyzing the intensity of Hoechst33342 staining. As the fluorescence intensity directly correlates with the DNA content, conclusions concerning the actual cell cycle state can be drawn. For image analysis, another protocol was developed using the ASSAYbuilder Cellcycle Analyst software.

Following default settings were used:

- Ch1 = nucleus
- Nucleus Identification and Selection see settings in chapter 2.2.6.1
- Settings: Cellcycle Intensity, Peaks_one class for ctl cells

2.3 *In vitro* stability and metabolism

2.3.1 Human liver microsomes

Pooled human liver microsomes (HLM) derived from 50 adult donors of mixed gender and with a total protein concentration of 20 mg/mL were purchased from Live Technologies (HMMC-PL; 0.5 mL). They were stored in aliquots at -80 °C prior to use to avoid frequent freeze-thaw cycles.

2.3.2 Chemicals, reagents

| | |
|--|--|
| Potassium dihydrogen phosphate p.a. | Merck, Darmstadt |
| Di-Potassium hydrogen phosphate p.a. | Merck, Darmstadt |
| Magnesium chloride hexahydrate p.a. | Merck, Darmstadt |
| Nicotinamide adenine dinucleotide phosphate reduced tetrasodium salt | Calbiochem [®] , Merck, Darmstadt |
| Nicotinamide adenine dinucleotide phosphate sodium salt hydrate | Sigma-Aldrich, Taufkirchen |
| Glucose-6-phosphate sodium salt | Sigma-Aldrich, Taufkirchen |
| Glucose-6-phosphate dehydrogenase 100 UN | Sigma-Aldrich, Taufkirchen |
| Uridine 5'-diphosphoglucuronic acid trisodium salt | Sigma-Aldrich, Taufkirchen |
| Alamethicin from <i>Trichoderma viride</i> | Sigma-Aldrich, Taufkirchen |

The metabolism studies were carried out in 0.1 M potassium phosphate buffer (**PO₄ buffer**). Therefore, 2.76 g of KH₂PO₄ (A) and 4.56 g of K₂HPO₄ (B) were dissolved in ultra-pure water to a volume of 100 mL (0.2 M) respectively. 19.0 mL of solution A and 81.0 mL of solution B were mixed and adjusted to a pH of 7.40 using a pH meter. The adjusted buffer was diluted 1:1 in ultra-pure water to obtain a concentration of 0.1 M. Afterward, the buffer was sterile-filtered and stored at 4 °C.

Stock solutions of glucose-6-phosphate (110 mM, **G-6-P**), magnesium chloride hexahydrate (110 mM, **MgCl₂**), nicotinamide adenine dinucleotide phosphate (43 mM, **NADP**), reduced nicotinamide adenine dinucleotide phosphate (10 mM, **NADPH**), and uridine 5'-diphosphoglucuronic acid (40 mM, **UDPGA**) were prepared in potassium phosphate buffer. The glucose-6-phosphate dehydrogenase (**G-6-P-DH**) was diluted in 5 mM sodium citrate solution to a concentration of 40 U/mL. The pore-forming peptide alamethicin (**Ala**) was dissolved in methanol and ultra-pure water (2%, v/v) to a final concentration of 0.5 mg/mL. All reagents were stored in aliquots at -20 °C.

2.3.3 Microsomal metabolism of chalcones and identification of phase I and phase II metabolites

2.3.3.1 Incubation systems

The metabolite profiling of flavokawains was conducted in different microsomal incubation systems investigating both phase I and II reactions. As only membrane-bound enzymes are present in microsomal preparations (see chapter 5.1.1), the set of phase II enzymes is limited to UDP-glucuronosyltransferases (UGTs). Therefore, phase II reactions are limited to glucuronidation reactions. Phase I and II reactions (**Ph I**, **Ph II**) can be studied separately by addition of either NADPH or UDPGA equivalents, but also in combination (**Ph I+II**) by co-activation of phase I enzymes and UGTs within one system [105]. Suitable negative controls without microsomes (**w/o micr**) or without cofactors (**w/o cof**) have to be included to the sample set to avoid false conclusions because of unspecific reactions or stability problems. In addition, stability of the parent compound in the buffer system without any supplements has to be proven (**stabi**). Furthermore in preliminary experiments, 7-ethoxycoumarin (7-EC) was used as positive control to check whether the incubations systems and metabolizing enzymes are working properly. 7-EC is a commonly used probe for *in vitro* metabolism studies: both oxidative metabolism (deethylation, hydroxylation) and conjugation to glucuronic acid can be investigated [106].

Microsomal incubation systems for *in vitro* metabolism studies are very well established. The incubation systems were composed in accordance with literature data and available manuals [37]. For phase I metabolism, a NADPH regeneration system was used consisting of 3.3 mM MgCl₂, 3.3 mM Glc-6-P, 0.4 U/mL Glc-6-P-DH, and 1.3 mM NADP. For phase II metabolism, 2 mM UDPGA has to be added as activated substrate for UGTs. The pore-forming peptide alamethicin (25 µg/mL) helps the substrate to penetrate to the active site of the UGTs, which is localized inside the endoplasmic reticulum and thereby facilitates the glucuronidation reaction [107]. Stock solution (**Stock**) of 7-EC was prepared in MeOH (100 mM). The test chalcones were dissolved in DMSO (10 mM), again diluted in EtOH (1:10, 1 mM), and stored at 4 °C. The end concentration in the incubation system was 250 µM for the positive control and 10 µM for the flavokawains. Table 2.3 presents a pipetting scheme for the seven different test reactions, exemplarily for an end-volume of 1 mL.

Table 2.3: Pipetting scheme for the different incubation systems. Volumes are given in μL .

| | incubation systems | | | | | | |
|------------------------------|--------------------|-------|----------|---------|------|-------|---------|
| | matrix | stabi | w/o micr | w/o cof | Ph I | Ph II | Ph I+II |
| PO₄ buffer | 775 | 990 | 790 | 845 | 865 | 835 | 765 |
| MgCl₂ | 30 | - | 30 | 30 | 30 | 30 | 30 |
| Glc-6-P | 30 | - | 30 | 30 | 30 | - | 30 |
| Glc-6-P-DH | 10 | - | 10 | 10 | 10 | - | 10 |
| Ala | 50 | - | 50 | 50 | - | 50 | 50 |
| Micr | 25 | - | - | 25 | 25 | 25 | 25 |
| Stock | - | 10 | 10 | 10 | 10 | 10 | 10 |
| NADP | 30 | - | 30 | - | 30 | - | 30 |
| UDPGA | 50 | - | 50 | - | - | 50 | 50 |

All reagents were gently defrosted and kept on ice during the experiment. The PO₄ buffer was pre-warmed to room temperature and the required volume was transferred to 2 mL Eppendorf tubes. The reagents were pipetted in descending order. After addition of the microsomes, the samples were carefully vortexed and pre-warmed in a stirred water bath at 37 °C for 5 min. Subsequently, the chalcone stock solution was added and the samples were agitated again. By addition of NADP and/or UDPGA the reaction was started. The tubes were quickly transferred into the water bath and incubated at 37 °C. At defined time points (0-60 min), the metabolic reaction was stopped. Therefore, samples were taken and pipetted in another tube already containing the same volume of ice-cold EtOH in case of the chalcones or 5% (v/v) HCl (1:5) for 7-EC. The samples were vortexed vigorously for 5 min. Precipitated proteins were removed by centrifugation at 14 000 rpm for 5 min. The supernatant was used for HPLC and liquid chromatography–mass spectrometry (LC–MS) analyses.

2.3.3.2 Analytical high pressure liquid chromatography

Metabolized samples of 7-ethoxycoumarin (**C1**) and flavokawains (**C2**) were subjected to HPLC analysis (Table 2.4). Separation was performed on a C18-column (Hibar® 250-4, Purosphere, 5 μm). Temperature was set at 40 °C for the column oven and 4 °C for the autosampler.

Table 2.4: Methods for analytical HPLC. M method, A and B eluents A and B, t time [min], A/B solvent composition, f flow [mL/min], V injection volume [μ L], λ detection wavelength [nm]. FA 98% p.a., MeCN for HPLC.

| M | A | B | t | A/B | f | V | λ |
|----|---------|-------------------|-------|-------------|---|----|-----------|
| C1 | 0.1% FA | 95% MeCN (v/v) | 0-20 | 90/10→40/60 | 1 | 10 | 320 |
| | | | 20-22 | 40/60 | | | |
| | | | 22-23 | 40/60→90/10 | | | |
| | | | 25-30 | 90/10 | | | |
| C2 | 0.1% FA | 95% MeCN (v/v) | 0-20 | 70/30→0/100 | 1 | 10 | 364 |
| | | | 23-24 | 0/100 | | | 343 |
| | | | 24-25 | 0/100→70/30 | | | 368 |
| | | | 25-30 | 0/100→80/20 | | | |

2.3.3.3 Liquid chromatography–high resolution electrospray ionization mass spectrometry

Samples for liquid chromatography–high resolution electrospray ionization mass spectrometry (LC–HRESIMS) analysis (phase I, phase II, phase I+II, negative controls) were prepared at two time points (0 min and 60 min) according to the previously described method in chapter 2.3.3.1. Matrix samples without test compounds referred as blank controls (**matrix**). All samples were stored in HPLC vials (Wicom, Heppenheim) at -20 °C prior to analysis.

High resolution LC–MS was performed using UHPLC Agilent 1290 infinity, DAD G4212A, MS Agilent 6540 UHD Q-TOF with positive and negative electrospray ionization (ESI) using dual ion source. For separation, a Thermo Accucore aQ column (C18, 50x2.1 mm, 2.6 μ m) and the following solvents were used: eluent A was 0.1% formic acid (FA), eluent B 100% acetonitrile (MeCN) supplemented with 0.1% FA. A volume of 5 μ L (5 μ M chalcone solution) was injected. An oven temperature of 40 °C and a flow of 0.6 mL/min were set. Separation of the sample was conducted using the following gradient system:

0-10 min 100/0→2/98, 10-11 min 2/98 A, 11-11.1 min 2/98→100/0, 11.1-13 min 100/0.

Data analysis was performed with MassHunter software (B.05.00, Agilent) using automatic mass spectrum integration. The compound tables were manually compared to negative and matrix control samples and screened for corresponding metabolite masses.

2.3.3.4 High pressure liquid chromatography–nuclear magnetic resonance spectroscopy

For structure elucidation of major metabolites by means of high pressure liquid chromatography–nuclear magnetic resonance spectroscopy (HPLC–NMR), samples were sent to the NMR Group of the Max Planck Institute for Chemical Ecology in Jena.

Samples (combined phase I and II metabolism) were prepared according to the described method in chapter 2.3.3.1. The sample size was increased to 5 mL and the concentration of chalcones was raised to 100 μ M due to lower detection limit of NMR. A longer incubation

time of 4 h was chosen in order to achieve a maximized transformation rate of the initial compound and consequently an increased metabolite concentration. Reaction was again stopped by the addition of ice-cold EtOH (1:1). Samples were vortexed and centrifuged as described before. To improve storage stability, EtOH was carefully evaporated; samples were refilled with ultra-pure water, and frozen at $-20\text{ }^{\circ}\text{C}$ overnight. After freeze-drying, the samples were shipped on dry ice and stored at $-20\text{ }^{\circ}\text{C}$ prior to analysis.

Structure isolation and elucidation were conducted by the working group of Dr. Bernd Schneider at the Max Planck Institute Jena.

Isolation and structure elucidation of **FKA** metabolites

The provided sample was suspended in ultra-pure water ($\sim 3\text{ mL}$) and extracted with 5 mL of EtOAc by stirring for 30 minutes. The procedure was repeated 5 times. The EtOAc layers were joined and the solvent was evaporated under vacuum. The same was done for the remaining water fraction. The samples were dissolved in a minimum amount of HPLC solvents and HPLC fractionation was performed using an Agilent HP1100 Series equipped with binary pump G1312A, degaser G1322A, autoinjector G1367A, column oven G1316, and G1315B diode array detector controlled with ChemStation Rev.A.08.04. (1008) software. The chromatographic separation was performed on a LiChrospher RP-18 column (5 mm, 250 \times 4 mm; Merck KGaA, Darmstadt, Germany) with a guard column (5 mm, 4 \times 4 mm) using a linear binary gradient of ultra-pure H_2O containing 0.1% (v/v) TFA (solvent A) and MeCN (solvent B) with a flow rate of 0.8 mL/min.

For the EtOAc part the following gradient profile was used: 0 min, 5% B; 10 min, 20% B; 45 min, 100% B; 55 min, 100% B; 57 min, 5% B. Injection volumes: 10 + 10 + 20 + 30 + 40 + 40 + 40 μL . Column temperature: $30\text{ }^{\circ}\text{C}$.

For the water part the following gradient profile was used: 0 min, 20% B; 30 min, 80% B; 35 min, 80% B; 37 min, 20% B. Injection volume: 50 μL * 19 times. Column temperature: $30\text{ }^{\circ}\text{C}$.

Isolated samples were dissolved in 100 μL $\text{MeOH-}d_4$ and measured in 2 mm capillary NMR tubes. $^1\text{H-NMR}$ spectra were recorded with a Bruker Avance 500 NMR spectrometer (Bruker-Biospin, Karlsruhe, Germany) operating at 500.13 MHz and equipped with a 5 mm TCI cryoprobe. TMS was used as an internal standard. The manually calibrated spectra were phase and baseline corrected by TopSpin 3.1 software.

Isolation and structure elucidation of **FKB** and **FKC** metabolites

An Agilent 1100 chromatography system (quaternary solvent delivery pump G1311A, autosampler G1313A; Agilent Technologies, Waldbronn, Germany) and a J&M photodiode array detector (DAD, detection 200-700 nm; J&M Analytik AG, Aalen, Germany) was used to

separate metabolites from crude assay mixtures and recording UV spectra. The LC system was controlled by Bruker software HyStar 3.2 (Bruker-Biospin, Rheinstetten, Germany).

Column: Nucleodur C18 (5 μ m, 250 \times 4.6 mm; Macherey & Nagel, Düren, Germany) with a flow rate of 1 mL/min. A binary linear solvent system of H₂O (solvent A) and MeCN containing 0.1% FA (solvent B), was used as follows: 0 min: 20% B, 30 min: 80% B, 35 min: 80% B, 37 min: 20% B. UV detection was performed at a monitoring wavelength of 254 and 343 nm for **FKB** metabolites and of 254 and 368 nm for **FKC** metabolites.

NMR spectra (¹H-NMR, ¹H,¹H-COSY, ¹H,¹³C-HMBC, ¹H,¹³C-HSQC) were measured on a Bruker Avance 500 NMR spectrometer (Bruker-Biospin, Karlsruhe, Germany), operating at a resonance frequency of 500.13 MHz for ¹H and 125.75 MHz for ¹³C. The spectrometer was equipped with a TCI cryoprobe (5 mm) and 2 mm capillaries (80 μ L MeOH-d₄) were used for measuring NMR spectra with standard Bruker pulse sequences.

HRESIMS of FKC-3 was recorded on a LC-MS/MS system consisting of an Ultimate 3000 series RSLC (Dionex, Sunnyvale, CA, USA) system and an Orbitrap mass spectrometer (Thermo Fisher Scientific, Bremen, Germany). HRESIMS data were analyzed using XCALIBUR (Thermo Fisher Scientific, Waltham, MA, USA) software.

2.3.4 *In vitro* degradation stability and microsomal metabolism of the tacrine-silibinin codrug

2.3.4.1 Analytical methods

For determination of codrug amount in the incubation medium and the microsomal incubation systems, two different HPLC methods (Table 2.5) and calibrations (see chapter 2.3.4.2 and 2.3.4.3) were applied. Separation was performed on a C18-column (Hibar® 250-4, Purosphere, 5 μ m). Oven temperature was set at 40 °C.

Table 2.5: Methods for analytical HPLC. M method, A and B eluents A and B, t time [min], A/B solvent composition, f flow [mL/min], V injection volume [μ L], λ detection wavelength [nm]. FA 98% p.a., MeCN for HPLC.

| M | A | B | t | A/B | f | V | λ |
|-----------|---------|-------------------|-------|-------------|---|----|-----------|
| C3 | 0.1% FA | 95% MeCN (v/v) | 0-20 | 80/20→0/100 | 1 | 10 | 287 |
| | | | 20-24 | 0/100 | | | |
| | | | 24-25 | 0/100→80/20 | | | |
| | | | 25-30 | 80/20 | | | |
| C4 | 0.1% FA | 95% MeCN (v/v) | 0-3 | 80/20 | 1 | 20 | 287 |
| | | | 3-23 | 80/20→20/80 | | | |
| | | | 23-24 | 20/80→0/100 | | | |
| | | | 24-29 | 0/100 | | | |
| | | | 29-30 | 0/100→80/20 | | | |
| | | | 30-33 | 80/20 | | | |

LC–HRESIMS was performed using UHPLC Agilent 1290 infinity, DAD G4212A, MS Agilent 6540 UHD Q-TOF with positive and negative electrospray ionization. For separation, a Thermo Accucore aQ column (C18, 50x2.1 mm, 2.6 μm) and the following solvents were used: eluent A was 0.1% FA, eluent B 100% MeCN supplemented with 0.1% FA. A volume of 7 μL was injected. An oven temperature of 40 $^{\circ}\text{C}$ and a flow of 0.6 mL/min were set. Separation of the sample was conducted using the following gradient system: 0-8 min 95/5 \rightarrow 50/50, 8-9 min 50/50 \rightarrow 2/98 A, 9-10 min 2/98, 10-10.1 min 2/98 \rightarrow 95/5, 10.1-11 min 95/5. The metabolites were detected at two wavelengths (287 nm and 337 nm).

2.3.4.2 Stability of the codrug under *in vitro* assay conditions

The codrug (50 μM) was incubated for 24 h in Dulbecco's Modified Eagle's Medium (DMEM, Invitrogen) containing 10% heat-inactivated FCS at standard cell culture conditions (37 $^{\circ}\text{C}$, 5% CO_2) in 96 well plates as they were used for *in vitro* assays. After 0, 2, 4, 8, 12, and 24 h, 100 μL hereof were added to 900 μL ice-cold EtOAc, vortexed for 5 min and centrifuged for another 5 min at 14 000 rpm at 4 $^{\circ}\text{C}$. Afterwards, 720 μL of the upper EtOAc phase was evaporated under nitrogen stream to dryness and resolved in 80 μL MeOH + 1% FA for HPLC quantification using method **C3** (see chapter 2.3.4.1). For calibration the peak areas of 2.5, 5, 10, 20, 40, and 60 μM codrug in MeOH + 1% FA were determined using the same HPLC method. The experiment was conducted three times in triplicates. The recovery rate of the codrug was $87 \pm 4\%$.

2.3.4.3 Microsomal metabolism and metabolic stability in microsomal incubation systems

Microsomal metabolism was investigated in five different incubation systems. Metabolism of the codrug (50 μM) was performed in 0.1 M PO_4 buffer (pH 7.4) at 37 $^{\circ}\text{C}$ in a water bath. For phase I metabolism the incubation system consisted of 0.5 mg/mL HLM (20 mg/mL), 3.3 mM MgCl_2 (110 mM in buffer) and 1 mM NADPH (10 mM in buffer). For the investigation of glucuronidation in phase II metabolism, HLM were incubated together with 3.3 mM MgCl_2 , 25 $\mu\text{g/mL}$ alamethicin (0.5 mg/mL in 2% MeOH) and 2 mM UDPGA (40 mM in buffer). Finally, both phase I and II reactions, were studied in a combined incubation system including NADPH as well as UDPGA equivalents. Furthermore, incubation systems without microsomes or cofactors served as negative controls.

The reaction was stopped at different time points (0, 1, 2, 4, 6 h) by adding 100 μL ice-cold MeOH to 100 μL of the incubation solution. The mixture was vortexed 5 min and centrifuged at 14 000 rpm for 5 min. The supernatant was used for HPLC (method **C4**) and LC–MS analysis (see chapter 2.3.4.1). For calibration the peak areas of 1, 2.5, 5, 10, 20, 30, 40, 50, and 60 μM codrug in a MeOH-buffer mixture were determined in three replicates. The recovery rate of the codrug in the microsomal incubation system was $105 \pm 5\%$.

2.4 Test compounds, solvents, and other chemicals

Tested kavalactones

| | |
|--------------------------|---------------------------------|
| Desmethoxyyangonin (DMY) | isolated from Kava Kava rhizome |
| Dihydrokawain (DHK) | isolated from Kava Kava rhizome |
| Dihydromethysticin (DHM) | isolated from Kava Kava rhizome |
| Kawain (K) | isolated from Kava Kava rhizome |
| Methysticin (M) | isolated from Kava Kava rhizome |
| Yangonin (Y) | isolated from Kava Kava rhizome |

Tested chalcones

| | |
|-----------------------------------|--------------------------------------|
| Alpinetin chalcone (A) | synthesis [96-98] |
| 4-Acetyl-xanthohumol (4AcXAN) | synthesis [96-98] |
| Dihydroflavokawain C (dhFKC) | synthesis [99] |
| Dihydrohelichrysetin (dhHeli) | synthesis [99] |
| Dihydroxanthohumol C (dhXANC) | synthesis [96-98] |
| Flavokawain A (FKA) | synthesis [96-98] |
| Flavokawain B (FKB) | synthesis [96-98] |
| Flavokawain C (FKC) | synthesis [96-98] |
| Helichrysetin (Heli) | synthesis [96-98] |
| 3-Hydroxyhelichrysetin (3OHHeli) | synthesis [96-98] |
| 3-Hydroxyxanthohumol H (3OHXANH) | synthesis [96-98] |
| 3-Methoxyxanthohumol H (3OMeXANH) | synthesis [96-98] |
| 4-Methylxanthohumol (4MeXAN) | synthesis [96-98] |
| 4'-Methylxanthohumol (4'MeXAN) | synthesis [96-98] |
| Pinostrobin chalcone 91% (P) | PhytoLab, Vestenbergsgreuth, Germany |
| Tetrahydroxanthohumol C (thXANC) | synthesis [99] |
| Xanthohumol 98% (XAN) | Nookandeh Institut, Hamburg, Germany |
| Xanthohumol C (XANC) | synthesis [96-98] |
| Xanthohumol H (XANH) | synthesis [96-98] |

Tacrine-silibinin codrug

| | |
|---------------------------------|--------------------------------------|
| Silibinin 98% (S) | PhytoLab, Vestenbergsgreuth, Germany |
| Tacrine HCl \geq 99% (T) | Sigma-Aldrich, Taufkirchen, Germany |
| Tacrine hemi succinamide (THSA) | synthesis [100] |
| Tacrine-silibinin codrug (C) | synthesis [100] |

Positive controls

| | |
|--------------------------|---|
| 7-Ethoxycoumarin (7-EC) | Sigma-Aldrich, Taufkirchen, Germany |
| Staurosporine \geq 99% | Cell Signaling Technology, Danvers, USA |

Solvents

NMR spectra were recorded in deuterated chloroform (Sigma-Aldrich, Taufkirchen) or deuterated acetone (acetone-d₆, Deutero, Kastellaun). For HPLC analyses methanol (Merck, LiChroSolv), acetonitrile (Merck, LiChroSolv), and ultra-pure water were used as mobile phase. If not mentioned otherwise, solvents for fractionation, isolation, (HP)TLC analyses, and studies of microsomal metabolism had pro analysi (p.a.) quality and derived from Merck or Arcos. For preparing stock solutions for cellular assays and microsomal metabolism, either dimethyl sulfoxide (p.a. Merck), ethanol (absolute, Baker), or PBS (Biochrom) was used.

Other chemicals

| | |
|-------------------------------------|----------------------------|
| Ammonia solution 28-30% p.a. | Merck, Darmstadt |
| Diethylamine > 99% | Merck, Darmstadt |
| Diphenylboryloxyethylamine > 97% | Sigma-Aldrich, Taufkirchen |
| Formic acid 98% p.a. | Merck, Darmstadt |
| Glacial acid 100% anhydrous | Merck, Darmstadt |
| Lichroprep RP-18 (25-40 μ m) | Merck, Darmstadt |
| <i>p</i> -Methoxybenzaldehyde > 98% | Merck, Darmstadt |
| Polyethylene glycol 400 | Merck, Darmstadt |
| Silica gel 60 (40-63 μ m) | Merck, Darmstadt |
| Sulfuric acid 95-97% p.a. | Merck, Darmstadt |
| Trifluoroacetic acid 99% | Sigma-Aldrich, Taufkirchen |

2.5 Laboratory instruments

| | |
|--------------------|---|
| Analytical balance | R 160 P, Sartorius, Göttingen |
| Cell incubator | Nu-5500, Nuair, Plymouth, USA Cellstar 300 compact, Queue Systems, Asheville, USA |
| Cell observer | AxioObserver.Z1, Incubator XL-S1 with TempModule S, CO ₂ Module S and Heating Unit XL S, motorized stage, stage Incubator PM S1, HXP120, AxioCam HRm, AxioVision 4.8.1 software, Carl Zeiss, Göttingen |
| Centrifuges | Megafuge 1.0, Heraeus Sepatech, Osterode BR4i, Thermo electron corporation, Langenselbold |

| | |
|-------------------------------------|--|
| Flash chromatography system | Spot Liquid Chromatography Flash, Armen Glider Flash software V 2.3, Armen, Saint Ave, France |
| Freeze dryer | P 10 with pump PK8D, Ilmvac, Ilmenau |
| Heating plate | Thermoplate S, Desaga, Wiesloch |
| HPLC system, analytical | Elite LaChrom: autosampler L-2200, pump L-2130, column oven L-2350, diode array detector L-2455, EZChromElite 3.1.7 software, VWR-Hitachi, Darmstadt |
| HPLC system, semi-prep | ProStar: autosampler 410, pumps 210, detector 335, Galaxie Chromatography Data System, Varian, Darmstadt |
| (HP)TLC device | Linomat 5, Reprostar 3, automatic ADC2 Chamber, WinCATS 1.4.2 software, Camag, Muttenz, Switzerland |
| Inverted light microscope | CK X 41, Olympus, Hamburg |
| Laboratory balance | MC 1, Sartorius, Göttingen |
| Laboratory mill | A10, IKA, Staufen |
| Laminar flow bench | HERAsafe KS, Thermo SK 1200, BDk, Sonnenbühl |
| Magnetic stirrer | RCT basic, IKA, Staufen |
| Mass spectrometer | Q-TOF 6540 UHD, Agilent |
| NMR spectrometer | Avance 600 Kryo, Avance 400, Avance 300, Topspin 2.1 software, Bruker, Ettlingen |
| pH meter | inoLab pH Level 1, electrode SenTix Mic, WTW, Weilheim |
| Pipettes | Research, Research Pro, Eppendorf, Hamburg |
| Pipettor | Accu jet pro, Brand, Wertheim |
| Plate reader | SpectraFluor Plus, Xfluor4 V 4.40 software, Tecan, Crailsheim |
| Rotary evaporator | Laborota 4003 control, Rotavac vario control, Heidolph, Schwabach |
| Thermometer | ETS-D4 fuzzy, IKA, Staufen |
| Ultrapure water purification system | Astacus LS, Membra pure, Bodenheim |
| Ultrasonic Cleaner | USC 1700 TH, VWR, Darmstadt |
| Vortex mixer | Vortex Genius 3, IKA, Staufen |
| Water bath | WB 22, Memmert, Schwabach |

2.6 Statistical analysis

If not mentioned otherwise for the data subjected to statistical analysis, experiments were conducted in (at least) triplicates and repeated independently not less than three times. The results of the assays are presented as the mean \pm SD. For cell-based assays untreated control cells referred as 100% values.

Statistical analysis was performed applying either GraphPad Prism 4 or PASW Statistics 18 software. Gaussian distribution of values was tested prior to statistical analysis. Data were subjected to one-way ANOVA followed by appropriate post-hoc tests. P values < 0.05 were considered statistically significant.

3 Isolation of kava constituents and reevaluation of their hepatotoxic potential

3.1 Introduction

3.1.1 Botany

The kava plant (*Piper methysticum* FORST., Piperaceae) is an up to 7 m high, robust, fairly succulent, erect, perennial shrub with heart-shaped, pointed, smooth, on both sides green leaves of about 15 cm length. Petioles are up to 6 cm long. At maturity, after 3-5 years of growth, the root can reach 60 cm in length and 8 cm in diameter and may eventually occur as a heavy knotted mass. Flowers appear in irregular inconspicuous spadices of 3-9 cm length (Figure 3.1).

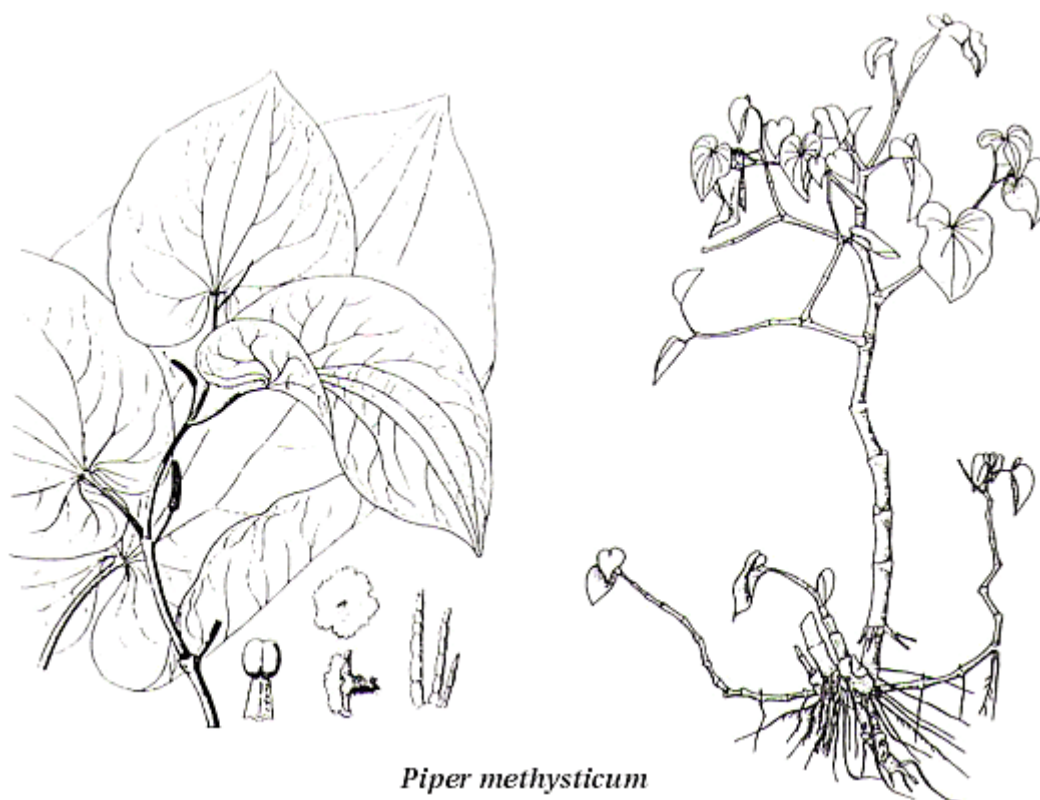


Figure 3.1: The habitus of kava-kava, *Piper methysticum* FORST., Piperaceae. (http://www.naturepacific.com/contents/en-us/d59_kava.html)

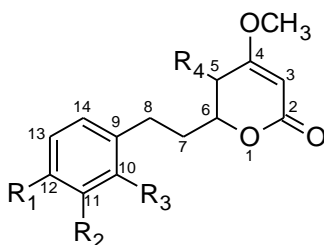
Kava originates mainly from Western Polynesia. However, it is found and cultivated nearly all over the Pacific Islands, from Hawaii to Papua New Guinea, with exception of New Caledonia, New Zealand, and most of the Solomon Islands. Its widespread cultivation, attended by various morphological characteristics of the kava plant, led to classification of

different varieties of *Piper methysticum* by the native people with vernacular names, i.e. *apu*, *makea*, *liwa*, *mo'i*, or *papa*. These varieties also differ in traditional use [108].

The herbal drug consists of the dried (and peeled) rhizomes (*Piperis methystici* rhizoma; DAC 1998) from which roots are mostly removed. The drug is irregularly cut in transverse and longitudinal pieces of varying size and shape. Fractures are coarsely fibrous. The outer surface appears light yellowish or greyish brown with thin bark. The inner surface is colored yellow-white [109]. A kavalactone content of at least 3.5% was demanded by the German monograph (DAC 1998).

3.1.2 Chemical constituents

The major constituents and pharmacologically active compounds of kava are the kavalactones (also called kavapyrones). They possess a typical arylethylene- α -pyrone skeleton (Figure 3.2).



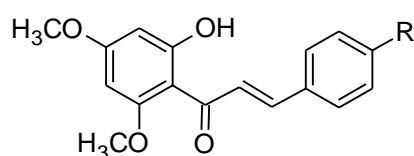
| | R ₁ | R ₂ | R ₃ | R ₄ | C ₅ -C ₆ | C ₇ -C ₈ |
|------------------------------------|------------------|--------------------|------------------|------------------|--------------------------------|--------------------------------|
| 7,8-Dihydrokawain | | | | | | |
| Hydroxykawain | | | | OH | | = |
| Kawain | | | | | | = |
| 11-Hydroxy-12-methoxydihydrokawain | OCH ₃ | OH | | | | |
| 11-Methoxy-12-hydroxydehydrokawain | OH | OCH ₃ | | | = | = |
| 7,8-Dihydro-5-hydroxykawain | | | | β -OH | | |
| 11,12-Dimethoxydihydrokawain | OCH ₃ | OCH ₃ | | | | |
| Methysticin | | OCH ₂ O | | | | = |
| Dihydromethysticin | | OCH ₂ O | | | | |
| 5,6-Dehydromethysticin | | OCH ₂ O | | | = | = |
| Desmethoxyyangonin | | | | | | = |
| Yangonin | OCH ₃ | | | | = | = |
| 5,6,7,8-Tetrahydroyangonin | OCH ₃ | | | | | |
| 5,6-Dihydroyangonin | OCH ₃ | | | | | = |
| 7,8-Dihydroyangonin | OCH ₃ | | | | = | |
| 10-Methoxyyangonin | OCH ₃ | | | OCH ₃ | = | = |
| 11-Methoxyyangonin | OCH ₃ | | OCH ₃ | | = | = |
| 11-Hydroxyyangonin | OCH ₃ | | OH | | = | = |
| 11-Methoxy-5,6-dihydroyangonin | OCH ₃ | | OCH ₃ | | | = |

Figure 3.2: Kavalactones in kava kava rhizome (modified according to [110]).

The content of kavalactones in dried rhizomes varies from 3-20%. Six major kavalactones account for 96% of the kavalactone content in extracts namely (+)-kawain (**K**), (+)-methysticin (**M**), desmethoxyyangonin (**DMY**), yangonin (**Y**), (+)-dihydrokawain (**DHK**), and (+)-dihydromethysticin (**DHM**) [111].

The first isolated compound was reached by Goble (1860) and Cuzent (1861) and has been later identified as **M**. In 1874, a further crystalline substance was isolated, which was named **Y** by Lewin in 1886. Winzheimer succeeded in isolating **DHM** in 1908 [108]. More extensive investigations by Brosche and coworkers in the first half of the 20th century yielded the isolation of **K** and **DHK** together with structure elucidation of previously isolated compounds [112]. Moreover, synthesis routes for kavalactones and derivatives were investigated [113]. **DMY** was finally isolated by Klohs et al. in 1959 [108]. Achenbach recorded NMR spectra of kavalactones and contributed to structure elucidation and configuration [114]. To date at least 19 kavalactones have been isolated and/or identified by various working groups (Figure 3.2).

In addition, several chalcones (Figure 3.3) and flavanones can be found in *Piper methysticum*. Hänsel et al. were the first who isolated two yellow pigments from a chloroform extract [115]. These compounds were identified as methoxylated chalcones and named flavokawain A (**FKA**) and flavokawain B (**FKB**) due to their color. In 1972, the orange colored flavokawain C (**FKC**) was isolated from a benzene extract [116]. The total content of flavokawains in an ethanolic kava extract was determined at 1.1% [117].



| | R |
|---------------|------------------|
| Flavokawain A | OCH ₃ |
| Flavokawain B | H |
| Flavokawain C | OH |

Figure 3.3: Chalcones in kava kava rhizome.

Flavanones like pinostrobin and 5,7-dimethoxyflavanone are present in kava root extracts as minor constituents [118]. C-glycoside flavonoids were identified in kava leaf extracts [119].

Furthermore, different alkaloids are found in kava as minor constituents. Cepharadione A [120] and two pyrrolidine alkaloids [121] have been isolated from kava roots. Investigating aerial parts of the plant, the piperidine alkaloids pipermethysticine [122], 3 α ,4 α -epoxy-5 β -pipermethysticine, and awaine [123] were discovered in leaves and stems.

Besides, steroids like stigmasterol, long-chained alcohols [124], derivatives of cinnamic acid [125], little essential oil, and starch is present in *Piper methysticum*. A tabulation of constituents is compiled in [126].

3.1.3 Traditional use

Kava (*kava kava*, *kawa*, *ava*, *awa*, *yagona*) is the term given by the Pacific Islanders to both the plant and the psychoactive beverage made from the rhizome. The meaning of the name kava is quite broad and ranges from 'bitter', 'sour', 'acidic', 'salty', 'sharp' or 'pungent' to just 'beverage' [108].

The origin of kava drinking dates back centuries and is not exactly known. Kava is used as intoxicating beverage for many sociocultural or religious aspects by the natives of Oceania perhaps comparable to the use of other psychoactive drugs like the peyote by the Native Americans. In the 18th century, European discoverers first got in contact with the Oceanic plant and the ceremony of kava drinking.

The preparation of the beverage requires the dried kava root (particles or powder), a bowl, a drinking cup, a strainer, and water. The plant material is either mechanically pulverized with a mortar and a pestle or it is chewed by young men or women prior to preparation of the infusion. The powdered or chewed material is put in the bowl, doused with water, macerated some time, and finally strained. The beverage is handed in special cups for ceremonial drinking.

Mostly, kava is used for social ceremonial reason e.g. as a welcome drink for honored guests. Besides, it is employed for magico-religious purpose out of respect to gods or spirits. Additionally, it plays an important role in traditional medicine. In general, kava drinking is thought to have beneficial effect on health. More precise, kava is applied to soothe the nerves, induce relaxation and sleep, combat fatigue, reduce weight, and treat asthma, common cold, headaches, urinary and fungal infections, and gonorrhoea.

3.1.4 Experimental pharmacology

Kava extracts and in particular the biologically active kavalactones are extensively analyzed toward their activity on central nervous system (CNS) receptors (especially γ -aminobutyric acid (GABA) receptors) and neurotransmitters as well as toward the modulation of voltage-dependent Na^+ and Ca^{2+} channels. An overview of biochemical mechanisms and possible molecular targets is given in [127,128].

Due to similar pharmacological properties of kavalactones and benzodiazepines, the GABA receptors as possible targets were investigated. Enhanced binding of the GABA receptor-agonist [3H]muscimol to GABA_A receptors has been described for kavalactones with EC_{50} values ranging from 200 to 300 μM using membrane fractions from different rat brain regions [129]. Kavalactone-binding to GABA receptors was discussed and investigated in brainstem models [130]. However, isolated kavalactones showed only weak binding to GABA_A receptors and lacked any binding to GABA_B [131]. Dinh and coworkers tested

methanolic kava extracts from different cultivars on several CNS receptors and found as well only weak binding to benzodiazepine binding site of GABA_A. In contrast to previous findings, a potent binding inhibition was observed for the GABA binding site [132]. In summary, the modulation of GABAergic activity seems to contribute in any case to the overall pharmacological effects of kavalactones.

Alterations in noradrenaline (NA) uptake and monoamine oxidase B (MAO-B) inhibition seem to be involved in the psychotropic activity of kava. Inhibition of [³H]NA uptake was observed for **K** (70-80% vs. control) and less distinct for **M** [133]. One *in vitro* study examined the inhibition of MAO-B in comparison to established antidepressants. Kava extract reversibly inhibited MAO-B in intact platelets (IC₅₀ 24 μM) and disrupted platelet homogenates (IC₅₀ 1.2 μM). The most potent kavalactone was **DMY** (IC₅₀ 28 μM and IC₅₀ 0.12 μM) [134].

For kava, also anticonvulsive and local anesthetic activities are postulated. Indeed, kavalactones exhibit an effect on ion channels and neuronal transmission similar to approved mood stabilizers like lamotrigine [135]. The influence of (±)-**K** on voltage-dependent Na⁺-channels was investigated. By veratridine elevated [Na⁺]_i concentrations were rapidly reduced to 30% by **K** with an IC₅₀ of 86 μM [136,137]. (±)-**K**'s effect on voltage-dependent Ca²⁺ and Na⁺ channels was further investigated using rodent dorsal root ganglion cells. A pronounced decrease of both Ca²⁺ and Na⁺ currents was observed [138]. In hippocampal neurons, (+)-**M** and (±)-**K** showed a voltage-dependent inhibition of Na⁺ channels by interaction with closed and inactivated states of Na⁺ channels [139]. Isolated guinea-pig ileum was used to examine the Ca²⁺ channel blocking (spasmolytic) properties of **K** on evoked contractile activity. **K** inhibited dose-dependently the contractile response induced by carbachol, but not by caffeine. After nifedipin and pertussis toxin pretreatment of carbachol induced ileum contractions, **K** was able to block the remaining response in high concentrations (400 μM). However, **K** showed no effect on Ca²⁺ elicited contractions [140]. Moreover, kava's pharmacological properties may as well be mediated through additive effects on serotonin 5-HT_{1A} receptors and activation of glutamate (NMDA, *N*-methyl-D-aspartate) receptors [141].

Compounds of kava root extracts showed COX inhibitory activities. Major kavalactones and **FKA** were tested for COX-I and COX-II inhibition. All compounds demonstrated similar or even better COX-I and COX-II inhibition activity than ibuprofen, naproxen, and acetylsalicylic acid with **DHK** and **Y** being the most potent inhibitors at 100 μg/mL. Moreover, for **Y** and **M**, free radical-scavenging capacity against stable DPPH radicals was found [142]. A bornyl ester of cinnamic acid derivative and **FKB**, both isolated from a methanol extract, exhibited

the strongest COX-I enzyme inhibition at 100 µg/mL. Also, a moderate COX-II inhibitory activity was found for extracted compounds [118].

K and **DHK** were positively screened for their ability to inhibit tumor necrosis factor alpha (TNF-α) secretion by lipopolysaccharide (LPS)-stimulated THP-1 cells and to reduce levels of the p65 subunit in cell lysate. *In vivo*, **K** pretreated mice were rendered immune to lethal doses of LPS [143]. Folmer et al. investigated the influence of kava compounds on the nuclear factor NF-κB signaling pathway and discovered a dose-dependent inhibition of TNF-α induced NF-κB-DNA binding for **K**, **DHK**, and the chalcones **FKA** and **FKB**. The latter also inhibited various protein kinases [144]. In contrast, another working group identified **M** as a potent and non-toxic NF-κB inhibitor (IC₅₀ 0.19 ± 0.01 µg/mL) by assay guided fractionation [145].

The kavalactones' influence on P-glycoprotein (Pgp) was investigated in a fluorescent calcein uptake assay. All kavalactones increased intracellular calcein concentration at two digit micromolar IC₅₀ values among **DMY** being the most potent (17.1 µM ± 0.6 µM) [146]. Weiss et al. observed an inhibition of Pgp in a Pgp-overexpressing cell line by kava extracts (80% inhibition at 170 µg/mL) and by individual kavalactones over a concentration range of 17-90 µM [147].

Recently, kavalactones were tested for cannabinoid (CB) receptor affinity and inhibitory activity of two major metabolic enzymes of the endocannabinoid system, fatty acid amine hydrolase and monoacylglycerol lipase. No inhibitory activity of these enzymes could be observed for the test compounds. **Y** exhibited selective CB₁ receptor affinity with K_i of 0.72 µM (CB₂ K_i > 10 µM). These results suggest that the endocannabinoid system might also be involved in pharmacological activity of kava [148].

3.1.5 Preclinical studies

Neurological and sedative effects, and anticonvulsive, muscle relaxing, and spasmolytic activity of kava extracts or kavalactones have been examined in several *in vivo* studies, mainly in rats and mice. A dichloromethane extract of kava rhizome (150 mg/kg) decreased motility and reduced motor control in mice. Besides, at this dose hypnosis and analgesia were observed [149]. Apomorphine induced hyperactivity was reduced in rats after intraperitoneal administration of an aqueous or dichloromethane extract of the rhizome (120 mg/kg) [150]. Administration of kava extract (50-100 mg/kg) or (±)-**K** (10-50 mg/kg) led to reduce muscle tone in cats [151]. A depression of the CNS occurred in rodents after intraperitoneal administration of an aqueous rhizome extract [152]. Modulatory effects of

kava extracts and kavalactones on the dopaminergic system of rats were detected by Baum et al. [153]. Co-administration of kavalactones and pentobarbital in mice potentiated their sleeping-time up to 400% for **DHM** [154]. Neuroprotective effects of kavalactones were investigated in a model of focal cerebral ischemia in mice and rats and compared to memantine. The kava extract, **M**, and **DHM** showed protective effects against ischemic brain damage [155]. Analgesic activity of an aqueous and a dichloromethane extract of kava rhizome was observed in mice measured by tail-flick reaction times [156]. Also anticonvulsant activity of kava extracts on strychnine-induced convulsions was investigated in mice [154]. **DHM** and **DHK** reduced electroshock-induced seizures in mice and rats [157].

3.1.6 Clinical pharmacology

Several double-blind, randomized, controlled trials have been conducted to proof the efficacy of kava extracts in treatment of anxiety disorders. Warnecke et al. performed a study in two groups of 20 women with anxiety due to climacteric syndrome [158]. Patients were treated with kava WS 1490 extract 300 mg/day (210 mg kavalactones) or placebo for 8 weeks. The Hamilton Anxiety scale (HAM-A) was used as rating target. A significant improvement of anxiety symptomology associated with very good tolerance was found in the kava group.

Kinzler et al. investigated the clinical efficacy of kava extracts in patients with non-psychotic anxiety syndrome in a double-blind, placebo controlled study (two groups à 29 patients) over a period of 4 weeks [159]. Again, the HAM-A score was significantly reduced in the drug receiving group. No adverse reactions were observed within the 4 weeks of treatment with kava WS 1490 extract.

A placebo-controlled, double-blind study with 101 patients suffering from anxiety of non-psychotic origin was conducted by Volz et al. with kava extract WS 1490 over a period of 25 weeks [160]. There was a significant improvement of anxiety symptoms in the kava group starting from week 8. After 24 weeks the HAM-A score of WS 1490 group was 9.7 compared to placebo with a value of 15.2.

Malsch et al. investigated the efficacy of kava WS 1490 extract in benzodiazepine pretreated patients with non-psychotic anxiety disorders [161]. Patients received either 300 mg/day of kava extract or placebo while benzodiazepine dose was tapered off over 2 weeks followed by 3 weeks of monotherapy with drug or placebo. The outcome was measured with the HAM-A scale, and again WS 1490 was superior to placebo associated with high tolerance of the drug.

Gastpar et al. examined the efficacy and tolerability of 150 mg/day (105 mg kavalactones) of kava WS 1490 in 141 patients suffering from neurotic anxiety [162]. The post-treatment score of the Anxiety Status Inventory (ASI) observer rating scale did not significantly differ between the two groups. However, there was a significant difference between treatment end and

baseline, with a superiority of the herbal extract over placebo. Compared to previous studies investigating higher doses of kava extracts, the beneficial effects of kava remained relatively small. WS 1490 was well tolerated and did not impair liver functions.

Lehrl et al. tested the clinical efficacy of kava WS1490 extract in 61 patients with anxiety associated sleeping disturbances [163]. Patients were treated with either 200 mg/day (140 mg kavalactones) of extract or placebo for 4 weeks. Efficacy was measured by a sleep questionnaire (SF-B) and by HAM-A. After 4 weeks, significant differences between the two groups were observed with superiority of herbal treatment for both the quality and recuperative effect of sleep and the HAM-A score.

Geier et al. investigated lower doses of WS 1490 (150 mg/day) in 50 patients in a placebo-controlled, double-blind trial for 4 weeks and found a relevant reduction in anxiety versus placebo [164].

A recent study of Sarris et al. compared effects of a standardized aqueous kava extract (60 mg kavalactones) to oxazepam treatment in a randomized, placebo-controlled, double-blind study [165]. Patients received kava extract (3 x 60 mg/day), oxazepam (30 mg), or placebo for one week. For oxazepam there was a significant reduction in anxiety, which was not found for kava treatment under applied conditions.

Pittler and Ernst compiled 12 double-blind, randomized, controlled trials and performed a meta-analysis of data using total score on the HAM-A [166]. The results suggest significant reduction of the HAM-A score in patient receiving kava extract (total of 197 patients) compared with patients receiving placebo (total of 183 patients) although the effect seems to be weak. Within the 1-24 weeks of treatment, data imply safety of kava extracts. However, authors recommend long-term safety studies with larger sample sizes.

Another meta-analysis was conducted in 2005, investigating the efficacy of acetonetic kava WS 1490 extract in patients with non-psychotic anxiety disorders [167]. Individual patient data of 6 placebo-controlled, randomized trials were included. HAM-A score was used as endpoint parameter. Data analysis showed an improvement on the HAM-A scale with WS 1490 extract, on average achieving 5.49 points less than the placebo. Therefore, the authors suggest acetonetic kava extracts to be effective and to constitute a therapeutic alternative to benzodiazepines and antidepressants in the treatment of non-psychotic anxiety disorders.

3.1.7 Pharmacokinetic studies

Bioavailability of kavalactones in ethanolic and aqueous extracts was studied *in vitro* using Caco-2 cell monolayers [168]. The extracts showed only minor differences in ratio of kavalactones (in contrast to investigations of Côté [111]) but there was a difference in total amount (204 mg/mL in ethanolic and 103 mg/mL in aqueous extracts). Good bioavailability

was found for kavalactones as they rapidly crossed the Caco-2 monolayers. Apparent permeability (P_{app}) calculated from uptake data from 10 to 90 min was for all $> 40 \times 10^{-6}$ cm/s. Complete intestinal absorption is considered for $P_{app} > 1 \times 10^{-6}$ cm/s. **Y** was potentially retained in Caco-2 cells as recovery on the apical side was only 40%. Permeability of purified **K** was significantly lower compared to **K** uptake from extracts. Bioavailability was not affected by the extraction method.

Pharmacokinetics of **K** has been investigated in rats [169] and humans [170]. Tarbah et al. studied kinetics after administration of a single oral dose of 800 mg **K** in a self-medication study. **K** metabolites were detected in serum and urine samples. The main metabolite of **K** is *p*-hydroxykawain, which was found in serum and urine in its free (~ 10% in serum) and conjugated forms (glucuronide and sulfate). Further metabolization takes place to *p*-hydroxy-7,8-dihydrokawain, which was only detected in urine in form of its conjugates. Opening of the lactone ring, demethylation, decarboxylation and oxidation leads to 6-phenyl-5-hexene-2,4-dione which was detected in urine after 24 h. **K** is furthermore dehydrated to form 5,6-dehydrokawain (**DMY**). The latter molecule is hydroxylated and demethylated to *o*-desmethyl-hydroxy-5,6-dehydrokawain. Serum concentrations within 1-4 h after oral uptake ranged between 40 and 10 ng/mL for **K**, 300 and 125 ng/mL for *p*-hydroxykawain, and 90 and 40 ng/mL for *o*-desmethyl-hydroxy-5,6-dehydrokawain. The major metabolite *p*-hydroxykawain appears in serum in free and conjugated forms with a lag time of 0.25 h and peaks after 0.75 h. The half-lives of free and conjugated forms range between 0.7 and 1.9 h indicating that **K** metabolites can be found up to 10 h in serum samples.

Mathews and coworkers dealt with **K** pharmacokinetics in rats [169]. After intravenous administration of 7 mg/kg **K**, an initial plasma concentration of 7.2 μ g/mL was determined. **K** was rapidly eliminated with a mean half-life of 0.63 h. Oral administration of 100 mg/kg **K** resulted in ~ 50% bioavailability, C_{max} of 2.6 μ g/mL, and a mean half-life of 1.3 h. They could also show that **K** bioavailability is improved with co-administration of kava extract. C_{max} doubled to 5.4 μ g/mL. This is in accordance to findings of Matthias et al. [168].

Fu et al. studied the microsomal metabolism of kavalactones [171,172]. A HPLC quantitative assay was established and validated for **K**, **M**, and **DMY**. *P*-hydroxykawain, *m,p*-dihydroxykawain, and *p*-hydroxyyangonin were identified as primary metabolites [171]. Moreover, cytochrome P450 isoforms responsible for kavalactone metabolism were examined [172]. CYP3A1/3A23 was found to be responsible for kavalactone metabolism in female rats, CYP3A2 in male rats. For **DMY**, CYP2C6 and CYP2C11 were involved in males and CYP2C12 in females. Kavalactone metabolism was also investigated in the isolated perfused rat liver [173]. The rat livers were exposed to **K**, **M**, and **DMY** for 120 min.

Metabolism was found to be of first-order nature with similar half-lives of decay (1.2 – 3 h). *P*-hydroxykawain and *m,p*-dihydroxykawain were found as metabolites. Biliary excretion of kavalactones was negligible.

3.1.8 Adverse reactions and drug interactions

An observatory study involving 4049 patients consuming orally 105 mg kavalactones per day (standardized extract of *Piperis methystici* rhizoma) for seven weeks revealed 61 cases (1.5%) of adverse reactions [174]. The major reactions were gastrointestinal disturbances or allergic skin reactions. Another study with 3029 patients taking 240 mg of a standardized kava extract orally for four weeks reported similar side effects in 2.3% of patients. Chronic administration of kava rhizome preparations may cause a transient yellow discoloration of the skin and nails. Furthermore, disturbances in visual accommodation occurred after ingestion of large doses of kava [109]. Anti-dopaminergic side effects were reported in 4 patients with symptoms similar to Parkinson's disease [175].

Aqueous kava kava extracts have been used for centuries for medicinal, ceremonial and sociocultural purpose by different ethnic groups from Pacific Islands (see chapter 3.1.3). In 1990, standardized acetonetic or ethanolic kava rhizome extracts were established on the German market (e.g. Kavasedon[®], Laitan[®], Kava ratiopharm[®]) for symptomatic treatment of mild states of anxiety and nervous disorders. The pharmacology of kava extracts is extensively investigated. Numerous data of experimental pharmacology as well as clinical studies are available, which proof the efficacy of the drug (see chapters 3.1.4 and 3.1.6). Longtime, Kava was also considered to be safe with a very favorable risk profile and kavalactone extracts were estimated as valuable drugs in rational phytotherapy.

Since 1998, several cases of severe hepatotoxic side effects arose that were connected to kava intake [79,176–184] (an overview of case reports is given by Teschke and Stickel [64,79,80]). As a consequence, kava containing drugs were banned from the German market by the BfArM in 2002. Other European countries, Canada and Australia reacted equally, even so a reevaluation of the case reports of the Commission E [185] and the Society of Medicinal Plant Research [186] revealed some inconsistencies like double reports of identical cases, probable influence of co-medication, and alcohol abuse or over-dosage. Pursuant to Schmidt and Nahrstedt [185], only 4 of 78 originally reported cases could be reasonably connected to adverse events against kava and only one could be attributed directly to kava intake in conform dosages (120 mg/d) recommended by the monograph of the German commission [176]. However, authors only consider direct hepatotoxicity of kava although indirect mechanisms may lead to toxic effects as well [187,188]. Putative

hepatotoxicity of kava, kava extracts and kava constituents and possible mechanisms are extensively discussed in chapter 3.3.3.

Drug interaction potential of kava is extensively treated in literature [189,190]. Kava extracts and the active principle, the kavalactones, have shown to be potent inhibitors of cytochrome P450 enzymes [169,191–193].

Mathews et al. investigated the inhibition of cytochrome P450 enzymes of a kava extract normalized to 100 μM kavalactones as well as the effect of individual kavalactones [191]. The kava extract (100 μM) markedly inhibited CYP2C9, CYP2C19, and CYP3A4 about 78% to 92%. An effect was already present at a kavalactone concentration of 10 μM . CYP1A2 (56% inhibition), CYP2D6 (73%), and CYP4A9/11 (65%) were also significantly affected. Kavalactones were tested in concentrations of 1 and 10 μM . With exception of **K**, cytochrome inhibition was detected for all assayed kavalactones at 10 μM : CYP2C9 was inhibited by **DMY** (42%), **M** (58%), and **DHM** (69%); CYP2C19 by **DHM** (76%); CYP2D6 by **M** (44%); and CYP3A4 by **DMY** (40%), **M** (27%), and **DHM** (54%) [191]. An extended study by Mathews et al. revealed inhibition of CYP2C9, CYP2C19, CYP2D6, and CYP3A4 by a composite formulation of kavalactones. They investigated the inhibition kinetics of **M**, **DHM**, and **DMY** with regard to the mostly affected isoforms CYP2C9 and CYP2C19. K_i values for CYP2C9 inhibition were 5 μM for **M** and 9 μM for **DMY**, and 7 μM for **DHM** inhibiting CYP2C19 [169]. Furthermore, the influence of kava extracts and sub-fractions on CYP3A4 was analyzed. The fraction containing kavalactones was identified as major inhibitory principle with 60% inhibition [192].

Zou and coworkers examined the influence of the six major kavalactones on recombinant human CYP isoforms CYP1A2, CYP2C9, CYP2C19, CYP2D6, and CYP3A4, the most important isoforms involved in drug metabolism. A distinct inhibitory activity (IC_{50}) was found for CYP1A2 by **DMY** (1.70 μM), for CYP2C19 by **DHM** (0.43 μM), **DMY** (0.51 μM), **M** (0.93 μM), and **K** (4.86 μM), and for CYP3A4 by **M** (1.49 μM) and **DHM** (2.69 μM). Partly, enzyme inhibitory activity was equal to or even more pronounced than that of used positive controls (furafylline for CYP1A2 1.65 μM ; tranlycypromine for CYP2C19 5.46 μM). **Y** could not be investigated due to its native fluorescence [193]. In summary, collected data suggest a high potential for pharmacokinetic herb-drug interactions as a number of CYP enzymes is significantly affected by kava extracts and especially kavalactones.

Additionally, several putative pharmacodynamic drug interactions have been reported for kava and are listed in [189]. The impact of a simultaneous intake of kava extract and ethanol was evaluated in two volunteer clinical studies [194,195]. Whereas Herberg et al. did not detect any effect of kava in combination with alcohol, Foo et al. found a potentiated sedation,

intoxication, and impairment of cognition/coordination. The interaction potential of kava with bromazepam was examined in a double-blind, randomized, cross-over trial on 18 volunteers receiving either 800 mg of a kava extract, 9 mg bromazepam, or both for 14 days. No significant differences between groups were observed. In contrast, a human case report was published connecting kava and alprazolam intake, which led to a comatose state in a 54-year-old man [196].

Schelosky et al. reported a possible interaction of kava with levodopa in a 76-year-old man suffering from Parkinson's disease. Frequency and duration of "off-periods" were increased [175].

Rhabdomyolysis was observed in a 29-year-old man who took a herbal product containing caffeine, *Ginkgo biloba*, and kava extract. A putative interaction between the methylxanthine effects and the antidopaminergic activities of kava were discussed [197]. However, this is the only case report suggesting an interaction between kava and caffeine.

3.1.9 Kava extracts, approved indication, posology

In contrast to traditionally used water infusions, most commercially available kava extracts are prepared by ethanolic or acetonetic extraction of rhizomes. Whereas no qualitative differences of traditional and industrial kava extracts were detected by TLC [198], aqueous and organic kava extracts differ in total amount and ratio of kavalactones [111]. The kavalactone content of extracts ranges from 30 to 70%; 96% of kavalactone content is contributed to the six major constituents.

Kava extracts were approved for treatment of mild states of anxiety or insomnia due to nervousness, stress, or tension. The daily dosage advised by the German monograph was 60-120 mg of kavalactones (commission E).

In 2002, all kava containing drugs were banned from the German market due to argued hepatotoxic side effects.

3.2 Aim of the study

Standardized acetonetic kava root extracts have widely been used as approved herbal remedies for treatment of non-psychotic anxiety disorders. In recent years, several cases of hepatic necrosis have been reported as severe side effects in connection to intake of commercially available kava products.

Hence, this study was aimed to isolate and identify major constituents of an acetonetic extract of rhizome of *Piper methysticum*. Since the ban of kava in Germany in 2002, kava hepatotoxicity has been extensively reviewed [187,188,199–205], albeit it still remains a controversial issue: possible mechanisms as well as different constituents responsible for

hepatotoxic effects are discussed. However, above all there is a lack of novel experimental data investigating the toxic potential of individual major and minor constituents. With regard to still incomplete data, the study should give a comparative insight into the *in vitro* hepatotoxicity of major kavalactones and chalcones in order to identify putative toxic compounds and estimate the overall hepatotoxicity of kava.

3.3 Results and discussion

3.3.1 Fractions and isolated structures

The extraction method is described in chapter 2.1.1. The fractionation and isolation was carried out mainly by medium pressure liquid chromatography (MPLC) / flash chromatography (see chapter 2.1.2). The complete fractionation scheme is presented in Figure 3.4. One part of the crude extract (≈ 5 g) was used for establishment and optimization of the flash chromatographic methods (see chapter 2.1.2.1). First, 11.86 g of the crude extract was separated into eight fractions (A-H) using method **F1**. Fraction B (0.11 g, $R_t \sim 36$ -43 min) contained mainly a chalcone, which was identified as **FKB**. Fraction D and E contained a further chalcone, namely **FKA** (0.1 g and 0.2 g, $R_t \sim 56$ -61 min). The kavalactone fraction (fraction G, 7.91 g, $R_t \sim 62$ -84 min) was separated from most other constituents. Thereby, two compounds already precipitated in the tubes: the yellow needles (0.49 g) and white crystals (0.69 g) were sucked off and dried in an exsiccator. The precipitates were further purified by recrystallization (see chapter 2.1.2.3) and pure **Y** (0.41 g) and **M** (0.45 g) were finally obtained. Fraction G, containing all kavalactones, was further separated in seven sub-fractions (G1-G7) using method **F2**. Mainly, fraction G2 (5.46 g, $R_t \sim 25$ -35 min) and G4 (1.33 g, $R_t \sim 47$ -68 min) had considerable contents. In fraction G2, **DHK**, **K**, **DHM**, and **M** were separated from **DMY** and **Y** in fraction G4. Moreover, **DMY** (0.35 g) partly precipitated in the tubes and was carefully sucked off and dried. Subsequently, fractions G2 and G4 were subjected once again to flash chromatography using methods **F3** and **F4** respectively. Separation of G2 resulted in eight sub-fractions. Quite pure isolates were obtained for G2.2 (**DHK**, 1.14 g, $R_t \sim 40$ -43 min), G2.4 (**K**, 1.83 g, $R_t \sim 47$ -55 min), and G2.6 (**DHM**, 0.24 g, $R_t \sim 60$ -61 min). Part of the fraction G2.4 was recrystallized in methanol due to still present impurities (see chapter 2.1.2.3). Additionally, methods **F5-F7** were used for purification and yielded in 0.45 g pure **DHK** ($R_t \sim 33$ -37 min) and 0.31 g **K** ($R_t \sim 33$ -40 min). For fraction G2.6', the HPLC method **H1** (see chapter 2.1.2.2) was applied to finally obtain pure **DHM** (0.17 g, $R_t = 18$ min). Finally, fraction G4.2 and precipitated **DMY** were purified using method **F8**. At the end, 0.16 g of **DMY** ($R_t \sim 47$ -57 min) was isolated.

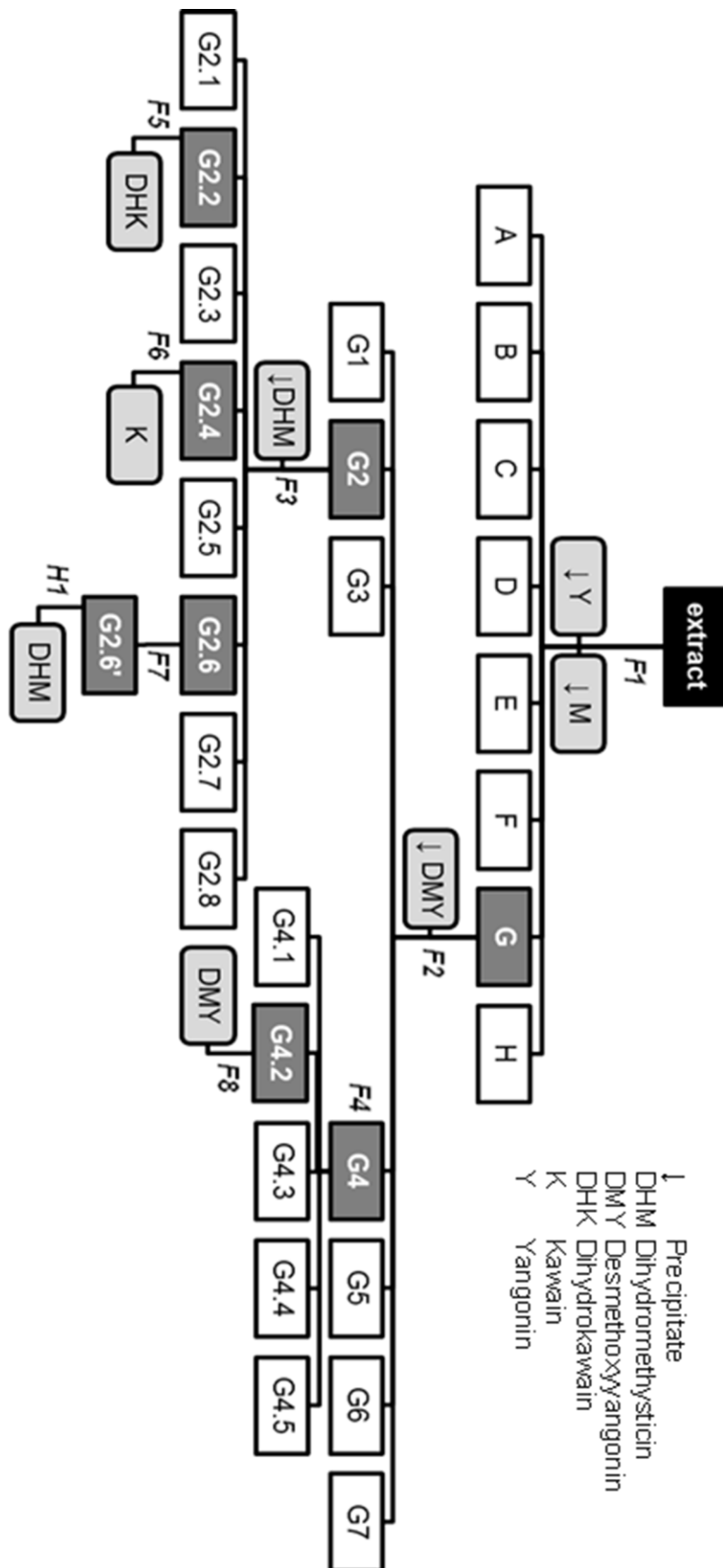


Figure 3.4: Fractionation scheme. Used methods are describe in chapters 2.1.2.1 and 2.1.2.2.

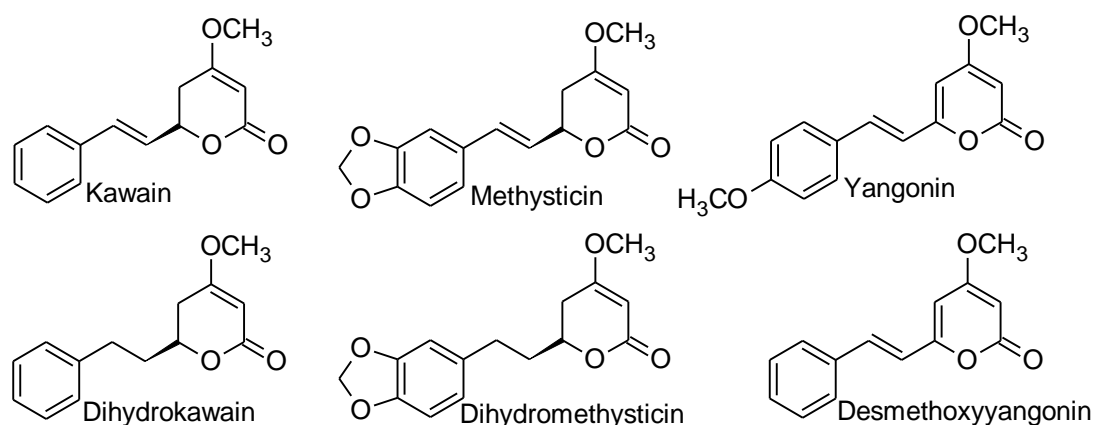


Figure 3.5: Chemical structures of isolated kavalactones.

The six major kavalactones (Figure 3.5) were isolated in sufficient amounts with a very high degree of purity using flash techniques. **FKB** and **FKA** were identified in fraction B and fractions D/E, respectively. **FKC** was not found, probably due to a kavalactone like chromatographic behavior. Fractionated chalcones were not further purified as they were synthesized by our working group for pharmacological testing.

3.3.2 Analytical characterization of isolated kavalactones

Identity of isolated compounds was confirmed by ^1H NMR spectroscopy (see chapter 2.1.3.2). Chemical shifts were compared to literature [206]. Purity of isolated kavalactones was determined by HPTLC (1 mg/mL, 7.5 μL) with solvent system **T1** (see chapter 2.1.3.1) and HPLC (1 mg/10 mL; 10 μL) using method **P1** (see chapter 2.1.3.3).

Table 3.1: HPTLC and HPLC analysis of kavalactones.

| | HPTLC | | | HPLC | | |
|------------|--------|-----------------------------------|----------------|----------------|----------------------|------------|
| | 365 nm | AA/H ₂ SO ₄ | R _f | λ [nm] | R _t [min] | purity [%] |
| K | - | red | 0.23 | 244 | 11.75 | 99 |
| DHK | - | brown | 0.25 | 236 | 11.93 | 99 |
| M | - | grey | 0.17 | 264 | 11.29 | 95 |
| DHM | - | blue | 0.21 | 235 | 11.39 | 98 |
| Y | blue | green | 0.24 | 356 | 12.57 | 100 |
| DMY | - | violet | 0.30 | 255 | 12.63 | 98 |

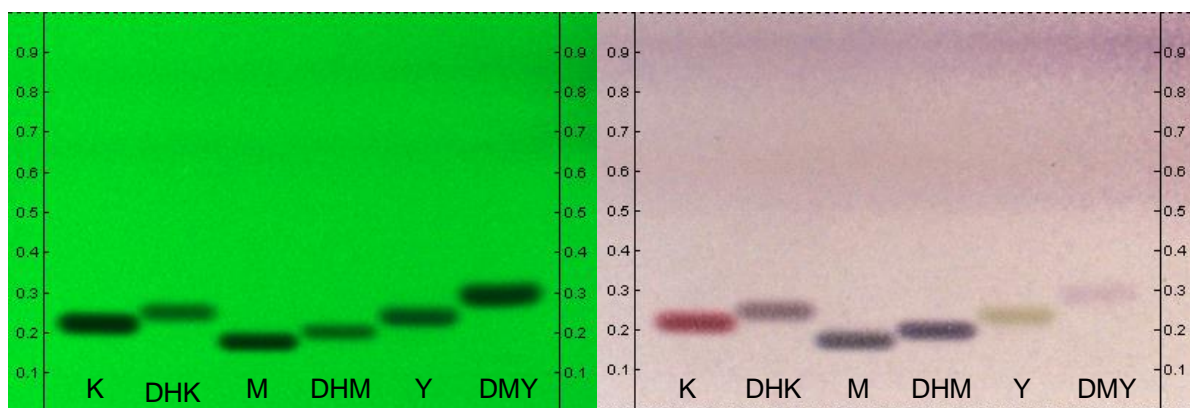


Figure 3.6: HPTLC of isolated kavalactones. On the left: 254 nm, on the right: daylight after derivatization with anisaldehyde reagent.

The results of the HPTLC (Figure 3.6) show no detectable impurities at 254 nm, 365 nm, and daylight. All kavalactones quench fluorescence at 254 nm; **Y** exhibits a blue fluorescence at 365 nm. After derivatization with anisaldehyde reagent, the kavalactones react to bright colored products. Due to similar chemical structures of the kavalactones, their chromatographic behavior resembles as can be seen from R_f and R_i values. Therefore, **DMY** is estimated to be the most lipophilic and **M** the most hydrophilic of the compounds. LogP values confirm these findings and were calculated for **M** as 1.51, for **DHM** as 1.81, for **K** as 1.65, for **Y** as 1.99, and for **DMY** as 2.05 [207]. The purity of the isolates was confirmed by HPLC (Table 3.1). For all compounds, a purity of at least 95% was found.

The analytical characterization of the synthesized kavachalcones (**FKA-C**) is described in chapter 4.3.1.

3.3.3 *In vitro* cytotoxicity of kavalactones and chalcones, major and minor constituents in kava rhizome extract

Since in 2002 kava containing products were banned by German health authorities, a controversial dispute broke out concerning putative culprits and possible mechanism of kava hepatotoxicity. Despite the necessity of novel approaches, still quite little new experimental data are available which evaluate and compile the toxic potential of individual kava constituents. Thus, the hepatotoxic potential of the six kavalactones and three chalcones, major and minor constituents of the acetonic kava rhizome extract, was (re)assessed using two human hepatoma cell lines (HepG2, HuH-7), and for comparative evaluation of potentially liver-specific effects, an intestinal cell line (Caco-2, see chapter 2.2.2.3). Cells were cultivated and treated as described in chapter 2.2.4. Used cell culture reagents and expendables are listed in chapters 2.2.1, 2.2.2 and 2.2.3. The influence of the individual compounds on viability or metabolic activity and cell proliferation was investigated with MTT (see chapter 2.2.5.1) and CV (see chapter 2.2.5.2) assay, respectively. The test concentration ranged from 10 to 100 μ M and the incubation period was 24 h.

The question of suitability of the test concentration range can be answered by a theoretical approach and *in vivo* pharmacokinetic data. Maximum daily oral dose of kavalactones is 120 mg, resulting in an average dose of 20 mg for each kavalactone. After a single oral dose of 200 mg (\pm)-**K** in human, a maximum plasma concentration of 18 $\mu\text{g/mL}$ was detected [24]; thus, bioavailability was approximately 50%. Other experiments in rats have shown increased absorbance of **K** in presence of other kavalactones [168] so that at least 50% bioavailability can be assumed for kavalactones ingested with kava extracts. Assuming an average molecular weight of 250 g/mol, a blood volume of 6 L, and a minimum bioavailability of 50%, blood concentrations of 2 $\mu\text{g/mL}$ (\sim 8 μM) might be reached. In tissues like the liver, concentrations may even be higher. As short-term toxicity of kavalactones in liver cells is addressed, the concentration range of 10-100 μM is considered adequate.

Table 3.2 shows the results of the MTT and CV assay for all tested kavalactones indicating all concentrations with significant effects on cell viability and proliferation. The two hydrated compounds **DHK** and **DHM** had no significant influence on viability and cell number up to the highest concentration tested. **K** and **M** decreased viability of HepG2 cells significantly already at low concentrations (10 μM and 30 μM respectively). Interestingly, the effect seemed to be dose independent as viability remained constant at around 70-80% even at 100 μM . There was no measurable influence on cell proliferation. **DMY** exhibited a slight but significant effect on both viability of HepG2 and HuH-7 and cell proliferation of HuH-7 and Caco-2. Viability of **DMY** treated cells remained at around 70% for HepG2 (50-100 μM) and 80% for HuH-7 (100 μM). Cell number of HuH-7 decreased to 80% starting at 80 μM , and to 80% at 100 μM for Caco-2. A pronounced and dose-dependent impact on cell viability of HepG2 and HuH-7 was found for **Y** starting already at 10 and 30 μM with higher concentrations being more toxic. Calculated IC_{50} values for HepG2 were $60 \pm 13 \mu\text{M}$ and for HuH-7 $52 \pm 9 \mu\text{M}$ (Table 3.3). Loss of cell viability was also observed for Caco-2. As it was less distinct and leveled off at 70% (50-100 μM), no IC_{50} value could be calculated. **Y** also impaired cell proliferation of HepG2 and HuH-7 already at low concentrations (10 μM). Cell number was decreased to 70% and 80% of control, respectively, unchanging over the whole concentration range. In comparison, cell number of Caco-2 was only affected at the highest test concentration.

Table 3.2: Toxicity of kavalactones on HepG2, HuH-7, and Caco-2 cells determined by MTT and CV assay. Concentrations [μM] are indicated for significant effects ($p < 0.05$): v [%] remaining viability, p [%] remaining cell number, referred to untreated control cells (100%); (-) no significant effect. Values are indicated as the means \pm SD ($n = 3$). Statistical analysis (one-way ANOVA followed by Dunnett's multi-comparison post-hoc test) was performed using GraphPad Prism 4 software.

| MTT and CV assay | | | | | | | |
|------------------|---------------------|-------------|------------|-------------|-------------|-------------|------------|
| | HepG2 | | | HuH-7 | | Caco-2 | |
| | c [μM] | v [%] | p [%] | v [%] | p [%] | v [%] | p [%] |
| DMY | 10 | - | - | - | - | - | - |
| | 30 | - | - | - | - | - | - |
| | 50 | 78 \pm 11 | - | - | - | - | - |
| | 60 | 67 \pm 10 | - | - | - | - | - |
| | 70 | 69 \pm 7 | - | - | - | - | - |
| | 80 | 72 \pm 10 | - | - | 82 \pm 11 | - | - |
| | 90 | 80 \pm 6 | - | - | 82 \pm 11 | - | - |
| | 100 | 73 \pm 11 | - | 81 \pm 4 | 81 \pm 17 | - | 80 \pm 4 |
| Y | 10 | 76 \pm 15 | 72 \pm 5 | - | 86 \pm 14 | - | - |
| | 30 | 62 \pm 5 | 69 \pm 9 | 70 \pm 6 | 85 \pm 6 | - | - |
| | 50 | 50 \pm 4 | 72 \pm 4 | 46 \pm 10 | 81 \pm 4 | 75 \pm 11 | - |
| | 60 | 46 \pm 7 | 70 \pm 4 | 40 \pm 8 | 80 \pm 4 | 69 \pm 10 | - |
| | 70 | 44 \pm 7 | 67 \pm 6 | 40 \pm 8 | 83 \pm 5 | 69 \pm 8 | - |
| | 80 | 43 \pm 2 | 70 \pm 3 | 39 \pm 8 | 76 \pm 5 | 71 \pm 7 | - |
| | 90 | 44 \pm 5 | 71 \pm 4 | 39 \pm 9 | 83 \pm 6 | 70 \pm 8 | - |
| | 100 | 52 \pm 9 | 75 \pm 5 | 40 \pm 10 | 79 \pm 4 | 70 \pm 6 | 81 \pm 1 |
| DHK | - | - | - | - | - | - | - |
| K | 10 | 76 \pm 3 | - | - | - | - | - |
| | 30 | 76 \pm 6 | - | - | - | - | - |
| | 50 | 71 \pm 2 | - | - | - | - | - |
| | 60 | 70 \pm 3 | - | - | - | - | - |
| | 70 | 74 \pm 4 | - | - | - | - | - |
| | 80 | 70 \pm 6 | - | - | - | - | - |
| | 90 | 77 \pm 5 | - | - | - | - | - |
| | 100 | 82 \pm 8 | - | - | - | - | - |
| DHM | - | - | - | - | - | - | - |
| M | 10 | - | - | - | - | - | - |
| | 30 | 84 \pm 12 | - | - | - | - | - |
| | 50 | 83 \pm 7 | - | - | - | - | - |
| | 60 | 75 \pm 4 | - | - | - | - | - |
| | 70 | 74 \pm 6 | - | - | - | - | - |
| | 80 | 72 \pm 8 | - | - | - | - | - |
| | 90 | 76 \pm 6 | - | - | - | - | - |
| | 100 | 76 \pm 2 | - | - | - | - | - |

Direct hepatotoxicity of kavalactones and kavalactone rich extracts has been assessed in numerous *in vitro* studies yielding different and partly inconsistent results. Tang et al. studied the *in vitro* toxicity of **Y**, **M**, and **K** in HepG2 cells using lactate dehydrogenase (LDH) release and ethidium bromide assay [208]. Toxic effects were observed for **M** and **K** at 100 and 200 μM , respectively. For **Y**, pronounced decrease of cell viability to 40% at 25 μM in the ethidium bromide assay was detected. Thus, these results are in good accordance to findings of the present study where **Y** also showed distinct cytotoxicity in HepG2. Furthermore, the mode of cell death was elucidated using acridine orange/ethidium bromide dual staining. Early and late apoptotic cells were detected after a treatment with 200 μM **M** and 25 μM **Y** but not with 200 μM **K**. Glutathione levels were not decreased by kavalactone treatment so glutathione depletion may not be the cause for observed toxicity.

These findings differ from other *in vitro* studies, which analyzed the effect of individual kavalactones on ATP levels in primary human hepatocytes [209]. **M** and **DMY** were found to be the most toxic and, surprisingly, **Y** the least toxic kavalactone.

Nerurkar et al. investigated the toxicity of **DMY** and **DHM** in HepG2 and found no increased LDH release up to 200 μM and 24 h of treatment [210]. In preliminary experiments individual kavalactones failed to show any toxic potential in HepG2 at concentrations less than 0.5 μM for up to two weeks. **DHM** and **DMY** exhibited no toxicity at 50 and 100 μM up to 8 days of treatment. Unfortunately, authors did show any data of long-term toxicity.

Gebhardt et al. examined the cytotoxicity of kava extracts and kavalactones in rat hepatocytes and HepG2 [211]. No cytotoxic effects of kavalactones were detected in HepG2 ($\text{IC}_{50} > 200 \mu\text{g/mL} \sim 800 \mu\text{M}$). **K** and **M** were the most toxic constituents in rat hepatocytes with IC_{50} values of 45 $\mu\text{g/mL}$ ($\sim 200 \mu\text{M}$) and 63 $\mu\text{g/mL}$ ($\sim 230 \mu\text{M}$). A native ethanolic kava extract was toxic in concentrations above 250 $\mu\text{g/mL}$, and the acetonic extract at concentrations above 125 $\mu\text{g/mL}$, whereas the commercial extracts did not exhibit any toxicity. Used assay systems were only insufficiently indicated.

Another study also identified **Y** as most hepatotoxic kavalactone in HepG2 ($\text{IC}_{50} \sim 100 \mu\text{M}$). However, no toxicity was observed in an immortalized human hepatocyte cell line L-02 [212]. Commercial kava extracts and kavalactones were also tested for mutagenicity and toxicity in L5178Y mouse lymphoma cells [213]. **DMY** and **Y** appeared to be the most toxic components. However, both extracts and individual kavalactones lacked any mutagenic response in the mutation assay with addition of human liver S9 activation.

Lüde et al. compared the hepatocellular toxicity of kava leaf and root extracts in HepG2 and isolated liver mitochondria [214]. Methanolic and acetonic root extracts contained approximately 80% kavalactones and 0.011% pipermethysticine whereas the methanolic leaf extract had 24% kavalactones and 1.34% pipermethysticine. The kava leaf extract showed lower cytotoxicity and less mitochondrial impairment compared to root extracts. The authors

draw the conclusion that rather the kavalactones than the alkaloid pipermethysticine can be considered as the toxic principle in kava extracts. These results contradict the findings of Nerurkar et al. who found more pronounced toxicity of pipermethysticine compared to individual kavalactones [210].

One reason for the huge differences in assay results could be the use of different assay systems with different sensitivity degrees. Furthermore, findings in HepG2 and primary hepatocytes (also the use of hepatocytes from different species) are not necessarily comparable. For example, cytochrome P450 enzymes are highly down-regulated in HepG2 whereas primary hepatocytes normally possess the whole range of metabolizing enzymes. Primary human hepatocytes - if available - still remain the "gold-standard" in any *in vitro* hepatotoxicity approach. Nevertheless, a re-evaluation of toxicity especially of **Y** in primary hepatocytes compared to liver cell lines would be a very interesting issue.

Not only the *in vitro* findings but also *in vivo* toxicity testing leads to different results concerning kavalactone or kava extract toxicity. Both aqueous and organic extracts as well as single kavalactones have been investigated. Sorrentino et al. assessed the long-term toxicity of an ethanolic kava extract (daily 73 mg kavalactones/kg) in rats over 6 month and found no signs of hepatotoxic effects [215]. Singh et al. investigated the effects of an aqueous kava extract on liver function in rats (daily 200-500 mg kavalactones/kg) for up to 4 weeks and detected no altered levels of ALT, AST, ALP, or LDH [216]. Clayton et al. examined the effects of an organic kava extract in concentrations from 0.25 up to 2 g extract/kg/day in rats [217]. Time- and dose-dependency of hepatotoxicity was revealed. No hepatotoxic effect was observed with doses of 0.25 g/kg/d. Toxicity of 1 g/kg/d appeared after 93 days of treatment and after 4 days with 2 g/kg/d. Another study from 2006, investigating the effect of an acetonic and an ethanolic extract at three different oral doses from 31 to 133 mg/kg in rats, observed no liver injury based on serum markers and serum lipid peroxidase status [218]. **K**'s effect on hepatic ultrastructure was tested by infusing 10 µg/mL **K** solution for 2 h in rats [219]. Histological analysis revealed severe vascular and endothelial damages in the livers of **K** treated rats compared to control. A recent study investigated the hepatotoxicity of **K** and **M** in perfused livers of rats, which were either pretreated with the macrophage intoxicant gadolinium chloride or not [220]. An extensive damage was observed in kavalactone-perfused livers whereas the damage was significantly lower with a gadolinium chloride pretreatment. These results indicate that the activation of liver macrophages may be a factor for observed hepatotoxicity of kavalactones.

In general, kavachalcones (Figure 3.7) exhibited a more pronounced cytotoxicity compared to kavalactones with exception of **Y** (Table 3.3). The most cytotoxic compound was **FKB**, followed by **FKC** and then **FKA**. The latter compound significantly reduced cell viability of

HepG2 and HuH-7 but not of Caco-2 cells. For HepG2, an IC_{50} of $73 \pm 10 \mu\text{M}$ (Table 3.3) was determined. Viability of HuH-7 cells was significantly decreased to 80% at $80 \mu\text{M}$ and to 67% at $100 \mu\text{M}$. Cell proliferation was impaired in all cell lines. For **FKA**, an IC_{50} of $71 \pm 8 \mu\text{M}$ was calculated for HepG2 and an IC_{50} of $90 \pm 12 \mu\text{M}$ for HuH-7. Cell number of Caco-2 was only affected at high concentrations and decreased to around 70% at $100 \mu\text{M}$. For **FKC**, a higher toxicity was observed in liver cell lines. IC_{50} values determined by MTT assay were $55 \pm 7 \mu\text{M}$ for HepG2 and $58 \pm 5 \mu\text{M}$ for HuH-7. In Caco-2 cells, **FKC** effects on viability were less pronounced and completely absent regarding cell proliferation. Viability at $100 \mu\text{M}$ was still 75% in comparison to only 28% in HepG2 and 19% in HuH-7. Cell number of HepG2 was significantly reduced at $60 \mu\text{M}$ and determined as 53% at $100 \mu\text{M}$; for HuH-7 an IC_{50} of $92 \pm 11 \mu\text{M}$ was found. **FKB** was by far the most toxic of all tested kava compounds in all three cell lines herein again the liver cell lines being more sensitive. IC_{50} values assessed by MTT assay were $33 \pm 1 \mu\text{M}$, $42 \pm 2 \mu\text{M}$, and $70 \pm 4 \mu\text{M}$ for HepG2, HuH-7, and Caco-2. Moreover, the compound exhibited a strong anti-proliferative and in higher concentrations also a cytotoxic effect. IC_{50} values in the CV assay were $35 \pm 3 \mu\text{M}$, $42 \pm 3 \mu\text{M}$, $91 \pm 17 \mu\text{M}$ for HepG2, HuH-7, and Caco-2, thus ranging in the same concentrations as IC_{50} values of cell viability. Accordingly, toxic potential of **FKB** is rather explainable due to decrease of cell number than due to enzymatic impairment.

Table 3.3: IC_{50} values of toxic kava constituents determined by nonlinear regression using GraphPad Prism 4 software. (-) IC_{50} value was not determinable in the test concentration range (10-100 μM). Calculated values are presented as mean \pm SE.

| | IC_{50} [μM] | | | | | |
|------------|-----------------------------|------------|------------|-------------|------------|-------------|
| | HepG2 | | HuH-7 | | Caco-2 | |
| | MTT | CV | MTT | CV | MTT | CV |
| Y | 60 ± 13 | - | 52 ± 9 | - | - | - |
| FKA | 73 ± 10 | 71 ± 8 | - | 90 ± 12 | - | - |
| FKB | 33 ± 1 | 35 ± 3 | 42 ± 2 | 42 ± 3 | 70 ± 4 | 91 ± 17 |
| FKC | 55 ± 7 | - | 58 ± 5 | 92 ± 11 | - | - |

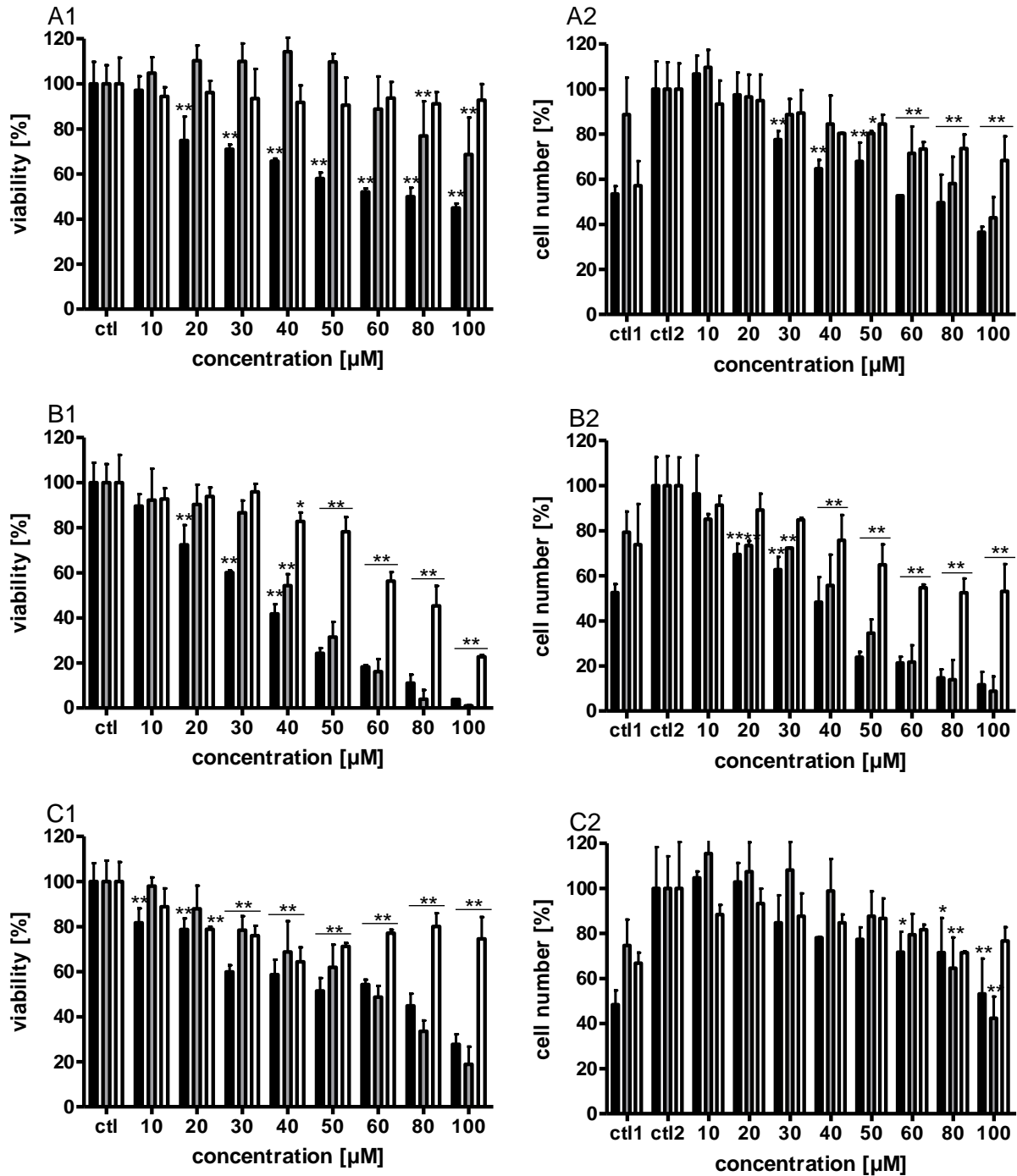


Figure 3.7: Toxicity of kavachalcones: A = FKA; B = FKB; C = FKC; 1 = MTT; 2 = CV; black bars HepG2; grey bars HuH-7; white bars Caco-2. Values are presented as means \pm SD ($n = 3$) referred to untreated control cells (ctl/ctl2 = 100%); ctl1 = initial cell density (before treatment). Statistical analysis (one-way ANOVA followed by Dunnett's multi-comparison post-hoc test) was performed using GraphPad Prism 4 software. Levels of significance * $p < 0.05$; ** $p < 0.01$.

FKB has been previously identified as cytotoxic constituent of a methanolic kava root extract by bioassay-guided fractionation [221]. The finally isolated compound exhibited pronounced cytotoxic effects on HepG2 in MTT (IC_{50} 8.4 $\mu\text{g/mL}$ \sim 30 μM), LDH, and AST assay comparable to the findings of our present study. **FKB** has also shown to be a potent COX-I and moderate COX-II inhibitor [142]. It is discussed whether this might contribute to the hepatotoxic potential [200]. A recent study investigated the molecular mechanisms of **FKB** toxicity in HepG2 and human hepatocytes L-02 and also evaluated the toxicity of **FKA** and **FKC** [212]. In accordance with our present study, **FKB** was found to be the most toxic compound in HepG2 (IC_{50} 15 μM ; 48 h incubation). **FKA** and **FKC** were also toxic in test concentrations of 10-50 μM . In L-02 cells, an IC_{50} of 32 μM was determined for **FKB** and 70 μM for **FKC**, whereas **FKA** was not toxic. Further investigations of cell morphology in L-02 cells and caspase-3 activation in HepG2 revealed apoptotic activity of **FKB** (30 μM). Caspase-3 was not cleaved with **FKA** and **FKC** treatment at same concentrations. Furthermore, **FKB** inhibited TNF- α induced activation of NF- κB (IC_{50} 10 μM) and activated mitogen-activated kinases (MAPKs) signaling pathways in HepG2. Transient activation of MAPKs like JNK leads to proliferation, whereas prolonged activation of JNK has been link to hepatocytic death. **FKB** also depleted glutathione (GSH) levels, and exogenous supplementation of GSH reduced **FKB**-induced hepatotoxicity. *In vivo*, hepatotoxic potential of **FKB** was investigated in mice that received daily oral doses of 25 mg/kg **FKB** over one week. Histological analysis revealed massive liver damage with hepatocellular swelling and vesiculated cytoplasm indicating inflammatory infiltration. AST and ALP levels were significantly increased in **FKB** treated mice. Additionally, LPS induced NF- κB activation was greatly reduced by **FKB** also *in vivo*. Taken together, this study emphasizes the overall hepatotoxic potential of **FKB**. *In vivo* toxicity of **FKA** and **FKC** has not been addressed yet, although they might also contribute to the observed liver toxicity, as they are also present in kava extracts.

FKB is only a minor constituent of *Piper methysticum* with an amount of < 1% of dry weight [200]. HPLC analysis of an ethanolic kava extract quantitated a total chalcone content of 1.1% [117]. However, flavokawain content seems to be highly dependent on the kava cultivar [201]. Different amounts of **FKB** were found in organic kava extracts varying from 0.54-7.06 mg equated to 120 mg kavalactones. In the worst case, 7.06 mg of **FKB** would be ingested with daily kava extract dose. Assuming complete oral absorption and an average blood volume of 6 L, blood/plasma concentrations of 1.2 $\mu\text{g/mL}$ (\sim 4 μM) may be predicted. *In vitro* hepatotoxicity was observed starting at 20 μM (Figure 3.7), a five-fold higher concentration. Nevertheless, it has to be kept in mind that only short-term toxicity (24 h) has been investigated yet. Further assays should examine the long-term toxicity of kavachalcones choosing longer incubation times (72 h) which may lead to much lower IC_{50}

values that might be dose-relevant then. To date, there are neither data available that address toxicity of kava-chalcones in primary human hepatocytes nor *in vivo* studies (except **FKB** in mice [212]) that take in account their hepatotoxic potential.

Another kava constituent, the alkaloid pipermethysticine has also been suspected to be the culprit of hepatotoxic events. Pipermethysticine was isolated from aerial parts of the plant (leaves, stem peelings) [123]. Nerurkar et al. compared the toxicity and apoptotic potential of pipermethysticine to that of **DHM** and **DMY** in HepG2 cells [210]. The alkaloid significantly increased LDH release at 50 μM (65%) and 100 μM (90%) within 24 h whereas the kavalactones showed no alterations. Furthermore, pipermethysticine depleted ATP levels at same concentrations by 70-90% and increased caspase-3 activity by 250 and 575%. A decrease of mitochondrial membrane potential and increased ROS production was observed as well at 50 and 100 μM , respectively. In contrast to these findings, a methanolic kava leaf extract containing 1.34% pipermethysticine was less toxic than an acetonic and methanolic root extract containing only 0.011% pipermethysticine [214]. These results suggest rather the kavalactones than pipermethysticine being the toxic principle. An *in vivo* study in F-344 rats investigated the short-term toxicity (2 weeks) of pipermethysticine (10 mg/kg) and an acetonic kava rhizome extract (100 mg/kg) [222]. Both lacked significant changes in liver function tests (ALT and AST levels, lipid peroxidation) or severe hepatotoxic injury. Pipermethysticine treatment, however, led to increased markers of oxidative stress such as elevated glutathione levels, and enhanced cytosolic superoxide dismutase activity and TNF- α mRNA expression. Alteration of CYP2E1 and 1A2 was also reported, which may lead to drug interactions. It is discussed whether pipermethysticine can be found in raw material of kava rhizomes and roots [201]. Pipermethysticine could not be detected in commercially available kava products from Germany. However, it may be present in kava products of poorer quality or due to adulterations with aerial parts. In summary, the evidence for pipermethysticine as culprit of kava's hepatotoxicity remains unclear.

Beside the direct hepatotoxicity of kava constituents, also indirect mechanisms may cause kava's hepatotoxicity. Indeed, several models of indirect kava toxicity are discussed. Kava extracts and kavalactones possess a high potential of cytochrome P 450 enzyme alteration (see 3.1.8 drug interactions). A set of important drug metabolizing cytochrome enzymes is significantly inhibited [169,191–193]. As kava extracts were sold as over the counter drugs and have been likely used in combination with other remedies, a high potential of pharmacokinetic drug interactions theoretically exists, which may have led to intoxicative complications in certain combinations. In addition, these toxic drug interactions are not likely

detected in a clinical test surrounding where co-medication is strictly monitored. On the other hand, surveillance studies neither did reveal toxic events due to drug interactions.

Moreover, metabolic interaction of kava and alcohol is suggested as possible mechanism of kava hepatotoxicity [223]. Ethanol is partly metabolized by the hepatic cytochrome P450 enzymes, especially CYP2E1, which was found to be inhibited in a test group consuming kava.

Due to two case reports in patients with a deficiency in CYP2D6, it is discussed whether genetic polymorphism of CYP2D6 is responsible for hepatotoxicity of kava in the Caucasian population (~ 10% of poor metabolizers) [203].

Another assumption attributes COX inhibitory activity to possible hepatotoxicity of kava [204]. Kava constituents like **Y** and **DHK** have been shown to be COX-II inhibitors [142]. COX-II is known to mediate hepatoprotective factors, and other COX-II inhibitors (e.g. NSAIDs) have shown hepatotoxic potential as well [224].

Whitton and coworkers postulated that observed hepatotoxic side effects might arise from different extraction process of commercial kava extracts compared to traditional ones [225]. Aqueous extracts contain glutathione, which is absent in standardized organic extracts. *In vitro* experiments showed that glutathione binds irreversibly to kavalactones by a Michael type reaction, due to opening of the lactone ring. This might also be the detoxifying phase II reaction *in vivo*. Whitton et al. argue that glutathione depletion after intake of standardized kavalactone extracts might be the reason for observed hepatotoxic effects. This theory is critically questioned by Schmidt et al. [202], doubting the *in vivo* relevance as kavalactones are absorbed intact from intestine, and because they are undoubtedly the carriers of pharmacological actions.

Differences between traditional and commercial kava extracts were also discussed in another context. Since aqueous kava extracts have been longtime used by the Pacific Islanders without reports of liver toxicity and necrotic hepatitis appeared in Western countries after intake of ethanolic and acetonetic kava extracts, different composition of traditional and commercial extracts might be the reason for hepatotoxicity. Actually, differences in total kavalactone amount, in kavalactone distribution, and inhibitory activity of cytochrome enzymes was detected for organic and aqueous extracts [111]. Generally, aqueous extracts contained less kavalactones, above all less **Y**. However, Teschke et al. composed clinical data of 5 patients with suspected liver disease in association with the use of traditional aqueous kava extracts [226]. This data rather suggest that kava hepatotoxicity is independent from extraction procedure. In fact, a recent German case of toxic hepatitis in a 42-year-old man was reported after consumption of traditional kava beverage during his stay in Samoa [183].

Johnson and coworkers identified electrophilic *o*-quinone metabolites of **M** and **DHM** via GSH trapping and LC–MS after incubation of a kava extract with liver microsomes. These electrophilic metabolites, however, could not be detected *in vivo* [227]. Zou et al. tested the toxification of kavalactones in MCL-5 cells, which were transfected with 5 human P450 enzymes, and a control cell line (cH2) without these metabolizing enzymes. They detected that both cell lines were equally sensitive to the test compounds. These results suggest that kavalactones are not activated to toxic metabolites [228].

Teschke et al. proposed that poor kava cultivar (export of substandard cultivars) or plant part quality (root peelings, aerial parts), adulterants, or mold hepatotoxins (due to insufficient drying and inaccurate storing) may be responsible for observed hepatotoxic side effects [188,229–231].

Summing up, there is a broad spectrum of possible explanations for kava hepatotoxicity. Probably, not only one single toxic principle or mechanism can explain all cases of hepatotoxic side effects. Nevertheless, there is evidence that direct hepatotoxic potential of kava constituents, above all **Y** and kava-chalcones, is present in human HepG2 and HuH-7. This fact should be considered for an over-all evaluation of hepatotoxic potential of kava. Furthermore, cytotoxicity was significantly more pronounced in the liver cell lines compared to Caco-2 cells. This finding suggests a certain liver specificity of toxic effects.

Further studies are needed that assess long-term toxicity and mechanism of toxicity of **Y** and flavokawains as well as their pharmacokinetics. In any case, the role of these potential hepatotoxins should be considered in further investigations.

3.4 Conclusion

Six major kavalactones were isolated in high purity degrees from an acetonic kava rhizome extract using mainly flash techniques. **FKA** and **FKB**, but not **FKC**, were identified in sub-fractions of the extract.

The evaluation of the *in vitro* hepatotoxicity of kavalactones and chalcones in human HepG2 and HuH-7 identified **Y** and flavokawains as toxic compounds. For comparison, the well-known hepatotoxine tacrine showed higher IC_{50} values in the MTT assay under same conditions (IC_{50} (HepG2) 64 μ M and IC_{50} (HuH-7) 94 μ M; see chapter 6.3.4 Table 6.2). Toxicity in descending order was found to be **FKB** > **FKC**~**Y** > **FKA**. While **FKA** and **FKB** affected cell viability and proliferation in nearly same extents, **FKC** and **Y** reduced mainly the metabolic activity of cells and less pronounced the cell number. This could be due to different mechanisms of toxicity. **K** and **M** showed a weak, dose-independent decrease of cell viability in HepG2 already at low concentrations. Toxicity was completely absent for the two hydrated

compounds **DHK** and **DHM** in all cell lines. This could be an indicator that the 7,8-double-bond triggers kavalactone toxicity.

The toxicity of **FKB** (which was also the most toxic compound in this study) is quite clearly estimated. Physiological relevance of test concentrations has to be integrated in the discussion as **FKB** is only a minor constituent in kava extracts. However, in account of and combination with **FKA** and **FKC**, the chalcones could contribute to kava hepatotoxicity. Further studies should be conducted concerning *in vivo* hepatotoxicity and pharmacokinetics (microsomal metabolism see chapter 5.3.2). **FKA** and **FKC** should attract more interest as they showed distinct toxicity in HepG2 and HuH-7 cells. Studies could be repeated in human primary hepatocytes with longer incubation times and lower concentrations to augment the physiological relevance.

Results concerning kavalactones remain contradictory. The toxicity and apoptotic potential of **Y** was detected in HepG2 before [208], however, it was completely absent in another study in HepG2 and primary cultured rat hepatocytes [211]. Some findings indicate hepatotoxicity of **K**, **M**, and kava extracts. Results of *in vivo* testings are as well ambiguous. The overall estimation of kavalactone toxicity stays a difficult issue. However, this study reveals the explicit toxicity of **Y** in comparison to other kavalactones. At least *in vitro*, toxicity of **K** and **M** should be considered as well.

A full evaluation of kava hepatotoxicity is still not possible. In summary, it seems to be very likely that not only one factor is responsible for the observed hepatotoxic side effects. Direct toxicity of constituents - as also shown in this study - as well as indirect mechanisms may be involved. Albeit very laborious, a case by case evaluation might be more suitable. Additionally, long-time safety studies of kava extracts are required. Taking in account the high hepatotoxic potential of flavokawains *in vitro* together with lacking pharmacological benefits, strict analytical characterization of kava extracts with respect to chalcone content or even the usage of chalcone-free extracts can be highly recommended.

4 Inhibitory activity of structurally related chalcones on activated human hepatic stellate cells

4.1 Introduction

4.1.1 The role of hepatic stellate cells in liver fibrosis

Liver fibrosis is considered as a wound-healing response to chronic liver injury, which is attended by exceeding production and deposition of extracellular matrix (ECM) proteins leading to disorganization of the normal liver architecture, portal hypertension, and cirrhosis in progressive stage [232].

Hepatic stellate cells (HSC) - also called vitamin A-storing cells, lipocytes, fat-storing cells, or Ito cells -, first described by Kupffer in 1876, have been identified as major cellular source of ECM and central mediators of hepatic fibrosis [9]. In normal liver, HSC account for 10-15% of the total cell number and are located in the perisinusoidal space of Disse in contact to both hepatocytes and the abluminal surface of sinusoidal endothelial cells, in proximity to hepatic nerves [233]. Physiologically, HSC are the major storage site for retinoids, thus responsible for the vitamin A homeostasis [234]. Retinoids are stored in form of their esters in cytoplasmic droplets. As a result of liver injury caused by e.g. viral infections, alcohol consumption, drug toxicity, autoimmune or metabolic disease, HSC undergo activation, transforming from resting vitamin A-rich cells into proliferative, fibrinogenic, and contractile myofibroblasts. This activation is considered as key step in the pathogenesis of hepatic fibrosis [10]. Initially, HSC activation is triggered by paracrine stimuli from injured hepatocytes, endothelial cells, Kupffer cells, and platelets, which release fibronectin, cytokines such as transforming growth factor β (TGF- β), platelet-derived growth factor (PDGF), and tumor necrosis factor α (TNF- α), reactive oxygen species (ROS), and others [235]. These factors mediate the phenotypic change of HSC, which yields in a quantitative and qualitative alteration of ECM. Due to an imbalance between ECM degradation and accumulation, total collagen content increases three to eight fold and the composition of ECM proteins shifts to predominantly fibrillar collagens (type I, III, and IV). ECM degradation is controlled by zinc-dependent matrix metalloproteinases (MMP) and their inhibitors, the tissue inhibitors of metalloproteinases (TIMP). In progressive fibrosis, TIMP-1 and TIMP-2 are up-regulated leading to a decreased activity of MMP-1 (interstitial collagenase, collagenase I) and therefore accumulation of ECM proteins [236]. Activated HSC themselves show up-regulated levels of alpha smooth muscle actin (α -SMA) and mitogenic (e.g. PDGF,

endothelin-1 ET-1), and fibrogenic (e.g. TGF- β 1) factors. Furthermore, released cytokines contribute to the perpetuation of HSC activation in an autocrine manner [235].

Longtime, therapeutic approaches have mainly focused on the suppression of hepatic inflammation and the removal of injurious stimuli [233]. In recent years, targeting of HSC as source of fibrinogenic mediators has awakened more and more interest [237]. The inhibition of HSC activation and proliferation is addressed by various strategies [238] including treatment with interferon, anti-oxidants, TGF- β antagonists, inhibitors of signal transduction or cell-matrix interaction, or herbal compounds [239] (e.g. Chinese herbs like extracts of Xiao Caihu Tang [240], glycyrrhizin [241], silymarin [242]). It is discussed whether reversion of activated HSC into the quiescent state, apoptotic clearance, or both mechanisms are involved in the resolution of the fibrotic process [243,244]. Hence, apoptosis-inducing agents constitute as well a therapeutic approach in treatment of hepatic fibrosis, however, specific effect on activated HSC remaining the bottleneck.

4.1.2 Pharmacological characterization of the test compounds

The compounds used in this study (Figure 4.1) comprise a set of natural and synthetic (dihydro)chalcones with different aryl substituents such as hydroxy-, methoxy-, and prenyl-groups. Biosynthetically, chalcones (1,3-diaryl-2-propen-1-ones) belong to the huge flavonoid family, more precisely they constitute flavanone precursors with open C ring, which arise from a mixed biosynthesis including both the shikimate (B ring, C₆-C₃) and the acetate malonate (A ring) pathway. Chalcones possess a wide range of biological activities such as anti-oxidant [245], anti-inflammatory [246,247], anti-cancer [248,249], and anti-infective effects [250,251], to mention just the most important ones (for an overview of chalcone effects see [252]). Moreover, chalcones constitute an interesting basic structure in medicinal chemistry to create derivatives with enhanced pharmacological properties and to investigate structure-activity relationships [253,254].

Xanthohumol (**XAN**), the most abundant prenylated chalcone in hop cons, has already been isolated and synthesized by various working groups [96,255–258]. Xanthohumol H (**XANH**), 4-acetylxanthohumol (**4AcXAN**), and 4-methylxanthohumol (**4MeXAN**) were found as metabolites of **XAN** in rat feces [259]. These compounds were included in the study to estimate the activity of putative **XAN** metabolites as they may occur after administration of **XAN** *in vivo*. Both 3-hydroxyxanthohumol H (**3OHXANH**) and 3-methoxyxanthohumol H (**3OMeXANH**) are synthetic derivatives of the metabolite **XANH**. The non-natural chalcone 4'-methylxanthohumol (**4'MeXAN**) was included as it is a prenyl structure analogue of flavokawain C (**FKC**). Xanthohumol C (**XANC**), 1'',2''-dihydroxanthohumol C (**dhXANC**), and **FKC** were found as minor constituents in *Humulus lupulus* L. [260,261]. **FKC** was also

identified in *Piper methysticum* FORST., as well as flavokawain A (**FKA**) and flavokawain B (**FKB**) (see chapter 3.1.2). The latter compound and alpinetin chalcone (**A**) were isolated from *Alpinia rafflesiana* WALL. EX BAKER [262]. **FKA** was also identified in aerial parts of *Goniothalamus gardneri* HOOK F. ET. THOMS [263]. Pinostrobin chalcone (**P**) was found amongst others in *Alpinia mutica* ROXB. rhizome [264]. Helichrysetin (**Heli**) is a natural chalcone derived from *Helichrysum odoratissimum* L. [265]. 3-Hydroxyhelichrysetin (**3OHHeli**) is a synthetic derivative possessing a catecholic substitution of the B ring. Furthermore, three synthetic dihydrochalcones, dihydroflavokawain C (**dhFKC**), dihydrohelichrysetin (**dhHeli**), and tetrahydroxanthohumol C (**thXANC**), were investigated to evaluate the impact of the α,β -unsaturated ketone structure element on the chalcone activity.

The pharmacological properties of **XAN** are well studied and enclose a broad spectrum of effects and modes of action described in a large number of publications, which mainly address its anti-infective, anti-inflammatory, anti-oxidant, anti-obesity, anti-osteoporosis, anti-invasive, anti-angiogenic, and pro-apoptotic activities (for an overview [261,266–268]). Decisively for this study, **XAN** has already demonstrated inhibitory effects on hepatic inflammation and fibrosis in *in vitro* and *in vivo* studies (see chapter 4.1.3).

FKA caused strong anti-proliferative and apoptotic effects in human bladder cancer cell lines. Apoptosis was mediated by a Bax protein-dependent pathway involving loss of mitochondrial membrane potential and release of cytochrome c [269]. Furthermore, **FKA** reduced the overexpression of anti-apoptotic factors (X-linked inhibitor of apoptosis, survivin). Bladder tumor growth in mice was inhibited to 57%. The effect of **FKA** on the cell cycle was investigated in wild type (RT4) and different p53 mutant bladder cancer cell lines [270]. Differences in cell cycle arrest occurred: cyclin-dependent kinase-2 (CDK2) activity was decreased in RT4 cells, which led to G₁ arrest; in contrast, G₂/M arrest was observed in p53 mutants attended by enhanced growth-inhibitory effects of **FKA** in these cell lines. The regulation of the cell cycle in bladder cancer cells seems to be associated with the p53 status, favoring **FKA** for the treatment of p53 mutant-cancers.

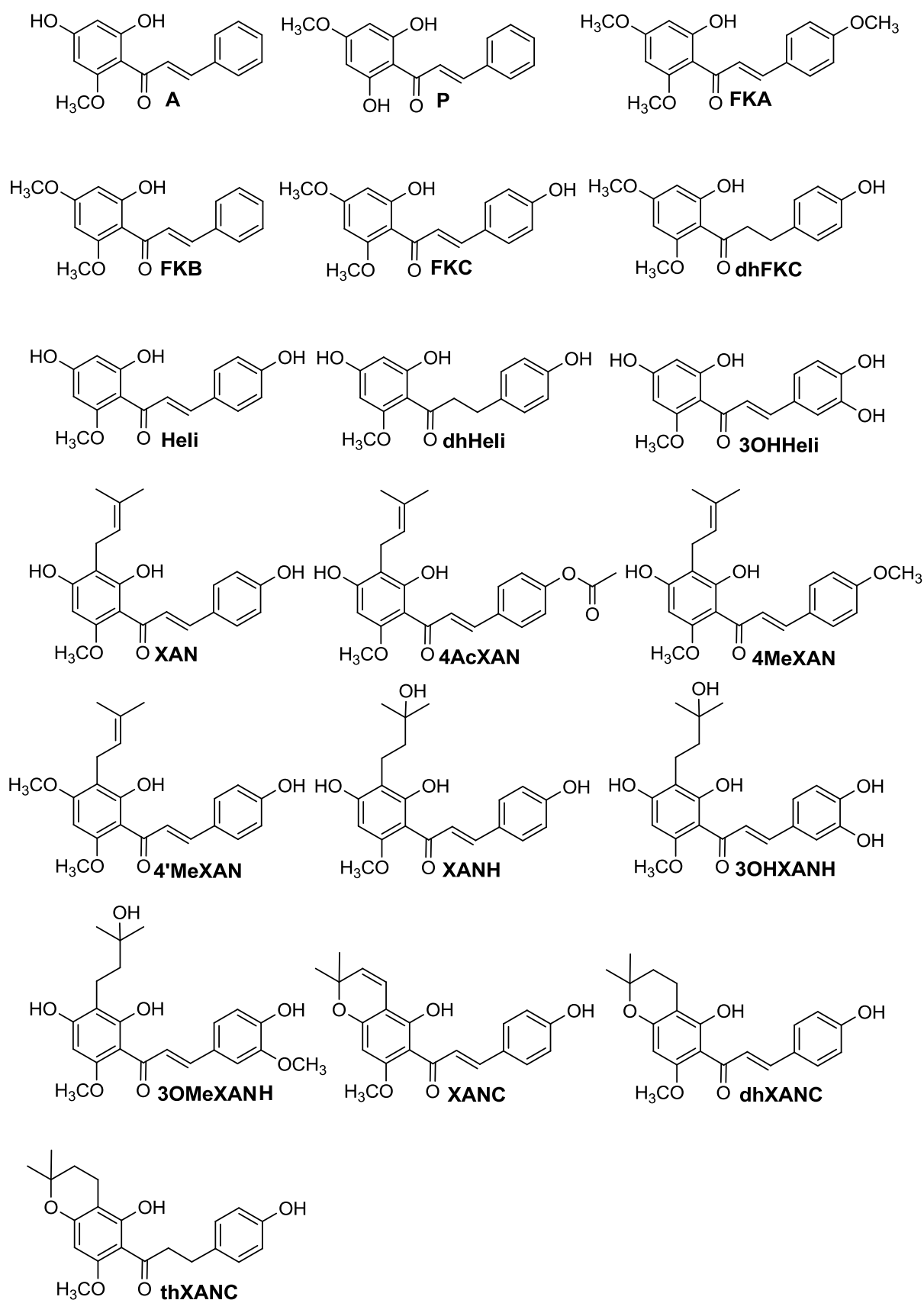


Figure 4.1: Structures of the investigated prenylated and non-prenylated chalcones.

FKB exhibited apoptosis-inducing activities in several cancer cell lines by affecting different molecular targets. In a uterine leiomyosarcoma cell line (SK-LMS-1) growth inhibition was associated with a G₂/M arrest [271]. Besides, **FKB** increased the expression of death receptor (DR5) and mitochondrial pro-apoptotic proteins (Bim, Puma) indicating that both apoptotic pathways may be involved. Similar effects were observed in a hormone-refractory prostate cancer cell line (HRPC) [272] and in synovial sarcoma cell lines (SYO-I, HS-SY-II) [273]. **FKB** was also effective against oral cancer cell lines. **FKB** inhibited the proliferation of oral adenoid cystic cancer cells by causing cell cycle G₂/M arrest and apoptosis via up-regulation of pro-apoptotic proteins (Bim, Bax, Bak) and down-regulation of Bcl-2 [274]. In oral carcinoma HSC-3 cells, **FKB** induced again G₂/M cell cycle arrest through inhibition of cyclin-dependent kinases (Cdc2) [275]. Different pathways of apoptosis were addressed by **FKB**. Apoptotic cell death was induced through the intrinsic pathway evident by dysregulation of the Bax/Bcl-2 ratio, cytochrome c release, and caspase-9/-3 activation and the extrinsic pathway by induction of Fas/FasL expression and caspase-8 activation. Activation of Bax, caspase-4 and -12 suggest that ER stress pathway was involved as well. **FKB** increased intracellular ROS apparent by up-regulation of oxidative stress markers (HO-1, Nrf2). Moreover, **FKB** inhibited Akt/p38 MAPK signaling pathways which both play a critical role in the regulation of cell proliferation and apoptosis. The same observations were made in a human squamous carcinoma (KB) [276]: **FKB** induced apoptosis involving both mitochondrial and death cell receptor mediated pathway. Again, G₂/M arrest was caused by repression of cyclin A, cyclin B₁, Cdc2, and Cdc25C. Interestingly, **FKB** had also an impact on MMP and TIMP, which play a role in tumor metastasis and - as mentioned above - in pathogenesis of liver fibrosis. **FKB** led to mitochondrial dependent apoptosis in colon cancer cells (HCT116) [277]. Again, ROS and ER-dependent mechanism are discussed. GADD153 (growth arrest and DNA damage-inducible gene 153), a marker for ER stress, was up-regulated by **FKB** treatment. Consistently, expression of Bcl-2 was reduced whereas pro-apoptotic Bim was up-regulated causing mitochondrial apoptosis. Like in other cell lines, proliferation was inhibited via induction of G₂/M arrest. Finally, autophagy signs were observed after **FKB** treatment. **FKB** targeted mitochondrial dependent pathways (dysregulation of Bcl/Bax, cytochrome c release, caspase activation) and mitogen-activated protein kinase (JNK) in lung cancer cells (H460) [278]. The anti-proliferative activity of **FKB** is once again in accordance with caused G₂/M cell cycle arrest.

Moreover, the anti-inflammatory potential of **FKB** was assessed: **FKB** showed potent COX-I inhibitory activity [118]. The LPS-induced generation of NO and PGE₂ was significantly decreased by **FKB** in RAW 264.7 cells [279]. NF-κB translocation was inhibited by **FKB**, which was connected to prevention of IκB degradation. Furthermore, **FKB** (200 mg/kg)

decreased the NO concentration after LPS treatment in mouse serum and suppressed the expression of pro-inflammatory proteins (iNOS, COX-2, NF- κ B) in mouse liver.

However, **FKB** raised suspicion of being responsible for the hepatotoxic side effects observed after consumption of kava (see chapter 3.3.3). Zhou et al. demonstrated enhanced cytotoxicity in human hepatoma HepG2 cells (IC_{50} 15.3 μ M) and the human hepatocyte cell line L-02 (IC_{50} 32 μ M) using MTT assay [212]. The mechanism discussed for apoptosis-inducing effects in several cancer cell lines may in the same way affect normal cells, in particular hepatocytes. **FKB** induced oxidative stress and depleted GSH levels leading to sustained activation of mitogen activated protein-kinases (mainly p38 and JNK) and subsequent cell death. Through inhibition of I κ B kinase (IKK) followed by down-regulation of NF- κ B transcriptional activity, hepatocellular survival is impaired. Interestingly, exogenous supply with GSH normalized NF- κ B and MAPK signaling suggesting that GSH depletion is basically responsible for observed toxicity. *In vivo*, **FKB** (25 mg/kg/d, one week) inhibited hepatic NF- κ B transcriptional activity and caused severe liver damage in mice. Li and coworkers evaluated the cytotoxicity of flavokawains (**FKA**, **FKB**, and **FKC**) and **A** on HepG2 and L-02 using MTT assay [280]. Toxicity was found to be **A** (IC_{50} 31 \pm 4 μ M) > **FKB** (IC_{50} 35 \pm 3 μ M) > **FKC** (IC_{50} 57 \pm 2 μ M) for L-02 and **A** (IC_{50} 23 \pm 3 μ M) > **FKB** (IC_{50} 59 \pm 3 μ M) > **FKC** (IC_{50} 62 \pm 5 μ M) for HepG2. The findings suggest a certain hepatotoxic potential of these compounds, which has to be incorporated in the valuation of the results determined on activated HSC. For additional information, the hepatotoxic potential of flavokawains is extensively discussed in chapter 3. Toxicity studies of suspicious compounds, especially flavokawains and **A**, on primary human hepatocytes (PHH) are urgently required. Validation of assay results obtained with HSC will be not possible until impairment of "healthy" liver cells, especially hepatocytes, is excluded. For **XAN**, lacking hepatotoxicity has already been proven on PPH and *in vivo* [281,282].

The anti-inflammatory activity of **A** (also known as cardamonin) is addressed in several publications. Lee et al. first identified **A** as potent inhibitor of NF- κ B activation in LPS-stimulated RAW 264.7 cells [283]. TNF α and NO production as well as the expression of iNOS and COX-2 were decreased by **A** in a dose-dependent manner. Thereby, **A** inhibited the translocation of NF- κ B through suppression of I κ B degradation and phosphorylation and IKK activation. Another study on IFN- γ and LPS-induced RAW 264.7 cells largely confirmed these results [284]. Authors found that reduced NO and PGE2 production was attributed to down-regulation of both inducible enzymes, iNOS and COX-2, and not to direct enzyme inhibition. **A** showed similar inhibitory effects on these pro-inflammatory mediators in LPS/INF- γ -stimulated microglia cells (BV-2) [285], in LPS-stimulated ICR mice [286], and myeloma cells [287]. **A** exhibited also anti-inflammatory activity in whole blood systems by

decreasing both NO and PGE2 production after stimulation with LPS or INF- γ [288]. Moreover, thromboxane B2 (TxB2) secretion was suppressed with a certain selectivity of COX-2 pathway inhibition. Another study on human monocytes and murine macrophages (RAW) revealed again inhibition of NO production and iNOS expression, however, no effect on COX-2 expression was observed in this model [289]. In contrast to other studies, NF- κ B signaling pathways were affected through inhibition of NF- κ B-DNA binding and not through inhibition of I κ B degradation or phosphorylation of NF- κ B. Furthermore, no effect on MAPK phosphorylation was observed.

A induced apoptosis by enhancement of TNF-related apoptosis inducing ligand (TRAIL)-related pathways [290]. Apoptosis was mediated by up-regulation of death receptors (DR4 and DR5), decrease of Bcl-xL levels, and activation of caspases-8, 9, and 3. A further study could show that up-regulation of death receptors was due to induction of CCAAT/enhancer binding protein homologous protein (CHOP) and increased production of ROS [291]. Furthermore, the impact of **A** on the migration and invasion of sarcoma cells was investigated. **A** targeted the expression of transglutaminase-2 and several matrix metalloproteinases [292].

The cytotoxic effect of **P** was evaluated in several cancer cell lines, including HeLa and HepG2 [293], KB, MCF7, A549, Caski, HCT116, HT29, and non-human fibroblast cell line (MRC 5) [264]. Remarkable cytotoxic effects at low micromolar concentrations were observed on KB, MCF7, and Caski cells.

The influence of the test compounds on LPS-induced NO production and iNOS expression were examined in RAW 264.7 [101]. Dihydrochalcones and **3OHHeli** were the least active compounds. In the Griess assay, inducing NO production either with LPS or a combination of LPS and INF- γ , highest inhibitory activity was found for **FKB**, **FKC**, **A**, **Heli**, **XANH**, and pyrano-chalcones respectively. **A**, **Heli**, and **XANC** already reduced NO at low concentrations of 2 μ M. The expression of iNOS was significantly inhibited by all test compounds except **4MeXAN**, and **3OHHeli**. At 5 μ M, **A** was the most active compound, followed by **XANC**, **FKB**, **XANH**, and **Heli**. Summing up, chalcones in general possess a potential impact on LPS and INF- γ induced NO production and iNOS expression. The α,β -unsaturated ketone seems to be a required structure element as dihydrochalcones lacked distinct activity. Furthermore, additional hydroxylation in position 3 in case of **Heli** (**3OHHeli**) lowers the activity perhaps due to higher hydrophilicity and resulting lower intracellular concentration. Prenylation in position 3' does not enhance the biological activity. Non-prenylated chalcones (**A**, **FKB**, **Heli**) were more active.

The cytotoxicity of prenylated and non-prenylated chalcones with different substitution pattern was assessed in HeLa cells. IC_{50} values ranged in low two digit micromolar concentrations, **Heli** ($5.2 \pm 0.8 \mu\text{M}$) being the most cytotoxic of the test compounds [98,294]. Furthermore, anti-oxidant and anti-inflammatory properties were determined using oxygen radical absorbance capacity (ORAC)-fluorescein and ICAM-assay respectively [97]. Most compounds showed moderate to high anti-oxidant activities in a concentration range between 0.1 and 1.0 μM . The anti-oxidant capacity, expressed as Trolox (6-hydroxy-2,5,7,8-tetramethylchroman-2-carboxylic acid) equivalents, was highest for **XANH** (4.8 ± 0.1), **Heli** (4.4 ± 0.6), and **FKC** (4.0 ± 0.5). The TNF α -induced expression of the adhesion molecule ICAM-1 was most strongly inhibited by **3OHHeli** and **3OHXANH** both possessing caffeoyl substructure [97].

4.1.3 Chalcones with anti-fibrotic effects

To date, only a few chalcones have been analyzed regarding their inhibitory, anti-proliferative, or apoptotic effects on activated hepatic stellate cells *in vitro* and *in vivo*.

Zhang and coworkers discovered protective effects of hydroxysafflor yellow A (HSYA), a glucosylated chalcone derivative from safflower, against carbon tetrachloride-induced liver fibrosis in Sprague-Dawley rats [295]. Animals were subjected to CCl_4 injections twice a week, with or without additional intraperitoneal application of 5 mg/kg/d HSYA over a period of 12 weeks. Control animals received isovolumetric olive oil i.p. injections alone or in combination with HSYA at same doses. Liver histology and determination of hydroxyproline content, a marker of collagen disposition in the liver, resulted in a significant reduction of CCl_4 -elevated fibrotic areas and hydroxyproline levels in HSYA treated rats. Moreover, gene expression of α -SMA, collagen α type 1, TIMP-1, MMP-9 was inhibited by HSYA suggesting a suppression of HSC activation. In accordance to these effects, an inhibition of TGF- β signaling pathways leading to reduced phospho-Smad4 levels was observed within the HSYA group. Taken together, the data imply an anti-fibrotic effect of HSYA by blocking TGF- β 1-regulated HSC activation. An additional hepatoprotective potential is postulated as serum transaminase levels were significantly reduced by HSYA as well. Another study using the same experimental design explained the observed anti-fibrotic effects of HSYA by decreased expression levels of myocyte enhancer factor (MEF-2C), inhibition of ERK5 phosphorylation, and attenuated TGF- β signaling [296]. Furthermore, HSYA induced apoptosis in culture-activated stellate cells from rats by suppression of ERK1/2 activation, subsequent decrease of Bcl-2/Bax ratio, enhanced cytochrome c release, and caspase-9/-3 activation, suggesting the involvement of mitochondrial pathways [297].

Butein (2',3,4,4'-tetrahydroxychalcone) showed an anti-proliferative effect on cytokine stimulated rat stellate cells [298]. In addition, mRNA expression levels of key factors in

hepatic fibrogenesis, namely collagen I, α -SMA, and TIMP-1 were significantly suppressed after butein treatment. Taken together, these findings indicate an inhibition of HSC transformation and exuberant collagen deposition. A recent *in vitro* study investigated the protective effects of butein, betulin, and betulinic acid on acetaldehyde-induced cytotoxicity and activation of rat liver stellate cells [299]. Preincubation with betulin (10 μ M), but not with betulinic acid and butein, significantly decreased the toxicity of acetaldehyde on HSC. The intracellular levels of α -SMA and procollagen type 1, migration of HSC, TIMP-1/-2 and ROS production were significantly reduced by all three compounds. However, only butein (10 μ M) decreased the acetaldehyde-induced production of TGF- β 1 and TNF- α without having effects on MMP-2 concentrations. As described before, the chalcone butein is a potent inhibitor of lipid peroxidation and ROS generation. As ROS derived from Kupffer cells or damaged hepatocytes is known to mediate HSC activation, the anti-oxidant activity of butein may contribute to its inhibitory effects regarding HSC transformation.

The synthetic chalcone derivative 2',4',6'-tris(methoxymethoxy)chalcone (TMMC) exhibited anti-proliferative effects on activated rat HSC in a dose dependent manner (5-20 μ M) [300]. These findings were attributed to observed induction of heme oxygenase 1 (HO-1) by TMMC. HO-1 is expressed in HSC during chronic liver injury and its specific activation is discussed to trigger anti-proliferative effects and therefore may limit the progression of fibrosis. Furthermore, TMMC decreased intracellular GSH, which activates extracellular signal-regulated kinase (ERK) belonging to the family of MAPK. TMMC induced ERK activation and in turn led to transcriptional activation of activator protein 1 (AP-1), a major transcription factor involved in HO-1 gene transcription. Authors conclude that the described pathway is responsible for observed anti-proliferative effects of TMMC. Another study investigated the induction of apoptosis by TMMC on activated rat HSC [301]. As mentioned before, apoptosis of activated HSC is proposed as therapeutic strategy in the resolution of the fibrotic process. At concentrations of 30 to 50 μ M, TMMC induced apoptosis in activated HSC by a caspase-dependent pathway. Authors attribute the effects of TMMC on apoptosis to histone deacetylase (HDAC) inhibition which is involved in the expression of apoptosis-related genes. Indeed, TMMC enhanced the expression of Fas-ligand (FasL) which subsequently leads to caspase-3 activation and apoptosis. Moreover, TMMC exhibited protective effects in CCl₄-injured rat livers and reduced the expression and mRNA levels of α -SMA. Increased poly(ADP-ribose) polymerase (PARP) cleavage products after TMMC treatment suggest the elimination of CCl₄-activated HSC by apoptosis as PARP is a substrate of active caspase-3.

Similar effects on the proliferation of serum or growth factor-induced rat HSC were demonstrated for isoliquiritigenin (2',4,4'-trihydroxychalcone) [302]. Again, the induction of

HO-1 expression and the involvement of mitogen-activated protein kinase and phosphatidylinositol 3-kinase-Akt-p70^{S6K} pathways could be shown *in vitro*.

Six flavonoids, including chalcone and the dihydrochalcone phloretin, were tested on stimulated HSC-T6 [303]. All compounds inhibited the proliferation of activated HSC in low micromolar concentration ranges. Ring-closed flavonoids and chalcones showed similar activities. The hydroxylation in position 4' enhanced the anti-proliferative activity.

XAN, which was also investigated in the present study, demonstrated inhibitory effects on liver inflammation and fibrosis both *in vitro* and *in vivo* [281]. *In vitro*, the mRNA expression of two markers of HSC activation, α -SMA and collagen type I, were significantly reduced after treatment with 5 μ M and 10 μ M **XAN** for 3 days. Apoptosis was induced in activated HSC already at low concentrations of 5 μ M. Noteworthy, cytotoxic effects of **XAN** were absent in PHH up to concentrations of 50 μ M. The expression of pro-inflammatory cytokines, MCP-1 and IL-8, was reduced in HSC and PHH respectively. Both basal and TNF induced NF- κ B activity was significantly decreased by **XAN** (5 μ M). NF- κ B is a central factor responsible for HSC activation and resistance to apoptosis and regulates as well the expression of pro-inflammatory chemokines. *In vivo*, the effect of **XAN** was assessed in a murine model of NASH which is characterized by fatty infiltration (cholesterol) of the liver, leading to inflammation, hepatocellular damage, and fibrosis. Although **XAN** (1% w/w in the chow) showed no effects on hepatic steatosis, hepatic inflammation was inhibited by **XAN** treatment displayed in the suppression of TNF, IL-1, MCP-1, and ALT and AST serum levels. Furthermore, the expression of the pro-fibrogenic genes TGF- β and TIMP-1 was reduced by **XAN** nearly to control state. The elevated collagen type I mRNA levels were as well decreased in mice receiving **XAN**. In addition to the NASH model, protective effects of **XAN** feeding (1 mg/g body weight) were studied in carbon tetrachloride-induced liver fibrosis in mice [304]. Liver weight and serum transaminase levels were significantly elevated 72 h after CCl₄-injection in both the control and **XAN** group. Nevertheless, **XAN** exhibited a distinct inhibitory activity on pro-inflammatory (TNF, IL-1, MCP-1, ICAM-1, NF- κ B) and pro-fibrogenic (TGF- β , collagen I, TIMP-1, α -SMA) gene expression. These results indicate a suppressive effect of **XAN** on both hepatic inflammation and HSC activation, which protects against the progression of CCl₄-induced hepatic fibrosis. A previous study has shown that **XAN** feeding alone did not impair organ functions or homeostasis in mice [282].

Summing up, the chalcone structure comprises promising pharmacological properties for the prevention and treatment of hepatic fibrosis due to modulatory activity on ECM proteins, anti-inflammatory activity, and anti-proliferative and apoptosis-inducing effects. These encouraging results were picked up in the present study for further investigation of structurally related prenylated and non-prenylated chalcones and dihydrochalcones on activated human HSC.

4.2 Aim of the study

The study was aimed to evaluate the inhibitory activity of chalcones on activated human hepatic stellate cells. Therefore, the effect of the test compounds on cell viability and proliferation was assessed using MTT assay, CV assay, and fluorescence microscopy. Moreover, to investigate the impact on cell organelles, a high content analysis (HCA) assay was established on HSC applying fluorescent staining of nuclei, mitochondria, and F-actin. This allows a comparative and contemporaneous evaluation of chalcone-induced alterations on the organelle level. Furthermore, cytochrome c release as an early apoptosis marker was determined. By analyzing the fluorescence intensity of Hoechst-stained cell nuclei, the DNA content and herein the influence of the test compounds on the cell cycle phase distribution can be studied.

Finally, the objective of the study was to identify structure elements, which enhance or attenuate the activity on HSC. **XAN** has already shown protective effects against hepatic inflammation and fibrosis *in vitro* and *in vivo* [281,304]. This study provides additional information on **XAN** metabolites and other prenylated and non-prenylated derivatives that have not been tested on HSC yet. Based on the findings of this study, potent chalcones may be identified and elected for further pharmacological testing and elucidation of molecular mechanisms.

4.3 Results and discussion

4.3.1 Analytical characterization of test compounds

Prior to *in vitro* testing, the 21 structurally related test compounds were analytically characterized to ensure adequate purity degrees and to gain a first insight in lipophilicity of the test chalcones, which might have influence on cellular absorption, distribution, and finally biological activity. Therefore, also log P values as a measure of lipophilicity are indicated in Table 4.1. Among the test compounds, there were seven chalcones with variable methoxylation pattern of the A ring and different B ring moieties, four prenylated chalcones, three 3'-(3''-hydroxy-3''-methylbutyl)-derivatives, two pyrano-, and three dihydrochalcones (Figure 4.1).

XAN was provided by the Nookandeh Institute with a purity degree of 98%. **P** was purchased from PhytoLab with a purity degree of 91%. The other test chalcones were obtained by synthesis (see chapter 2.4).

Identity of synthesized chalcones was confirmed by ¹H NMR spectroscopy (see chapter 2.1.3.2). Purity of test compounds was determined by HPLC (10 μM; 20 μL) using method **P2** (see chapter 2.1.3.3). Additionally, for estimation of purity and lipophilicity, HPTLC analysis

(500 μ M; 7.5 μ L) was performed using solvent system **T1+FA** and derivatization reagent **D2** (see chapter 2.1.3.1).

Table 4.1: Analytical features of the test compounds. R_f values for estimation of lipophilicity determined by HPTLC. Purity (p [%]) analysis was performed by HPLC (P2). Log P values are derived from SciFinder. (*) not tested, (-) not determined.

| | Compound | systematic name | R _f | p | log P |
|----|-------------------|---|----------------|----|-----------------|
| 1 | FKA | 2'-Hydroxy-4,4',6'-trimethoxychalcone | 0.49 | 99 | 4.24 \pm 0.42 |
| 2 | FKB | 2'-Hydroxy-,4',6'-dimethoxychalcone | 0.56 | 94 | 4.21 \pm 0.37 |
| 3 | FKC | 2',4-Dihydroxy-,4',6'-dimethoxy-chalcone | 0.25 | 99 | 4.00 \pm 0.41 |
| 4 | A | 2',4'-Dihydroxy-6'-methoxychalcone | 0.31 | 99 | 3.61 \pm 0.34 |
| 5 | P | 2',6'-Dihydroxy-4'-methoxychalcone | 0.34 | 91 | 4.22 \pm 0.35 |
| 6 | 4AcXAN | 4-Acetoxy-2',4'-dihydroxy-6'-methoxy-3'-prenylchalcone | 0.25 | 96 | 4.49 \pm 0.41 |
| 7 | dhXANC | 2'',2''-Dimethyl-3'',4''-dihydro-(2H)-pyrano[2'',3'':3',4']-2',4-dihydroxy-6'-methoxychalcone | 0.35 | 98 | 4.47 \pm 0.42 |
| 8 | XANC | 2'',2''-Dimethylpyrano[2'',3'':3',4']-2',4-dihydroxy-6'-methoxychalcone | 0.33 | 97 | 4.84 \pm 0.40 |
| 9 | XANH | 2',4',4-Trihydroxy-3'(3''-hydroxy-3''-methylbutyl)-6'-methoxychalcone | 0.08 | 97 | 3.24 \pm 0.41 |
| 10 | 4MeXAN | 2',4'-Dihydroxy-4,6'-dimethoxy-3'-prenylchalcone | 0.29 | 96 | 5.08 \pm 0.41 |
| 11 | Heli | 2',4,4'-Trihydroxy-6'-methoxychalcone | 0.14 | 99 | 3.41 \pm 0.37 |
| 12 | 3OHHeli | 2',3,4,4'-Tetrahydroxy-6'-methoxychalcone | 0.07 | 98 | 2.63 |
| 13 | XAN | 2',4'-Dihydroxy-6'-methoxy-3'-prenylchalcone | 0.15 | 98 | 4.82 \pm 0.42 |
| 14 | SV 171 (*) | 2',4,4',6'-Tetrahydroxy-3'-prenylchalcone | 0.09 | 86 | - |
| 15 | 4'MeXAN | 2',4-Dihydroxy-4',6'-dimethoxy-3'-prenylchalcone | 0.21 | - | 5.52 \pm 0.43 |
| 16 | SV 249 (*) | 4,6'-Dihydroxy-2',4'-dimethoxy-3'-prenylchalcone | 0.34 | - | - |
| 17 | 3OHXANH | 2',3,4,4'-Tetra(hydroxy)-3'(3''-hydroxy-3''-methylbutyl)-6'-methoxychalcone | 0.04 | - | 2.90 \pm 0.42 |
| 18 | 3OMeXANH | 2',4',4-Tri(hydroxy)-3'(3''-hydroxy-3''-methylbutyl)-3,6'-dimethoxychalcone | 0.06 | - | 3.20 \pm 0.42 |
| 19 | dhHeli | 2',4,4'-Trihydroxy-6'-methoxy-dihydrochalcone | 0.10 | 88 | 3.36 |
| 20 | dhFKC | 2',4-Dihydroxy-,4',6'-dimethoxy-dihydrochalcone | 0.23 | 94 | 3.98 \pm 0.38 |
| 21 | thXANC | 2'',2''-Dimethyl-3'',4''-dihydro-(2H)-pyrano[2'',3'':3',4']-2',4-dihydroxy-6'-methoxy-dihydrochalcone | 0.34 | 87 | - |

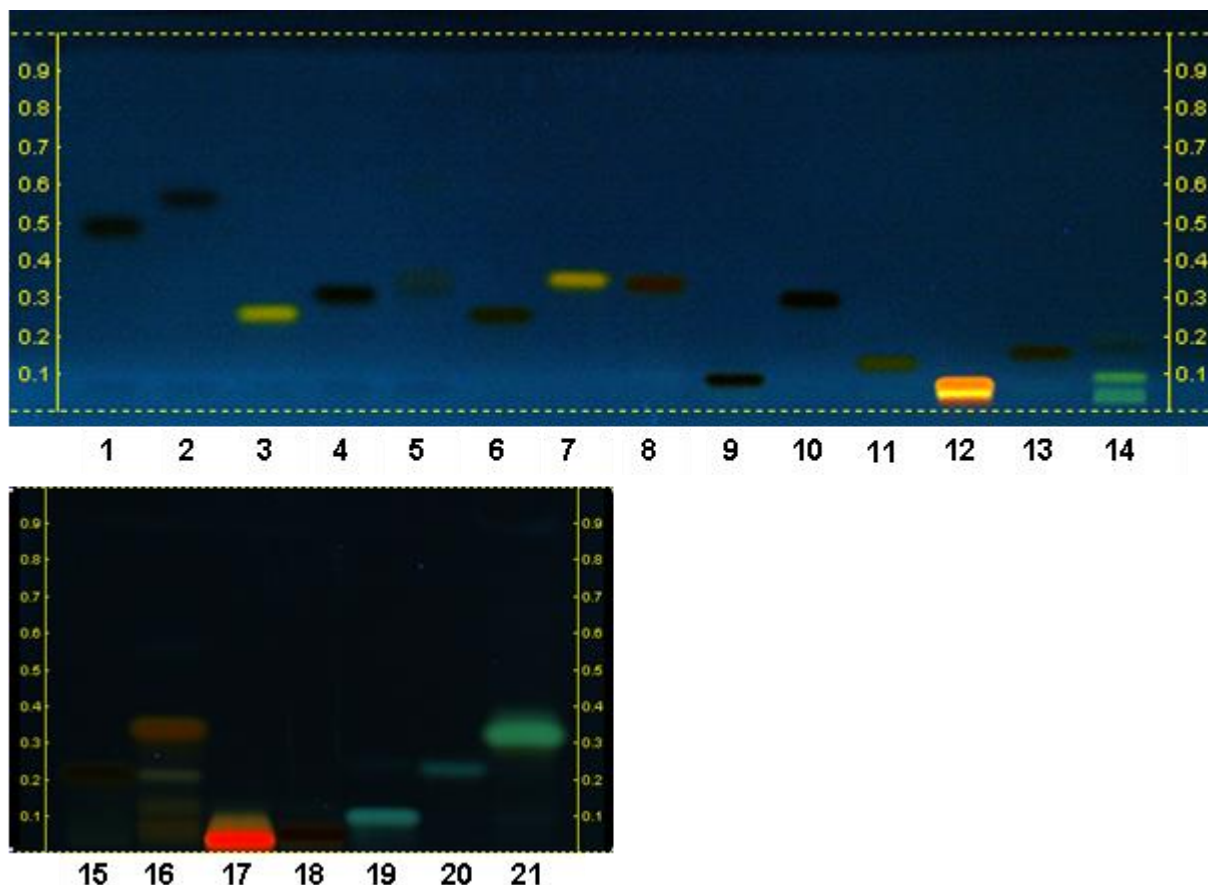


Figure 4.2: HPTLC of test chalcones. Numbers correspond to the compounds listed in Table 4.1. Images were recorded after derivatization with natural product reagent and macrogol (D2) under UV 365 nm.

The purity of the test compounds ranged from 87 to 99%, most chalcones exhibiting a purity degree greater than 95% (Table 4.1). Compound **14** and **16** were excluded from testing due to insufficient purity (< 87%).

Figure 4.2 shows the results of the HPTLC analysis on silica coated glass plates. R_f values of the chalcones in descending order were found to be **2** > **1** > **7** > **5** = **21** > **8** > **4** > **10** > **3** = **6** > **20** > **15** > **13** > **11** > **19** > **9** > **7** > **18** > **17**. Log P values approximately ranged between 3 and 5. **XANH** and derivatives, **Heli** and **3OHHeli** are the most hydrophilic test compounds. Chalcones with unsubstituted B ring exhibit a higher lipophilicity (**FKB**, **A**, **P**). Added prenyl- and methoxy-groups render the molecule even more lipophilic (**FKA**, **XAN** derivatives) whereas hydroxyl groups increase the hydrophilicity. The impact of lipophilicity and structural alterations on the biological effects is discussed in the following chapter.

4.3.2 Effects on cell viability and proliferation

Initially, the influence of selected test compounds on cell viability and proliferation of HSC was assessed in the MTT and CV assay respectively (see chapters 2.2.5.1 and 2.2.5.2). Therefore, the cells were treated with 10, 20, 30, 40, 50, 60, 80, and 100 μM of the test chalcones for 24 h (see chapter 2.2.4.3). Sigmoidal response curves were used for nonlinear

regression and calculation of IC_{50} values. Furthermore, the effect of the compounds on the remaining cell number was analyzed by fluorescence microscopy in the context of HCA (see chapter 2.2.6.1). Test concentrations ranged from 1 to 50 μM . After staining and cell fixation, the fluorescent cell nuclei were automatically counted and the number of nuclei was equated with the number of cells. The number of untreated control cells was set as 100% value and the amount of remaining cells after treatment was referred to this control value. This convenient assay approach directly provides information about the influence on cell proliferation and cytotoxicity comparable to the CV assay.

A summary of assay results is given in Table 4.2. Whenever possible, IC_{50} values were calculated.

Table 4.2: IC_{50} values of chalcones in the different assays determined by nonlinear regression using GraphPadPrism 4 software. Values are expressed as mean \pm SE [μM]. (*) values determined by Dr. Magdalena Motyl [101], (NA) not analyzed, (#) non-sigmoidal behavior of dose response, (no effect) no significant influence up to the highest test concentration (100 and 50 μM respectively).

| Compound | IC_{50} [μM] | | |
|----------|-----------------------------|--------------|-------------|
| | MTT | CV | HCA |
| A | # | > 100 | > 50 |
| P | no effect | no effect | no effect |
| FKA | 90 \pm 12 | > 100 | > 50 |
| FKB | 39 \pm 3 | 68 \pm 8 | 43 \pm 10 |
| FKC | 76 \pm 8 | > 100 | > 50 |
| dhFKC | NA | NA | no effect |
| Heli | 97 \pm 2* | > 100* | > 50 |
| dhHeli | NA | NA | no effect |
| 3OHHeli | no effect* | no effect* | no effect |
| XAN | 65 \pm 4* | 78 \pm 3* | > 50 |
| 4AcXAN | 75 \pm 7* | 87 \pm 17* | > 50 |
| 4MeXAN | #* | #* | no effect |
| 4'MeXAN | NA | NA | 30 \pm 5 |
| XANH | 49 \pm 6* | > 100* | no effect |
| 3OHXANH | NA | NA | > 50 |
| 3OMeXANH | NA | NA | > 50 |
| XANC | 69 \pm 3* | 74 \pm 9* | > 50 |
| dhXANC | 55 \pm 4* | 55 \pm 7* | > 50 |
| thXANC | NA | NA | no effect |

Figure 4.3 compares the compounds' effects on the cell number determined by fluorescence microscopy (HCA). Significant deviations to control cells are indicated above the bar diagrams.

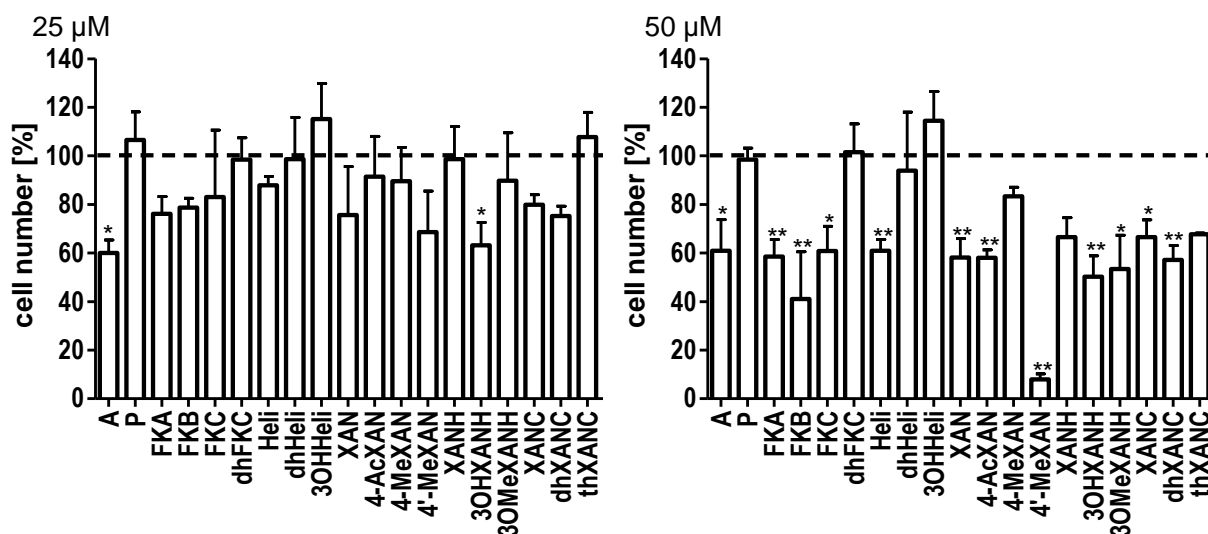


Figure 4.3: Cell number determined by fluorescence microscopy in the context of HCA for test concentrations of 25 µM (left) and 50 µM (right). Values are presented as mean ± SD (n = 3) and refer to untreated control cells (ctl, 100%). Statistical analysis (one-way ANOVA following Dunnett's multi-comparison post-hoc test) was performed using GraphPad Prism 4 software. Levels of significance *p < 0.05, **p < 0.01 vs. ctl cells.

None of the test compounds had significant effects on the cell number at concentrations of 1 and 10 µM (data not shown). Neither **P** nor **3OHHeli** affected cell viability or proliferation up to the highest test concentration of 100 µM (Table 4.2). The dihydrochalcones (**dhFKC**, **dhHeli**, **thXANC**) as well did not show significant influence on the cell number although for **thXANC** a slight decrease could be observed at 50 µM (Figure 4.3).

The mono-, di-, and trimethoxylated compounds **Heli**, **FKC**, and **FKA** exhibited similar effects on cell viability, proliferation, and cell number. IC₅₀ values of 97 ± 2, 76 ± 8, and 90 ± 12 µM were determined in the MTT assay, whereas for the CV assay, IC₅₀ values ranged above 100 µM (Table 4.2). The compounds showed significant cytotoxicity at a concentration of 50 µM (Figure 4.3). In comparison, the B ring unsubstituted chalcones **A** and **FKB** decreased viability and cell number to a higher extent. Albeit no IC₅₀ could be determined for **A** due to non-sigmoidal behavior of dose response curves, the substance significantly affected metabolic functions and cell number at low concentrations of 10 and 25 µM respectively. For **FKB**, IC₅₀ values of 39 ± 3 µM (MTT assay), 68 ± 8 µM (CV assay), and 43 ± 10 µM (HCA) were found (Table 4.2). Thereby, this chalcone constitutes one of the most potent of all test compounds.

The prenylated chalcone **XAN** and its acetylated metabolite **4AcXAN** had comparable IC₅₀ values in the MTT (65 ± 4 and 75 ± 7 µM) and the CV assay (78 ± 3 and 87 ± 17 µM, Table 4.2), and both reduced the cell number to around 60% at 50 µM determined by fluorescence

microscopy (Figure 4.3). However, **4MeXAN** behaved differently. This compound significantly decreased cell viability already at low concentrations (20 μM) in a dose-independent manner without having significant impact on the cell number. In contrast, **4'MeXAN** exhibited strong inhibitory effects regarding the cell number. In the fluorescence microscopic assay, an IC_{50} value of $30 \pm 5 \mu\text{M}$ was calculated for **4'MeXAN** (Table 4.2), thus being the most cytotoxic compound in this set-up.

XANH decreased the cell viability of HSC with an IC_{50} of $49 \pm 6 \mu\text{M}$ whereas the cell number was not significantly affected up to 50 μM . The very polar 3-OH and 3-OCH₃ derivatives of **XANH** significantly reduced the cell number at 25 and 50 μM respectively.

The pyrano-chalcones **XANC** and **dhXANC** diminished the cell viability and proliferation to same extents (IC_{50} for MTT 69 ± 3 and $74 \pm 9 \mu\text{M}$, for CV 55 ± 4 and $55 \pm 7 \mu\text{M}$). At 50 μM , a significant reduction of the cell number was detected for both compounds.

The investigated chalcones show structural similarity regarding the 2' hydroxyl moiety. Jin et al. demonstrated that this structure element has a strong impact on the anti-inflammatory activity of chalcones [305]. Pharmacological properties of chalcones (such as NF- κB inhibition) are often attributed to nucleophilic reactions with the α,β unsaturated ketone. The authors suggest that the electrophilicity of the α,β unsaturated ketone is increased by the 2' hydroxyl group due to formation of a hydrogen bond with the electron pair of the ketone. Furthermore, electron-donating groups in the A ring (e.g. methoxy groups) stabilize the Michael adduct by lowering the acidity of the α -hydrogen. Indeed, this effect could be observed for the test compounds regarding their ability to inhibit NO production and iNOS expression [101]. Inhibitory effects on HSC activation have already been demonstrated for chalcones such as butein [298], isoliquiritigenin [302], and **XAN** [281], all of which exhibiting anti-inflammatory properties. Hence, these properties constitute a beneficial pharmacological feature in the treatment of fibrosis, which is connected to chronic inflammation and inflammatory signals playing also a crucial role in activation of HSC. Moreover, the 2' hydroxyl group increased the anti-proliferative activity of chalcones on HepG2 [306].

From assay results, further structure elements can be identified that enhance or reduce the effect of chalcones on activated HSC. First, the B ring moieties influence both the lipophilicity and the activity. In comparison, the B ring unsubstituted chalcones **A** and **FKB** show a high anti-proliferative potential. **A** and especially **FKB** exhibited a distinct anti-proliferative activity in several cancer cell lines (see chapter 4.1.2). Li et al. found as well that cytotoxic potential of chalcones lacking B ring substitution was enhanced [307]. Hydroxylated or methoxylated derivatives (**FKA**, **FKC**, **Heli**) affected also viability and cell proliferation, however, they were less active. Similar effects were observed on HepG2. The absence of methoxy moieties in the B ring increased the activity [308]. The 4-acetylated **XAN** derivative (**4AcXAN**) behaved

similarly to **XAN** itself. This might be due to rapid deacetylation by cellular esterases. The same observations were made with human hepatoma cell lines (HuH-7, HepG2). Both compounds inhibited cell viability and proliferation to nearly same extents [101]. In contrast, methylation of the hydroxyl group lowered the activity as **4MeXAN** lacked significant effects on the cell proliferation but showed a decline of cell viability already at low concentrations.

The catechol group in ring B constitutes an important structure element favoring the anti-oxidant activity of chalcones [97,309]. However, the ortho-dihydroxy group led to loss of activity in case of **3OHHeli** whereas for **3OHXANH** cytotoxicity was increased compared to **XANH**. Nevertheless, the enhanced radical scavenger activity of 3,4-dihydroxylated chalcones such as butein [310] may contribute to the anti-fibrotic effects due to inhibition of ROS, a mediator of HSC activation. Additional methoxylation in position 3 of **XANH** (**3OMeXANH**) slightly augmented the compound's impact on the cell number at higher concentrations.

The substitution pattern of the A ring triggered as well the pharmacological properties of the chalcones. Contrarily to the B ring substitution, additional methoxy groups in the A ring seem to enhance the activity of the chalcones. A structure activity relationship study found enhanced anti-cancer and NF- κ B inhibitory activity of A ring methoxylated compounds [311]. The 4'-methoxylated **FKC** (IC_{50} 76 ± 8) showed a stronger effect on cell viability of HSC than **Heli** (IC_{50} 97 ± 2). However, these slight effects were absent concerning cell proliferation. The activity of **XAN** was significantly increased with an additional methoxy group (**4'MeXAN**) which led to a noteworthy increase of cytotoxicity. The 3'-prenyl side chain contributes to the chalcones' effects on HSC. Prenyl side chains are associated with different pharmacological effects. For example, the prenyl group contributes to the anti-oxidant [98,312] and cytotoxic [313–315] activity of flavonoids. Compared to **Heli**, the 3'-prenylated **XAN** exhibits stronger effects on cell viability and proliferation. Even more pronounced, this effect can be observed for **4'MeXAN**, which is the 3'-prenylated derivative of **FKC** and shows, as mentioned before, a very strong anti-proliferative activity.

Oxidation of the prenyl side chain results in the formation of phase I metabolite **XANH**. Compared to the parent structure of **XAN**, **XANH** had unexpectedly a distinct impact on cell viability of HSC but only a weak effect on cell proliferation was observed. After formation of an epoxide and subsequent ring closure, the pyrano-chalcone **XANC** and its hydrated analog **dhXANC** arise from **XAN** metabolism. **XAN** has shown to affect viability and induce apoptosis in activated human HSC before [281]. This *in vitro* study now included the investigation of putative **XAN** metabolites, which might occur *in vivo*. Despite the structural variation, the biological activity was quite similar to the parent chalcone concerning their influence on viability and proliferation of HSC, **dhXANC** being slightly more potent. Thus, these **XAN** metabolites may contribute to **XAN**'s anti-fibrotic activity *in vivo* [304].

The Michael system (acceptor of nucleophilic species like GSH or cysteine residues on proteins) has been identified as crucial structure element for biological activity of chalcones before. Hydrogenation of the α,β double bond often led to loss or attenuation of biological activity [305,316,317]. However, the dihydrochalcone phloretin exhibited anti-proliferative activity on stimulated HSC-T6 [303]. In this study, the hydrated derivatives **dhFKC** and **dhHeli** lacked any effects on the cell number of HSC. **thXANC** showed a weak inhibition of cell proliferation which was not significant in the test concentration range. This compound might cause different effects due to the pyrano structure element. Nevertheless, once more the α,β -unsaturated ketone seems to presuppose the chalcone reactivity.

A possible explanation of inactivity of **P** could be the unprotected OH-group in position 6'. This may lead to formation of the corresponding flavanone pinostrobin and account for the loss of activity compared to structurally related chalcones.

No direct correlation between log P and anti-proliferative activity can be observed. The cytotoxic activity of the chalcones rather seems to be influenced by the substitution pattern than by lipophilicity. However, the quite lipophilic **A** (log P 3.61), **FKB** (log P 4.21), and **4'MeXAN** (log P 5.52) were the most active compounds regarding the anti-proliferative activity on activated HSC.

4.3.3 Effects on cell organelles

The influence of the test compounds on different cellular compartments was investigated by HCA (see chapter 2.2.6.1) to identify possible targets or mechanism of toxicity and draw connections between structure elements and biological activity. In general, HCA assays combine a multi-parameter setup usually together with automatic data acquisition and analysis for a fast and information-rich screening of test compounds. In this study, fluorescence microscopy was applied to investigate the influence of the test chalcones on cell organelles of HSC. For this, cell nuclei were stained with Hoechst 33342 and the mean nucleus area was analyzed. Fluorescently labeled actin filaments were used to detect cytoskeleton reorganization and morphological changes. Finally, the mean fluorescence intensity of stained mitochondria served as an indicator for mitochondrial impairment attended by loss of mitochondrial membrane potential.

The alteration of the nucleus area came along with the observed cytotoxic effects of the test compounds (Figure 4.4). The changes of the nucleus area were absent for compounds which neither have shown effects on the cell number before (**P**, **dhFKC**, **dhHeli**, **3OHHeli**, **4MeXAN**, **thXANC**). **A** increased the nucleus area to 1.13 ± 0.06 at 25 μM where it reduced the cell number to 60%. For **FKB** and **4'MeXAN**, a slight decrease of the nucleus area was observed at 50 μM . These compounds are highly toxic and only cell fragments were detected at this concentration. For the other chalcones, a significant increase of the nuclear area was found at 50 μM .

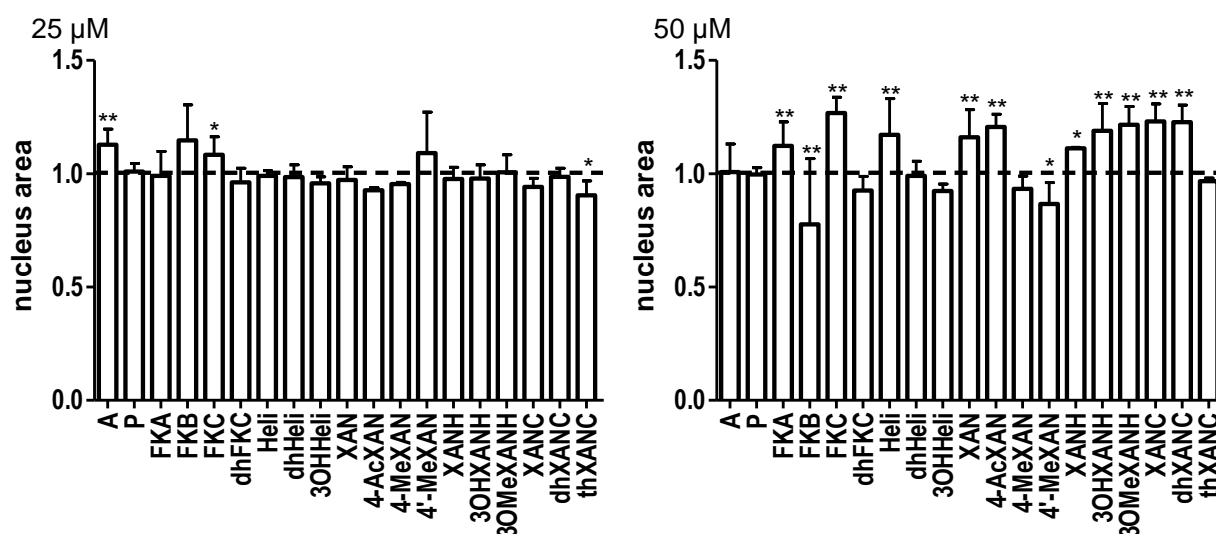


Figure 4.4: Influence of the test compounds on mean nucleus area at 25 μM (left) and 50 μM (right). The mean nucleus area of untreated cells was used as reference and a value of 1.0 was defined for these control cells. The values are presented as the mean \pm SD. Statistical analysis (one-way ANOVA following Dunnett's multi-comparison post-hoc test) was performed using GraphPad Prism 4 software. Levels of significance *p < 0.05, **p < 0.01 vs. ctl cells.

Alteration of the nuclear area is a frequently used marker of cytotoxicity in high content screening [318]. In summary, the influence on the nucleus area can serve as a sensitive marker for cytotoxicity but in the present study it did not reveal pre-lethal effects as alterations only occurred when cell number was already significantly affected.

The dying cell undergoes several morphological and biochemical changes. Necrosis leads to loss of membrane integrity, swelling, and disruption of the cells whereas apoptosis is characterized by membrane blebbing, cell shrinkage, chromatin condensation, and DNA fragmentation. During apoptosis, the reorganization of the cytoskeleton is a crucial process [319]. First, the formation of stress fibers (short, bundled actin filaments) and lamellipodia can be observed leading to cell rounding and detachment from ECM. Cell rounding is accompanied by actin-reorganization into a peripheral ring. Myosin light chain phosphorylation leads to contraction of the actin ring and formation of membrane protrusions

(blebs). These blebs play a major role for chemotaxis and recognition by phagocytes. Finally, actin is depolymerized and the cell is dismantled into apoptotic bodies [319].

Interestingly, the area of detected actin filaments was more selectively affected by the test chalcones (Figure 4.5). Significant effects were only present for **A**, **FKA**, **FKB**, and **4'MeXAN**. The latter two compounds exhibit strong cytotoxic effects at 50 μ M and the results have to be assessed carefully. Although the prenylated chalcones, the **XANC**, and the **XANH** derivatives significantly reduced the cell number, no alterations of the actin area were observed. **Heli** and **FKC** neither affected the actin area, contrarily to the structurally related **A** and **FKA** which might be due to a different mechanism of action.

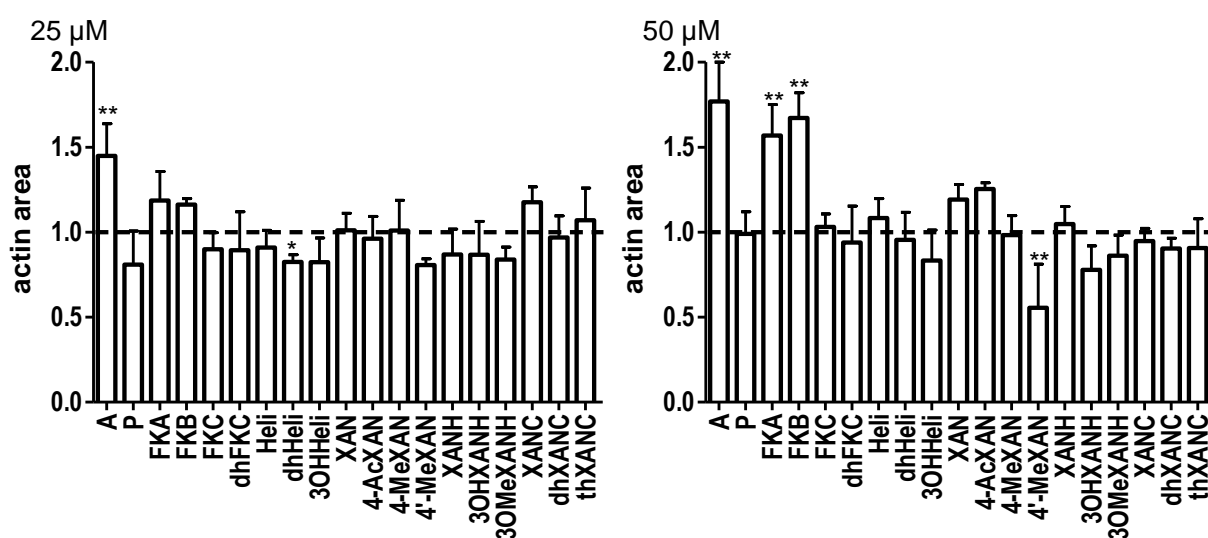


Figure 4.5: Influence of the test compounds on mean area of detected actin filaments at 25 μ M (left) and 50 μ M (right). The mean actin area of untreated cells was used as reference and a value of 1.0 was defined for these control cells. The values are presented as the mean \pm SD. Statistical analysis (one-way ANOVA following Dunnett's multi-comparison post-hoc test) was performed using GraphPad Prism 4 software. Levels of significance *p < 0.05, **p < 0.01 vs. ctl cells.

Overall, within the used image analysis protocol, the observed effects on actin were only weak. For a more sensitive and precise analysis of the effects on actin, protocols should further be refined and adapted. Moreover, by choosing suitable positive controls the influence on actin polymerization and depolymerization could be studied.

Mitochondria fulfill numerous tasks. They are responsible for the energy supply and the Ca^{2+} homeostasis in cells, and occupy as well a regulatory role in apoptosis [320]. In early stages of programmed cell death, mitochondrial transition pore opening leads to dissipation of mitochondrial transmembrane potential, and permeabilization of the mitochondrial outer membrane [321,322]. The fluorescence intensity of mitochondria was analyzed to detect impairment of these organelles by the test compounds. Mitochondria constitute sensitive and

early indicators of cellular dysfunction that are affected long before cell number decreases. Either an increase or a decrease in mitochondrial fluorescence intensity indicates a disturbance of the mitochondrial health of the cell. An increase of fluorescence intensity shows an accumulation of the fluorescent dye often attended by swelling of mitochondria and loss of function. A decrease of fluorescence intensity indicates a loss of mitochondrial membrane potential, which can precede both necrotic and apoptotic cell death.

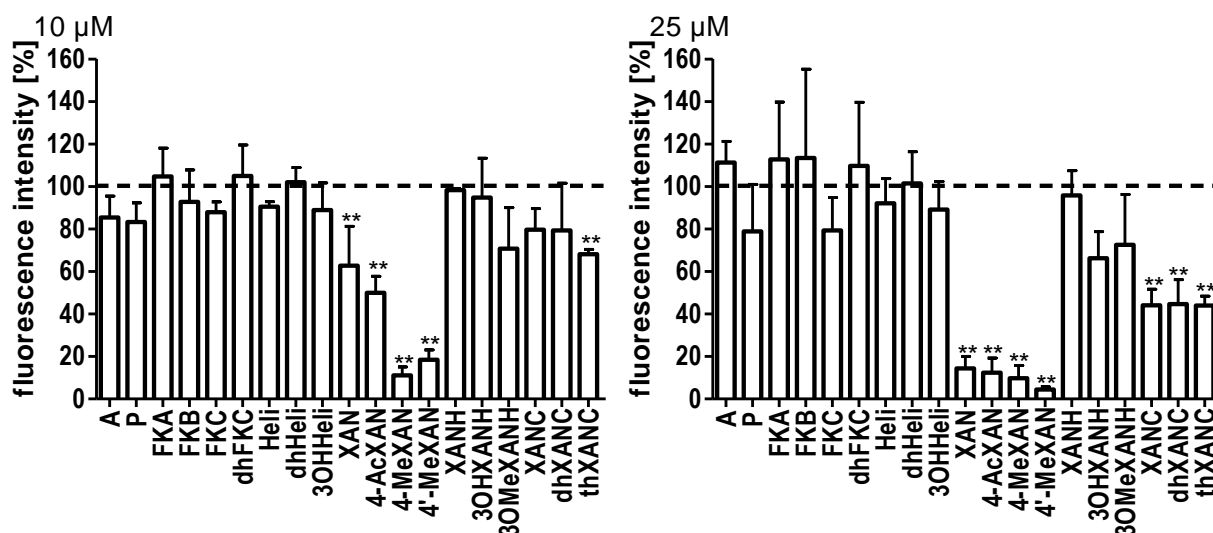


Figure 4.6: Influence of the test compounds on the fluorescence intensity of mitochondria at 10 µM (left) and 25 µM (right). The mean total fluorescence intensity of mitochondria of untreated cells was set as 100% value. Values are presented as mean \pm SD. Statistical analysis (one-way ANOVA following Dunnett's multi-comparison post-hoc test) was performed using GraphPad Prism 4 software. Levels of significance * $p < 0.05$, ** $p < 0.01$ vs. ctl cells.

Effects on the mitochondrial fluorescence intensity could be observed already at low concentrations starting at 10 µM (Figure 4.6). Remarkably, only the 3'-prenylated compounds and the dihydrochalcone **thXANC** showed a significant decrease of the fluorescence intensity at this concentration. At 25 µM, besides the prenylated chalcones, also the pyrano-chalcones reduced the mitochondrial fluorescence intensity. Neither the 3'-unsubstituted chalcones nor the **XANH** derivatives exhibited significant effects at this concentration. This constitutes a quite interesting finding since on the one hand the potent decrease of fluorescence intensity is limited to the prenyl- and pyrano-chalcones and on the other hand this effect can be observed at pre-lethal concentrations where the cell number is not yet affected.

For **A** ($232 \pm 80\%$), **FKA** ($163 \pm 39\%$), and **FKB** ($463 \pm 180\%$) a strong increase of fluorescence intensity was measured at 50 µM. This might be due to the observed cytotoxicity of these test compounds, which is attended by mitochondrial damage. Despite the structural relation, **Heli** showed no influence on the fluorescence intensity although being cytotoxic at this concentration. For **FKC** ($62 \pm 29\%$) and **3OHXANH** ($37 \pm 5\%$) a significant fluorescence intensity reduction was detected at 50 µM. **P**, **dhFKC**, **dhHeli**, **3OHHeli**, **XANH**,

and **3OMeXANH** lacked any effects on the fluorescence intensity of mitochondria even at 50 μ M.

The impact of hydroxychalcones on the mitochondrial membrane potential has been examined before in cancer cell lines [323] and rat hepatocytes [324]. GSH depletion and the generation of ROS were observed. Both trigger the formation and opening of mitochondrial transition pores, leading to loss of mitochondrial transmembrane potential and the release of pro-apoptotic factors [322].

4.3.4 Cytochrome c release

Apoptosis (programmed cell death) is essential for embryogenesis, tissue homeostasis, and the removal of unwanted cells. Dysregulation of this crucial event can lead to immunodeficiency, autoimmune disorders, and cancer in the last resort. Aberrant apoptosis is also linked to the progression of chronic liver diseases such as liver fibrosis [243]. Hence, the apoptotic clearance of activated hepatic stellate cells, the key mediators in the fibrinogenic process, constitutes an interesting therapeutic tool in the resolution of hepatic fibrosis [244].

Two major pathways of apoptosis are known: the extrinsic (death receptor pathway) and the intrinsic pathway (mitochondrial pathway) [325]. Besides, alternative signaling pathways exist (e.g. autophagy, ER stress pathway). Furthermore, considerable cross talk between the different pathways can be observed. Based on the observed effects on the fluorescent intensity of mitochondria in the HCA assay, further studies concerning mitochondria-related apoptosis were conducted. Therefore, cytochrome c release as an early apoptosis marker was investigated. The intrinsic apoptosis is mainly controlled by the family of B-cell lymphoma 2 (Bcl-2) proteins [326]. Activation of pro-apoptotic proteins Bax and Bak initiate the permeabilization of the outer mitochondrial membrane, which leads to the release of cytochrome c and other pro-apoptotic factors from the mitochondrial inter-membrane space to the cytosol. Here, cytochrome c interacts with apoptotic protease-activating factor-1 (Apaf-1), which leads to ATP-dependent conformational changes, self-aggregation and oligomerization (formation of apoptosome), recruitment of procaspase 9 and its subsequent proteolytic activation. Caspase 9 directly activates effector caspases 3 and 7, which consequently leads to cell death due to controlled proteolytic cleavage of multiple downstream targets [327].

To investigate the cytochrome c release, HSC were seeded in 96-well plates and treated with 10, 25, 50 μ M of test compounds for 24 h (see chapters 2.2.4.2 and 2.2.4.3). The assay was performed according to the described methodology (see chapter 2.2.6.2). Cytochrome c was detected by immunofluorescence. Apoptotic signals lead to a release of cytochrome c from

mitochondria, which then diffuses into the cytosol and nucleus (Figure 4.7, staurosporine-treated cells). This translocation of cytochrome c was used for analysis. Staurosporine, known to trigger cytochrome c release from apoptotic mitochondria, was used as a positive control (p.ctl) for assay protocol development and served also as reference system (100% value).

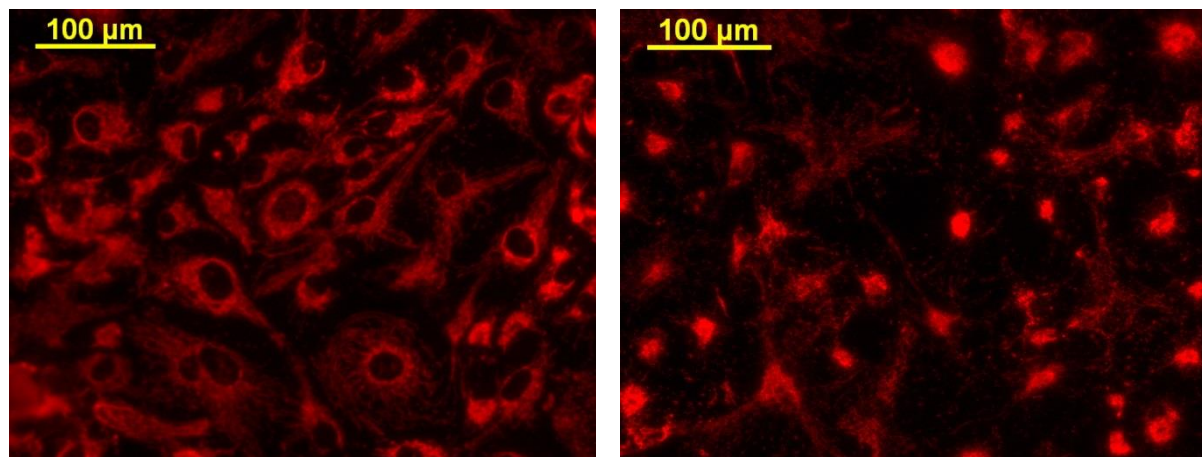


Figure 4.7: Immunofluorescent staining of cytochrome c in untreated (n.ctl, left) and staurosporine (4h, 1 µM)-treated (p.ctl, right) HSC.

Cytochrome c release was detected first in cells treated with 10 µM of **A**, **FKB**, **XAN**, **4AcXAN**, **4MeXAN**, **XANH**, **XANC**, or **dhXANC**, and 25 µM of **FKA**, **Heli**, **4'MeXAN**, and **XANH** derivatives (Figure 4.8).

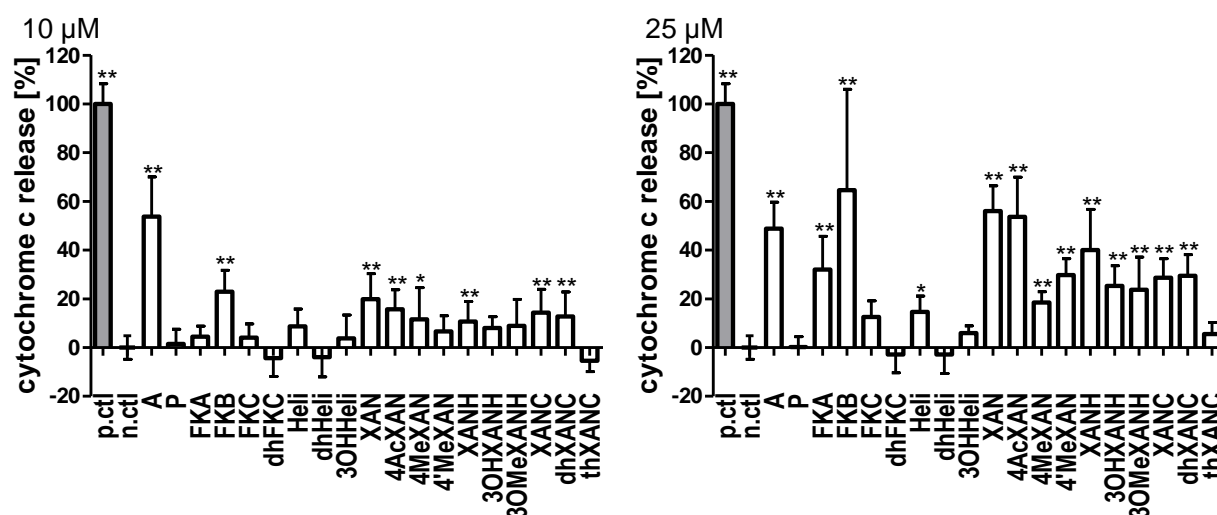


Figure 4.8: Cytochrome c release [%] from HSC after treatment with 10 and 25 µM of test compounds for 24h. Staurosporine (1 µM, 4h) was used as positive control (p.ctl) and reference system (staurosporine effect = 100%) for chalcone effects. Untreated cells (n.ctl) were set as zero value. Values are presented as the mean \pm SD. Statistical analysis (one-way ANOVA following Dunnett's multi-comparison post-hoc test) was performed using GraphPad Prism 4 software. Levels of significance * $p < 0.05$, ** $p < 0.01$ vs. n.ctl cells.

These results are partly consistent with the results obtained by the analysis of mitochondrial fluorescence intensity (see chapter 4.3.3). Whereas the prenyl- and pyrano-chalcones have

shown effects on the mitochondria in the HCA before, cytochrome c release was also observed for **XANH** and its derivatives, **A**, **FKA**, **FKB**, and **Heli**, obviously independent from mitochondrial transmembrane depolarization. There is evidence that cytochrome c release can occur prior to the loss of mitochondrial membrane potential [328]. However, **thXANC** exhibited a strong effect on the mitochondrial fluorescence intensity without inducing cytochrome c release at these concentrations. At 50 μM , the effects were very unspecific. Nearly all compounds (except **P**, **dhFKC**, **dhHeli**) caused a significant increase. These results have to be rated carefully as the release of cytochrome c constitutes an early step of apoptosis and should be observed in pre-lethal states where cell number is not affected yet. Perhaps, also a shorter incubation period would have as well enhanced the specificity of observed effects. At a concentration of 50 μM test compound, also cell morphology was partly altered what limited interpretation of data.

The mitochondrial dependent pathway is an important target of chalcones triggering apoptosis. **FKA** induced apoptosis in bladder cancer cells causing loss of mitochondrial membrane potential and release of cytochrome c via Bax-mediated pathway [269]. As more precisely described in chapter 4.1.2, **FKB** induced apoptosis in several cancer cell lines via the mitochondrial-dependent pathway [274–277]. Enhanced ROS production observed in HCT-116 and HSC-3 seems to serve as a catalyst. **XAN** is known to induce apoptosis in a broad panel of cell lines [101]. Thereby, dependent on the cell type and expression levels, different cell death mechanisms are addressed. Regarding mitochondrial dependent apoptosis, a connection to ROS production was drawn by Strathmann et al. [329]. **XAN** increased the production of superoxide radical anion in isolated mouse liver mitochondria, affected the ATP concentration and mitochondrial membrane potential and led to release of cytochrome c in cancer cells. The same effects were observed in mouse embryo fibroblasts by Yang et al. [330]. **XAN** increased the ROS production which was directly associated with its apoptosis-inducing effects displayed in loss of mitochondrial membrane potential, cytochrome c release, and PARP cleavage. Moreover, **XAN** induced apoptosis in human glioblastoma cells [331]. Increased intracellular ROS was again made responsible for the activation of the intrinsic pathway. Indeed, cytochrome c release, caspase 9 and 3 activation, and down-regulation of Bcl-2 indicated that apoptosis is mediated by mitochondria. Furthermore, **XAN** induced mitochondria-dependent apoptosis in human colon [332] and prostate cancer cells [333]. Taken together, a clear correlation between the enhanced production of ROS, GSH depletion, and the activation of the mitochondrial pathway is likely for the investigated chalcones and has been already demonstrated for **FKB**, **XAN**, and several hydroxychalcones.

Summing up, the prenyl- and pyrano-chalcones provoke a loss of mitochondrial fluorescence intensity followed by a significant release of cytochrome c. The latter is also caused by

XANH and its derivatives but to a lesser extent. **XANH** has shown to evoke a considerable effect on cell viability of HSC, but it did not cause any impairment of the mitochondrial transmembrane potential. Cytochrome c release is also observed after **A**, **FKB**, and **FKA** treatment. None of these compounds induced a loss of mitochondrial fluorescence intensity. However, a distinct increase of fluorescence intensity at 50 μ M suggests a remarkable mitochondrial damage. Compared to their 3'-prenylated analogs, **Heli** and **FKC** only exhibited a weak effect, which even was not significant in case of **FKC**. The two compounds neither affected the fluorescence intensity of mitochondria at same concentrations. As expected from previous results, the dihydrochalcones, **P**, and **3OHHeli** constituted again the least active compounds.

4.3.5 DNA content and cell cycle analysis

Furthermore, the DNA content of treated and untreated HSC was analyzed in the context of HCA. For that purpose, the fluorescence intensity of Hoechst 33342 stained cell nuclei was determined (see chapter 2.2.6.3). As the fluorescence intensity is proportional to the DNA content, the corresponding cell cycle state can be determined and potential influences of the test compounds can be assessed.

DNA replication and cell division are the two primary events in cell proliferation. The cell cycle is divided in sequential phases (Figure 4.9 left):

- the first gap phase (G_1), in which the cell prepares for DNA replication,
- the period of DNA synthesis (S), during which a second copy of the genetic material is generated,
- the second gap phase (G_2), in which the cell prepares for division,
- the mitosis phase (M), during which the two copies of DNA are segregated into two daughter cells.

Cell cycle progression is regulated by an ordered activation of different cyclin-dependent kinases (Cdk). Activation of the Cdk requires the presence of different cyclins, which show altered protein levels during cell cycle. Several checkpoints ensure the proper order and timing of events. Loss of cell integrity or DNA damage leads to arrest of the cell cycle at these checkpoints. Deprivation of growth factors, modulation of Cdk-cyclin activity and other signaling proteins, DNA damage, inhibition of DNA synthesis, interference with topoisomerase II and microtubules, and various apoptotic stimuli may cause cell cycle arrest at different stages. As is known, modulation and arrest of the cell cycle is an important target of anti-proliferative and apoptosis-inducing chalcones [334].

To get an insight into the distribution of cell cycle phases in a normal cell population, the DNA content of untreated control cells was analyzed first (Figure 4.9 right).

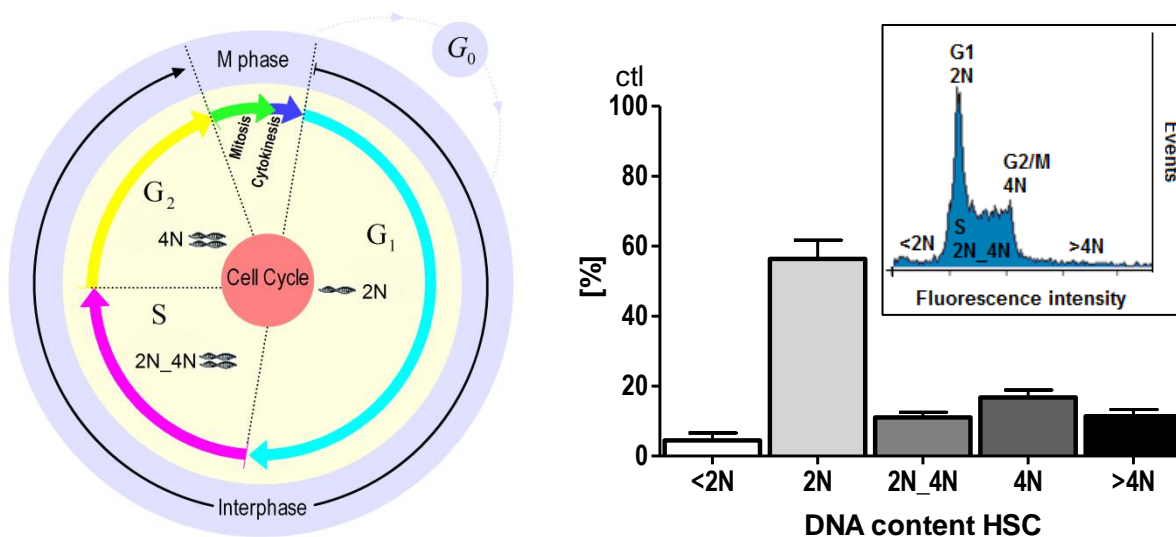


Figure 4.9: Left: Correlation of cell cycle phases and DNA content of the cells. The DNA content of cells can be determined by measurement of fluorescence intensity of Hoechst33342 stained cell nuclei. Right: DNA content of untreated HSC (ctl) ; DNA content (cell cycle phase): 2N (G₀/G₁), 2N_4N (S), 4N (G₂/M), <2N and >4N (abnormal).

In a normal cell population, the major number of the cells should be in the G₁/G₀ phase (2N), a smaller in the G₂/M phase (4N), and a small number in the S phase (2N_4N). This was confirmed by our results. Approximately 56% of the cells had a DNA content of 2N, 11% of 2N_4N, 17% of 4N, 5% of less than 2N, and 11% more than 4N. Hence, round about half of the cell population was in the G₀/G₁ phase and one third in the S/G₂/M phase.

For studying the chalcones' effect on the DNA content of HSC, the ratio of cells with 2N and 4N DNA content was calculated and compared to untreated control cells with a ratio of 3.3 (Figure 4.10). The ratio of 2N/4N is a commonly used value in cell cycle analysis to describe influences of test compounds on cell cycle phase distribution. An increase of the quotient compared to control value indicates an arrest in G₁/G₀ whereas a G₂/M arrest is reflected by a decrease of this ratio.

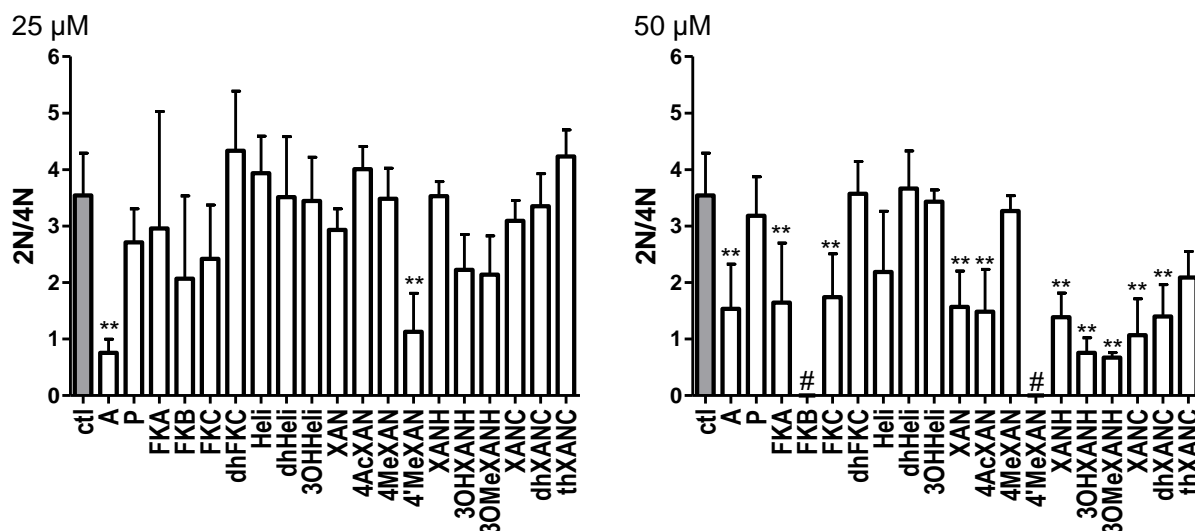


Figure 4.10: Ratio of cells [%] with DNA content of 2N (G₁) and 4N (G₂) (2N/4N) at 25 µM (left) and 50 µM (right). (#) not determined. Values are presented as the mean ± SD. Statistical analysis (one-way ANOVA following Dunnett's multi-comparison post-hoc test) was performed using GraphPad Prism 4 software. Levels of significance *p < 0.05, **p < 0.01 vs. ctl cells.

At 50 µM, all compounds which significantly inhibited cell proliferation showed a reduced ratio of 2N to 4N. For the highly cytotoxic chalcones **A** and **4'MeXAN** this effect already occurred at 25 µM. For **FKB** and **4'MeXAN**, the ratio could not be determined at 50 µM due to low amount of viable cells, however, **FKB** lacked significant effects at lower concentrations either. Again, significant effects were absent for the dihydrochalcones, **P**, and **3OHHeli** which is attended by the low toxicity of these compounds on HSC. **4MeXAN** that affected both cell viability and mitochondrial membrane potential did not have any influence on the DNA content of cells. This finding correlates well with its missing anti-proliferative activity.

The antimitotic activity of chalcones has been recognized quite early [335]. Colchicine, a reversible inhibitor of microtubule assembly, referred as a model substrate for the synthesis of 3',4',5'-trimethoxylated chalcones. Previous SAR studies on colchicine have revealed the importance of the methoxy substituents and the carbonyl group for binding to tubulin. These structure elements were incorporated into the synthesized chalcones. Indeed, these compounds revealed anti-mitotic effects in HeLa comparable to colchicine. The effect of 2'-oxygenated chalcones on cell cycle phase distribution has been studied before in human cancer cell lines (Jurkat, U937) [336]. A distinct anti-proliferative activity and altered distribution of cell cycle phases was observed for the hydroxylated and methoxylated chalcones, 2'-hydroxy-2,3,4',6'-tetramethoxychalcone being the most active and causing G₂/M arrest. A recent study investigated the antimitotic effect of chalcones against leukemia cells K562 [337]. Propidium iodide staining was used for determination of cell cycle state. Several compounds induced G₂/M arrest comparable to vincristine. The methoxylation pattern of the A ring influenced the antimitotic activity clearly favoring di- and trimethoxylation at 2',4',6'-carbons. Substitution of the B ring was found to be less important, however, dimethoxylation

in position 2 and 6 seems to be relevant. In fact, for the 4',6'-dimethoxylated compounds **FKA** [270] and **FKB** [271,274–278], G₂/M arrest was made responsible for their anti-proliferative effect in several cancer cell lines. Also **FKA** led to G₂/M arrest in HSC. **XAN** caused S arrest in breast cancer cells (MDA-MB-435) [338] and S/G₂/M arrest in ovarian cancer cell lines (SKOV3, OVCAR3) [339]. The compounds' influence on the cell cycle is dependent on the cell type, test concentration, and other factors. On activated HSC, **XAN** and its structure analogs induced G₂/M arrest: the number of cells in G₁ was decreased whereas the number of cells in G₂/M increased (Figure 4.10).

The analysis of the DNA content can help to understand and interpret the anti-proliferative activity of the chalcones. The amount of cells with a DNA content of 2N is decreased in favor of cells with a content of 4N. Thus, cells still proceed through the G₁ and S phase but remain in the G₂/M phase whereby normally following cell division is blocked. This is reflected in a decreased cell number after chalcone treatment. Thereby, **A** and **4'MeXAN** showed the strongest impact on the cell cycle phase distribution already at 25 μM.

4.4 Conclusion

The chalcones possess a favorable pharmacological profile for the treatment of diseases, which are attended by inflammatory processes. Moreover, their anti-proliferative and pro-apoptotic activities are broadly investigated in numerous cellular and animal models. Some chalcones have already been tested with regard to their activity against activated hepatic stellate cells, which are considered as the most important cellular target in the treatment of hepatic fibrosis.

A high content analysis (HCA) assay was established to determine effects on the organelle level. This multi-parameter approach enables the detection of pre-lethal effects and can also be combined with other established viability and toxicity assays. HCA therefore constitutes an interesting tool for the quick and simultaneous investigation of several cellular parameters and qualifies this method for structure activity relationship studies.

Table 4.3 summarizes the assay results and effects of the investigated chalcones. For more detailed information about assay results, see the supplementary data in chapter 10.1 (Figure 10.1 – Figure 10.19).

Table 4.3: Overview of assay results. Viability (MTT), prolif (cell proliferation by CV and HCA cell number), nucleus (HCA nucleus area), actin (HCA actin area), mito (HCA mitochondrial fluorescence intensity), cyto c (cytochrome c release), DNA (HCA DNA content). (+ +) strong increase, (+) increase, (- -) strong decrease, (-) decrease, (~) weak effect, (NA) not analyzed.

| | viability | prolif | nucleus | actin | mito | cyto c | DNA |
|-----------------|-----------|-----------|-----------|-----------|-----------|-----------|-----------|
| A | - | -- | + | ++ | ++ | ++ | ++ |
| P | no effect | no effect | no effect | no effect | no effect | no effect | no effect |
| FKA | - | - | + | + | + | + | + |
| FKB | -- | -- | | + | ++ | ++ | ~ |
| FKC | - | - | + | no effect | ~ | no effect | + |
| dhFKC | NA | no effect | no effect | no effect | no effect | no effect | no effect |
| Heli | - | - | + | no effect | no effect | + | ~ |
| dhHeli | NA | no effect | no effect | no effect | no effect | no effect | no effect |
| 3OHHeli | no effect | no effect | no effect | no effect | no effect | no effect | no effect |
| XAN | - | - | + | no effect | -- | ++ | + |
| 4AcXAN | - | - | + | no effect | -- | ++ | + |
| 4MeXAN | - | ~ | - | no effect | -- | + | no effect |
| 4'MeXAN | NA | -- | - | - | -- | + | + |
| XANH | -- | ~ | + | no effect | no effect | + | + |
| 3OHXANH | NA | -- | + | no effect | ~ | + | + |
| 3OMeXANH | NA | - | + | no effect | no effect | + | + |
| XANC | - | - | + | no effect | - | + | + |
| dhXANC | - | - | + | no effect | - | + | + |
| thXANC | NA | ~ | no effect | no effect | -- | no effect | ~ |

XAN was identified as effective inhibitor of hepatic inflammation and fibrosis *in vitro* and *in vivo*. The present *in vitro* study first provides information concerning the activity of **XAN** metabolites and other structurally related 2'-hydroxy chalcones on activated HSC. **XAN** treatment led to apoptosis in HSC through activation of caspase 3 [281]. This study proposes a mitochondrial mediated pathway, attended by loss of mitochondrial membrane potential and subsequent cytochrome c release already at low concentrations of 10 μ M. Interestingly, this was also observed for the **XAN** metabolites **4'AcXAN**, **4MeXAN**, **XANC**, and **dhXANC**. Thereby, the effect on cell viability and proliferation compared to **XAN** was slightly enhanced for the pyrano-chalcones and decreased for **4MeXAN** which did not affect cell number or cell cycle distribution up to a concentration of 50 μ M. **XANH** decreased cell viability but had a weaker impact on cell proliferation. However, **XANH** induced G₂/M arrest and release of cytochrome c without affecting mitochondrial membrane potential. The different behavior might be due to higher hydrophilicity (log P), lower cellular absorption, and altered cellular distribution. Nevertheless, data suggest that tested **XAN** metabolites contribute to **XAN**'s effects *in vivo* affecting same cellular targets and pathways. Data of conjugated **XAN**

metabolites (glucuronides, sulfates) are still missing and should be addressed in future studies because of high *in vivo* relevance (see chapter 5.1.2 for **XAN** metabolism).

In addition, the study was aimed to identify structure elements, which influence the activity of chalcones on HSC (Figure 4.11).

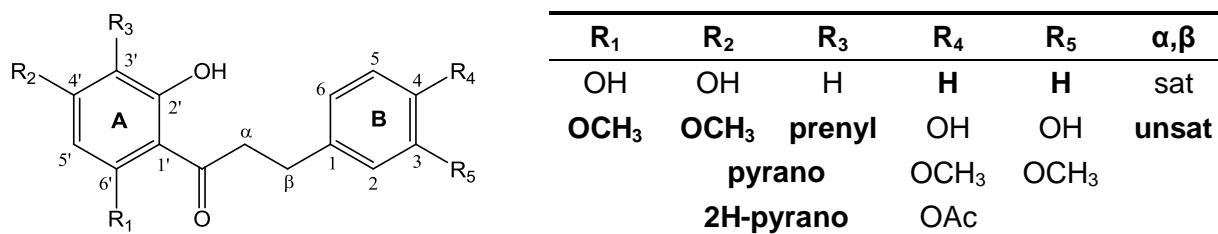


Figure 4.11: General structure and substitution pattern of investigated 2'-hydroxy chalcones. Structure elements, which enhance the activity on activated HSC, are indicated in bold letters.

Like described before, the double bond in α,β position to the carbonyl group is required for the activity of the chalcones. Hydrogenation led to complete loss of activity in case of **dhFKC** and **dhHeli** whereas for **thXANC** still mitochondrial fluorescence intensity was affected. Thus, the Michael system constitutes a crucial structure element, however, substitution of the A ring as well triggers the chalcone activity. **P** with an unprotected hydroxyl group in position 6' lacked any influence on HSC. Perhaps, the cyclisation to the corresponding flavanone is attended by loss of activity. Further investigations of 2',6'-dihydroxy chalcones and corresponding flavanones could verify this assumption. The substitution pattern of the A ring clearly influence the chalcone effects. By comparison, B ring substituents had a weaker impact, even favoring unsubstituted compounds such as **A** and **FKB**. The 3'-prenyl group enhanced the activity of chalcones: in comparison to **FKC** and **Heli** the prenylated analogs **4'MeXAN** and **XAN** were more effective. Furthermore, a prenyl group or a pyrano substitution seems to be a structural requirement for interaction with the mitochondrial membrane. Distinct decrease of mitochondrial fluorescence intensity was selectively observed for these chalcones. In contrast to the B ring, further methoxy groups in the A ring increased particularly the anti-proliferative activity: the 4'-methoxy derivatives **FKB** and **4'MeXAN** were more cytotoxic than **A** and **XAN**. As mentioned above, no explicit connection of log P and activity of the chalcones was found. In general, log P values between 1 and 4 are considered as beneficial for absorption [340]. For quite lipophilic chalcones like **XAN**, rapid cellular uptake, accumulation, and intracellular formation of protein complexes (thiol adducts) were observed in hepatic stellate cells [341]. Chalcones with similar log P might show analog kinetics.

The structural alterations uncovered several chalcones with enhanced *in vitro* activity against activated HSC. Among the test compounds, **A**, **FKB**, and **4'MeXAN** were the most potent. They exhibit strong anti-proliferative activity, induce a release of cytochrome c, and cause

G₂/M arrest. The distinct anti-inflammatory activity of chalcones could turn out to be advantageous for treatment of hepatic fibrosis. **A**, **FKB**, **XAN**, and other chalcones have shown to inhibit NF-κB pathways. Enhanced NF-κB activity plays a central role in HSC activation and perpetuation of hepatic inflammation. Further pharmacological testing of the chalcones should be conducted to illuminate the mechanism of HSC inhibition on the molecular level. The study provides information about structure elements, which contribute to biological effects. Hence, further structures could be synthesized and evaluated concerning their inhibitory activity on activated HSC. In addition, toxicity studies of the compounds are strongly needed. **FKB** is suspicious causing hepatotoxic effects, which would exclude this compound from therapeutic application. *In vitro* evaluation of toxicity on primary human hepatocytes therefore is an indispensable issue.

5 *In vitro* metabolism of chalcones: identification and structure elucidation of microsomal metabolites

5.1 Introduction

5.1.1 *In vitro* metabolism systems and their applications

In vitro metabolism studies constitute an important tool in fundamental research and preclinical screening of drug-like properties [342]. As is known, metabolism is carried out in two general phases: in phase I polar groups are either introduced by oxidation, reduction, and hydrolysis, or uncovered by dealkylation. In phase II polar groups are conjugated with glucuronic acid, sulfate, glycine, glutamine, glutathione, acetate, or methyl groups in order to render the molecule more polar and facilitate the excretion [343]. Metabolites are often less active than the parent drug or even inactive. Sometimes however, biotransformation products show enhanced bioactivity or toxicity. In case of prodrugs, biotransformation is even necessary to convert the drug in its active form as the parent drug is inactive. Metabolism may consequently be involved in both “activation or toxification” and “inactivation or detoxification” [344]. The liver is the major site for metabolism although other tissues as well as the bacterial flora of the gastrointestinal tract contribute to overall biotransformation reactions.

Most important enzymes in drug metabolism are the cytochrome P450 monooxygenases (CYP450) followed by uridine diphosphoglucuronosyl transferases (UGT) and esterases [345]. The cytochrome P450 system consists of a superfamily of isoenzymes with different tissue distribution, regulation, and of course substrate affinity. Two protein components, a heme protein (substrate and oxygen binding site) and a flavoprotein (electron carrier), compose the enzyme system [344]. Cytochrome P450 enzymes are present in the endoplasmic reticulum, thus can be found in microsomal preparations. To date, about 36 human isoforms are known [346]. However, only nine isoforms are mainly involved in drug metabolism, CYP3A4 being the most important isoenzyme responsible for the metabolism of around 50% of approved drugs, followed by CYP2C9, CYP2C19, and CYP2D6 [345,347]. Table 5.1 compiles the main human CYP isoforms, their tissue distribution, model substrates, (selective) chemical inhibitors and inducers.

Table 5.1: Compilation of major human CYP isoforms involved in drug metabolism, their occurrence, model substrates used for quantification of enzyme activity, selective inhibitors, and known inducers of enzyme activity. ^[1] Recommendation of FDA, American Association of Pharmaceutical Sciences (AAPS), and the European Federation of Pharmaceutical Sciences; ^[2] according to Khojasteh et al. [348]; ^[3] according to Brandon et al. [349].

| Isoform | Occurrence | Model substrate ^[1] | Inhibitor ^[2] | Inducer ^[3] |
|----------------|------------------------------|--|--|---|
| CYP1A1 | Mainly extrahepatic | 7-Ethoxyresofurin O-deethylation | (α -Naphtho-flavone) | Polycyclic hydrocarbons |
| CYP1A2 | Liver | Phenacetin O-deethylation | Furafylline | Smoking 3-Methylchol-anthrene Char-grilled meat |
| CYP2A6 | Liver | Coumarin C7-hydroxylation | Tranylcypromine | Pyrazoles Barbiturates |
| CYP2B6 | Liver | (S)-Mephenytoin N-desmethylation | 2-Phenyl-2-(1-piperdiny)propane (Sertraline) | |
| CYP2C9 | Liver, intestine | (S)-Warfarin C6-, C7 hydroxylation | Sulfaphenazol | Rifampicine Phenobarbital |
| CYP2C19 | Liver | (S)-Mephenytion C4'-hydroxylation | (-)-N-3-Benzyl-phenobarbital (Ticlopidine) | Rifampicine Carbamazepine |
| CYP2D6 | Liver, intestine, kidney | Bufuralol C1'-hydroxylation Dextromorphan O-demethylation | Quinidine | |
| CYP2E1 | Liver, intestine, leucocytes | Chlorzoxazone C6-hydroxylation | 4-Methylpyrazole | Ethanol |
| CYP3A4 | Liver, GIT | Midazolam C1'-hydroxylation Testosterone C6- β -hydroxylation | Ketoconazol | Rifampicine Barbiturates |

Flavin monooxygenases (FMO) are involved in oxidation of heteroatoms such as nitrogen and sulfur. These membrane-bound enzymes can be found in microsomes as well.

Monoamine oxidases are responsible for oxidation of endogenous and exogenous amines [350].

Further important for phase I metabolism are the previously mentioned esterases (as well as serum esterases present in blood), and the cytosolic enzymes carbonyl reductases and alcohol and aldehyde dehydrogenases. Moreover, also the microsomal and soluble epoxide hydrolases may play a role in drug metabolism.

The membrane-bound UGTs catalyze the conjugation of glucuronic acid at hydroxyl, amine, and carboxylic acid groups of endo- and exogenous molecules. UGTs are grouped in two subfamilies, UGT1A and UGT2B, which each contain again several isoforms. UGT1A1, UGT1A6, and UGT2B7 are the most important ones for drug metabolism. UGTs can be found in liver, gastrointestinal tract, kidney, brain, mammary, and prostate [351].

The cytosolic sulfotransferases (SULT) are responsible for the transfer of sulfate to their substrates. Again, several isoforms are known with different sites of expression (liver, GIT, skin, prostate, placenta, platelets, adrenal, endometrium, brain, fetal kidney and lung). Sulfation is known to be involved in the metabolism of e.g. acetaminophen, minoxidil, and salbutamol [352].

Other important phase II enzymes are the glutathione-S-transferases (GST), the *N*-acetyltransferases (NAT), and the methyltransferases (such as catechol-*O*-methyltransferase).

Except the membrane-bound UGTs, microsomal preparations lack these conjugation enzymes, thus they are limited in their ability of phase II metabolite formation.

For *in vitro* metabolism studies, a number of different systems has been established. However, the suitable application should be chosen carefully because each system is associated with advantages, disadvantages, and limitations (see Table 5.2).

In vitro metabolism techniques are a valuable tool in preclinical testing to screen and characterize drug metabolites, elucidate the metabolic pathways, and assess metabolic stability as a first approach to pharmacokinetic parameters. Additionally, they constitute an important tool for prediction of drug-drug interactions, enzyme inhibition, or induction [342].

Supersomes are microsomes, which consist of vesicles of the hepatocyte ER of human CYP- or UGT-transfected insect cells. They are suitable for the determination of metabolite formation with regard to individual isoforms. Moreover, they are used for drug-interaction studies and examination of the impact of enzyme polymorphism on drug biotransformation. Another application is the specific formation of metabolites for isolation purpose. As the perhaps most “non-physiological” model, *in vivo* correlation is a doubtful issue.

The use of subcellular fractions (S9, cytosol, microsomes) is very common, well established and characterized. Fractions are obtained from (liver) tissue by differential centrifugation steps. The S9 fraction contains both phase I and II enzymes, thus can be used for metabolite profiling choosing individual, species-, or gender-specific probes. However, enzyme activities are lower than in microsomal or cytosolic preparations so that some metabolites may not be detected.

Table 5.2: Overview of *in vitro* metabolism systems and their advantages and disadvantages. From top to bottom increasing resemblance of true *in vivo* situation. The table was compiled and adapted according to Brandon et al. [349], Jia et al. [347], Asha et al. [353] and FDA Guidance for Industry (Drug metabolism/Drug interaction; Studies in vitro).

| <i>In vitro</i> system | Advantages | Disadvantages |
|-------------------------------|---|---|
| Supersomes | easy to use studies of individual enzyme isoforms and different genotypes high enzyme activity | only CYP, FMO, UGT, GST, SULT available difficult correlation to <i>in vivo</i> no induction models |
| Microsomes | easy to use, cheap individual, gender- and species-specific studies | incomplete metabolic profile addition of cofactors no induction models |
| Cytosol | phase II metabolism of different enzymes can be studied separately high enzyme activities easy to use, cheap individual, gender- and species-specific studies | incomplete metabolic profile, only NAT, SULT, GST addition of cofactors no induction models |
| S9 fraction | phase I and II metabolism easy to use, cheap individual, gender- and species-specific studies | low enzyme activities than in microsomes addition of cofactors no induction models |
| Liver cell lines | easy to culture quite stable enzyme activities CYPs inducible | low expression levels |
| Hepatocytes | whole metabolic profile self-sufficient cofactors well established and characterized induction models pools for cryopreserved cells presence of drug transporters good <i>in vivo</i> correlation | quite expensive complex isolation batch variability instability of enzyme activity and down regulation of transporters loss of cell viability damage of cells during isolation |
| Liver slices | whole metabolic profile intact cellular association morphological studies interindividual studies good <i>in vivo</i> correlation | expensive <i>ex vivo</i> animal trial complex methodology and high technical effort penetration problems limited viable period damaged cells on the edges batch variability |
| Perfused liver | whole metabolic profile bile formation three dimensional architecture best <i>in vivo</i> correlation | very costly <i>ex vivo</i> animal trial complex methodology and high technical effort limited viable period poor reproducibility no human livers |

Microsomes constitute a popular and affordable model for metabolic screening. Individual, gender-specific, and pooled probes from different species are commercially available. They are used for assessing the metabolic stability (kinetics, estimation and extrapolation of hepatic clearance) as well as for interspecies comparisons of metabolic profile. The latter can give valuable hints for choosing the appropriate animal model for subsequent *in vivo* investigations. Nevertheless, it has to be noted that only membrane-bound enzymes (CYPs, UGTs) are enclosed. Due to the lack of many conjugation enzymes, microsomes are mainly applied for phase I studies, and for identification of metabolic pathways by selective inhibition of CYP isoforms with either chemical inhibitors or antibodies. Glucuronidation can be examined by addition of uridine diphosphoglucuronic acid.

The cytosol fraction contains the soluble phase II enzymes (SULT, NAT, GST etc.). Metabolism of individual enzymes can be studied by addition of enzyme specific cofactors. However, due to the lack of phase I enzymes the metabolic profile remains incomplete.

On the cellular level, both cell lines and primary cultured hepatocytes are applied. The most common liver cell line is the human hepatocellular carcinoma cell line HepG2. As basal enzymes activity is very low, CYP enzymes have to be induced by supplementation of inducers to the culture medium. Cell lines are generally easier in handling as primary hepatocytes and show relatively stable enzyme concentrations. However, they are rarely used because of low expression levels of most metabolizing enzymes, which may lead to detection problems of formed metabolites.

Primary hepatocytes are a popular and physiological *in vitro* system for any studies of drug metabolism. The whole range of metabolizing enzymes is present as well as drug specific transporters. The isolation of primary hepatocytes is a quite complex procedure and in conventional cultures there is a rapid loss in transporter and enzyme activity. However, nowadays with establishment of cryopreservation techniques, hepatocytes from different species as well as pooled probes are commercially available and enzyme activity can be maintained by special culture methods (e.g. sandwich-culture in collagen matrix).

Tissue cultures and studies on isolated perfused livers are the high-end models in *in vitro* biotransformation studies with best *in vivo* correlation due to presence of three-dimensional structures and cell-cell interactions. Both techniques are very complex and make a high demand on technical equipment. Due to practical inconveniences, poor reproducibility, high costs, and short viable period, perfused organs are seldomly used for biotransformation studies only when bile excretion is necessary. Liver slices and hepatocyte culture constitute the more feasible methodology with good *in vivo* correlation.

5.1.2 Absorption, bioavailability, and metabolism of flavonoids and chalcones

Chalcones (derivatives of *trans*-1,3-diphenyl-2-propen-ol) belong to the large group of polyphenolic compounds, more precise they are flavonoid derivatives (C₆-C₃-C₆) lacking the heterocyclic C ring [354]. For chalcones many interesting pharmacological activities have been discovered, such as anti-infective, anti-oxidative, anti-inflammatory, chemopreventive, and anti-cancer effects [250] (see chapter 4). Sometimes, chalcones may also contribute to toxicity observed for drugs (e.g. kava-chalcones, see chapter 3.3.3). In any case, chalcones as small molecules seem to possess a very high and widespread ability for pharmacological interactions. Chalcones may be ingested (as minor constituents) via dietary sources (e.g. phloretin/phloridizin in apple, naringenin chalcone in tomato, xanthohumol in beer) or herbal drugs (e.g. isosalipurposide in willow bark, flavokawains in kava kava root, isoliquiritigenin/isoliquiritin and licochalcone A in licorice, cardamonin in TCM drugs like *Alpinia katsumada*). Although pharmacological properties of chalcones are extensively investigated, little is known about their absorption, bioavailability, and metabolism in general [355].

In contrast, pharmacokinetics of C ring-closed flavonoids (flavones, flavonols, flavanones, catechins, anthocyanidines, and isoflavones) are far better investigated as they are abundant in plant foods and connected to constitutional and protective effects [356–359]. Mainly, dietary flavonoids, except catechins, are present in plants as β -glycosides. Longtime, very poor absorption was predicted for glycosylated flavonoids. However, hydrolyzation by bacterial enzymes might take place in lower parts of the intestine and liberated aglycones might be partly absorbed or further metabolized [356] (Figure 5.1). On the contrary, Hollmann et al. could show that quercetin glucosides are obviously absorbed intact in the small intestine via the sodium-dependent glucose transporter 1 (SGLT1) [360]. In further investigations, however, no intact quercetin-glucosides were detected in plasma [361]. Alternative mechanisms of absorption were proposed such as the pre-involvement of hydrolyzing enzymes of the small intestine (broad-specific β -glucosidase enzyme (BS β G) and lactase phloridizin hydrolase (LPH)). Substrate specificity of these enzymes highly depends on the sugar moiety and only rarely on the aglycone part [362]. Efficacy of absorption of certain flavonoid glycosides might also be decreased by efflux transporters as the multidrug resistance-associated protein 2 (MRP2) [363].

Glycosides which are not substrates of SGLT1 or LPH (e.g. quercetin-3- β -rutinose) will be transported toward the colon where they are hydrolyzed by bacterial enzymes. Liberated aglycones either can be absorbed in colon as well (but in a lesser extent than in the small intestine), or further metabolism and degradation by microorganisms to a variety of hydroxylated phenyl carboxylic acids and CO₂ takes place. A rash of these “colon-

metabolites" namely benzoic acids, phenylacetic acids, and phenylpropionic acids were detected in urine and plasma [364].

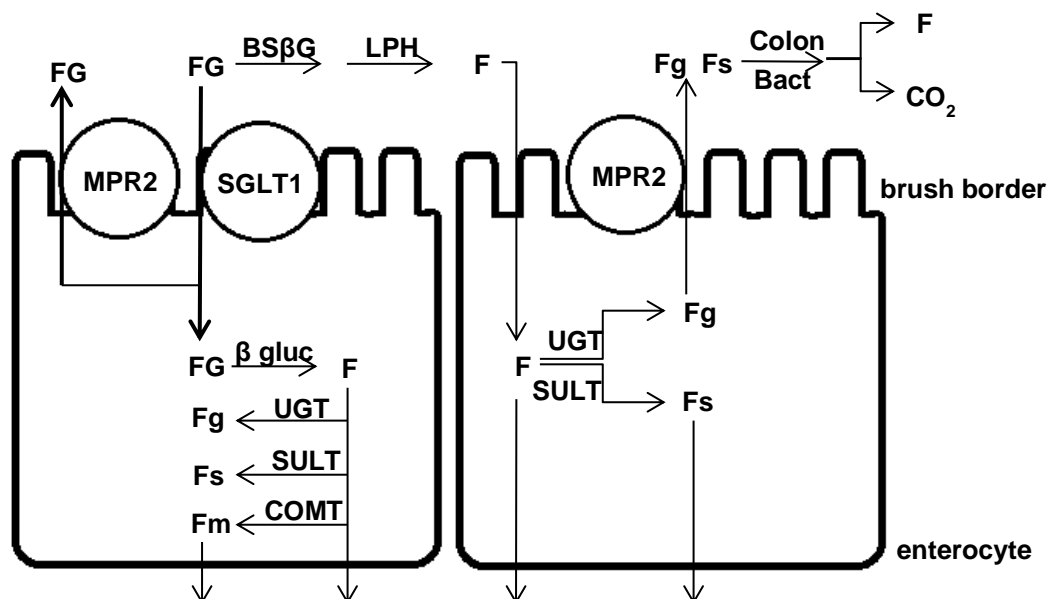


Figure 5.1: Absorption, transport pathways, and metabolism of flavonoid glycosides (FG) and aglycones (F) in enterocytes. SGLT1 sodium dependent glucose transporter 1, MPR2 multidrug resistance-associated protein 2, BS β G broad-specific β -glucosidase, LPH lactase phloridizin hydrolase, β gluc β -glucosidase, UGT uridine diphosphoglucuronosyl transferase, SULT sulfonyletransferase, COMT catechol-O-methyltransferase, Bact bacterial enzymes, Fg flavonoid glucuronide, Fs flavonoid sulfate, Fm methylated flavonoid. Adapted from [359,356].

Also bioavailability of flavonoid aglycones and glycosides has been examined. The best-studied aglycone is quercetin. In a study using [14 C]quercetin, absorption of 36-53% was found, however, nearly no free quercetin could be detected in plasma. This is due to extensive metabolism to conjugated metabolites, mainly glucuronides [365].

The quite lipophilic flavone chrysin showed very poor oral bioavailability of 0.003-0.02% albeit high membrane permeability. However, it was extensively metabolized by intestinal cells to glucuronic acid and sulfate metabolites, which were almost quantitatively eliminated via efflux proteins [366].

Bioavailability of flavonoid glycosides is strongly determined by the sugar moiety as could be shown for different quercetin glycosides [362]. Original quercetin glycosides are not detectable in plasma. Instead, deconjugation (hydrolysis) and re-conjugation to phase II metabolites occurs in the intestinal cells. Meanwhile, bioavailability studies have been conducted for different flavonoid subclasses, such as catechins, anthocyanines, and isoflavones [357].

For metabolism of flavonoids, mainly two compartments are important: on the one hand tissues like the small intestine and the liver, on the other hand the microorganisms of the colon (as previously mentioned). Conjugation of hydroxyl groups with glucuronic acid (by UGTs), sulfate (by SULTs), or glycine has been reported for different flavonoids. For

catechol-like structure elements (e.g. B ring of quercetin) also O-methylation by cytosolic catechol-O-methyltransferase (COMT) plays a role. Isorhamnetin was found as quercetin metabolite in human [367].

As oxidative metabolism of drugs and other xenobiotics often has a key role in biotransformation, the influence of cytochrome P450 enzymes on flavonoid metabolism has been focused as well. Exemplarily, *in vitro* studies with human liver microsomes identified kaempferol as primary metabolite of both galangin, by ring hydroxylation (CYP2C9), and kaempferide, by O-demethylation (CYP1A2) [368]. In contrast, metabolism studies of galangin in primary hepatocyte culture and with S9 fraction have rather revealed the importance of conjugated metabolites (glucuronides and sulfates) while kaempferol was only found as minor metabolite [369]. Hence, *in vivo* relevance of CYP mediated metabolism of flavonoids is ambiguous in many cases and generally, conjugated metabolites seem to dominate the biotransformation of most abundant flavonoids.

However, the absorption and metabolism of chalcones may differ from “normal” flavonoids due to their different molecule structure and chemical properties. Thus, as chalcones constitute the molecules of interest in this study, their metabolism is treated separately and more detailed in the following.

In comparison to other chalcones, metabolism of xanthohumol (**XAN**), a prenylated chalcone from hop cones, is quite extensively examined. So far, both *in vitro* and *in vivo* studies have been conducted. First, the *in vitro* inhibition of cytochrome P450 enzymes by prenylated flavonoids from hops was investigated using cDNA-expressed human CYP1A1, CYP1B1, CYP1A2, CYP3A4, and CYP2E1 [370]. At 10 μM , **XAN** almost inhibited completely the activity of CYP1A1 and CYP1B1, and partly the activity of CYP1A2 (~35%). Most potent CYP1A2 inhibitors (> 90%) at 10 μM were the prenylated flavanones 8-prenylnaringenin and isoxanthohumol. The isoenzymes CYP3A4 and CYP2E1 were only marginally affected by prenylated flavonoids. Yilmazer et al. studied the metabolism of **XAN** using rat liver microsomes [371] and also **XAN** glucuronidation by rat and human microsomes [372]. Three major phase I metabolites were identified in the microsomal incubation assay. Structure elucidation of formed metabolites was performed by LC–MS and ^1H NMR. Major metabolites were formed via oxidation of the prenyl side chain (epoxidation) and subsequent ring closure, which yielded isopropylidihydrofurano metabolites (K_m 20 ± 9 and $119 \pm 39 \mu\text{M}$) of **XAN**. The third metabolite constitutes a derivative with an additional hydroxyl group at the B ring (K_m $246 \pm 116 \mu\text{M}$). Besides, pretreatment with isosafrole and β -naphthoflavone (inducers of CYP1A) led to formation of a nonpolar metabolite, which was found to be dehydrocycloxanthohumol. The formation of multiple phase I metabolites suggests the involvement of different CYP isoforms. Indeed, incubation with CYP inhibitors of CYP1A and

CYP3A did not lead to complete inhibition of metabolite formation [371]. *In vitro* glucuronidation of **XAN** by liver microsomes yielded two major glucuronides, the C-4' and C-4 monoglucuronide of **XAN** [372]. Biotransformation of **XAN** was also performed using human liver microsomes [373]. For major and two minor metabolites of **XAN** were found and identified by liquid chromatography / tandem mass spectrometry. The major metabolites were mono-oxidation products of **XAN** among hydroxylation of the terminal methyl group of the prenyl moiety being the most abundant. The latter metabolite has not been identified with rat liver microsomes. Hydroxylation of the prenyl group also took place at the 2''-carbon changing the double bond to the terminal position. However, epoxidation of the prenyl moiety and subsequent ring closure to isopropylidihydrofurano and dimethylpyrano derivatives was observed as well with human microsomes. Ruefer and coworkers examined the involvement of phase II isoenzymes on **XAN** metabolism using nine recombinant human UGT and five SULT [374]. Mainly, UGT 1A8, 1A9, and 1A10 are predominantly responsible for the glucuronidation. In addition, sulfatation was observed but to lesser extent. Mainly, SULT 1A1*2, 1A2, and 1E1 were involved. The isoenzymes can be found in the liver as well as in the gastrointestinal tract. All three possible hydroxyl groups were conjugated; however, position for conjugation could not be identified with the used analytical methods.

Bioavailability and metabolism of **XAN** was also studied *in vivo*. Nookandeh et al. analyzed **XAN** metabolism after a single oral dose of 1 g/kg and identified 22 metabolites in the feces of rats using LC–MS and LC–NMR techniques [259]. Three metabolites with hydroxylated prenyl side chain (position 2'', 3'', 5''), four metabolites with substituted (C4' O-glucuronide, C4 methoxy and acetoxy derivatives) or altered (α,β -epoxide) chalcone moiety, two flavanones (isoxanthohumol and 3''-OH isoxanthohumol), eight benzodihydro-/benzofurane derivatives, and five benzoisochromane-/chromene derivatives were identified. Bioavailability and metabolism of **XAN** was studied with focus on the impact of gut flora in germ-free (GF) and human microbiota-associated (HMA) rats [375]. After application of 17 mg/kg **XAN**, **XAN** itself, **XAN** conjugates, and isoxanthohumol conjugates were detected in blood of rats (concentration range 0.11-4.87 μ M). Isoxanthohumol only occurred in the blood of HMA rats (1.04 μ M). Total excretion of **XAN** and its metabolites was only 4.2% in HMA rats and 4.6% in GR rats, feces being the major route of excretion. Low urinary excretion was found for **XAN** and its metabolites (< 0.1% of dose). Interestingly, 8-prenylnaringenin was detected only in feces of HMA rats, indicating that O-demethylation is catalyzed by intestinal bacteria. Thus, impact of the gut flora in **XAN** metabolism has to be considered.

Jirásko et al. detected further phase II metabolites in rats after administration of hop extract [376]. Metabolites were extracted from feces. Mainly, sulfatation, oxidation, and hydrogenation of initial hop compounds were observed.

Legette and coworkers dealt with pharmacokinetics of **XAN** after oral and intravenous administration in rats [377]. Rats received either 1.86 mg/kg i.v. or low (1.86 mg/kg), medium (5.64 mg/kg), or high (16.9 mg/kg) oral doses of **XAN**. Resulting bioavailability of total **XAN** (free and conjugated) was found to be 33%, 13%, and 11% for low-, medium-, and high dose-group, showing dose-dependency of oral bioavailability.

Motyl et al. recently investigated the absorption, the distribution in different compartments, and the phase II metabolism of **XAN** in mice, particularly with regard to matrix effects of other hop polyphenolics present in the extract [101]. Dose-dependency of **XAN** bioavailability was observed as well; mainly, however, an increased absorption of **XAN** in presence of other hop polyphenolics could be shown. Relevant concentrations of **XAN** conjugates were found in all analyzed compartments whereas the concentration of free **XAN** was significantly lower. This once more highlights the importance of investigations concerning the biological effects of phase II metabolites as they may contribute to pharmacological actions *in vivo* or even constitute the active principle. Besides, **XAN** and **XAN** metabolites accumulated in liver tissue and, above all, the bile where the highest concentrations were detected.

The metabolism of isoliquiritigenin (2',4',4'-trihydroxychalcone), a chalcone in licorice, was assessed using human liver microsomes [378]. Seven metabolites were found and identified by liquid chromatography-tandem mass spectrometry. In addition to hydroxylated metabolites (2', 4, 4', 5'-tetrahydroxychalcone and butein), also hydrogenation of the double bond (dihydroisoliquiritigenin) and cyclization to liquiritigenin and (*E/Z*)-6,4'-dihydroxyaurone was observed. Finally, by incubation with monoclonal antibody inhibitors of CYP isoforms, CYP2C19 could be identified as significant enzyme for isoliquiritigenin hydroxylation to butein. Furthermore, the involvement of reactive oxygen species and peroxidases, responsible for the formation of aurones, was discussed. Guo et al. further examined the phase II metabolism of isoliquiritigenin using human hepatocytes and liver microsomes [379]. Five monoglucuronides of both isoliquiritigenin and liquiritigenin were detected whereas conjugation to sulfate was not observed. UGT1A1 and UGT1A9 were responsible for the formation of the major glucuronide, isoliquiritigenin-4'-*O*-glucuronide, and UGT1A1 and UGT1A10 for the 2'-*O*-glucuronide. Unexpectedly, the 4-*O*-glucuronide was the least abundant isoliquiritigenin glucuronide. The half-life of isoliquiritigenin in the incubation assay was determined at 25 min. The estimated intrinsic clearance was calculated to be 36 mL/min/kg.

The metabolism of other chalcones is rarely investigated, as they usually constitute minor compounds in drugs or extracts. However, data are available for chalcones that have showed pronounced pharmacological actions or can be found in food.

Cardamonin (alpinetin chalcone), a mono-methoxylated chalcone with anti-inflammatory, iNOS-inhibitory, and vasorelaxant effects was metabolized using human and animal liver microsomes [380]. Two hydroxylated metabolites (B ring, double bond of α,β -unsaturated ketone) could be identified by MS fragmentation. Furthermore, kinetic parameters of cardamonin hydroxylation were calculated (K_m 32 μ M, V_{max} 35 pmol/min/mg) and responsible CYP isoenzymes were identified by incubation with selective chemical CYP inhibitors. Furfaylline and clomethiazole significantly inhibited the hydroxylation of cardamonin. Thus, CYP1A2 and CYP2E1 seem to be responsible for biotransformation of cardamonin. However, no IC_{50} values were determined. Interestingly, they compared the hydroxylation capacities of different species to metabolism by human microsomes and found the metabolic activity of guinea pigs being closest to human in this case. Hence, they suggest using guinea pigs for *in vivo* pharmacokinetic studies.

Kohono et al. assessed the metabolism of chalcone and *trans*-4-phenyl-3-buten-2-one (PBO) in rat liver microsomes [381]. Oxidative metabolism led to formation of the major metabolites 4-OH chalcone (CYP1A1/2) and 4-OH PBO (CYP2C6, 1A2) which possess estrogenic activity. Minor metabolites observed for the chalcone were the 4'-OH (CYP1A1, 2C6) and 2-OH (CYP3A1, 1A1) derivative. PBO is also converted by liver cytosolic double bond reductase to 4-phenyl-2-butanone, which is further oxidized to 4-hydroxyphenyl-2-butanone. Both show no estrogenic activity.

Two glycosylic dihydrochalcones of rooibos (*Aspalathus linearis* (N.L.BURM.) R.DAHLGR.), aspalathin and nothofagin, were investigated with regard to phase II metabolism using rat liver microsomes and cytosolic fractions [382]. Following LC-MS analysis revealed the presence of two glucuronides for aspalathin (3-OH, 4-OH) and nothofagin (4-OH, 6'-OH), respectively, whereas only for aspalathin also sulfation was observed.

Moreover, the biotransformation of synthesized chalcone analogues with anti-plasmodial properties has been studied *in vitro* using human liver microsomes [383,384].

A further study deals with the *in vivo* metabolism of naringenin chalcone, present in tomato skin, after oral administration (20 mg/kg) in rats [385]. Urine and plasma samples were analyzed. Naringenin chalcone-2'-O- β -D-glucuronide was the major metabolite found both in urine and plasma samples. Besides, naringenin-7-O- β -D-glucuronide and naringenin-4'-O- β -D-glucuronide were found in urine but not in plasma. The peak plasma level (5.0 ± 1.0 μ M) of naringenin chalcone-2'-O- β -D-glucuronide was reached within 1 h and its half-life was 5.5 ± 1.7 h. Total recovery of the metabolites in urine was only 21% of the dosage which may be due to the high ingested dose.

5.2 Aim of the study

Chalcones possess a broad spectrum of biological activities and a high potential for therapeutic application (see chapter 4). In contrast to the large number of publications dealing with the pharmacological effects, only few studies have focused on the bioavailability and metabolism of chalcones. Nevertheless, besides the pharmacodynamic interactions, pharmacokinetic parameters are indispensable for a complete pharmacological profile.

Hence, this study examines the microsomal metabolism of flavokawains (**FKA**, **FKB**, and **FKC**) and alpinetin chalcone (**A**) which have already been introduced as test compounds in the previous chapters 3 and 4. Different microsomal incubation systems are used (including suitable negative and positive controls) to study both phase I and phase II metabolism. For identification and structure elucidation of microsomal metabolites, LC–HRESIMS and HPLC–NMR techniques are applied to propose a metabolic profile of these chalcones. To date, only phase I metabolism of alpinetin chalcone (cardamomin) has been studied. Phase II metabolism and the biotransformation of flavokawains have not been examined yet.

5.3 Results and discussion

5.3.1 Preliminary experiments

For the establishment of the microsomal incubation systems, 7-ethoxycoumarin (7-EC) was chosen as a cheap and commonly used probe for the investigation of both phase I metabolism and glucuronidation reaction. Samples were prepared and processed as described in chapter 2.3.3.1. HPLC analysis was performed using method **C1** (see chapter 2.3.3.2). Furthermore, for identification of metabolite masses, samples were subjected to liquid chromatography–high resolution electrospray ionization mass spectrometry (LC–HRESIMS, see chapter 2.3.3.3).

As metabolism of 7-EC is well described, 7-EC served as positive control for qualification of the different incubation systems comparing the formation of metabolites to literature data. Oxidative deethylation of 7-EC by CYP1A2 and CYP2E1 to 7-hydroxycoumarin (7-HC, umbelliferone, **M3**) is used as a model reaction for specific P450 enzyme activity [387]. 7-HC is further transformed by yet uncharacterized UGT isoforms to the corresponding 7-HC glucuronide (**M4**). Fisher et al. identified two novel metabolites of 7-EC resulting from 3-hydroxylation (**M1**) and subsequent glucuronidation (**M2**) [386]. Figure 5.2 illustrates the proposed metabolism scheme for 7-EC in alamethicin-treated human liver microsomes supplemented with NADPH and UDPGA.

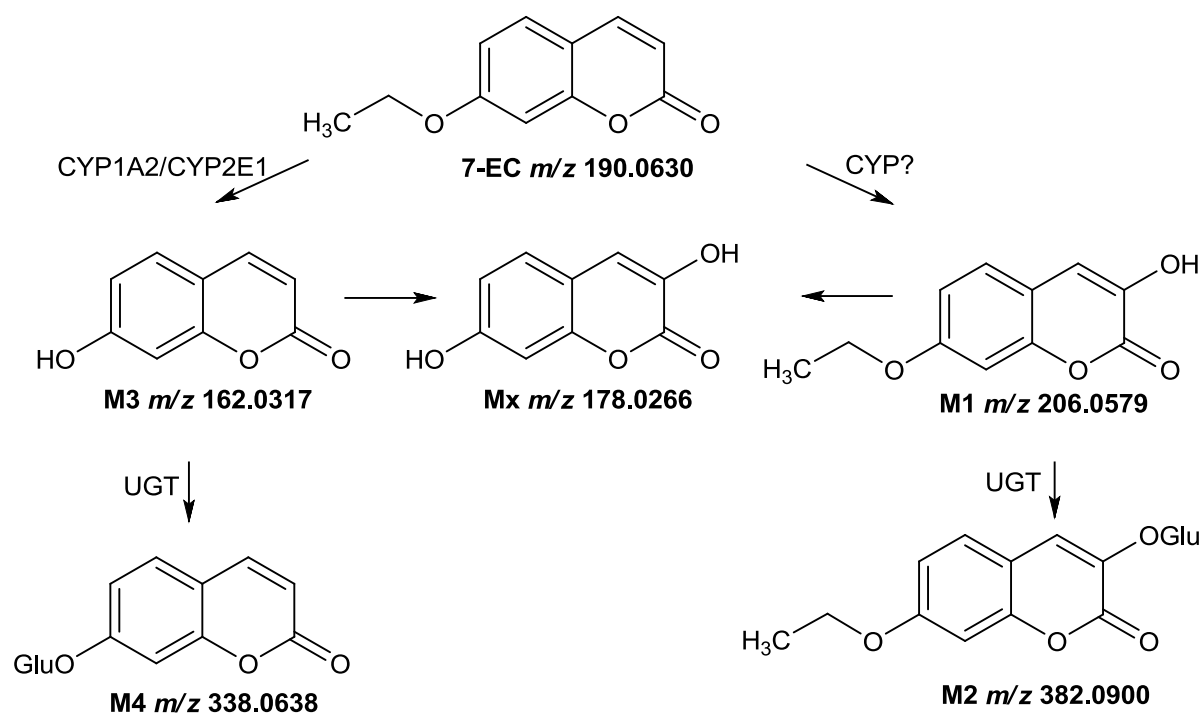


Figure 5.2: Suggested metabolism scheme of 7-EC according to Fisher et al. [386]. Metabolites were identified by LC–NMR and LC–MS.

Table 5.3: Results of high resolution LC–MS using positive electrospray ionization.

| detected metabolites of 7-EC | | | | | |
|------------------------------|-------------|-----------------------------------|--|---|------------|
| | Rt [min] | m/z [M+H] ⁺ found | m/z [M+H] ⁺ calculated | M formula | metabolite |
| 7-EC | 3.78 | 191.0706 | 191.0703 | C ₁₁ H ₁₀ O ₃ | parent |
| Ph I | 2.00 | 163.0391 | 163.0390 | C ₉ H ₆ O ₃ | M3 |
| | 3.48 | 207.0675 | 207.0652 | C ₁₁ H ₁₀ O ₄ | M1 |
| Ph II | - | - | - | - | - |
| Ph I+II | 1.32 | 339.0711 | 339.0711 | C ₁₅ H ₁₄ O ₉ | M4 |
| | 2.00 | 163.0389 | 163.0390 | C ₉ H ₆ O ₃ | M3 |
| | 2.56 | 383.0976 | 383.0973 | C ₁₇ H ₁₈ O ₁₀ | M2 |

As can be seen from results of LC–MS analysis (Table 5.3), all described metabolites were also detected within the used incubation systems. Phase I metabolism generated both 7-HC (**M3**) and the 3-hydroxy metabolite of 7-EC (**M1**). As expected, no metabolites are formed in incubation systems with only UDPGA supplementation, as no reactive groups are available for glucuronidation. For combined phase I and II metabolism, the masses of 7-HC (**M3**) and its glucuronide (**M4**) were detected whereas the 3-hydroxy metabolite (**M1**) was completely converted into its corresponding glucuronide (**M2**). Moreover, using negative electrospray ionization, a fifth compound (**Mx**) could be identified in phase I metabolism (m/z [M-H]⁻ found 177.0197, calculated 177.0193, C₉H₆O₄) which corresponds to 3,7-dihydroxycoumarin. The latter compound has been identified as metabolite of coumarin using liver microsomes [388], but has not been described for 7-EC metabolism yet.

Taken together, the formerly known microsomal metabolites of 7-EC were confirmed in the different incubation systems. In addition, a further phase I metabolite was detected. Hence, the suitability of applied incubation systems studying phase I, phase II, and combined metabolism is approved regarding the use for metabolite profiling.

5.3.2 Identification of microsomal chalcone phase I and II metabolites

The microsomal metabolism of four chalcones (10 μ M) **FKA**, **FKB**, **FKC**, and **A**, was studied within an incubation period of 60 min. Meanwhile, the compounds' stability in the phosphate incubation buffer (**stabi**) was controlled by HPLC. Furthermore, no unspecific metabolism or degradation of the compounds was observed in incubation systems without microsomes (**w/o micr**) or cofactors (**w/o cof**).

For metabolite profiling, the chalcones were incubated in the established microsomal systems for investigation of phase I (**Ph I**), phase II (**Ph II**), and combined metabolism (**Ph I+II**) as described in chapter 2.3.3.1. Additionally, the compounds' stability was controlled in incubation systems without microsomes (**w/o micr**) or cofactors (**w/o cof**). Obtained samples were subjected to HPLC analysis using method **C2** (see chapter 2.3.3.2). Exact metabolite masses were determined by LC–HRESIMS using positive and negative electrospray ionization (see chapter 2.3.3.3).

For **FKA**, two phase I metabolites (demethyl and bisdemethyl **FKA**) were found (Table 5.4). According to the retention times of 4.02 and 5.07 min, the metabolites were identified as **FKC** and helichrysetin (**Heli**), **FKC** being the major phase I metabolite of **FKA**. Despite only one available OH group (C-2'), two **FKA** glucuronides (Rt 3.38 min and 3.50 min) were detected. Most likely, *cis-trans* isomerization of **FKA** might be an explanation (see chapter 5.3.3). For combined phase I and II metabolism, besides the **FKA** glucuronide (Rt 3.50 min), also two masses corresponding to **FKC** glucuronides (Rt 2.81 min and 3.87 min) were found. Additionally, two metabolite masses corresponding to OH-**FKA** glucuronides (Rt 3.71 and 3.81 min) were identified as minor phase II metabolites of **FKA**. According to MS data, Figure 5.3 proposes a metabolism scheme for **FKA**.

Table 5.4: High resolution LC–MS of FKA samples using positive and negative electrospray ionization. (Corresponding mass spectra see Figure 10.20).

| detected metabolites of FKA | | | | | | |
|-----------------------------|----------|--------------------------------|-------------------------------------|--------------------------------|-------------------------------------|---|
| | Rt [min] | m/z [M+H] ⁺ found | m/z [M+H] ⁺ calculated | m/z [M-H] ⁻ found | m/z [M-H] ⁻ calculated | M formula |
| FKA | 6.18 | 315.1234 | 315.1227 | - | - | C ₁₈ H ₁₈ O ₅ |
| Ph I | 4.02 | - | - | 285.0766 | 285.0768 | C ₁₆ H ₁₄ O ₅ |
| | 5.07 | 301.1073 | 301.1071 | 299.0925 | 299.0925 | C₁₇H₁₆O₅ |
| Ph II | 3.38 | 491.1150 | 491.1548 | 489.1402 | 489.1402 | C ₂₄ H ₂₆ O ₁₁ |
| | 3.50 | 491.1151 | 491.1548 | 489.1405 | 489.1402 | C₂₄H₂₆O₁₁ |
| Ph I+II | 2.81 | 477.1389 | 477.1391 | 475.1238 | 475.1246 | C ₂₃ H ₂₄ O ₁₁ |
| | 3.50 | 491.1549 | 491.1548 | 489.1399 | 489.1402 | C₂₄H₂₆O₁₁ |
| | 3.71 | - | - | 505.1345 | 505.1351 | C ₂₄ H ₂₆ O ₁₂ |
| | 3.81 | - | - | 505.1345 | 505.1351 | C ₂₄ H ₂₆ O ₁₂ |
| | 3.87 | 477.1391 | 477.1391 | 475.1239 | 475.1246 | C ₂₃ H ₂₄ O ₁₁ |
| | 5.07 | 301.1072 | 301.1071 | 299.0920 | 299.0925 | C ₁₇ H ₁₆ O ₅ |

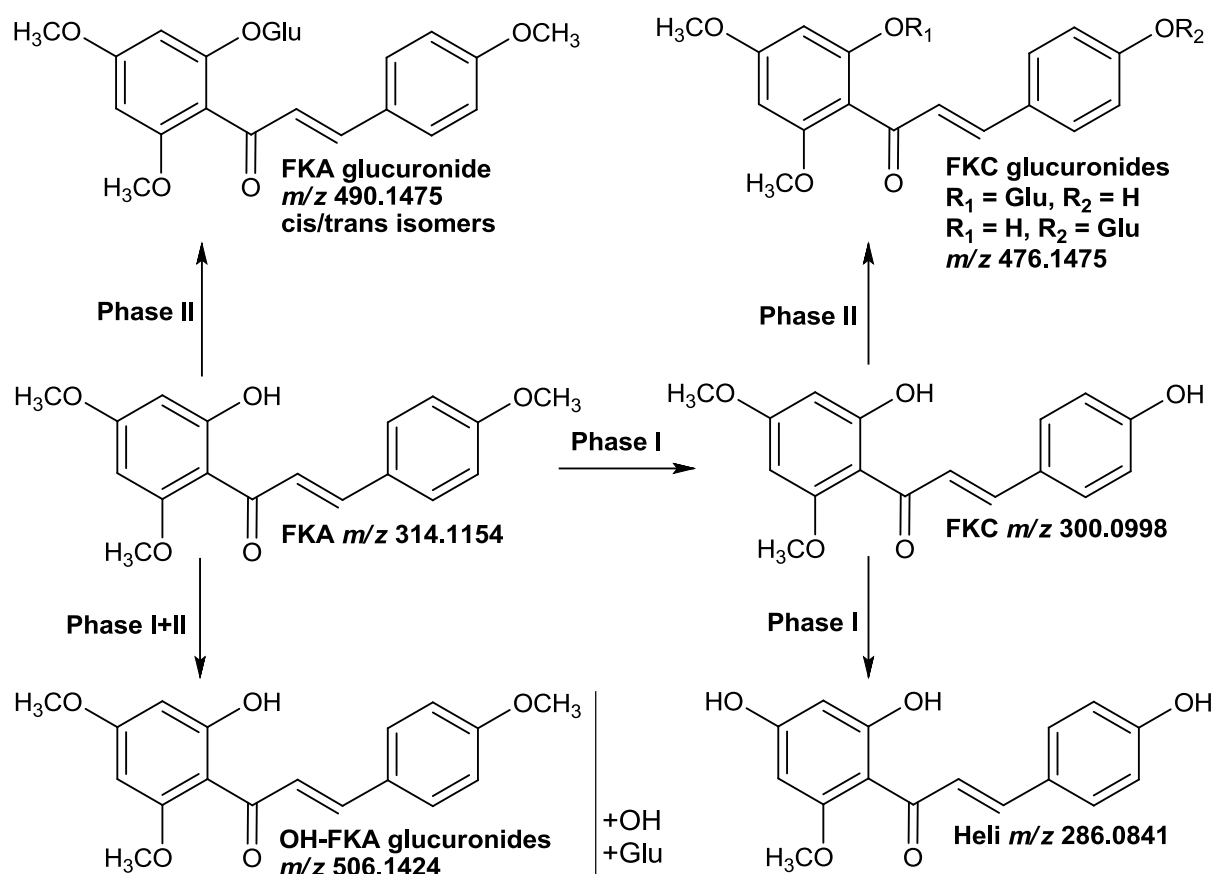


Figure 5.3: Suggested metabolism scheme of FKA using human liver microsomes. Metabolites were identified by LC–ESI–MS in different incubation systems.

For **FKB**, also **FKC** (Rt 5.07 min) was detected as major phase I metabolite after hydroxylation in position C-4 (Table 5.5). Demethylation in position C-4' and C-6', leads to formation of **A** (Rt 5.17 min) and 2',4',6'-trihydroxychalcone (Rt 4.48 min), respectively. The 2'-O-glucuronide of **FKB** (Rt 3.46 min) was found as phase II metabolite. Combined metabolism resulted in the formation of 2'-O-Glu-**FKB** and four glucuronides with corresponding masses of 476.1319 g/mol. Two of them (Rt 2.81 min and 3.87 min) were identified as the 2'- and 4-O-glucuronide of **FKC**. Furthermore, the phase I metabolite **A** was conjugated to glucuronic acid (Rt 3.95 min) either at positions C-2' or C-4'. The suggested metabolism of **FKB** is pictured in Figure 5.4.

Table 5.5: High resolution LC–MS of FKB samples using positive and negative electrospray ionization. (Corresponding mass spectra see Figure 10.21).

| detected metabolites of FKB | | | | | | |
|-----------------------------|-------------|-------------------------------------|--|-------------------------------------|--|---|
| | Rt [min] | <i>m/z</i> [M+H] ⁺ found | <i>m/z</i> [M+H] ⁺ calculated | <i>m/z</i> [M-H] ⁻ found | <i>m/z</i> [M-H] ⁻ calculated | M formula |
| FKB | 6.26 | 285.1125 | 285.1121 | - | - | C ₁₇ H ₁₆ O ₄ |
| Ph I | 4.48 | - | - | 255.0659 | 255.0663 | C ₁₅ H ₁₂ O ₄ |
| | 5.07 | 301.1070 | 301.1071 | 299.0927 | 299.0925 | C₁₇H₁₆O₅ |
| | 5.17 | - | - | 269.0819 | 269.0819 | C ₁₆ H ₁₄ O ₄ |
| Ph II | 3.46 | 461.1445 | 461.1442 | 459.1297 | 459.1297 | C₂₃H₂₄O₁₀ |
| Ph I+II | 2.81 | - | - | 475.1239 | 475.1246 | C ₂₃ H ₂₄ O ₁₁ |
| | 3.15 | - | - | 475.1239 | 475.1246 | C ₂₃ H ₂₄ O ₁₁ |
| | 3.46 | 461.1441 | 461.1442 | 459.1293 | 459.1297 | C₂₃H₂₄O₁₀ |
| | 3.75 | 477.1388 | 477.1391 | 475.1241 | 475.1246 | C ₂₃ H ₂₄ O ₁₁ |
| | 3.87 | - | - | 475.1241 | 475.1246 | C ₂₃ H ₂₄ O ₁₁ |
| | 3.95 | - | - | 445.1123 | 445.1140 | C ₂₂ H ₂₂ O ₁₀ |
| | 5.07 | - | - | 299.0920 | 299.0925 | C ₁₇ H ₁₆ O ₅ |

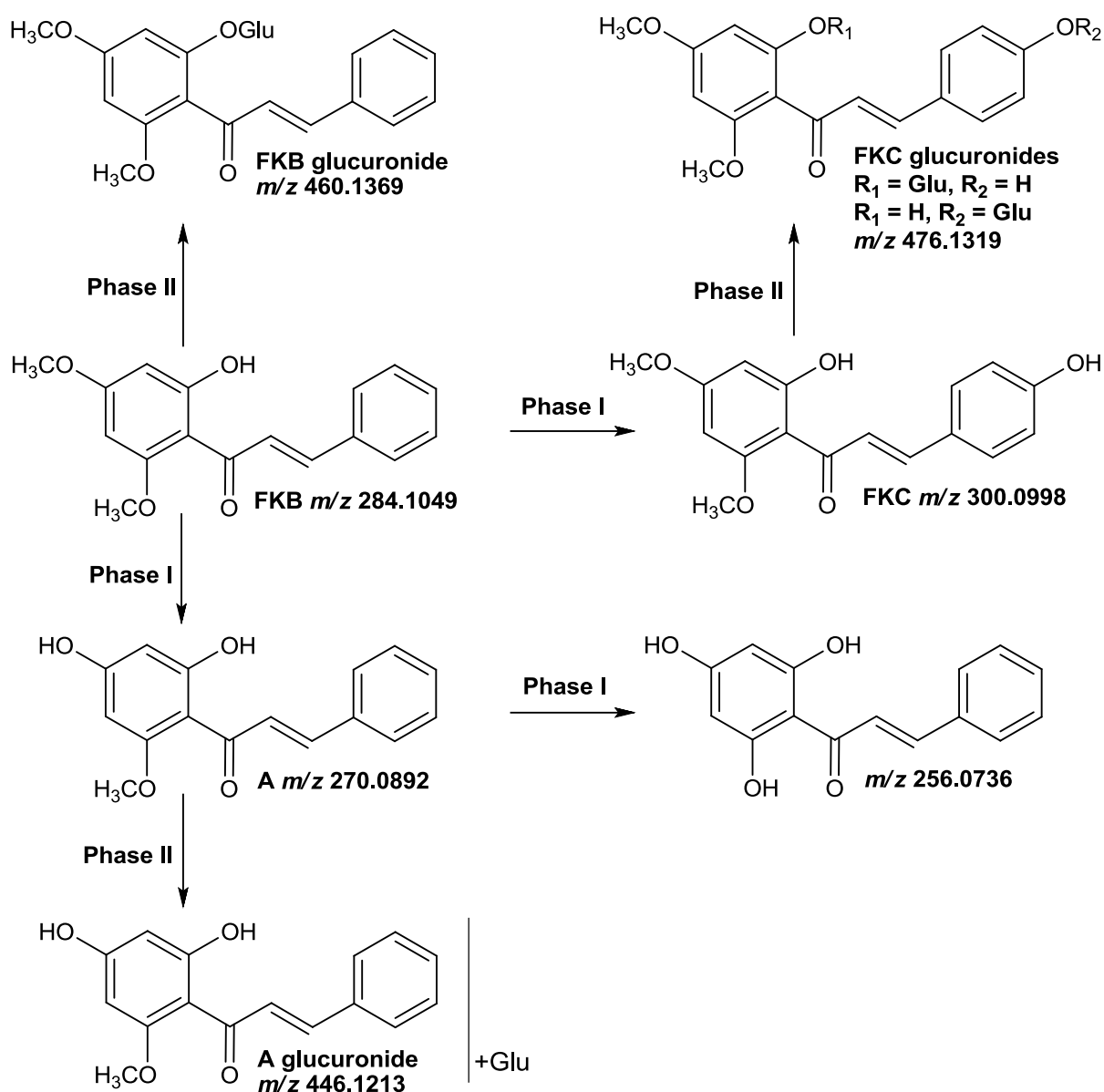
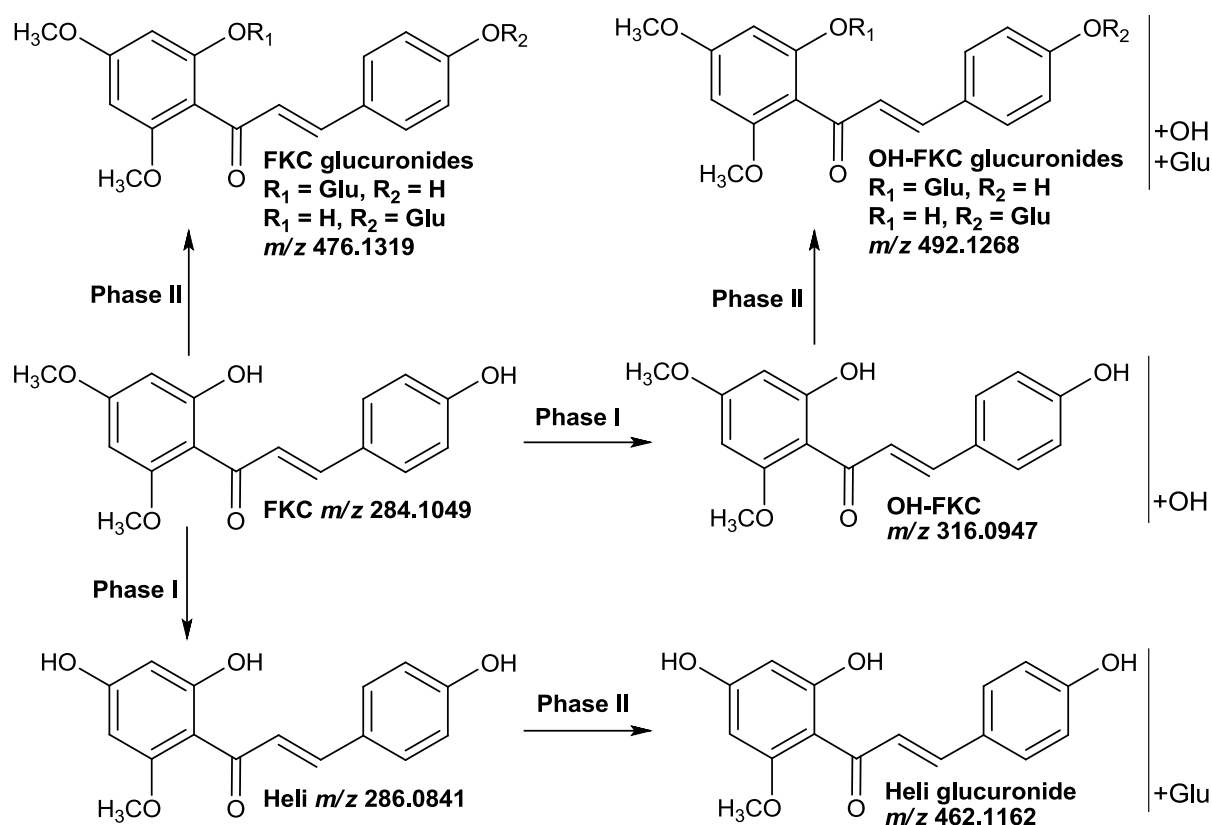


Figure 5.4: Suggested metabolism scheme of FKB using human liver microsomes. Metabolites were identified by LC-ESI-MS in different incubation systems.

In phase I metabolism of **FKC**, demethylation to **Heli** (Rt 4.03 min) and hydroxylation at unknown position (Rt 4.00 min and 4.52 min) occurred (Table 5.6). Three **FKC**-glucuronides were detected in phase II metabolism. Two major glucuronides (Rt 2.81 min and 3.86 min) might correspond to 2'-O- and 4'-O-Glu-**FKC** respectively. The third minor glucuronide (Rt 2.71 min) could possibly arise from flavanone- or *cis-trans*-isomerization (see chapter 5.3.3). In combined phase I and II metabolism, additionally a glucuronide of **Heli** (Rt 3.03 min) and three different glucuronides of OH-**FKC** (Rt 2.83 min, 3.18 min, and 3.72 min) were found. Figure 5.5 proposes a possible metabolism scheme for **FKC**.

Table 5.6: High resolution LC–MS of FKC samples using positive and negative electrospray ionization. (Corresponding mass spectra see Figure 10.22).

| detected metabolites of FKC | | | | | | |
|-----------------------------|-------------|--------------------------------|-------------------------------------|--------------------------------|-------------------------------------|---|
| | Rt [min] | m/z [M+H] ⁺ found | m/z [M+H] ⁺ calculated | m/z [M-H] ⁻ found | m/z [M-H] ⁻ calculated | M formula |
| FKC | 5.07 | 301.1071 | 310.1070 | 299.0926 | 299.0925 | C ₁₇ H ₁₆ O ₅ |
| Ph I | 4.00 | - | - | 315.0872 | 315.0874 | C ₁₇ H ₁₆ O ₆ |
| | 4.03 | 287.0911 | 287.0914 | 285.0767 | 285.0768 | C₁₆H₁₄O₅ |
| | 4.52 | 317.1019 | 317.1019 | 315.0871 | 315.0874 | C ₁₇ H ₁₆ O ₆ |
| Ph II | 2.71 | 477.1389 | 477.1391 | 475.1244 | 475.1246 | C ₂₃ H ₂₄ O ₁₁ |
| | 2.81 | 477.1392 | 477.1391 | 475.1245 | 475.1246 | C₂₃H₂₄O₁₁ |
| | 3.86 | 477.1395 | 477.1391 | 475.1248 | 475.1246 | C₂₃H₂₄O₁₁ |
| Ph I+II | 2.71 | - | - | 475.1241 | 475.1241 | C ₂₃ H ₂₄ O ₁₁ |
| | 2.81 | 477.1391 | 477.1391 | 475.1241 | 475.1241 | C₂₃H₂₄O₁₁ |
| | 2.83 | - | - | 491.1183 | 491.1195 | C ₂₃ H ₂₄ O ₁₂ |
| | 3.03 | 463.1234 | 463.1235 | 461.1085 | 461.1089 | C ₂₂ H ₂₂ O ₁₁ |
| | 3.18 | - | - | 491.1188 | 491.1195 | C ₂₃ H ₂₄ O ₁₂ |
| | 3.72 | - | - | 491.1187 | 491.1195 | C ₂₃ H ₂₄ O ₁₂ |
| | 3.86 | 477.1390 | 477.1390 | 475.1241 | 475.1241 | C₂₃H₂₄O₁₁ |

**Figure 5.5: Suggested metabolism scheme of FKC using human liver microsomes. Metabolites were identified by LC–ESI-MS in different incubation systems.**

Three hydroxylated metabolites of **A** were identified in phase I metabolism. One phase I metabolite could be identified as **Heli** (Rt 4.03 min) which is the 4-OH derivative of **A** (Table 5.7). Hydroxylation might also occur at different positions of the molecule including A and B ring and the α,β double bond. For the two other metabolites (Rt 4.43 min and 4.52 min), the exact position of the OH group could not be elucidated. He and coworkers have investigated the CYP450 dependent metabolism of **A** before [380]. Two monohydroxylated metabolites were identified by MS fragmentation. For the major metabolite (M1), the exact position of hydroxylation in the B ring could not be determined, however, the authors suggest C-4 being the most likely position. C-4 has also been identified before as preferential for hydroxylation of chalcone [381]. Accordingly, 4-OH-**A** would correspond to **Heli** that has been as well detected in this study. In addition, fragment ions suggest the hydroxylation in β -position of the unsaturated ketone (M2), which might correspond to another hydroxyl-derivative in this study (Rt 4.43 min or 4.52 min). In contrast to our findings, a third hydroxylated metabolite of **A** was not described by He et al. Three glucuronides of **A** were detected in phase II metabolism (Rt 2.67 min, 3.01 min, and 3.95 min). Again, despite only two free OH groups, a third corresponding mass suggests the presence or formation of **A** isomers. Besides the **A**-glucuronides, one glucuronide of OH-**A** (Rt 3.58 min) was found in combined metabolism. Figure 5.6 suggests a metabolism scheme for **A**.

Table 5.7: High resolution LC–MS of **A samples using positive and negative electrospray ionization. (Corresponding mass spectra see Figure 10.23).**

| | detected metabolites of A | | | | | |
|----------------|----------------------------------|--------------------------------|-------------------------------------|--------------------------------|-------------------------------------|---|
| | Rt [min] | m/z [M+H] ⁺ found | m/z [M+H] ⁺ calculated | m/z [M-H] ⁻ found | m/z [M-H] ⁻ calculated | M formula |
| A | 5.17 | 271.0970 | 271.0965 | 269.0820 | 269.0819 | C ₁₆ H ₁₄ O ₄ |
| Ph I | 4.03 | 287.0915 | 287.0914 | 285.0763 | 285.0768 | C₁₆H₁₄O₅ |
| | 4.43 | 287.0917 | 287.0914 | 285.0763 | 285.0768 | C ₁₆ H ₁₄ O ₅ |
| | 4.52 | 287.0917 | 287.0914 | 285.0762 | 285.0768 | C ₁₆ H ₁₄ O ₅ |
| Ph II | 2.67 | 447.1286 | 447.1286 | 445.1141 | 445.1140 | C ₂₂ H ₂₂ O ₁₀ |
| | 3.01 | 447.1282 | 447.1286 | 445.1138 | 445.1140 | C ₂₂ H ₂₂ O ₁₀ |
| | 3.95 | 447.1287 | 447.1286 | 445.1140 | 445.1140 | C₂₂H₂₂O₁₀ |
| Ph I+II | 2.67 | 447.1284 | 447.1284 | 445.1135 | 445.1140 | C ₂₂ H ₂₂ O ₁₀ |
| | 3.00 | 447.1283 | 447.1283 | 445.1136 | 445.1140 | C ₂₂ H ₂₂ O ₁₀ |
| | 3.58 | 463.1232 | 463.1235 | 461.1081 | 461.1089 | C ₂₂ H ₂₂ O ₁₁ |
| | 3.95 | 447.1287 | 447.1286 | 445.1135 | 445.1140 | C₂₂H₂₂O₁₀ |

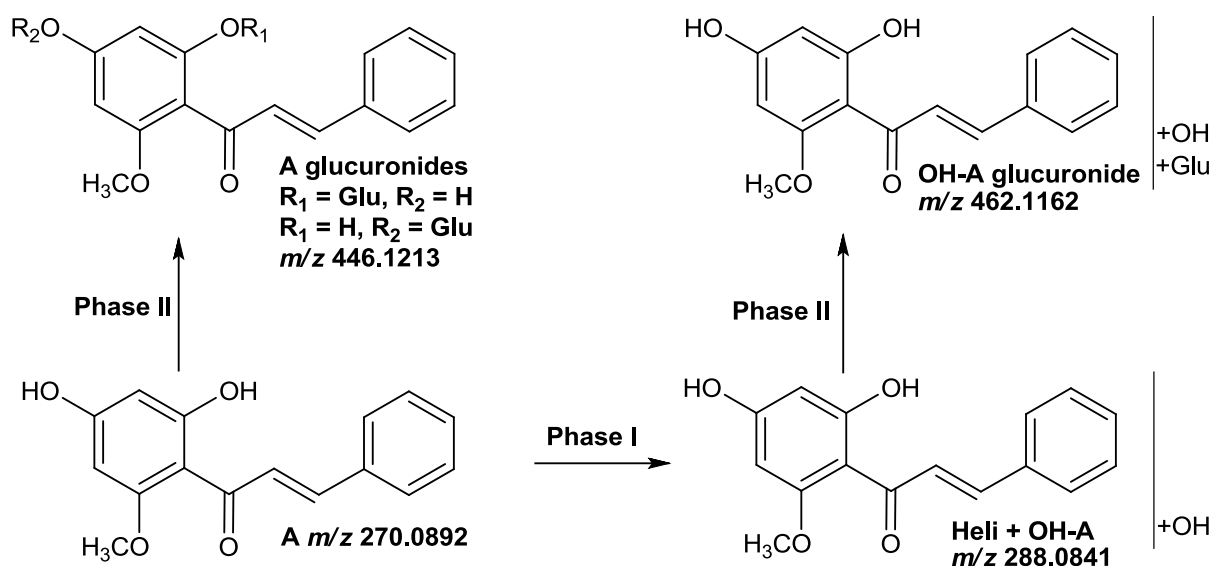


Figure 5.6: Suggested metabolism scheme of A using human liver microsomes. Metabolites were identified by LC–ESI–MS in different incubation systems.

5.3.3 Structure elucidation of major flavokawain metabolites

For structure elucidation of flavokawain A, B, and C metabolites, samples of combined phase I and II metabolism (**Ph I+II**) were prepared and subjected to HPLC–NMR analysis as described in chapter 2.3.3.4 using one- (^1H) and two-dimensional ($^1\text{H}, ^1\text{H}$ -COSY, $^1\text{H}, ^{13}\text{C}$ -HSQC, $^1\text{H}, ^{13}\text{C}$ -HMBC) NMR techniques. Due to the higher detection limit of NMR compared to MS, only the structures of major metabolites could be elucidated.

Trans-flavokawain A-2'-O-glucuronide (Figure 5.7) was identified as major metabolite of **FKA**. The metabolite was manually isolated via HPLC fraction collection and subjected to ^1H NMR and COSY analysis (see chapter 2.3.3.4). In HSQC and HMBC experiments, the signals appeared too weak for a full ^{13}C assignment. Similarity of the ^1H NMR spectra of the major **FKA** metabolite with parent compound clearly shows slightly changed chemical shifts for the protons in ring B while a clear change in the chemical shift position occurs for H-3' and H-5' and for the two olefinic protons α/β (Table 5.8). The same was observed for **FKB** and **FKC** (Table 5.9 and 5.10) and constitutes evidence of the glucuronide moiety being attached to the OH in position 2'. The resonances from the glucuronide moiety could not be assigned due to the presence of the *cis* isoform and 3 methoxy groups that create an overlap of signals also in the COSY spectrum. The two detected metabolite masses of FKA-monoglucuronides in Table 5.4 can now be assigned to the major *trans* and the minor *cis* isoform (Table 5.8). The latter might constitute an artifact that is formed during incubation, sample processing, or isolation procedure.

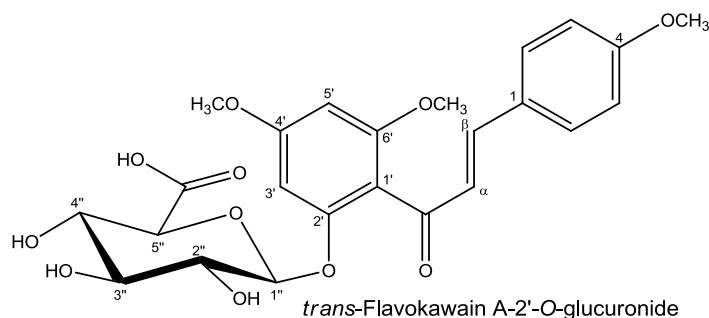


Figure 5.7: Major metabolite of FKA.

Table 5.8: $^1\text{H-NMR}$ data of FKA, *trans*- and *cis*-FKA-2'-O-glucuronide. Recording conditions see chapter 2.3.3.4.

| # | Flavokawain A | FKA-2'-O-glucuronide | |
|---------------------|-------------------------------|---|---|
| | δ (ppm), m, J (Hz) | Trans form (major) δ (ppm), m, J (Hz) | Cis form (minor, artifact) δ (ppm), m, J (Hz) |
| 3' | 6.11 (d, 1H, $J = 2.3$) | 6.57 (d, 1H, $J = 2.3$) | 6.48 (d, 1H, $J = 2.3$) |
| 5' | 6.09 (d, 1H, $J = 2.3$) | 6.36 (d, 1H, $J = 2.3$) | 6.15 (d, 1H, $J = 2.3$) |
| α | 7.71 (d, 1H, $J = 15.9$) | 6.96 (d, 1H, $J = 15.9$) | 6.39 (d, 1H, $J = 12.8$) |
| β | 7.81 (d, 1H, $J = 15.9$) | 7.39 (d, 1H, $J = 15.9$) | 6.88 (d, 1H, $J = 12.8$) |
| 2/6 | 7.60 (AA', 2H, d, $J = 8.7$) | 7.58 (2H, m) | 7.56 (2H, m) |
| 3/5 | 6.98 (AA', 2H, d, $J = 8.7$) | 6.95 (3H, m) | 6.81 (3H, m) |
| 4'-OCH ₃ | 3.95 (3H, s) | 3.83 (3H, s) | 3.79 (3H, s) |
| 6'-OCH ₃ | 3.84 (3H, s) | 3.78 (3H, s) | 3.73 (3H, s) |
| 4-OCH ₃ | 3.85 (3H, s) | 3.85 (3H, s) | 3.80 (3H, s) |
| 1'' | | Overlap with HDO signal | Overlap with HDO signal |
| 2'' | | | |
| 3'' | | 3.5 – 3.6 (m) | 3.5 – 3.6 (m) |
| 4'' | | | |
| 5'' | | Overlap with OCH ₃ signals | Overlap with OCH ₃ signals |

Trans-flavokawain B-2'-O-glucuronide (Figure 5.8) constitutes the major metabolite of **FKB** identified by ^1H NMR, COSY, HSQC, and HMBC (see chapter 2.3.3.4). Similarity of the ^1H NMR spectrum of the major **FKB** metabolite with that of the parent compound clearly shows slightly changed chemical shifts for the protons in ring B while a clear change in the chemical shift position occurs for H-3' and H-5' and for the two olefinic protons α/β (Table 5.9). Signals from the glucuronide moiety are recognized and COSY spectrum enabled their assignment even if some signals overlapped. The proton at the anomeric C-1'' is partially suppressed and H-5'' is overlapped by the methoxy signal. ^{13}C resonances were deduced from HMBC and in some cases it was not possible to discriminate close resonances as they were found in the ring B (Table 5.9). ^{13}C NMR chemical shifts of C-2' and the COOH carbon atom were not detected (n.d.) because of low signal-to-noise ratio of the HMBC spectrum.

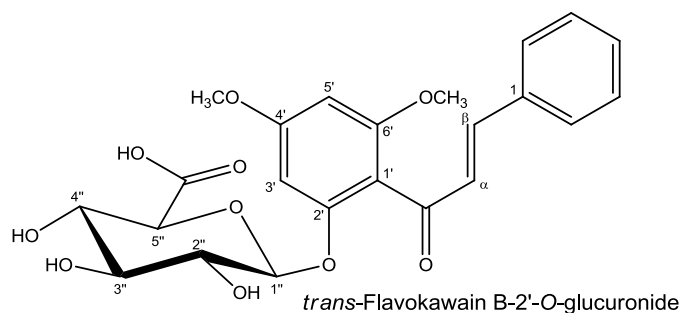


Figure 5.8: Major metabolite of FKB.

Table 5.9: ^1H - and ^{13}C -NMR data of FKA and *trans*-FKB-2'-O-glucuronide. Recording conditions see chapter 2.3.3.4.

| # | Flavokawain B | | <i>trans</i> -FKB-2'-O-glucuronide | |
|---------------------|-------------------------------|---|------------------------------------|--|
| | δ (ppm), m, J (Hz) | ^1H δ (ppm), m, J (Hz) | ^{13}C δ (ppm) | |
| 1' | | | 113.5 | |
| 2' | | | n.d. | |
| 3' | 6.12 (d, 1H, $J = 2.3$) | 6.55 (d, 1H, $J = 2.0$) | 95.3 | |
| 4' | | | 164.1 | |
| 5' | 6.10 (d, 1H, $J = 2.3$) | 6.37 (d, 1H, $J = 2.0$) | 93.8 | |
| 6' | | | 160.1 | |
| <u>C=O</u> | | | 196.0 | |
| α | 7.72 (d, 1H, $J = 15.9$) | 7.09 (d, 1H, $J = 15.9$) | 129.5 | |
| β | 7.92 (d, 1H, $J = 15.9$) | 7.42 (d, 1H, $J = 15.9$) | 145.7 | |
| 1 | | | 136.2 | |
| 2-6 | 7.65 (2H, m) | 7.62 (2H, m) | 129.5 | |
| 3-5 | 7.42 (3H, m) | 7.39 (3H, m) | 129.9 | |
| 4 | | | 131.6 | |
| 4'-OCH ₃ | 3.95 (3H, s) | 3.85 (3H, s) | 55.8 | |
| 6'-OCH ₃ | 3.84 (3H, s) | 3.79 (3H, s) | 56.1 | |
| 1'' | | 5.02 (d, 1H, $J = 7.8$) | 102.5 | |
| 2'' | | 3.38 (m, 1H) | 74.6 | |
| 3'' | | | 77.3 | |
| 4'' | | 3.49 (m, 2H) | 73.3 | |
| 5'' | | 3.85 (overlap with OCH ₃) | 76.3 | |
| <u>COOH</u> | | | n.d. | |

Two monoglucuronides of **FKC** (4-O- and 2'-O-glucuronide named as FKC-1 and FKC-2; Figure 5.9) were found as major and 5,7-dimethoxy-flavanone-4'-O-glucuronide (named as FKC-3; Figure 5.10) as minor **FKC** metabolite by the means of HPLC-NMR (see chapter 2.3.3.4). Similarity of the ^1H NMR spectrum of FKC-1 with that of the parent compound clearly shows slightly changed chemical shifts for H-3' and H-5' and the olefinic protons α/β while a clear change in chemical shift is detected for the protons in ring B indicating a substitution (Table 5.10). Signals from the glucuronide moiety are recognized also based on the data from the other metabolites. The anomeric proton is partially suppressed due to the

proximity of the water signal, but it is visible. The other protons of the glucuronide moiety seem to collapse in two distinct signals present in the region 3.5 – 3.7 ppm. Integrals are not helpful but resonances have been assigned, considering also the other metabolites, as reported.

Similarity of the ^1H NMR spectrum of FKC-2 with that of the parent compound clearly shows slightly changed chemical shifts for the protons in ring B while a clear change in the chemical shift position occurs for H-3' and H-5' and for the two olefinic protons α/β (Table 5.10). Signals from the glucuronide moiety were clearly recognized and COSY spectrum enabled assignment of the single protons. An HMBC correlation between H-5'' and a ^{13}C at 171.9, typical chemical shift for carboxylic carbons, proves the presence of the glucuronide. HMBC enabled assignment of those ^1H resonances that would be otherwise interchangeable like the methoxy groups or protons H-3' and H-5'.

For FKC-3 (Figure 5.10), the disappearance of the olefinic protons α/β together with the appearance of new resonances enables the recognition of the aglycone skeleton as a flavanone (Table 5.11). The molecule was fully assigned by means of 1D and 2D NMR spectra. There is some overlap among the glucuronide H-2'', H-3'', and H-4'' in the ^1H NMR spectrum but the glucuronide moiety is clearly recognized. The signals of the H-3 proton appear as a “double pseudotriplet”. The reason might be that the compound is a racemate, consisting of two diastereomers with opposite configuration at C-2. The signals of H-2 of the 2*R*- and the 2*S*-form as well as the signals of the H-3a at 3.04 ppm are isochronic. Only the dd signals of H-3b appear at slightly different chemical shifts ($\Delta\delta \sim 0.01$ ppm). If this hypothesis is correct, it can be assumed that the FKC-3 is formed by a non-enzymatic chemical reaction and is possibly an artifact (similar to the *cis* isoforms of FKA and FKB metabolites). The HRESIMS spectrum (positive ionization) confirmed the structure (found 477.1374 $[\text{M}+\text{H}]^+$, calculated for $\text{C}_{23}\text{H}_{25}\text{O}_{11}^+$: 477.1391, see chapter 2.3.3.4).

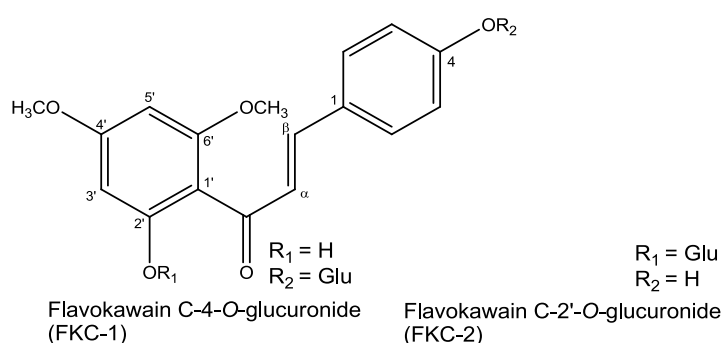
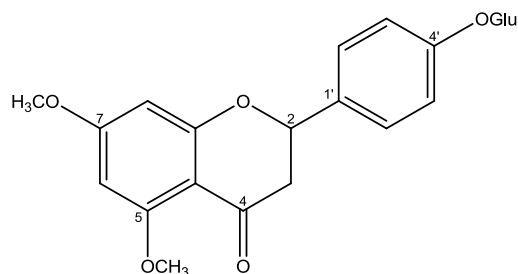


Figure 5.9: Metabolites of FKC.

Table 5.10: ^1H - and ^{13}C -NMR data of FKC, FKC-4-O-glucuronide (FKC-1), and FKC-2'-O-glucuronide (FKC-2). Recording conditions see chapter 2.3.3.4.

| # | Flavokawain C | FKC metabolite | | |
|---------------------|----------------------------|-------------------------------------|-------------------------------------|----------------|
| | δ (ppm), m, J (Hz) | FKC-1 δ (ppm), m, J (Hz) | FKC-2 δ (ppm), m, J (Hz) | δ (ppm) |
| 1' | | | | 113.7 |
| 2' | | | | 157.8 |
| 3' | 6.10 (d, 1H, J = 2.0) | 6.12 (d, 1H, J = 2.3) | 6.49 (d, 1H, J = 2.0) | 95.1 |
| 4' | | | | 163.8 |
| 5' | 6.09 (d, 1H, J = 2.0) | 6.10 (d, 1H, J = 2.3) | 6.38 (d, 1H, J = 2.0) | 93.8 |
| 6' | | | | 160.0 |
| <u>C=O</u> | | | | 196.4 |
| α | 7.71 (d, 1H, J = 15.6) | 7.71 (d, 1H, J = 15.5) | 6.89 (d, 1H, J = 16.0) | 126.4 |
| β | 7.77 (d, 1H, J = 15.6) | 7.84 (d, 1H, J = 15.5) | 7.34 (d, 1H, J = 16.0) | 147.4 |
| 1 | | | | 127.2 |
| 2/6 | 7.51 (AA', 2H, d, J = 8.7) | 7.62 (AA', 2H, d, J = 8.7) | 7.48 (AA', 2H, d, J = 8.9) | 131.6 |
| 3/5 | 6.82 (AA', 2H, d, J = 8.7) | 7.15 (AA', 2H, d, J = 8.7) | 6.80 (AA', 2H, d, J = 8.9) | 116.6 |
| 4 | | | | 161.5 |
| 4'-OCH ₃ | 3.94 (3H, s) | 3.95 (3H, s) | 3.85 (3H, s) | 55.7 |
| 6'-OCH ₃ | 3.84 (3H, s) | 3.85 (3H, s) | 3.78 (3H, s) | 56.1 |
| 1'' | | 5.05 (d, 1H, J = 7.7) | 5.05 (d, 1H, J = 7.7) | 102.4 |
| 2'' | | 3.52 (2H, m) | 3.37 (dd, 1H, J = 7.7, 9.1) | 74.2 |
| 3'' | | | 3.46 (dd, 1H, J = 9.1, 9.1) | 76.9 |
| 4'' | | 3.65 (m) | 3.56 (dd, 1H, J = 9.6, 9.1) | 72.5 |
| 5'' | | 3.93 (m) | 3.97 (d, 1H, J = 9.6) | 76.3 |
| <u>COOH</u> | | | | 171.9 |



5,7-Dimethoxyflavanone-4'-O-glucuronide (FKC-3)

Figure 5.10: Metabolite of FKC.

Table 5.11: ^1H - and ^{13}C -NMR data of 5,7-dimethoxyflavanone-4'-*O*-glucuronide (**FKC-3**). Recording conditions see chapter 2.3.3.4.

| # | FKC metabolite | |
|---------------------------------|---|-----------------------------------|
| | ^1H δ (ppm), m, J (Hz) | ^{13}C δ (ppm) |
| 2 | 5.43 (dd, 1H, $J = 12.8, 3.0$) | 79.9 |
| 3 | 3.04 (dd, 1H, $J = 16.4, 12.8$) 2.72 (dt, 1H, $J = 16.4, 3.0$) | 46.2 |
| 4 | | 192.4 |
| 5 | | 163.6 |
| 6 | 6.20 (d, 1H, $J = 2.0$) | 93.7 |
| 7 | | 168.3 |
| 8 | 6.22 (d, 1H, $J = 2.0$) | 94.9 |
| 9 | | 167.5 |
| 10 | | 106.3 |
| 1' | | 134.2 |
| 2'/6' | 7.44 (AA', 2H, d, $J = 8.7$) | 128.7 |
| 3'/5' | 7.14 (AA', 2H, d, $J = 8.7$) | 117.8 |
| 4' | | 158.9 |
| 5- and 7-OCH₃ | 3.84 (6H, s) | 56.2 |
| 1'' | 4.98 (d, 1H, $J = 7.5$) | 102.3 |
| 2'' | | 74.6 |
| 3'' | 3.51 (m, 2H) | 77.3 |
| 4'' | 3.59 (m, 1H) | 73.1 |
| 5'' | 3.92 (d, 1H, $J = 9.6$) | 76.3 |
| COOH | | 173.5 |

5.4 Conclusion

The *in vitro* metabolism of **FKA**, **FKB**, **FKC**, and **A** was studied using pooled human liver microsomes. For a metabolic profile, different microsomal incubation systems were established including phase I, phase II (glucuronidation), and combined reactions. Metabolites were identified by LC–HRESIMS. Moreover, the structure of major flavokawain metabolites was elucidated by the means of LC–NMR.

In phase I metabolism, demethylation in position C-4 or C-4' and hydroxylation predominantly in position C-4 occurs. This leads to the formation of **FKC** as major phase I metabolite of **FKA** and **FKB** and **Heli** as major phase I metabolite of **FKC** and **A**. Metabolites were assigned to found molecular masses (HRESIMS) and exact accordance to the retention times of the references (**FKC** and **Heli**) in the chromatographic system. Moreover, other monohydroxylated products were found as minor metabolites of **FKC** and **A**, but the position of hydroxylation could not be determined by mass spectrometric methods. The compounds

were even more extensively metabolized in presence of UDPGA by microsomal UGTs. For all test chalcones, the corresponding monoglucuronides were detected as the major metabolites in phase II and combined metabolism. The structures of the major flavokawain-glucuronides were elucidated by LC–NMR techniques. The detection of two metabolite masses of 490.1475 g/mol corresponding to **FKA**-glucuronides can be explained by the coexistence of the major *trans* and the minor *cis* isomer. For both, ¹H NMR signals were detected. Besides the 2'-O- and 4-O-chalcone-monoglucuronides of **FKC**, also the corresponding flavanone-glucuronide was identified by LC–NMR. This result is in accordance with MS data showing three metabolite masses of 476.1319 g/mol. The predominance of glucuronides over phase I metabolites generally emphasizes the important role of conjugated chalcones metabolites as possible *in vivo* active principles. This has also been shown for different flavonoids and chalcones such as **XAN** [101,376]. It has to be noticed that the extent of conjugated metabolites may even be underestimated by the use of microsomes, as phase II reactions are limited to glucuronidation reactions. Therefore, the concentration of conjugated metabolites *in vivo* may even be higher. Nevertheless, regarding the *in vitro* biological activity or toxicity of the chalcones, conjugated metabolites are to date not included in testing although they may rapidly be formed *in vivo* and therefore may constitute the actual active principles. Hence, the direct testing of phase II metabolites in *in vitro* assays would be an interesting issue. Toxicity studies - like performed for flavokawains in chapter 3 - should also be conducted in absence or presence of metabolizing enzymes to clarify if the compounds might be (de-)toxified. In comparison to e.g. **FKB**, which showed distinct toxicity against hepatoma cell lines, its major metabolite the 2'-O-glucuronide might show altered behavior.

Summing up, a metabolic profile of investigated chalcones is proposed. Furthermore, major phase I and II metabolites were identified based on MS and NMR data. Like for other flavonoids, conjugation to glucuronic acid seems to be a major route in chalcone metabolism. In future studies, microsomal incubation systems can be used to identify involved cytochrome P450 enzymes by selective inhibition of isoenzymes. Moreover, kinetic studies could be performed. The synthesis, characterization, and testing of chalcones glucuronides and other phase II metabolites remains a challenging issue as it is likely that those metabolites predominate *in vivo*.

6 *In vitro* stability, metabolism, and hepatotoxicity of a tacrine-silibinin codrug *)

6.1 Introduction

In recent years, much effort has been put into discovering new drugs for therapy of Alzheimer's disease (AD), the most prominent form of dementia [389]. To date there are only few approved drugs available. In 1993, tacrine (**1**, Figure 6.1) was approved as a potent acetylcholinesterase (AChE) inhibitor for treatment of AD. It was withdrawn from the market because of its hepatotoxic effects *in vivo* [390–393].

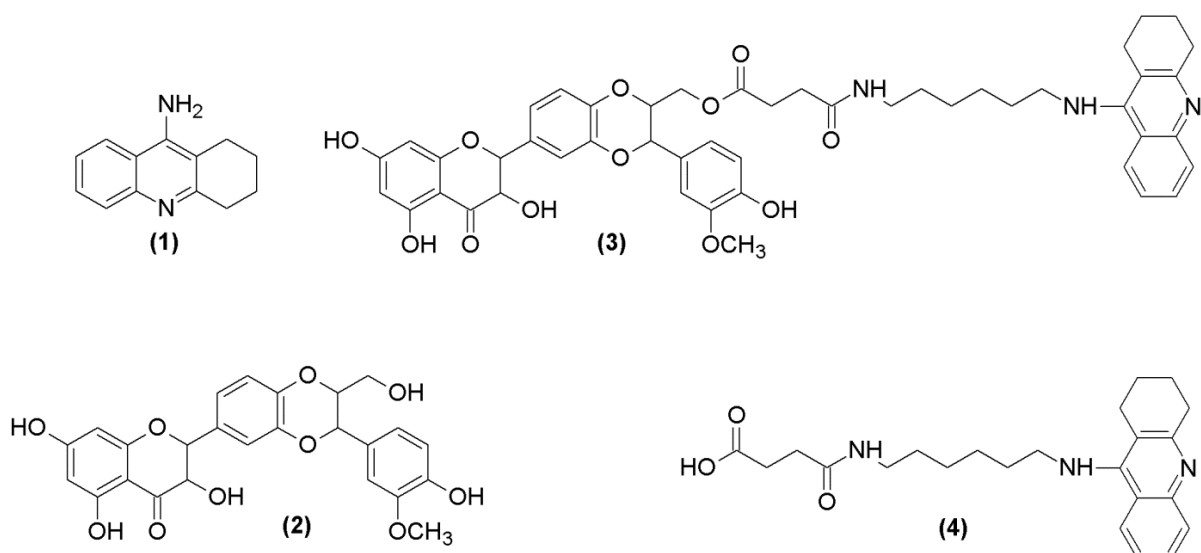


Figure 6.1: Structures of the AChE inhibitor tacrine (1), hepatoprotective flavonolignan silibinin (2), succinic acid-bridged tacrine-silibinin codrug (3), and its metabolite tacrine hemisuccinamide (4).

In order to face this problem there have been several approaches in medicinal chemistry to create hybrid [394,395] or multitarget [396,397] compounds by addressing more than one relevant pharmacological target with additive beneficial effects. A novel approach was realized by combining tacrine with the natural product silibinin (**2**, Figure 6.1), a flavonolignan known for its hepatoprotective and potentially anti-oxidant activities, in the form of a “codrug”. Like hybrid molecules this codrug molecule combines two pharmacologically active molecules within one molecule. In a hybrid such a connection is stable, whereas in the codrug approach at least one connecting chemical bond should be cleavable *in vivo*.

*) Part of the data presented in this chapter are published in Chen et al., Tacrine-silibinin codrug shows neuro- and hepatoprotective effects *in vitro* and pro-cognitive effects *in vivo*, *J Med Chem* 55 (2012) 5231-5242 and in Zenger et al., In-vitro stability and metabolism of a tacrine-silibinin codrug, *JPP* (2013) accepted.

Therefore, Chen et al. synthesized a codrug (**3**, Figure 6.1) consisting of a tacrine-based AChE inhibiting part and silibinin, respectively, linked by an ester bond. Since the structure of the codrug does not release tacrine but a related compound after cleavage, it is not a classical prodrug. Furthermore, a codrug releases two, not one biologically active compound after activation. The pharmacological properties of this tacrine-silibinin codrug were evaluated in comparison to tacrine and an equimolar mixture of tacrine and silibinin. The codrug showed quite promising pharmacological effects like AChE and butyrylcholinesterase (BChE) inhibitory activity, being slightly less potent than tacrine. Moreover, the codrug exhibited a neuroprotective effect against glutamate-induced toxicity using a neuronal cell line (HT-22). Finally, in a behavioral study, the codrug reversed scopolamine-induced cognitive impairment to the same extent as tacrine [100].

Beyond the pharmacological investigations, the objective of this study was to evaluate possible hepatotoxic or hepatoprotective effects of the codrug compared to tacrine and an equimolar mixture of tacrine and silibinin. In addition, it should be clarified if the chemical connection supplies any advantages over a physical mixture of components.

Furthermore, open questions remained regarding the stability and metabolism of the codrug in the *in vitro* incubation assays and *in vivo* testings, respectively. Accordingly, it had to be elucidated if it is the codrug, any cleaved product, or metabolite that is responsible for the pharmacological actions.

In our study, *in vitro* incubation conditions were mimicked in order to evaluate stability of the codrug during the incubation period of 24 h like in the *in vitro* assays [100]. In addition, the microsomal metabolism was examined to determine the stability in presence of metabolizing enzymes (metabolic stability). Moreover, this work was aimed to identify possible metabolites of the codrug, which may also occur *in vivo* and constitute the active principle of the compound. It can be assumed from the molecule structure that the ester bond of the codrug is easily cleaved and the tacrine-part of the molecule, a tacrine hemi succinamide (**4**, Figure 6.1), is generated.

Microsomal metabolism of both tacrine and silibinin has been well described in literature [398,399]. For tacrine, hydroxylated metabolites are most important. Cytochrome P4501A2 (CYP1A2) was identified as major enzyme involved in tacrine metabolism and is responsible for the formation of both stable (1,2,4-OH tacrine) and protein-reactive metabolites (7-OH tacrine) [400,401]. Both *in vitro* [402] and *in vivo* [403] fluvoxamine (CYP1A2 inhibitor) was identified as potent inhibitor of tacrine metabolism. For silibinin, glucuronidated metabolites play the major role. The major sites for glucuronidation are the phenolic OH groups at C-20 and C-7 [404].

Investigating the microsomal metabolism of the codrug creates valuable data concerning possible metabolites, which can putatively be found also *in vivo* and reveals interesting aspects of identifying the active principle of the codrug.

Tacrine's liver toxicity is extensively described in literature [405]. Among other aspects it is controversially discussed whether toxicity of tacrine is mediated by CYP1A2 or not [406,407]. With respect to unknown metabolism of the codrug, the study also deals with the evaluation of putative toxicity of metabolites.

6.2 Aim of the study

As the tacrine-silibinin codrug offers promising pharmacological properties, this study should assess its *in vitro* hepatotoxicity in comparison to tacrine and an equimolar of tacrine and silibinin in order to reveal any beneficial effect of the codrug design. For valuation of the *in vitro* and *in vivo* testings, particularly with regard to the identification of the active principle, the degradation and metabolic stability of the codrug should be investigated in different *in vitro* incubation systems. These data would supply useful information about the stability, possible degradation products, and metabolites of the codrug. Furthermore, the toxicity of the codrug cleavage products should be studied, as they constitute the primary metabolites *in vitro* and likely occur *in vivo*.

Taken together, this study was aimed to supplement preclinical data of the codrug in terms of drug toxicity and metabolism by choosing appropriate *in vitro* assays.

6.3 Results and discussion

6.3.1 Analytical characterization of the test compounds

Structure confirmation of ((2*S*,3*S*)-3-(4-hydroxy-3-methoxyphenyl)-6-((2*R*,3*R*)-3,5,7-trihydroxy-4-oxochroman-2-yl)-2,3-dihydrobenzo[*b*][1.4]dioxin-2-yl)-methyl 4-oxo-4-(6-(1,2,3,4-tetrahydroacridin-9-ylamino)-hexylamino)butanoate hydrochloride (**3**) and 4-oxo-4-(6-(1,2,3,4-tetrahydroacridin-9-ylamino)butanoic acid (**4**) was carried out by Dr. Xinyu Chen applying NMR spectroscopy (see chapter 2.1.3.2) [100].

Purity of synthesized compounds was determined by HPLC using method **P3** for the codrug and method **P4** for the tacrine hemi succinamide (see chapter 2.1.3.3). For both compounds, a purity of 96% was found.

For evaluation of chromatographic behavior and rough estimation of purity and lipophilicity, HPTLC analysis was performed on silica coated glass plates with the solvent system **T2** (see chapter 2.1.3.1).

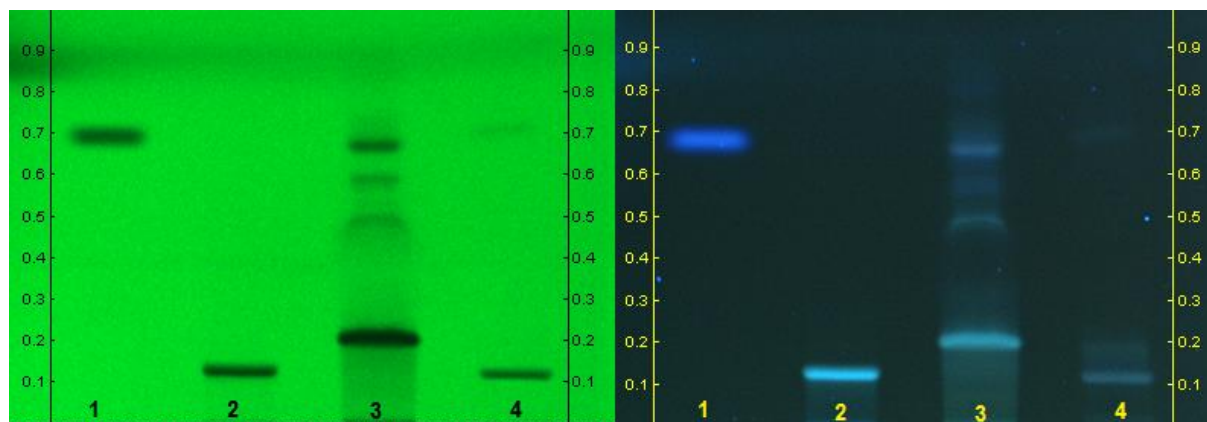


Figure 6.2: HPTLC of test compounds. Tacrine (1), silibinin (2), tacrine-silibinin codrug (3), tacrine hemi succinamide (4). Plates were analyzed under UV light: 254 nm (left) and 365 nm (right). R_f values (1) 0.70, (2) 0.13, (3) 0.22, (4) 0.12. Basic solvent system T2.

Under alkaline solvent conditions, **1** likely exists as a free base clarifying its high R_f value. Both **3** and **4** are negatively charged leading to high affinity on silica gel and relatively low R_f values. However, for **3** and **4** some impurities are detectable (Figure 6.2).

Table 6.1: Calculated pK_a and $\log P$ values. (*) SciFinder, (#)

| | | 1 | 3 | 4 |
|-------------|-------------------|----------|----------------|----------------|
| pK_a^* | most acidic group | - | 7.39 ± 0.6 | 4.75 ± 0.1 |
| | most basic group | 9.94 | 9.10 ± 0.2 | 9.10 ± 0.2 |
| $\log P^\#$ | | 3.3 | 6.7 | 3.1 |

Based on calculated pK_a values (Table 6.1) the state of charge at physiological pH value can be estimated. For the most part, **1** and **3** are positively charged at pH 7.4. For **4**, zwitterion structure can be assumed at a physiological pH value. This “amino-acid” like property might be an explanation for its different solubility, distribution, and metabolism. However, in consideration of $\log P$ values (Table 6.1), **3** is supposed to be the most lipophilic of the compounds followed by **1** and **4**.

Previous studies have not addressed oral bioavailability. Nevertheless, drug-like properties of the codrug can be assessed by its physical and chemical characteristics applying Lipinski’s Rule of Five [340,342]. This rule predicts absorption or permeation problems for chemicals that possess the following characteristics:

- H-bond donors > 5
- A molecular weight > 500
- A ClogP > 5
- A sum of Ns and Os > 10.

As the codrug fulfills Lipinski's Rule of Five in all regards, poor oral bioavailability is expected. For an encompassing evaluation, however, screening assays for intestinal permeability have to be conducted in future studies. For highly lipophilic compounds like the codrug, transcellular absorption through the lipid bilayer might be possible anyway. The intestinal permeability can be examined e.g. in *in vitro* cell culture assays using Caco-2 cells. Differentiated Caco-2 cells develop tight junctions as well as uptake/efflux transporters mimicking intestinal mucosa epithelium.

From a biopharmaceutical point of view, assays concerning drug absorption, disposition, and excretion should be addressed in further preclinical studies to enlarge the already existing data of *in vitro* metabolism and toxicity.

6.3.2 Degradation stability under *in vitro* assay conditions

For pharmacological evaluation, the codrug has been tested in several *in vitro* assays to investigate its neuro- and hepatoprotective activities [100]. So far, it could not be excluded that during the incubation period of 24 h the compound is cleaved or decomposed into other (active) products. For this reason, the stability of the codrug under *in vitro* assay conditions was investigated (see chapter 2.3.4.2). The concentration of the codrug was determined by HPLC using method C3 (see chapter 2.3.4.1).

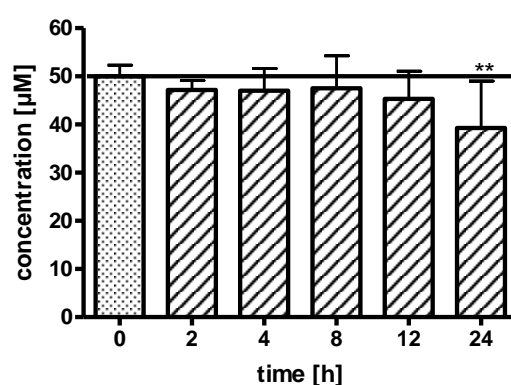


Figure 6.3: Degradation stability of the codrug in culture medium under *in vitro* assay conditions (37 °C, 5% CO₂). Concentrations were determined by HPLC calibration (method C3). Data are shown as mean \pm SD; n = 3. Statistical analysis was performed by one-way ANOVA followed by Dunnett's multiple comparison post-hoc test. **p < 0.01 vs. 0 h.

As illustrated in Figure 6.3, the concentration of the compound in the incubation medium was not markedly reduced during incubation time. Even after 24 h, around 80% of the initial concentration was detectable. Thus, these results suggest that the codrug and not cleaved products contribute to *in vitro* activities. Nevertheless, it has to be kept in mind that the stability assay was conducted in a cell-free system so that influence of cells on the stability cannot be excluded. In further studies, cellular uptake and intracellular codrug concentration should be investigated as the codrug is also supposed to be cleaved by cellular esterases.

6.3.3 Microsomal metabolism and metabolic stability in microsomal incubation systems

Furthermore, stability of the codrug was examined in several microsomal incubation systems (see chapter 2.3.4.3). Samples were taken at different time points and subjected to HPLC analysis (method C4 chapter 2.3.4.1) for quantification of codrug amount (Figure 6.4). In addition, samples (6 h) were analyzed using LC-MS (see chapter 2.3.4.1) in order to determine metabolite masses and identify possible metabolites (Figure 6.5).

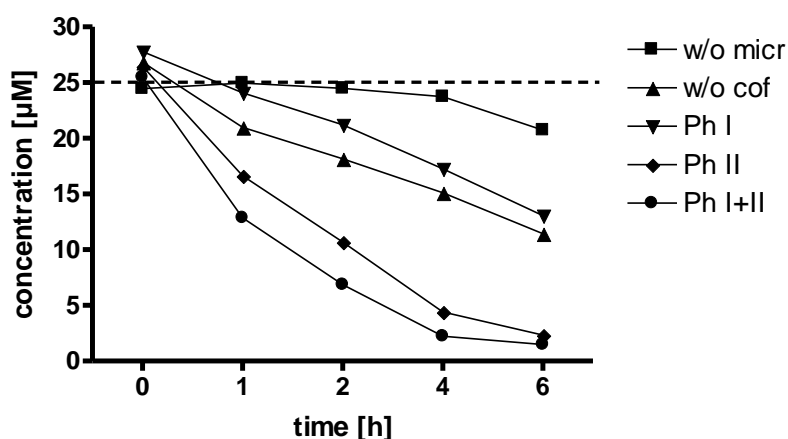


Figure 6.4: Metabolic stability of the codrug in microsomal incubation systems for phase I (Ph I), phase II (Ph II), and combined (Ph I+II) metabolism within 6 h including stability controls without microsomes (w/o micr) or without cofactors (w/o cof). Initial concentration of the codrug: 25 μM . Concentrations were determined by HPLC (method C4).

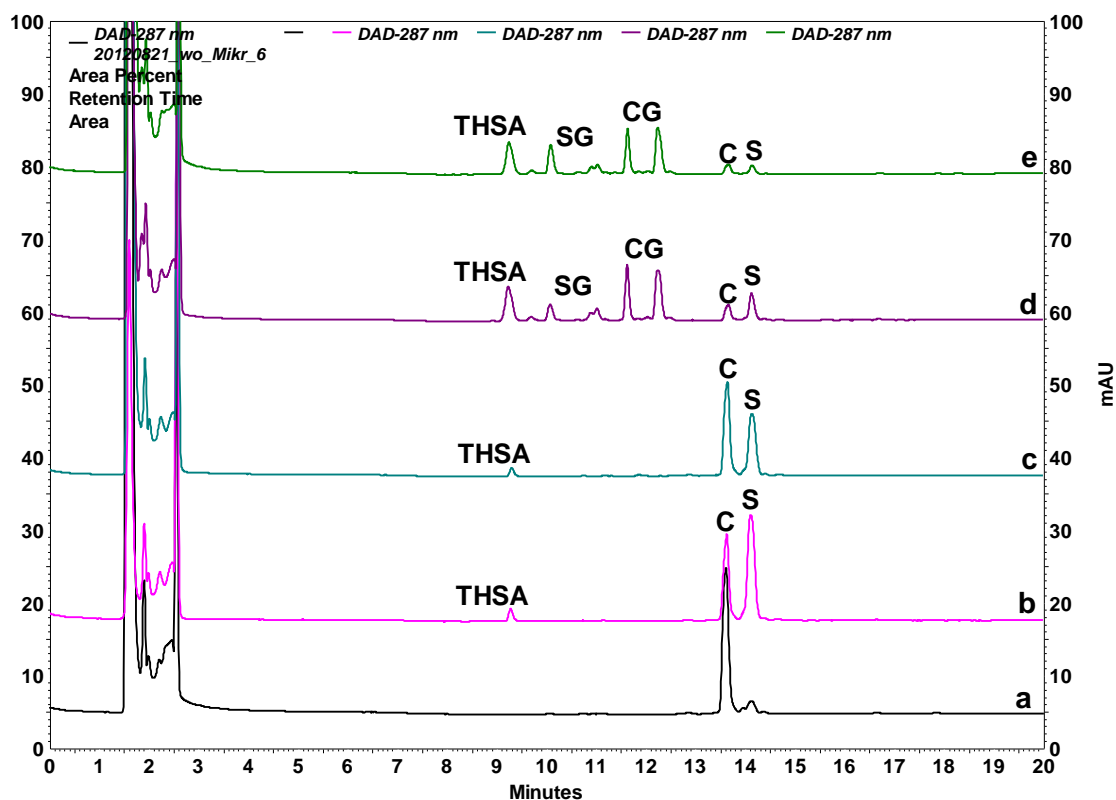


Figure 6.5: HPLC chromatogram of the microsomal incubation assay (6 h samples). a) without microsomes, b) without cofactors, c) phase I metabolism, d) phase II metabolism, e) combined phase I and II metabolism; $\lambda = 287$ nm. Structures were identified via LC–ESI–MS. Codrug (C), codrug glucuronides (CG), silibinin (S), silibinin glucuronides (SG), tacrine hemi succinamide (THSA).

As expected from the data acquired under in vitro conditions, the codrug showed good stability in the incubation system without microsomes. In the incubation system without NADPH and UDPGA no metabolism should take place as CYP reactions and glucuronidation cannot be performed without these cofactors/substrates. However, as can be seen from Figure 6.4, only half of the initial amount of codrug was detected after 6 h indicating that the compound is “metabolized” independently of CYP enzymes and UGTs. The structures formed were identified by LC–MS data as silibinin and tacrine hemi succinamide (Figure 6.5b). This indicates a cleavage of the ester bond by microsomal esterases – as expected from the design of the codrug. This ester bond is not cleaved at pH 7.4 in the buffer solution in absence of microsomes (Figure 6.4 and Figure 6.5a). In the set-up for phase I reaction the same products were detected as described for ester bond hydrolysis. The codrug is cleaved into two parts as indicated by the HPLC chromatogram (Figure 6.5c). No other metabolites were found by LC–MS. In contrast to known tacrine metabolism, the tacrine part of the codrug (the tacrine hemi succinamide) seems not to get hydroxylated anymore. Therefore, the compound is glucuronidated extensively. In phase II reactions two MS peaks corresponding to glucuronidated codrug molecules, the diglucuronide of the codrug, and silibinin glucuronides were identified besides the cleavage products (Figure 6.5d). The same compounds were detected in combined phase I and II metabolism (Figure 6.5e), but in higher

amounts. After 6 h (Figure 6.4) the codrug was converted completely to its glucuronides, silibinin glucuronides and the tacrine hemi succinamide. This reveals the importance of having a closer look on the tacrine hemi succinamide (and the codrug-glucuronides) as possible active principle of the codrug as it is possibly also formed quickly in vivo.

According to LC–MS data, a metabolism scheme of the codrug is proposed in Figure 6.6. Detailed information about calculated and found substance and metabolite masses can be found in chapter 10.3. Table 10.1 supplements the HPLC chromatogram in Figure 6.5.

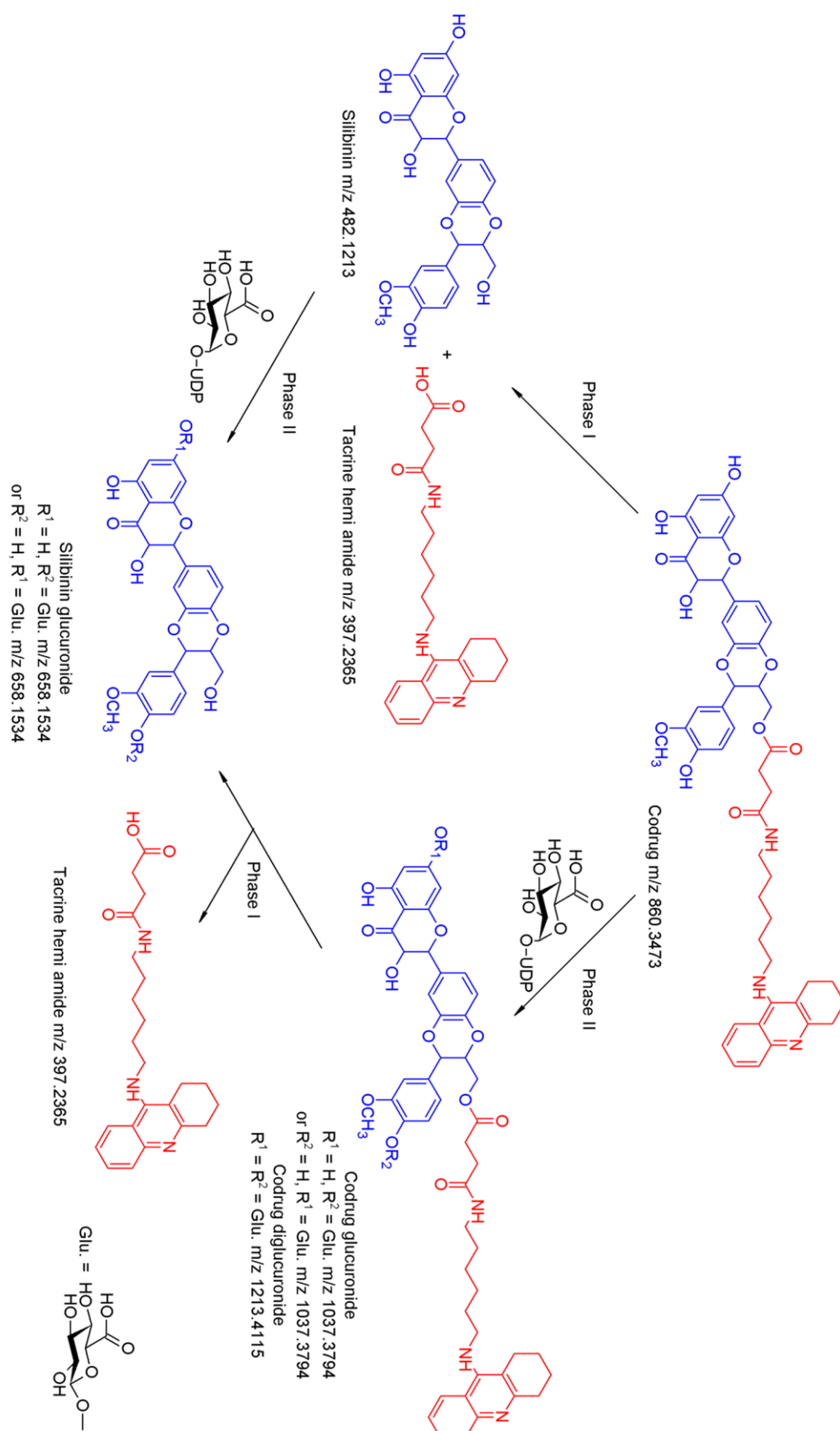


Figure 6.6: Suggested metabolism scheme of the codrug using human liver microsomes. Metabolites were identified in different incubation systems via LC-ESI-MS.

6.3.4 Comparative evaluation of the *in vitro* hepatotoxicity of tacrine, an equimolar mixture of tacrine/silibinin, and the codrug

To evaluate a possible hepatoprotective effect of the codrug and the tacrine/silibinin mixture compared to tacrine, the compounds' effect on human hepatic cell lines was investigated. For a first estimation of tacrine's hepatotoxicity, the influence of tacrine on the viability of three liver cell lines (see chapter 2.2.2.3) was determined by MTT assay (see chapter 2.2.5.1) choosing different incubation times (Table 6.2).

Table 6.2: Incubation time dependent IC₅₀ values [μM] of tacrine for three different cell lines determined from sigmoidal viability curves (MTT assay). MEAN ± SE (n = 3). Chosen cell line and incubation period for further testing is highlighted in grey.

| | 3 h | 6 h | 24 h | 48 h | 72 h |
|--------------|-----------|-----------|----------|---------|---------|
| HuH-7 | 749 ± 91 | 264 ± 65 | 94 ± 2 | 45 ± 6 | 37 ± 16 |
| HepG2 | 814 ± 126 | 395 ± 104 | 64 ± 9 | 30 ± 3 | 23 ± 2 |
| HSC | 471 ± 295 | 179 ± 81 | 128 ± 29 | 59 ± 12 | 25 ± 9 |

Tacrine showed a time and dose dependent toxicity on HuH-7, HepG2, and HSC. Determined IC₅₀ values ranged in comparable concentrations for the three cell lines. At short incubation times (3 h and 6 h) HSC prove to be the most sensitive and HepG2 the least sensitive; at longer incubation times (24 - 72 h) it was the other way round. The determined IC₅₀ values were compared to data from literature (HepG2) [408–411] which were found to be in the same concentration ranges.

All further assays were carried out on HSC as a representative model choosing an incubation time of 24 h because of already quite pronounced toxicity of tacrine and best applicable experimental setup.

Table 6.3: Influence of tacrine (T), an equimolar mixture of tacrine and silibinin (T + S), and the codrug (C) on viability and proliferation of HSC after 24 h incubation. Test concentration range 1-200 μ M. Concentrations are indicated for significant effects (mean \pm SD; $p < 0.01$).

| compound | MTT | | CV | |
|--------------|--------------------------|--------------------------|--------------------------|----------------------------|
| | concentration in μ M | remaining viability in % | concentration in μ M | remaining cell number in % |
| T | 10 | 77 \pm 4 | - | - |
| | 25 | 82 \pm 10 | - | - |
| | 50 | 90 \pm 5 | - | - |
| | 75 | 81 \pm 5 | 75 | 81 \pm 2 |
| | 100 | 64 \pm 10 | 100 | 79 \pm 8 |
| | 200 | 16 \pm 15 | 200 | 51 \pm 3 |
| T + S | 75 | 84 \pm 6 | 75 | 82 \pm 3 |
| | 100 | 64 \pm 3 | 100 | 74 \pm 8 |
| | 200 | 70 \pm 3 | 200 | 74 \pm 9 |
| C | 200 | 79 \pm 14 | no influence | |

First, the influence of test compounds on cell viability was determined by MTT assay (see chapter 2.2.5.1, Table 6.3). For tacrine, significant effects were detected already starting from 10 μ M. From a concentration of 100 μ M, cell viability was strongly affected by tacrine (see IC_{50} 128 μ M). For the equimolar mixture, significant impact on cell viability was detected starting at 75 μ M. At 100 μ M, cell viability decreased in the same way as for tacrine to 64%. At high concentrations (200 μ M), silibinin seems to exhibit a protective effect since viability was still 70% compared to only 16% for tacrine. The influence of the codrug on cell viability remained small and was significant only for the highest concentration tested.

Following, the compounds' effect on cell number was investigated by CV staining (see chapter 2.2.5.2, Table 6.3). Whereas both tacrine and the equimolar mixture had a significant impact on the cell number starting at a concentration of 75 μ M, the codrug showed no significant toxicity up to 200 μ M.

For a more precise analysis, we applied fluorescence microscopy and examined the influence on cell number and mitochondria (see chapter 2.2.6.1, Figure 6.7). Data confirmed the results of the crystal violet assay, being even more sensitive. As can be seen in Figure 6.7A, tacrine decreased the amount of cells already starting at a concentration of 50 μ M with higher concentrations being more toxic.

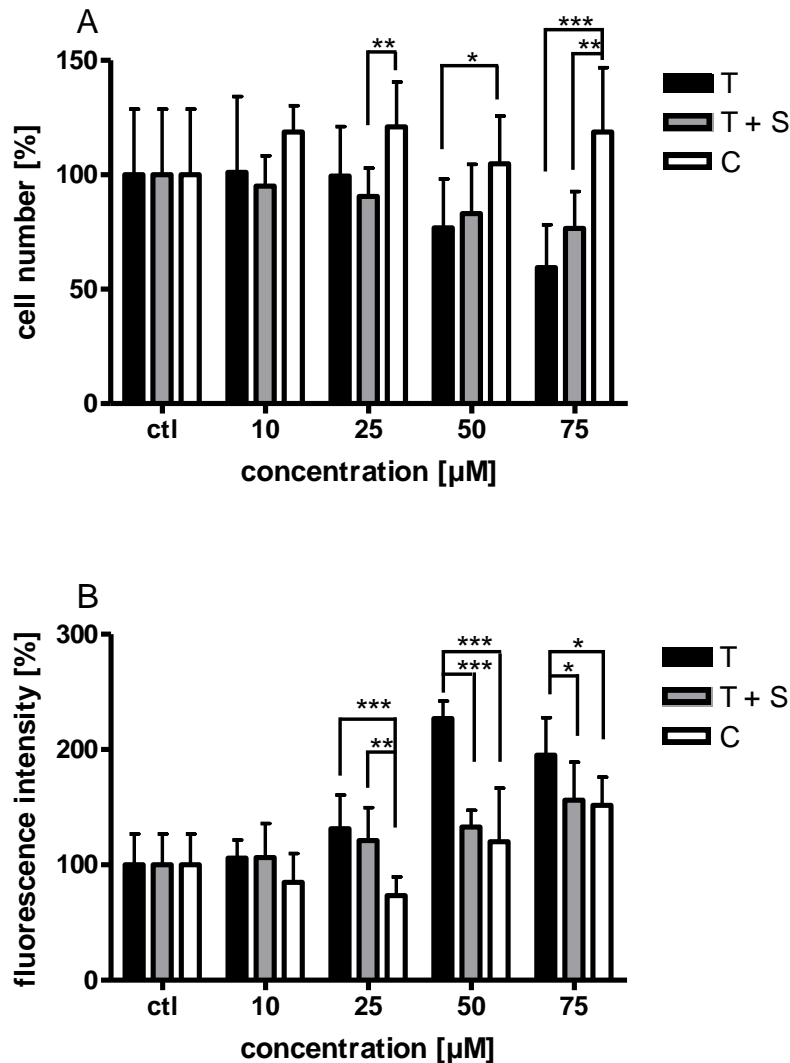


Figure 6.7: A Comparison of cell numbers determined by fluorescence microscopy after treatment of HSC with different concentrations of tacrine, an equimolar mixture of tacrine and silibinin, and codrug. B Fluorescence intensity of mitochondria after treatment of HSC with different concentrations of tacrine, an equimolar mixture of tacrine and silibinin, and codrug. Data were subjected to one-way ANOVA followed by Tukey's multiple comparison post-hoc test using GraphPad Prism 4 Software (Levels of significance * $p < 0.05$; ** $p < 0.01$; *** $p < 0.001$).

An interesting observation can be made when the influence of the codrug is compared with the tacrine/silibinin mixture (Figure 6.7A): Statistically significant differences were observed from a concentration of only 25 µM. The mixture shows lower cell viability and therefore higher cytotoxicity than the codrug. At concentrations where tacrine is toxic, also the mixture exhibits toxicity. Therefore, the codrug is greatly superior to the equimolar mixture in being non-toxic even at the highest concentration tested.

Additionally, we investigated the impact of the compounds on the mitochondria of HSC, as mitochondrial dysfunction is an important mechanism of hepatotoxicity [412] and is discussed to be involved in tacrine-induced liver toxicity [413]. One possible mechanism is the onset of mitochondrial permeability transition caused by opening of permeability transition pores in

the inner mitochondrial membrane. This pore opening causes mitochondrial depolarization, uncoupling, and large amplitude swelling and can lead to both necrotic and apoptotic cell death [321,414]. For mitochondrial analysis, mitochondria were stained after the treatment of cells with different concentrations of tacrine, tacrine/silibinin, and codrug, respectively, with a mitochondria specific dye that followed the determination of mitochondrial fluorescence intensity (figure 6.7B).

Mitochondrial fluorescence intensity dramatically increases after the treatment of cells with 50 μM tacrine to a value of 220% of the control. This increase in fluorescence intensity indicates a swelling of mitochondria and therefore mitochondrial dysfunction which can lead to necrotic or apoptotic cell death. This effect is significantly lower for the tacrine/silibinin mixture at 50 and 75 μM . The codrug shows the same effect as the mixture at these concentrations. In terms of hepatotoxicity indicated by increased mitochondrial fluorescence intensity in HSC, both the physical mixture and the codrug show greatly decreased toxicity compared to tacrine. Regarding the effect of the codrug at 25 μM , both tacrine and the tacrine/silibinin mixture show significantly higher fluorescence intensity, again indicating a superior effect of the codrug over the physical mixture of compounds.

Hepatotoxicity of tacrine and hepatoprotective activity of silibinin has been demonstrated before on HepG2 cells [415]. Our studies revealed also pronounced cyto- and mitotoxicity of tacrine on HSC. The mitotoxic effect is significantly lower for both the physical mixture of tacrine/silibinin and the codrug. Already at lower concentrations, the codrug's cytoprotective effect is more pronounced than that one of the mixture. Here the mixture was only moderately superior to tacrine's toxicity, whereas the codrug did not show any toxicity even at the highest concentration tested.

6.3.5 *In vitro* hepatotoxicity of the codrug's primary metabolites

In the previous chapter 6.3.4, the *in vitro* hepatotoxicity of tacrine was compared to an equimolar mixture of tacrine and silibinin and the codrug respectively.

The pronounced hepatotoxicity of tacrine has been shown before on several cell lines [407,416,417] and correlates well with our findings. In contrast, for the codrug, hepatotoxic effects were completely absent both *in vitro* and *in vivo* [100].

The codrug showed to be stable under *in vitro* assay conditions but is likely cleaved and metabolized quickly *in vivo*. Consequently, the effect of the codrug metabolites tacrine hemi succinamide and silibinin on viability, cell number, and mitochondria of HSC was examined in the same way.

Table 6.4: Influence of tacrine hemi succinamide (THSA), silibinin (S), and an equimolar mixture of tacrine hemi succinamide and silibinin (THSA + S) on viability and proliferation of HSC. Test concentration range 10-200 μ M. Concentrations are indicated for significant effects (mean \pm SD).

| compound | MTT | | CV | |
|-----------------|--------------------------|--------------------------|--------------------------|----------------------------|
| | concentration in μ M | remaining viability in % | concentration in μ M | remaining cell number in % |
| THSA | | no influence | | no influence |
| S | | no influence | | no influence |
| THSA + S | 200 | 77 \pm 7 | | no influence |

Viability of the cells was investigated by MTT assay (see chapter 2.2.5.1, Table 6.4). For the tacrine hemi succinamide and silibinin no influence on viability of HSC was detected. For the mixture of tacrine hemi succinamide and silibinin viability slightly decreased at 200 μ M. In comparison, tacrine affected cell viability already at 10 μ M and caused a decrease down to 16% at 200 μ M.

The influence of the compounds on the cell number was determined by CV staining (see chapter 2.2.5.2, Table 6.4). Comparable to the results of the codrug, there was no significant impact on the cell number within the highest concentration tested (200 μ M). In contrast, tacrine exhibited a concentration dependent toxicity starting at 75 μ M (Table 6.3).

Additionally, the effect of the codrug metabolites on cell number was analyzed by fluorescence microscopy applying Hoechst staining and counting cell nuclei (see chapter 2.2.6.1, Figure 6.8A). The number of cells remained unaffected by the compounds up to 75 μ M whereas tacrine decreased the cell number already starting at a concentration of 50 μ M (Figure 6.7A).

The influence of the compounds on mitochondria was investigated as mitochondrial impairment such as alterations in mitochondrial membrane potential can cause lethal cell death [414]. The mechanism of tacrine's toxicity is not yet fully investigated. However, a possible role of mitochondrial dysfunction and uncoupling is discussed in literature [413,416,418,419]. With respect to these findings, tacrine showed a significant increase in fluorescence intensity of mitochondria already at low concentrations (25 μ M) where it did not affect cell number yet (Figure 6.7B). While the influence on mitochondria already was significantly less pronounced for the codrug (Figure 6.7B), mitotoxicity was completely absent for tacrine hemi succinamide and silibinin in the tested concentration range (Figure 6.8B). Only the mixture of tacrine hemi succinamide and silibinin slightly decreased mitochondrial fluorescence intensity at a concentration of 75 μ M (Figure 6.8B).

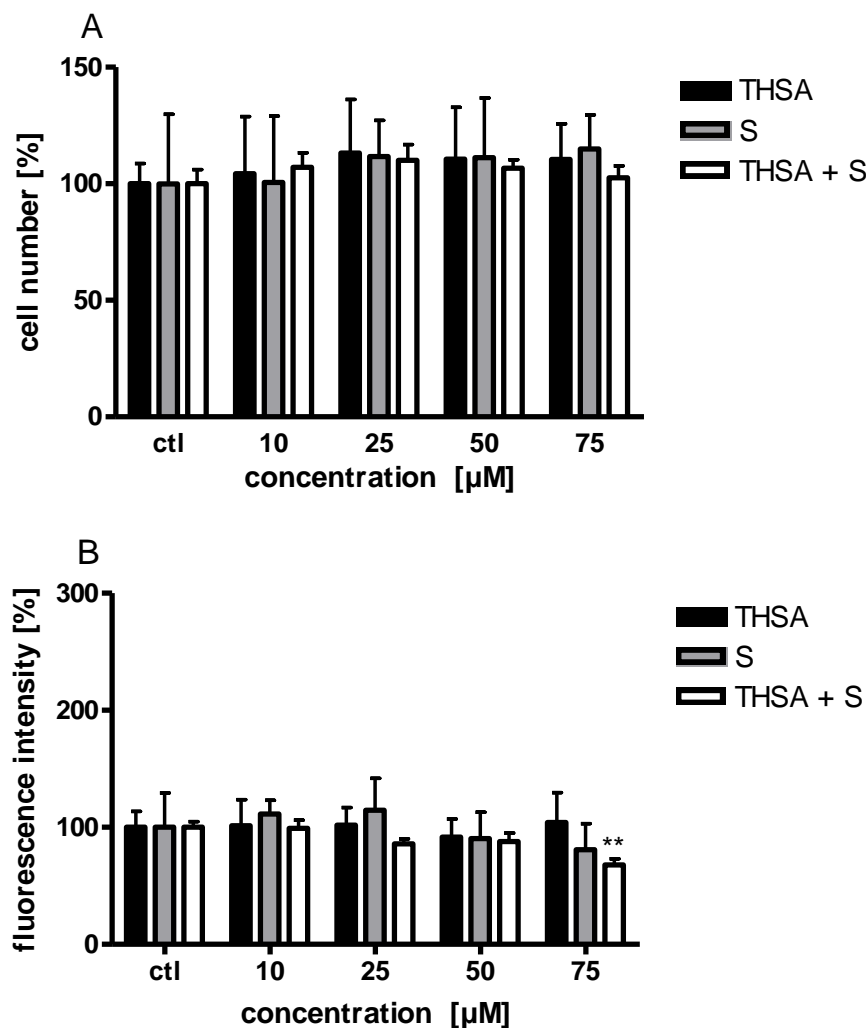


Figure 6.8: *In vitro* hepatotoxicity of the codrug's cleavage product tacrine hemi succinamide (THSA), silibinin (S), and equimolar mixture of THSA and silibinin (THSA + S) on HSC. A Cell number determined by fluorescence microscopy. B Fluorescence intensity of mitochondria. Untreated cells (ctl) were set as 100% values. Data are shown as mean \pm SD. Statistical analysis was performed by one-way ANOVA followed by Dunnett's multiple comparison post-hoc test. **p < 0.01 vs. ctl.

In summary, there was no detectable *in vitro* hepatotoxicity of tacrine hemi succinamide and silibinin, which might both be the primary metabolites of the codrug *in vivo*. The results also support and complete the already published findings of codrug's lacking hepatotoxicity *in vivo*. There probably would have been detectable hepatotoxic effects *in vivo* if the metabolites of the codrug exerted any toxicity.

6.4 Conclusion

In this study, the *in vitro* stability, hepatotoxicity, and metabolism of a tacrine-silibinin codrug with pro-cognitive effects was investigated. The results of the degradation assay implicate a good stability of the codrug in the incubation medium. However, in a microsomal incubation assay using HLM the codrug was rapidly cleaved and extensively metabolized into tacrine hemi succinamide and codrug- and silibininglucuronides. These findings have to be considered for evaluation of the *in vivo* results respectively the *in vivo* hepatotoxicity and behavioural studies. The data point out the role of the cleavage products especially the tacrine hemi succinamide as possible active principle *in vivo*. Indeed, the tacrine hemi succinamide showed also inhibition of AChE ($IC_{50} = 101.9$ nM) [100]. In further studies, the knowledge of microsomal metabolites can provide valuable hints for identification of metabolites in serum or tissue samples (e.g. liver, brain).

In a comparative evaluation of hepatotoxic effects on HSC, the physical mixture of tacrine and silibinin did not exhibit a significant improvement over tacrine regarding cell number whereas the codrug lacked cytotoxicity even at high concentrations. Both the codrug and the mixture, however, decreased mitochondrial fluorescence intensity compared to tacrine indicating a less pronounced mitotoxicity. Noteworthy, the *in vivo* hepatotoxicity testing in rats confirmed the *in vitro* hepatotoxicity findings showing a good predictability of the *in vitro* assay system in this case. Additionally, the *in vitro* hepatotoxicity testing revealed also the absence of any toxic effects of the codrug's cleavage products. This is again an advantage over tacrine whose protein-reactive metabolites, as it is known to date, exhibit harmful effects.

Taken together, the tacrine-silibinin codrug as well as its cleavage products lacked tacrine's therapy-limiting hepatotoxic effects. The stability studies help to understand and interpret the previous results and supply important information for further studies to finally identify the active principle of the codrug also *in vivo*. Whether the low *in vitro* hepatotoxicity of the metabolite tacrine hemi succinamide can explain the codrug's absence of hepatotoxicity *in vivo* or to which extent the silibinin part of the codrug actually contributes to the overall *in vivo* effects cannot be answered yet.

7 Summary

(1) Kava kava, traditionally used by the Pacific Islanders as a socio-ceremonial beverage and remedy, was approved as an anxiolytic drug in Western countries. However, the reports of severe hepatotoxic side effects led to the withdrawal of kava-containing products in most of these countries. Since then, responsible constituents and possible mechanisms of hepatotoxicity are controversially discussed.

To evaluate the hepatotoxic potential of single compounds, six kavalactones were isolated from an acetonic kava root extract and the three kava-chalcones (flavokawains) were obtained by synthesis. Subsequently, these major and minor constituents were tested towards their effects on cell viability and proliferation of human hepatoma cell lines. Whereas the toxicity of five tested kavalactones was found to be very low (**K**, **M**, **DMY**) or completely absent (**DHK**, **DHM**), distinct effects on both cell viability and proliferation were observed for the kavalactone **Y** and the kava-chalcones, **FKB** being the most toxic ($IC_{50} \sim 30 \mu\text{M}$ on HepG2 and $IC_{50} \sim 40 \mu\text{M}$ on HuH-7) of the test compounds.

The results of this study suggest that the flavokawains might contribute to the hepatotoxic potential of kava. Based on obtained *in vitro* toxicity data, further testing of long-term toxicity of **Y** and flavokawains is recommended preferably on primary human hepatocytes or *in vivo* in a suitable animal model.

(2) Therapy options for the treatment of Alzheimer's disease are still constricted to a few approved drugs. Facing the therapy limiting hepatotoxic side effects of tacrine in a new approach, a tacrine-silibinin codrug was synthesized that showed promising pharmacological properties such as AChE and BChE inhibitory activity *in vitro* and pro-cognitive effects *in vivo* in rats.

Driven by these promising results, the *in vitro* hepatotoxic potential of the codrug was assessed and compared to tacrine and an equimolar mixture of tacrine and silibinin. Therefore, the compounds' effects on cell number and fluorescence intensity of mitochondria of hepatic stellate cells were investigated. For both, the codrug and the physical mixture, reduced mitotoxicity compared to tacrine was observed. Additionally, the codrug did not show any influence on the cell number up to concentrations of $200 \mu\text{M}$. The results correlated well with the findings of the *in vivo* hepatotoxicity studies in rats. Furthermore, to find first hints of the active principle of the codrug, *in vitro* stability and microsomal metabolism studies were performed. In the presence of microsomes, the codrug was rapidly cleaved by esterases into tacrine hemi succinamide and silibinin. In phase II metabolism,

codrug- and silibininglucuronides were detected. As these metabolites are likely also formed *in vivo*, they may constitute the active principles of the codrug. Indeed the tacrine hemi succinamide showed pronounced AChE inhibition. Noteworthy, for the codrug cleavage products tacrine hemi succinamide and silibinin, toxicity in the *in vitro* HSC model was completely absent.

(3) Chalcones possess an interesting pharmacological profile for the treatment of hepatic fibrosis, as they comprise several favorable biological activities such as anti-inflammatory, anti-oxidant, antiviral, and apoptosis-inducing effects. The activation and the perpetuation of this activation of hepatic stellate cells are considered as the key steps in the pathogenesis of liver fibrosis. Hence, the inhibitory activity of structurally related prenylated and non-prenylated chalcones on activated human hepatic stellate cells was investigated.

With exception of the dihydrochalcones, **P**, and **3OHHeLi**, the investigated chalcones had a significant impact on cell viability, proliferation, cell organelles, and cytochrome c release. For the metabolites **4'AcXAN**, **XANC**, and **dhXANC**, similar activities were found as for the parent compound **XAN** whereas **4MeXAN** and **XANH** behaved differently. The induction of apoptosis via mitochondrial pathways is suggested as the test chalcones provoked a release of cytochrome c together with altered fluorescence intensity of mitochondria at low concentrations of 10 μ M. Several structure elements were identified which enhance or attenuate the activity of chalcones. The double bond in α,β position was essential for the activity. The unprotected hydroxyl group in position C-6' led to a complete loss of activity in case of **P**. Prenylation of C-3' and methoxy-groups in the A ring enhanced the activity whereas substituents in the B ring mostly attenuated the chalcones' effects. **4'MeXAN**, **A**, and **FKB** showed the strongest inhibitory effects on HSC. Based on the findings of this study, the most effective chalcones may be chosen to investigate the mechanisms on the molecular level. In addition, toxicity studies on primary human hepatocytes are needed.

(4) For studying the *in vitro* metabolism of flavokawains and alpinetin chalcone, different microsomal incubation systems were established. LC–HRESIMS was applied to identify phase I and II metabolites and to compile a metabolic profile for these compounds. Obtained data can be used to predict the *in vivo* metabolism and provide first information about main biotransformation pathways.

Demethylation (C-4, C-4') and hydroxylation (mainly C-4) constitute the major phase I reactions in flavokawain and **A** metabolism. **FKC** is generated as major metabolite of both **FKA** by demethylation and **FKB** by hydroxylation in position C-4. **HeLi** is formed as major metabolite of **FKC** and **A** after demethylation in position C-4' and hydroxylation of C-4 respectively. In phase II metabolism, extensive conjugation to glucuronic acid was observed.

In combined metabolism, the conjugated metabolites clearly predominated also. Glucuronidation of the parent chalcones is consequently considered as major reaction in the microsomal metabolism of investigated chalcones. The structures of major flavokawain-glucuronides were additionally elucidated using HPLC–NMR techniques. According to the results of this study, the chalcone monoglucuronides may constitute the major metabolites *in vivo*. It is not known if these metabolites contribute to pharmacological activities of chalcones. Regarding the observed *in vitro* hepatotoxicity of flavokawains, the biotransformation may also constitute a detoxifying reaction.

8 References

- [1] F.H. Netter, R. Mühlbauer, Atlas der Anatomie, Elsevier, Urban & Fischer, München, 2010.
- [2] A. Benninghoff, D. Drenckhahn, Taschenbuch Anatomie, Elsevier, Urban & Fischer, München, 2008.
- [3] H.F. Teutsch, The modular microarchitecture of human liver, *Hepatology* 42 (2005) 317–325.
- [4] R. Lüllmann-Rauch, Taschenlehrbuch Histologie: 10 Tabellen, Thieme, Stuttgart, New York, NY, 2012.
- [5] S. Sell, Heterogeneity and plasticity of hepatocyte lineage cells, *Hepatology* 33 (2001) 738–750.
- [6] C. Fahlke, W. Linke, B. Raßler, R. Wiesner, Taschenatlas Physiologie, Urban & Fischer, München, 2012.
- [7] E. Wisse, R.B. de Zanger, K. Charels, P. van der Smissen, R.S. McCuskey, The liver sieve: Considerations concerning the structure and function of endothelial fenestrae, the sinusoidal wall and the space of disse, *Hepatology* 5 (1985) 683–692.
- [8] E. Nemeth, A.W. Baird, C. O’Farrelly, Microanatomy of the liver immune system, *Semin Immunopathol* 31 (2009) 333–343.
- [9] H. Senoo, K. Yoshikawa, M. Morii, M. Miura, K. Imai, Y. Mezaki, Hepatic stellate cell (vitamin A-storing cell) and its relative – past, present and future, *Cell Biol Int* 34 (2010) 1247–1272.
- [10] C. Hellerbrand, Hepatic stellate cells-the pericytes in the liver, *Pflugers Arch* 6 (2013) 775–778.
- [11] E. Mutschler, G. Thews, H.-G. Schaible, P. Vaupel, Anatomie, Physiologie, Pathophysiologie des Menschen: 140 Tabellen, Wissenschaftliche Verlagsgesellschaft, Stuttgart, 2007.
- [12] P. Ginès, P.S. Kamath, V. Arroyo, Chronic liver failure: Mechanisms and management, Humana Press, New York, 2011.
- [13] S. Zanlungo, F. Nervi, The molecular and metabolic basis of biliary cholesterol secretion and gallstone disease, *Front Biosci* 8 (2003) 1166–1174.

- [14] D.K. Seviour, O. Pelkonen, J.T. Ahokas, Hepatocytes: The powerhouse of biotransformation, *Int J Biochem Cell Biol* 44 (2012) 257–261.
- [15] S. Silbernagl, A. Despopoulos, *Taschenatlas Physiologie*, Thieme, Stuttgart, 2012.
- [16] P. Nguyen, V. Leray, M. Diez, S. Serisier, J. Le Bloc'h, B. Siliart, H. Dumon, Liver lipid metabolism, *J Anim Physiol Anim Nutr* 92 (2008) 272–283.
- [17] J.L. Dixon, H.N. Ginsberg, Hepatic synthesis of lipoproteins and apolipoproteins, *Semin Liver Dis* 12 (1992) 364–372.
- [18] R. Sallie, J. Michael Tredger, R. Williams, Drugs and the liver part 1: Testing liver function, *Biopharm Drug Dispos* 12 (1991) 251–259.
- [19] G. Ramadori, F. Moriconi, I. Malik, J. Dudas, Physiology and pathophysiology of liver inflammation, damage and repair, *J Physiol Pharmacol* 59 (2008) 107–117.
- [20] M. Blachier, H. Leleu, M. Peck-Radosavljevic, D.-C. Valla, F. Roudot-Thoraval, The burden of liver disease in Europe: A review of available epidemiological data, *J Hepatol* 58 (2013) 593–608.
- [21] K. Walsh, Alcoholic liver disease, *Postgrad Med J* 76 (2000) 280–286.
- [22] W.W. Yip, A.D. Burt, Alcoholic liver disease, *Semin Diagn Pathol* 23 (2006) 149–160.
- [23] L.M. Alba, K. Lindor, Non-alcoholic fatty liver disease, *Aliment Pharmacol Ther* 17 (2003) 977–986.
- [24] P.L.M. Jansen, Non-alcoholic steatohepatitis, *Eur J Gastroenterol Hepatol* 16 (2004) 1079–1085.
- [25] J.P. Iredale, Models of liver fibrosis: exploring the dynamic nature of inflammation and repair in a solid organ, *J Clin Invest* 117 (2007) 539–548.
- [26] P.A. Farazi, R.A. DePinho, Hepatocellular carcinoma pathogenesis: from genes to environment, *Nat Rev Cancer* 6 (2006) 674–687.
- [27] V.J. Navarro, J.R. Senior, Drug-related hepatotoxicity, *N Engl J Med* 354 (2006) 731–739.
- [28] K.T. Suk, D.J. Kim, Drug-induced liver injury: present and future, *Clin Mol Hepatol* 18 (2012) 249–257.
- [29] M. Ghabril, N. Chalasani, E. Björnsson, Drug-induced liver injury: a clinical update, *Curr Opin Gastroenterol* 26 (2010) 222–226.
- [30] D. Schuppan, J.D. Jia, B. Brinkhaus, E.G. Hahn, Herbal products for liver diseases: a therapeutic challenge for the new millennium, *Hepatology* 30 (1999) 1099–1104.

- [31] A.S. Negi, J.K. Kumar, S. Luqman, K. Shanker, M.M. Gupta, S.P.S. Khanuja, Recent advances in plant hepatoprotectives: a chemical and biological profile of some important leads, *Med Res Rev* 28 (2008) 746–772.
- [32] F. Stickel, D. Schuppan, Herbal medicine in the treatment of liver diseases, *Dig Liver Dis* 39 (2007) 293–304.
- [33] R.K. Dhiman, Y.K. Chawla, Herbal medicines for liver diseases, *Dig Dis Sci* 50 (2005) 1807–1812.
- [34] A. Alvari, S.O.R. Mehrnaz, F.J. Ahmad, M.Z. Abdin, Contemporary overview on clinical trials and future prospects of hepato-protective herbal medicines, *Rev Recent Clin Trials* 7 (2012) 214–223.
- [35] E. Fogden, J. Neuberger, Alternative medicines and the liver, *Liver Int* 23 (2003) 213–220.
- [36] H. Wagner, P. Diesel, M. Seitz, Zur Chemie und Analytik von Silymarin aus *Silybum marianum* Gaertn, *Arzneimittelforschung* 24 (1974) 466–471.
- [37] R. Saller, J. Melzer, J. Reichling, R. Brignoli, R. Meier, An updated systematic review of the pharmacology of silymarin, *Forsch Komplementärmed* 14 (2007) 70–80.
- [38] P. Muriel, Y. Rivera-Espinoza, Beneficial drugs for liver diseases, *J Appl Toxicol* 28 (2008) 93–103.
- [39] S.C. Pradhan, C. Girish, Hepatoprotective herbal drug, silymarin from experimental pharmacology to clinical medicine, *Indian J Med Res* 124 (2006) 491–504.
- [40] C. Tamayo, S. Diamond, Review of clinical trials evaluating safety and efficacy of milk thistle (*Silybum marianum* [L.] Gaertn.), *Integr Cancer Ther* 6 (2007) 146–157.
- [41] B.P. Jacobs, C. Dennehy, G. Ramirez, J. Sapp, V.A. Lawrence, Milk thistle for the treatment of liver disease: a systematic review and meta-analysis, *Am J Med* 113 (2002) 506–515.
- [42] H.G. Jeong, H.J. You, S.J. Park, A.R. Moon, Y.C. Chung, S.K. Kang, H.K. Chun, Hepatoprotective effects of 18 β -glycyrrhetic acid on carbon tetrachloride-induced liver injury: inhibition of cytochrome P450 3E1 expression, *Pharmacol Res* 46 (2002) 221–227.
- [43] M. Yoshikawa, Y. Matsui, H. Kawamoto, N. Umemoto, K. Oku, M. Koizumi, J. Yamao, S. Kuriyama, H. Nakano, N. Hozumi, S. Ishizaka, H. Fukui, Effects of glycyrrhizin on immune-mediated cytotoxicity, *J Gastroenterol Hepatol* 12 (1997) 243–248.
- [44] T. Takahara, A. Watanabe, K. Shiraki, Effects of glycyrrhizin on hepatitis B surface antigen: a biochemical and morphological study, *J Hepatol* 21 (1994) 601–609.

- [45] T.G. van Rossum, A.G. Vulto, R.A. de Man, J.T. Brouwer, S.W. Schalm, Review article: glycyrrhizin as a potential treatment for chronic hepatitis C, *Aliment Pharmacol Ther* 12 (1998) 199–205.
- [46] J.-Y. Wang, J.-S. Guo, H. Li, S.-L. Liu, M.A. Zern, Inhibitory effect of glycyrrhizin on NF- κ B binding activity in CCl₄- plus ethanol-induced liver cirrhosis in rats, *Liver* 18 (1998) 180–185.
- [47] S.K. Acharya, S. Dasarathy, A. Tandon, Y.K. Joshi, B.N. Tandon, A preliminary open trial on interferon stimulator (SNMC) derived from *Glycyrrhiza glabra* in the treatment of subacute hepatic failure, *Indian J Med Res* 98 (1993) 69–74.
- [48] C. Girish, S.C. Pradhan, Drug development for liver diseases: focus on picroliv, ellagic acid and curcumin, *Fundam Clin Pharmacol* 22 (2008) 623–632.
- [49] R. Thapliyal, G.B. Maru, Inhibition of cytochrome P450 isozymes by curcumins in vitro and in vivo, *Food Chem Toxicol* 39 (2001) 541–547.
- [50] Y. Kiso, Y. Suzuki, N. Watanabe, Y. Oshima, H. Hikino, Antihepatotoxic principles of *Curcuma longa* rhizomes, *Planta Med* 49 (1983) 185–187.
- [51] Y.-J. He, J.-C. Shu, X. Lü, L. Fang, Y. Sheng, Prophylactic effect of curcumin on hepatic fibrosis and its relationship with activated hepatic stellate cells, *Zhonghua Gan Zang Bing Za Zhi* 14 (2006) 337–340.
- [52] R. Rukkumani, K. Aruna, P.S. Varma, V.P. Menon, Curcumin influences hepatic expression patterns of matrix metalloproteinases in liver toxicity, *Ital J Biochem* 53 (2004) 61–66.
- [53] Y. Fu, S. Zheng, J. Lin, J. Ryerse, A. Chen, Curcumin protects the rat liver from CCl₄-caused injury and fibrogenesis by attenuating oxidative stress and suppressing inflammation, *Mol Pharmacol* 73 (2008) 399–409.
- [54] K.V. Syamasundar, B. Singh, R.S. Thakur, A. Husain, Y. Kiso, H. Hikino, Antihepatotoxic principles of *Phyllanthus niruri* herbs, *J Ethnopharmacol* 14 (1985) 41–44.
- [55] J. Liu, H. Lin, H. McIntosh, Genus *Phyllanthus* for chronic hepatitis B virus infection: a systematic review, *J Viral Hepat* 8 (2001) 358–366.
- [56] H. Oka, S. Yamamoto, T. Kuroki, S. Harihara, T. Marumo, S.R. Kim, T. Monna, K. Kobayashi, T. Tango, Prospective study of chemoprevention of hepatocellular carcinoma with Sho-saiko-to (TJ-9), *Cancer* 76 (1995) 743–749.
- [57] A. Dhiman, A. Nanda, S. Ahmad, A recent update in research on the antihepatotoxic potential of medicinal plants, *Zhong Xi Yi Jie He Xue Bao* 10 (2012) 117–127.

- [58] G. Chaudhary, P. Kamboj, I. Singh, A. Kalia, Herbs as liver savers - A review, *Indian J Nat Prod Resour* 2010 (1) 397–408.
- [59] C. Stedman, Herbal hepatotoxicity, *Semin Liver Dis* 22 (2002) 195–206.
- [60] F. Stickel, E. Patsenker, D. Schuppan, Herbal hepatotoxicity, *J Hepatol* 43 (2005) 901–910.
- [61] S. Chitturi, G.C. Farrell, Herbal hepatotoxicity: an expanding but poorly defined problem, *J Gastroenterol Hepatol* 15 (2000) 1093–1099.
- [62] R. Venkataramanan, B. Komoroski, S. Strom, In vitro and in vivo assessment of herb drug interactions, *Life Sci* 78 (2006) 2105–2115.
- [63] L.B. Seeff, Herbal hepatotoxicity, *Clin Liver Dis* 11 (2007) 577–596.
- [64] R. Teschke, A. Wolff, C. Frenzel, J. Schulze, A. Eickhoff, Herbal hepatotoxicity: a tabular compilation of reported cases, *Liver Int* 32 (2012) 1543–1556.
- [65] F. Wilmot, G. Robertson, Senecio disease or cirrhosis of the liver due to senecio poisoning, *Lancet* 196 (1920) 848–849.
- [66] G. Bras, D. Jelliffe, K. Stuart, Venous-occlusive disease of the liver with non-portal type of cirrhosis occurring in Jamaica, *Arch Pathol Lab Med* 57 (1954) 285–300.
- [67] R.K. Tandon, B.N. Tandon, H.D. Tandon, M.L. Bhatia, S. Bhargava, P. Lal, R.R. Arora, Study of an epidemic of venoocclusive disease in India, *Gut* 17 (1976) 849–855.
- [68] H.D. Tandon, B.N. Tandon, A.R. Mattocks, An epidemic of veno-occlusive disease of the liver in Afghanistan. Pathologic features, *Am J Gastroenterol* 70 (1978) 607–613.
- [69] M. Roulet, R. Laurini, L. Rivier, A. Calame, Hepatic veno-occlusive disease in newborn infant of a woman drinking herbal tea, *J Pediatr* 112 (1988) 433–436.
- [70] A.S. Stillman, R. Huxtable, P. Consroe, P. Kohonen, S. Smith, Hepatic veno-occlusive disease due to pyrrolizidine (Senecio) poisoning in Arizona, *Gastroenterology* 73 (1977) 349–352.
- [71] N. Bach, S.N. Thung, F. Schaffner, Comfrey herb tea-induced hepatic veno-occlusive disease, *Am J Med* 87 (1989) 97–99.
- [72] L.D. DeLeve, H.M. Shulman, G.B. McDonald, Toxic injury to hepatic sinusoids: sinusoidal obstruction syndrome (veno-occlusive disease), *Semin Liver Dis* 22 (2002) 27–42.
- [73] T.W. Petry, G.T. Bowden, R.J. Huxtable, I.G. Sipes, Characterization of hepatic DNA damage induced in rats by the pyrrolizidine alkaloid monocrotaline, *Cancer Res* 44 (1984) 1505–1509.

- [74] A.R. Mattocks, Chemistry and toxicology of pyrrolizidine alkaloids, Academic Press, London, 1986.
- [75] A. Castot, D. Larrey, Hépatites observées au cours d'un traitement par un médicament ou une tisane contenant de la Germandrée petit-chêne. Bilan des 26 cas rapportés aux Centres Régionaux de Pharmacovigilance, *Gastroenterol Clin Biol* 16 (1992) 916–922.
- [76] J. Loeper, V. Descatoire, P. Letteron, C. Moulis, C. Degott, P. Dansette, D. Fau, D. Pessayre, Hepatotoxicity of germander in mice, *Gastroenterology* 106 (1994) 464–472.
- [77] D. Fau, M. Lekehal, G. Farrell, A. Moreau, C. Moulis, G. Feldmann, D. Haouzi, D. Pessayre, Diterpenoids from germander, an herbal medicine, induce apoptosis in isolated rat hepatocytes, *Gastroenterology* 113 (1997) 1334–1346.
- [78] A. Mattéi, P. Rucay, D. Samuel, C. Feray, M. Reynes, H. Bismuth, Liver transplantation for severe acute liver failure after herbal medicine (*Teucrium polium*) administration, *J Hepatol* 22 (1995) 597.
- [79] F. Stickel, H.-M. Baumüller, K. Seitz, D. Vasilakis, G. Seitz, H.K. Seitz, D. Schuppan, Hepatitis induced by Kava (*Piper methysticum rhizoma*), *J Hepatol* 39 (2003) 62–67.
- [80] R. Teschke, Kava hepatotoxicity--a clinical review, *Ann Hepatol* 9 (2010) 251–265.
- [81] F. Stickel, G. Egerer, H.K. Seitz, Hepatotoxicity of botanicals, *Public Health Nutr* 3 (2000) 113–124.
- [82] N.M. Sheikh, Chaparral-Associated Hepatotoxicity, *Arch Intern Med* 157 (1997) 913.
- [83] R. Agarwal, Z.Y. Wang, D.P. Bik, H. Mukhtar, Nordihydroguaiaretic acid, an inhibitor of lipoxygenase, also inhibits cytochrome P-450-mediated monooxygenase activity in rat epidermal and hepatic microsomes, *Drug Metab Dispos* 19 (1991) 620–624.
- [84] C. Daniele, S. Dahamna, O. Firuzi, N. Sekfali, L. Saso, G. Mazzanti, *Atractylis gummifera* L. poisoning: an ethnopharmacological review, *J Ethnopharmacol* 97 (2005) 175–181.
- [85] D.K. Obatomi, S. Brant, V. Anthonypillai, P.H. Bach, Toxicity of atractyloside in precision-cut rat and porcine renal and hepatic tissue slices, *Toxicol Appl Pharmacol* 148 (1998) 35–45.
- [86] J. Benninger, H.T. Schneider, D. Schuppan, T. Kirchner, E.G. Hahn, Acute hepatitis induced by greater celandine (*Chelidonium majus*), *Gastroenterology* 117 (1999) 1234–1237.
- [87] P.W. Whiting, A. Clouston, P. Kerlin, Black cohosh and other herbal remedies associated with acute hepatitis, *Med J Aust* 177 (2002) 440–443.

- [88] J. Levitsky, T.A. Alli, J. Wisecarver, M.F. Sorrell, Fulminant liver failure associated with the use of black cohosh, *Dig Dis Sci* 50 (2005) 538–539.
- [89] J. Harvey, D.G. Colin-Jones, Mistletoe hepatitis, *Br Med J* 282 (1981) 186–187.
- [90] G. Millonig, S. Stadlmann, W. Vogel, Herbal hepatotoxicity: acute hepatitis caused by a Noni preparation (*Morinda citrifolia*), *Eur J Gastroenterol Hepatol* 17 (2005) 445–447.
- [91] U. Beuers, U. Spengler, G.R. Pape, Hepatitis after chronic abuse of senna, *Lancet* 337 (1991) 372–373.
- [92] S. Hamid, S. Rojter, J. Vierling, Protracted cholestatic hepatitis after the use of prostata, *Ann Intern Med* 127 (1997) 169–170.
- [93] J.A. Bakerink, S.M. Gospe, R.J. Dimand, M.W. Eldridge, Multiple organ failure after ingestion of pennyroyal oil from herbal tea in two infants, *Pediatrics* 98 (1996) 944–947.
- [94] J.B. Sullivan, B.H. Rumack, H. Thomas, R.G. Peterson, P. Bryson, Pennyroyal oil poisoning and hepatotoxicity, *JAMA* 242 (1979) 2873–2874.
- [95] D. Thomassen, N. Knebel, J.T. Slattery, R.H. McClanahan, S.D. Nelson, Reactive intermediates in the oxidation of menthofuran by cytochromes P-450, *Chem Res Toxicol* 5 (1992) 123–130.
- [96] S. Vogel, *Synthese prenylierter Chalkone aus Hopfen und Bestimmung ihrer cytotoxischen und antioxidativen Aktivität*, Regensburg, 2008.
- [97] S. Vogel, M. Barbic, G. Jürgenliemk, J. Heilmann, Synthesis, cytotoxicity, anti-oxidative and anti-inflammatory activity of chalcones and influence of A-ring modifications on the pharmacological effect, *Eur J Med Chem* 45 (2010) 2206–2213.
- [98] S. Vogel, S. Ohmayer, G. Brunner, J. Heilmann, Natural and non-natural prenylated chalcones: Synthesis, cytotoxicity and anti-oxidative activity, *Bioorg Med Chem* 16 (2008) 4286–4293.
- [99] A. Mori, T. Mizusaki, Y. Miyakawa, E. Ohashi, T. Haga, T. Maegawa, Y. Monguchi, H. Sajiki, Chemoselective hydrogenation method catalyzed by Pd/C using diphenylsulfide as a reasonable catalyst poison, *Tetrahedron* 62 (2006) 11925–11932.
- [100] X. Chen, K. Zenger, A. Lupp, B. Kling, J. Heilmann, C. Fleck, B. Kraus, M. Decker, Tacrine-silibinin codrug shows neuro- and hepatoprotective effects in vitro and pro-cognitive and hepatoprotective effects in vivo, *J Med Chem* 55 (2012) 5231–5242.
- [101] M. Motyl, *The absorption of xanthohumol in in vitro and in vivo studies and the investigation of the biological activity of structurally related chalcones*, Regensburg, 2012.

- [102] B. Schnabl, Y.H. Choi, J.C. Olsen, C.H. Hagedorn, D.A. Brenner, Immortal activated human hepatic stellate cells generated by ectopic telomerase expression, *Lab Invest* 82 (2002) 323–333.
- [103] T. Mosmann, Rapid colorimetric assay for cellular growth and survival: application to proliferation and cytotoxicity assays, *J Immunol Methods* 65 (1983) 55–63.
- [104] K. Saotome, H. Morita, M. Umeda, Cytotoxicity test with simplified crystal violet staining method using microtitre plates and its application to injection drugs, *Toxicol In Vitro* 3 (1989) 317–321.
- [105] Z. Yan, G.W. Caldwell, Metabolic assessment in liver microsomes by co-activating cytochrome P450s and UDP-glycosyltransferases, *Eur J Drug Metab Pharmacokinet* 28 (2003) 223–232.
- [106] M.B. Fisher, Characterization by liquid chromatography-nuclear magnetic resonance spectroscopy and liquid chromatography-mass spectrometry of two coupled oxidative-conjugative metabolic pathways for 7-ethoxycoumarin in human liver microsomes treated with alamethicin, *Drug Metab and Dispos* 30 (2002) 270–275.
- [107] M.B. Fisher, K. Campanale, B.L. Ackermann, M. VandenBranden, S.A. Wrighton, In vitro glucuronidation using human liver microsomes and the pore-forming peptide alamethicin, *Drug Metab Dispos* 28 (2000) 560–566.
- [108] Y.N. Singh, Kava: an overview, *J Ethnopharmacol* 37 (1992) 13–45.
- [109] WHO, WHO monographs on selected medicinal plants: *Rhizoma Piperis Methystici*, <http://apps.who.int/medicinedocs/pdf/s4927e/s4927e.pdf> (2004).
- [110] A.R. Bilia, L. Scalise, M.C. Bergonzi, F.F. Vincieri, Analysis of kavalactones from *Piper methysticum* (kava-kava), *J Chromatogr B Analyt Technol Biomed Life Sci* 812 (2004) 203–214.
- [111] C.S. Côté, C. Kor, J. Cohen, K. Auclair, Composition and biological activity of traditional and commercial kava extracts, *Biochem Biophys Res Commun* 322 (2004) 147–152.
- [112] Borsche W., W. Peitzsch, Constituents of kava root. X. Kawain and dihydrokawain, *Berichte der Deutschen Chemischen Gesellschaft* (1927) 2414–2417.
- [113] W. Borsche, C. Bodenstein, M. Lewinsohn, Constituents of kava root. IX. Synthesis of yangonin, *Berichte der Deutschen Chemischen Gesellschaft* (1929) 2515–2523.
- [114] H. Achenbach, N. Theobald, Constituents of *Piper methysticum*. VII. Absolute configuration of kava lactones, *Chem Ber* 107 (1974) 735–737.

- [115] R. Hänsel, P. Bähr, J. Elich, Isolierung und Charakterisierung von zwei bisher unbekanntem Farbstoffen des Kava-Rhizoms Eine vorläufige Mitteilung, *Arch Pharm Pharm Med Chem* 294 (1961) 739–743.
- [116] C.P. Dutta, L.P.K. Ray, A. Chatterjee, Piperaceae: Constituents of *Piper methysticum*, *Phytochemistry* 11 (1972) 2891–2892.
- [117] O. Meissner, H. Häberlein, HPLC analysis of flavokavins and kavapyrones from *Piper methysticum* Forst, *J Chromatogr B Analyt Technol Biomed Life Sci* 826 (2005) 46–49.
- [118] Di Wu, M.G. Nair, D.L. DeWitt, Novel compounds from *Piper methysticum* Forst (Kava Kava) roots and their effect on cyclooxygenase enzyme, *J Agric Food Chem* 50 (2002) 701–705.
- [119] J.-W. Jhoo, C.Y.W. Ang, T.M. Heinze, J. Deck, L.K. Schnackenberg, R.D. Beger, K. Dragull, C.-S. Tang, Identification of C-glycoside flavonoids as potential mutagenic compounds in kava, *J Food Sci* 72 (2007) 120–125.
- [120] H. Jaggy, H. Achenbach, Cephadione A from *Piper methysticum*, *Planta Med* 58 (1992) 111.
- [121] H. Achenbach, W. Karl, Über die Isolierung von zwei neuen Pyrrolidinen aus Rauschpfeffer (*Piper methysticum* Forst), *Chem Ber* 103 (1970) 2535–2540.
- [122] R. Smith, Pipermethysticine, a novel pyridone alkaloid from *Piper methysticum*, *Tetrahedron* 35 (1979) 437–439.
- [123] K. Dragull, W.Y. Yoshida, C.-S. Tang, Piperidine alkaloids from *Piper methysticum*, *Phytochemistry* 63 (2003) 193–198.
- [124] L. Graeza, P. Ruff, Aliphatic and alicyclic alcohols of *Piperis methystici* rhizome, *Arch Pharmacol* 319 (1986) 475.
- [125] P. Jössang, D. Molho, Chromatographie sur couches épaisses non linées des constituants du rhizome de *Piper Methysticum*: isolement de deux nouvelles cétones, cinnamylacétone et méthylène dioxy-3,4 cinnamylacétone, *J Chromatogr* (1967) 375–383.
- [126] V.S. Parmar, S.C. Jain, K.S. Bisht, R. Jain, P. Taneja, Phytochemistry of the genus *Piper*, *Phytochemistry* 46 (1996) 597–673.
- [127] A.R. Bilia, S. Gallon, F.F. Vincieri, Kava-kava and anxiety: growing knowledge about the efficacy and safety, *Life Sci* 70 (2002) 2581–2597.
- [128] A. Rowe, R. Narlawar, P.W. Groundwater, I. Ramzan, Kavalactone pharmacophores for major cellular drug targets, *Mini Rev Med Chem* 11 (2011) 79–83.

- [129] A. Jussofie, A. Schmitz, C. Hiemke, Kavapyrone enriched extract from *Piper methysticum* as modulator of the GABA binding site in different regions of rat brain, *Psychopharmacology* 116 (1994) 469–474.
- [130] C.-S. Yuan, L. Dey, A. Wang, S. Mehendale, J.-T. Xie, H.H. Aung, M.K. Ang-Lee, Kavalactones and dihydrokavain modulate GABAergic activity in a rat gastric-brainstem preparation, *Planta Med* 68 (2002) 1092–1096.
- [131] G. Boonen, H. Häberlein, Influence of genuine kavapyrone enantiomers on the GABA-A binding site, *Planta Med* 64 (1998) 504–506.
- [132] L.D. Dinh, U. Simmen, K.B. Bueter, B. Bueter, K. Lundstrom, W. Schaffner, Interaction of various *Piper methysticum* cultivars with CNS receptors in vitro, *Planta Med* 67 (2001) 306–311.
- [133] U. Seitz, A. Schüle, J. Gleitz, [3H]-monoamine uptake inhibition properties of kava pyrones, *Planta Med* 63 (1997) 548–549.
- [134] R. Uebelhack, L. Franke, H.J. Schewe, Inhibition of platelet MAO-B by kava pyrone-enriched extract from *Piper methysticum* Forster (kava-kava), *Pharmacopsychiatry* 31 (1998) 187–192.
- [135] H. Grunze, J. Langosch, K. Schirmacher, D. Bingmann, J. von Wegerer, J. Walden, Kava pyrones exert effects on neuronal transmission and transmembraneous cation currents similar to established mood stabilizers--a review, *Prog Neuropsychopharmacol Biol Psychiatry* 25 (2001) 1555–1570.
- [136] J. Gleitz, A. Beile, T. Peters, (+/-)-Kavain inhibits veratridine-activated voltage-dependent Na(+)-channels in synaptosomes prepared from rat cerebral cortex, *Neuropharmacology* 34 (1995) 1133–1138.
- [137] J. Gleitz, A. Beile, T. Peters, (+/-)-Kavain inhibits the veratridine- and KCl-induced increase in intracellular Ca²⁺ and glutamate-release of rat cerebrocortical synaptosomes, *Neuropharmacology* 35 (1996) 179–186.
- [138] K. Schirmacher, D. Büsselberg, J.M. Langosch, J. Walden, U. Winter, D. Bingmann, Effects of (+/-)-kavain on voltage-activated inward currents of dorsal root ganglion cells from neonatal rats, *Eur Neuropsychopharmacol* 9 (1999) 171–176.
- [139] E.I. Magura, M.V. Kopanitsa, J. Gleitz, T. Peters, O.A. Krishtal, Kava extract ingredients, (+)-methysticin and (+/-)-kavain inhibit voltage-operated Na(+)-channels in rat CA1 hippocampal neurons, *Neuroscience* 81 (1997) 345–351.
- [140] U. Seitz, A. Ameri, H. Pelzer, J. Gleitz, T. Peters, Relaxation of evoked contractile activity of isolated guinea-pig ileum by (+/-)-kavain, *Planta Med* 63 (1997) 303–306.

- [141] J. Walden, J. von Wegerer, U. Winter, M. Berger, H. Grunze, Effects of kawain and dihydromethysticin on field potential changes in the hippocampus, *Prog Neuropsychopharmacol Biol Psychiatry* 21 (1997) 697–706.
- [142] D. Wu, L. Yu, M.G. Nair, D.L. DeWitt, R.S. Ramsewak, Cyclooxygenase enzyme inhibitory compounds with antioxidant activities from *Piper methysticum* (kava kava) roots, *Phytomedicine* 9 (2002) 41–47.
- [143] M.P. Pollastri, A. Whitty, J.C. Merrill, X. Tang, T.D. Ashton, S. Amar, Identification and characterization of kava-derived compounds mediating TNF-alpha suppression, *Chem Biol Drug Des* 74 (2009) 121–128.
- [144] F. Folmer, R. Blasius, F. Morceau, J. Tabudravu, M. Dicato, M. Jaspars, M. Diederich, Inhibition of TNFalpha-induced activation of nuclear factor kappaB by kava (*Piper methysticum*) derivatives, *Biochem Pharmacol* 71 (2006) 1206–1218.
- [145] A.A. Shaik, D.L. Hermanson, C. Xing, Identification of methysticin as a potent and non-toxic NF-kappaB inhibitor from kava, potentially responsible for kava's chemopreventive activity, *Bioorg Med Chem Lett* 19 (2009) 5732–5736.
- [146] S. Zhou, L.Y. Lim, B. Chowbay, Herbal modulation of P-glycoprotein, *Drug Metab Rev* 36 (2004) 57–104.
- [147] J. Weiss, A. Sauer, A. Frank, M. Unger, Extracts and kavalactones of *Piper methysticum* G. Forst (kava-kava) inhibit P-glycoprotein in vitro, *Drug Metab Dispos* 33 (2005) 1580–1583.
- [148] A. Ligresti, R. Villano, M. Allarà, I. Ujváry, V. Di Marzo, Kavalactones and the endocannabinoid system: The plant-derived yangonin is a novel CB1 receptor ligand, *Pharmacol Res* 66 (2012) 163–169.
- [149] P.H. Duffield, D. Jamieson, Development of tolerance to kava in mice, *Clin Exp Pharmacol Physiol* 18 (1991) 571–578.
- [150] D.D. Jamieson, P.H. Duffield, D. Cheng, A.M. Duffield, Comparison of the central nervous system activity of the aqueous and lipid extract of kava (*Piper methysticum*), *Arch Int Pharmacodyn Ther* 301 (1989) 66–80.
- [151] E. Holm, U. Städt, J. Heep, C. Kotsik, Untersuchung zum Wirkprofil von D,L-Kavain, *Arzneimittelforschung* (1962) 673–683.
- [152] A.R. Furgiele, W.J. Kinnard, M.D. Aceto, J.P. Buckley, Central activity of aqueous extracts of *Piper methysticum* (kava), *J Pharm Sci* 54 (1965) 247–252.

- [153] S.S. Baum, R. Hill, H. Rommelspacher, Effect of kava extract and individual kavapyrones on neurotransmitter levels in the nucleus accumbens of rats, *Prog Neuropsychopharmacol Biol Psychiatry* 22 (1998) 1105–1120.
- [154] M.W. Klohs, F. Keller, R.E. Williams, M.I. Toekes, G.E. Cronheim, A chemical and pharmacological investigation of Piper methysticum Forst, *J Med Pharm Chem* 1 (1959) 95–103.
- [155] C. Backhauss, J. Kriegelstein, Extract of kava (Piper methysticum) and its methysticin constituents protect brain tissue against ischemic damage in rodents, *Eur J Pharmacol* 215 (1992) 265–269.
- [156] D.D. Jamieson, P.H. Duffield, The antinociceptive actions of kava components in mice, *Clin Exp Pharmacol Physiol* 17 (1990) 495–507.
- [157] R. Kretzschmar, H.J. Meyer, Vergleichende Untersuchungen über die antikonvulsive Wirksamkeit der Pyronverbindungen aus Piper methysticum Forst, *Arch Int Pharmacodyn Ther* 177 (1969) 261–267.
- [158] G. Warnecke, Psychosomatische Dysfunktionen im weiblichen Klimakterium. Klinische Wirksamkeit und Verträglichkeit von Kava-Extrakt WS 1490, *Fortschr Med* 109 (1991) 119–122.
- [159] E. Kinzler, J. Krömer, E. Lehmann, Wirksamkeit eines Kava-Spezial-Extraktes bei Patienten mit Angst-, Spannungs-, und Erregungszuständen nicht-psychotischer Genese. Doppelblind-Studie gegen Plazebo über 4 Wochen, *Arzneimittelforschung* 41 (1991) 584–588.
- [160] H.P. Volz, M. Kieser, Kava-kava extract WS 1490 versus placebo in anxiety disorders-- a randomized placebo-controlled 25-week outpatient trial, *Pharmacopsychiatry* 30 (1997) 1–5.
- [161] U. Malsch, M. Kieser, Efficacy of kava-kava in the treatment of non-psychotic anxiety, following pretreatment with benzodiazepines, *Psychopharmacology* 157 (2001) 277–283.
- [162] M. Gastpar, H.D. Klimm, Treatment of anxiety, tension and restlessness states with Kava special extract WS 1490 in general practice: a randomized placebo-controlled double-blind multicenter trial, *Phytomedicine* 10 (2003) 631–639.
- [163] S. Lehl, Clinical efficacy of kava extract WS 1490 in sleep disturbances associated with anxiety disorders. Results of a multicenter, randomized, placebo-controlled, double-blind clinical trial, *J Affect Disord* 78 (2004) 101–110.
- [164] F.P. Geier, T. Konstantinowicz, Kava treatment in patients with anxiety, *Phytother Res* 18 (2004) 297–300.

- [165] J. Sarris, A. Scholey, I. Schweitzer, C. Bousman, E. LaPorte, C. Ng, G. Murray, C. Stough, The acute effects of kava and oxazepam on anxiety, mood, neurocognition; and genetic correlates: a randomized, placebo-controlled, double-blind study, *Hum Psychopharmacol Clin Exp* 27 (2012) 262–269.
- [166] M.H. Pittler, E. Ernst, Kava extract versus placebo for treating anxiety, *Cochrane Database Syst Rev* 1 (2003).
- [167] S. Witte, D. Loew, W. Gaus, Meta-analysis of the efficacy of the acetonetic kava-kava extract WS1490 in patients with non-psychotic anxiety disorders, *Phytother Res* 19 (2005) 183–188.
- [168] A. Matthias, J.T. Blanchfield, K.G. Penman, K.M. Bone, I. Toth, R.P. Lehmann, Permeability studies of Kavalactones using a Caco-2 cell monolayer model, *J Clin Pharm Ther* 32 (2007) 233–239.
- [169] J.M. Mathews, Pharmacokinetics and disposition of the kavalactone kawain: interaction with kava extract and kavalactones in vivo and in vitro, *Drug Metabolism and Disposition* 33 (2005) 1555–1563.
- [170] F. Tarbah, H. Mahler, B. Kardel, W. Weinmann, D. Hafner, T. Daldrup, Kinetics of kavain and its metabolites after oral application, *J Chromatogr B Analyt Technol Biomed Life Sci* 789 (2003) 115–130.
- [171] S. Fu, B.N. Tattam, C.C. Duke, I. Ramzan, High-performance liquid chromatography assays for desmethoxyyangonin, methysticin, kavain and their microsomal metabolites, *Biomed Chromatogr* 23 (2009) 81–91.
- [172] S. Fu, A. Rowe, I. Ramzan, Kavalactone metabolism in rat liver microsomes, *Phytother Res* 26 (2012) 1057–1061.
- [173] S. Fu, A. Rowe, I. Ramzan, Kavalactone metabolism in the isolated perfused rat liver, *Phytother Res* 26 (2012) 1813–1816.
- [174] Siegers S.P., Ergebnisse der Anwendungsbeobachtung L 1090 mit Laitan Kapseln, *Äztliche Forschung* (1992) 6–11.
- [175] L. Schelosky, C. Raffauf, K. Jendroska, W. Poewe, Kava and dopamin antagonism, *J Neurol Neurosurg Psychiatry* 58 (1995) 639–640.
- [176] S. Strahl, V. Ehret, H.H. Dahm, K.P. Maier, Nekrotisierende Hepatitis nach Einnahme pflanzlicher Heilmittel, *Dtsch Med Wochenschr* 123 (1998) 1410–1414.
- [177] M. Kraft, T.W. Spahn, J. Menzel, N. Senninger, K.H. Dietl, H. Herbst, W. Domschke, M.M. Lerch, Fulminantes Leberversagen nach Einnahme des pflanzlichen Antidepressivums Kava-Kava, *Dtsch Med Wochenschr* 126 (2001) 970–972.

- [178] M. Escher, J. Desmeules, E. Giostra, G. Mentha, Hepatitis associated with Kava, a herbal remedy for anxiety, *BMJ* 322 (2001) 139.
- [179] L. Bujanda, A. Palacios, R. Silvariño, A. Sánchez, C. Muñoz, Hepatitis aguda icterica secundaria a Kava, *Gastroenterol Hepatol* 25 (2002) 434–435.
- [180] P.J. Gow, N.J. Connelly, R.L. Hill, P. Crowley, P.W. Angus, Fatal fulminant hepatic failure induced by a natural therapy containing kava, *Med J Aust* 178 (2003) 442–443.
- [181] C.L. Humberston, J. Akhtar, E.P. Krenzelok, Acute hepatitis induced by kava kava, *J Toxicol Clin Toxicol* 41 (2003) 109–113.
- [182] S. Russmann, Y. Barguil, P. Cabalion, M. Kritsanida, D. Duhet, B.H. Lauterburg, Hepatic injury due to traditional aqueous extracts of kava root in New Caledonia, *Eur J Gastroenterol Hepatol* 15 (2003) 1033–1036.
- [183] S.U. Christl, A. Seifert, D. Seeler, Toxic hepatitis after consumption of traditional kava preparation, *J Travel Med* 16 (2009) 55–56.
- [184] R.B. Brauer, M. Stangl, J.R. Stewart, R. Pfab, K. Becker, Acute liver failure after administration of herbal tranquilizer kava-kava (*Piper methysticum*), *J Clin Psychiatry* 64 (2003) 216–218.
- [185] M. Schmidt, Harsewinkel, A. Nahrstedt, Ist Kava wirklich lebertoxisch? Eine Analyse der bekannten Daten zum Lebrisiko von Kavapräparaten, *DAZ* (2002) 1006–1011.
- [186] Society of Medicinal Plant Research, Relevant hepatotoxic effects of kava still need to be proven, *Planta Med* 69 (2003) 971–972.
- [187] D.L. Clouatre, Kava kava: examining new reports of toxicity, *Toxicol Lett* 150 (2004) 85–96.
- [188] R. Teschke, Kava hepatotoxicity: pathogenetic aspects and prospective considerations, *Liver Int* 30 (2010) 1270–1279.
- [189] J. Anke, I. Ramzan, Pharmacokinetic and pharmacodynamic drug interactions with Kava (*Piper methysticum* Forst. f.), *J Ethnopharmacol* 93 (2004) 153–160.
- [190] Y.N. Singh, Potential for interaction of kava and St. John's wort with drugs, *J Ethnopharmacol* 100 (2005) 108–113.
- [191] J.M. Mathews, A.S. Etheridge, S.R. Black, Inhibition of human cytochrome P450 activities by kava extract and kavalactones, *Drug Metab Dispos* 30 (2002) 1153–1157.
- [192] M. Unger, U. Holzgrabe, W. Jacobsen, C. Cummins, L.Z. Benet, Inhibition of cytochrome P450 3A4 by extracts and kavalactones of *Piper methysticum* (Kava-Kava), *Planta Med* 68 (2002) 1055–1058.

- [193] L. Zou, M.R. Harkey, G.L. Henderson, Effects of herbal components on cDNA-expressed cytochrome P450 enzyme catalytic activity, *Life Sci* 71 (2002) 1579–1589.
- [194] K.W. Herberg, Zum Einfluss von Kava-Spezialextrakt WS 1490 in Kombination mit Ethylalkohol auf sicherheitsrelevante Leistungsparameter, *Blutalkohol* 30 (1993) 96–105.
- [195] H. Foo, J. Lemon, Acute effects of kava, alone or in combination with alcohol, on subjective measures of impairment and intoxication and on cognitive performance, *Drug Alcohol Rev* 16 (1997) 147–155.
- [196] J.C. Almeida, E.W. Grimsley, Coma from the health food store: interaction between kava and alprazolam, *Ann Intern Med* 125 (1996) 940–941.
- [197] V. Donadio, P. Bonsi, I. Zele, L. Monari, R. Liguori, R. Vetrugno, F. Albani, P. Montagna, Myoglobinuria after ingestion of extracts of guarana, Ginkgo biloba and kava, *Neurol Sci* 21 (2000) 124.
- [198] D. Loew, G. Franz, Quality aspects of traditional and industrial Kava-extracts, *Phytomedicine* 10 (2003) 610–612.
- [199] A. Rowe, L.Y. Zhang, I. Ramzan, Toxicokinetics of kava, *Adv Pharmacol Sci* 2011 (2011) 1–6.
- [200] L.R. Olsen, M.P. Grillo, C. Skonberg, Constituents in kava extracts potentially involved in hepatotoxicity: a review, *Chem Res Toxicol* 24 (2011) 992–1002.
- [201] R. Teschke, S.X. Qiu, V. Lebot, Herbal hepatotoxicity by kava: update on pipermethystine, flavokavain B, and mould hepatotoxins as primarily assumed culprits, *Dig Liver Dis* 43 (2011) 676–681.
- [202] M. Schmidt, Are kavalactones the hepatotoxic principle of kava extracts? The pitfalls of the glutathione theory, *J Altern Complement Med* 9 (2003) 183–188.
- [203] J. Anke, I. Ramzan, Kava hepatotoxicity: Are we any closer to the truth?, *Planta Med* 70 (2004) 193–196.
- [204] L.Y. Zhang, A. Rowe, I. Ramzan, Does inflammation play a role in kava hepatotoxicity?, *Phytother Res* 25 (2011) 629–630.
- [205] E. Ernst, A re-evaluation of kava (*Piper methysticum*), *Br J Clin Pharmacol* 64 (2007) 415–417.
- [206] H.R.W. Dharmaratne, N.P.D. Nanayakkara, I.A. Khan, Kavalactones from *Piper methysticum*, and their ¹³C NMR spectroscopic analyses, *Phytochemistry* 59 (2002) 429–433.

- [207] A. Avdeef, M. Strafford, E. Block, M.P. Balogh, W. Chambliss, I. Khan, Drug absorption in vitro model: filter-immobilized artificial membranes. 2. Studies of the permeability properties of lactones in Piper methysticum Forst, *Eur J Pharm Sci* 14 (2001) 271–280.
- [208] J. Tang, R.A. Dunlop, A. Rowe, K.J. Rodgers, I. Ramzan, Kavalactones yangonin and methysticin induce apoptosis in human hepatocytes (HepG2) in vitro, *Phytother Res* 25 (2010) 417–423.
- [209] L. Zou, G.L. Henderson, M.R. Harkey, Y. Sakai, A. Li, Effects of kava (kava-kava, 'awa, yaqona, Piper methysticum) on c-DNA-expressed cytochrome P450 enzymes and human cryopreserved hepatocytes, *Phytomedicine* 11 (2004) 285–294.
- [210] P.V. Nerurkar, K. Dragull, C.-S. Tang, In vitro toxicity of kava alkaloid, pipermethystine, in HepG2 cells compared to kavalactones, *Toxicol Sci* 79 (2004) 106–111.
- [211] R. Gebhardt, M. Schmidt, Cytotoxicity of kava extracts and kavalactones in primary cultured rat hepatocytes and human HepG2 cells, <http://www.herbresearch.de> (2005).
- [212] P. Zhou, S. Gross, J.-H. Liu, B.-Y. Yu, L.-L. Feng, J. Nolte, V. Sharma, D. Piwnicka-Worms, S.X. Qiu, Flavokawain B, the hepatotoxic constituent from kava root, induces GSH-sensitive oxidative stress through modulation of IKK/NF-kappaB and MAPK signaling pathways, *FASEB J* 24 (2010) 4722–4732.
- [213] P. Whittaker, J.J. Clarke, R.H.C. San, J.M. Betz, H.E. Seifried, L.S. de Jager, V.C. Dunkel, Evaluation of commercial kava extracts and kavalactone standards for mutagenicity and toxicity using the mammalian cell gene mutation assay in L5178Y mouse lymphoma cells, *Food Chem Toxicol* 46 (2008) 168–174.
- [214] S. Lüde, M. Török, S. Dieterle, R. Jäggi, K.B. Büter, S. Krähenbühl, Hepatocellular toxicity of kava leaf and root extracts, *Phytomedicine* 15 (2008) 120–131.
- [215] L. Sorrentino, A. Capasso, M. Schmidt, Safety of ethanolic kava extract: Results of a study of chronic toxicity in rats, *Phytomedicine* 13 (2006) 542–549.
- [216] Y.N. Singh, A. Devkota, Aqueous kava extracts do not affect liver function tests in rats, *Planta Med* 69 (2003) 496–499.
- [217] N.P. Clayton, K. Yoshizawa, G.E. Kissling, L.T. Burka, P.-C. Chan, A. Nyska, Immunohistochemical analysis of expressions of hepatic cytochrome P450 in F344 rats following oral treatment with kava extract, *Exp Toxicol Pathol* 58 (2007) 223–236.
- [218] R.A. DiSilvestro, W. Zhang, D.J. DiSilvestro, Kava feeding in rats does not cause liver injury nor enhance galactosamine-induced hepatitis, *Food Chem Toxicol* 45 (2007) 1293–1300.

- [219] S. Fu, E. Korkmaz, F. Braet, Q. Ngo, I. Ramzan, Influence of kavain on hepatic ultrastructure, *World J Gastroenterol* 14 (2008) 541–546.
- [220] L. Zhang, A. Rowe, F. Braet, I. Ramzan, Macrophage depletion ameliorates kavalactone damage in the isolated perfused rat liver, *J Toxicol Sci* 37 (2012) 447–453.
- [221] J.-W. Jhoo, J.P. Freeman, T.M. Heinze, J.D. Moody, L.K. Schnackenberg, R.D. Beger, K. Dragull, C.-S. Tang, C.Y.W. Ang, In vitro cytotoxicity of nonpolar constituents from different parts of kava plant (*Piper methysticum*), *J Agric Food Chem* 54 (2006) 3157–3162.
- [222] S.T. Lim, K. Dragull, C.-S. Tang, H.C. Bittenbender, J.T. Efird, P.V. Nerurkar, Effects of kava alkaloid, pipermethystine, and kavalactones on oxidative stress and cytochrome P450 in F-344 rats, *Toxicol Sci* 97 (2007) 214–221.
- [223] X.Z. Li, I. Ramzan, Role of ethanol in kava hepatotoxicity, *Phytother Res* 24 (2010) 475–480.
- [224] N.C. Teoh, G.C. Farrell, Hepatotoxicity associated with non-steroidal anti-inflammatory drugs, *Clin Liver Dis* 7 (2003) 401–413.
- [225] P.A. Whitton, A. Lau, A. Salisbury, J. Whitehouse, C.S. Evans, Kava lactones and the kava-kava controversy, *Phytochemistry* 64 (2003) 673–679.
- [226] R. Teschke, A. Genthner, A. Wolff, Kava hepatotoxicity: comparison of aqueous, ethanolic, acetic kava extracts and kava-herbs mixtures, *J Ethnopharmacol* 123 (2009) 378–384.
- [227] B.M. Johnson, S.-X. Qiu, S. Zhang, F. Zhang, J.E. Burdette, L. Yu, J.L. Bolton, R.B. van Breemen, Identification of novel electrophilic metabolites of piper methysticum Forst (Kava), *Chem Res Toxicol* 16 (2003) 733–740.
- [228] L. Zou, M.R. Harkey, G.L. Henderson, L.E. Dike, Kava does not display metabolic toxicity in a homogeneous cellular assay, *Planta Med* 70 (2004) 289–292.
- [229] R. Teschke, V. Lebot, Proposal for a kava quality standardization code, *Food Chem Toxicol* 49 (2011) 2503–2516.
- [230] R. Teschke, S.X. Qiu, T.D. Xuan, V. Lebot, Kava and kava hepatotoxicity: requirements for novel experimental, ethnobotanical and clinical studies based on a review of the evidence, *Phytother Res* 25 (2011) 1263–1274.
- [231] A. Rowe, I. Ramzan, Are mould hepatotoxins responsible for kava hepatotoxicity?, *Phytother Res* 26 (2012) 1768–1770.
- [232] D.C. Rockey, Translating an understanding of the pathogenesis of hepatic fibrosis to novel therapies, *Clin Gastroenterol Hepatol* 11 (2013) 224–231.

- [233] C.D. Zois, G.H. Baltayiannis, P. Karayiannis, E.V. Tsianos, Systematic review: hepatic fibrosis - regression with therapy, *Aliment Pharmacol Ther* 28 (2008) 1175–1187.
- [234] L. Atzori, G. Poli, A. Perra, Hepatic stellate cell: a star cell in the liver, *Int J Biochem Cell Biol* 41 (2009) 1639–1642.
- [235] D. Li, S.L. Friedman, Liver fibrogenesis and the role of hepatic stellate cells: new insights and prospects for therapy, *J Gastroenterol Hepatol* 14 (1999) 618–633.
- [236] E. Mormone, J. George, N. Nieto, Molecular pathogenesis of hepatic fibrosis and current therapeutic approaches, *Chem Biol Interact* 193 (2011) 225–231.
- [237] J. Wu, M.A. Zern, Hepatic stellate cells: a target for the treatment of liver fibrosis, *J Gastroenterol* 35 (2000) 665–672.
- [238] A.J. Thompson, K. Patel, Antifibrotic therapies: Will we ever get there?, *Curr Gastroenterol Rep* 12 (2010) 23–29.
- [239] F. Stickel, B. Brinkhaus, N. Krähmer, H.K. Seitz, E.G. Hahn, D. Schuppan, Antifibrotic properties of botanicals in chronic liver disease, *Hepatogastroenterology* 49 (2002) 1102–1108.
- [240] Y. Feng, K.-F. Cheung, N. Wang, P. Liu, T. Nagamatsu, Y. Tong, Chinese medicines as a resource for liver fibrosis treatment, *Chin Med* 4 (2009) 16.
- [241] Y. Qu, W.-H. Chen, L. Zong, M.-Y. Xu, L.-G. Lu, 18 α -Glycyrrhizin induces apoptosis and suppresses activation of rat hepatic stellate cells, *Med Sci Monit* 18 (2012) 24–32.
- [242] J.H. Tsai, J.Y. Liu, T.T. Wu, P.C. Ho, C.Y. Huang, J.C. Shyu, Y.S. Hsieh, C.C. Tsai, Y.C. Liu, Effects of silymarin on the resolution of liver fibrosis induced by carbon tetrachloride in rats, *J Viral Hepat* 15 (2008) 508–514.
- [243] J.B. Chakraborty, F. Oakley, M.J. Walsh, Mechanisms and biomarkers of apoptosis in liver disease and fibrosis, *Int J Hepatol* 2012 (2012) 1–10.
- [244] D. Kong, F. Zhang, Z. Zhang, Y. Lu, S. Zheng, Clearance of activated stellate cells for hepatic fibrosis regression: Molecular basis and translational potential, *Biomedicine & Pharmacotherapy* (2012).
- [245] M.L. Go, X. Wu, X.L. Liu, Chalcones: an update on cytotoxic and chemoprotective properties, *Curr Med Chem* 12 (2005) 481–499.
- [246] V.R. Yadav, S. Prasad, B. Sung, B.B. Aggarwal, The role of chalcones in suppression of NF- κ B-mediated inflammation and cancer, *Int Immunopharmacol* 11 (2011) 295–309.
- [247] C. Kontogiorgis, M. Mantzanidou, D. Hadjipavlou-Litina, Chalcones and their potential role in inflammation, *Mini Rev Med Chem* 8 (2008) 1224–1242.

- [248] A.-M. Katsori, D. Hadjipavlou-Litina, Chalcones in cancer: understanding their role in terms of QSAR, *Curr Med Chem* 16 (2009) 1062–1081.
- [249] B. Orlikova, D. Tasdemir, F. Golais, M. Dicato, M. Diederich, Dietary chalcones with chemopreventive and chemotherapeutic potential, *Genes Nutr* 6 (2011) 125–147.
- [250] Z. Nowakowska, A review of anti-infective and anti-inflammatory chalcones, *Eur J Med Chem* 42 (2007) 125–137.
- [251] T.T. Cushnie, A.J. Lamb, Recent advances in understanding the antibacterial properties of flavonoids, *Int J Antimicrob Agents* 38 (2011) 99–107.
- [252] D.I. Batovska, I.T. Todorova, Trends in utilization of the pharmacological potential of chalcones, *Curr Clin Pharmacol* 5 (2010) 1–29.
- [253] N.K. Sahu, S.S. Balbhadra, J. Choudhary, D.V. Kohli, Exploring pharmacological significance of chalcone scaffold: a review, *Curr Med Chem* 19 (2012) 209–225.
- [254] A.-M. Katsori, D. Hadjipavlou-Litina, Recent progress in therapeutic applications of chalcones, *Expert Opin Ther Pat* 21 (2011) 1575–1596.
- [255] F. Power, F. Tutin, H. Rogerson, The constituents of hops, *J Chem Soc* 103 (1913) 1267.
- [256] M. Verzele, J. Stockx, F. Fontijn, M. Anteunis, Xanthohumol, a new natural chalcone, *Bull Soc Chim Belges* 66 (1957) 452–475.
- [257] M. Vandewalle, On the Synthesis of xanthohumol and isoxanthohumol, *Bull Soc Chim Belges* 70 (1961) 163–167.
- [258] R.S. Khupse, P.W. Erhardt, Total synthesis of xanthohumol, *J Nat Prod* 70 (2007) 1507–1509.
- [259] A. Nookandeh, N. Frank, F. Steiner, R. Ellinger, B. Schneider, C. Gerhäuser, H. Becker, Xanthohumol metabolites in faeces of rats, *Phytochemistry* 65 (2004) 561–570.
- [260] L.R. Chadwick, D. Nikolic, J.E. Burdette, C.R. Overk, J.L. Bolton, R.B. van Breemen, R. Fröhlich, H.H.S. Fong, N.R. Farnsworth, G.F. Pauli, Estrogens and congeners from spent hops (*Humulus lupulus*), *J Nat Prod* 67 (2004) 2024–2032.
- [261] J.F. Stevens, A.W. Taylor, G.B. Nickerson, M. Ivancic, J. Henning, A. Haunold, M.L. Deinzer, Prenylflavonoid variation in *Humulus lupulus*: distribution and taxonomic significance of xanthogalenol and 4'-O-methylxanthohumol, *Phytochemistry* 53 (2000) 759–775.

- [262] H. Mohamad, F. Abas, D. Permana, N.H. Lajis, A.M. Ali, M.A. Sukari, T.Y.Y. Hin, H. Kikuzaki, N. Nakatani, DPPH free radical scavenger components from the fruits of *Alpinia rafflesiana* Wall. ex. Bak. (Zingiberaceae), *Z Naturforsch* 59 (2004) 811–815.
- [263] V. Seidel, F. Bailleul, P.G. Waterman, (Rel)-1beta,2alpha-di-(2,4-dihydroxy-6-methoxybenzoyl)-3beta, 4alpha-di-(4-methoxyphenyl)-cyclobutane and other flavonoids from the aerial parts of *Goniothalamus gardneri* and *Goniothalamus thwaitesii*, *Phytochemistry* 55 (2000) 439–446.
- [264] S.N.A. Malek, C.W. Phang, H. Ibrahim, N. Abdul Wahab, K.S. Sim, Phytochemical and Cytotoxic Investigations of *Alpinia mutica* Rhizomes, *Molecules* 16 (2011) 583–589.
- [265] L. van Puyvelde, N. de Kimpe, J. Costa, V. Munyjabo, S. Nyirankuliza, E. Hakizamungu, N. Schamp, Isolation of flavonoids and a chalcone from *Helichrysum odoratissimum* and synthesis of helichrysetin, *J Nat Prod* 52 (1989) 629–633.
- [266] C. Gerhäuser, Beer constituents as potential cancer chemopreventive agents, *Eur J Cancer* 41 (2005) 1941–1954.
- [267] P. Zanolli, M. Zavatti, Pharmacognostic and pharmacological profile of *Humulus lupulus* L, *J Ethnopharmacol* 116 (2008) 383–396.
- [268] P.J. Magalhães, D.O. Carvalho, J.M. Cruz, L.F. Guido, A.A. Barros, Fundamentals and health benefits of xanthohumol, a natural product derived from hops and beer, *Nat Prod Commun* 4 (2009) 591–610.
- [269] X. Zi, A.R. Simoneau, Flavokawain A, a novel chalcone from kava extract, induces apoptosis in bladder cancer cells by involvement of Bax protein-dependent and mitochondria-dependent apoptotic pathway and suppresses tumor growth in mice, *Cancer Res* 65 (2005) 3479–3486.
- [270] Y. Tang, A.R. Simoneau, J. Xie, B. Shahandeh, X. Zi, Effects of the kava chalcone flavokawain A differ in bladder cancer cells with wild-type versus mutant p53, *Cancer Prev Res (Phila)* 1 (2008) 439–451.
- [271] R.N. Eskander, L.M. Randall, T. Sakai, Y. Guo, B. Hoang, X. Zi, Flavokawain B, a novel, naturally occurring chalcone, exhibits robust apoptotic effects and induces G2/M arrest of a uterine leiomyosarcoma cell line, *J Obstet Gynaecol Res* 38 (2012) 1086–1094.
- [272] Y. Tang, X. Li, Z. Liu, A.R. Simoneau, J. Xie, X. Zi, Flavokawain B, a kava chalcone, induces apoptosis via up-regulation of death-receptor 5 and Bim expression in androgen receptor negative, hormonal refractory prostate cancer cell lines and reduces tumor growth, *Int J Cancer* 127 (2010) 1758–1768.

- [273] T. Sakai, R.N. Eskander, Y. Guo, K.J. Kim, J. Mefford, J. Hopkins, N.N. Bhatia, X. Zi, B.H. Hoang, Flavokawain B, a kava chalcone, induces apoptosis in synovial sarcoma cell lines, *J Orthop Res* 30 (2012) 1045–1050.
- [274] X. Zhao, Y.-L. Chao, Q.-B. Wan, X.-M. Chen, P. Su, J. Sun, Y. Tang, Flavokawain B induces apoptosis of human oral adenoid cystic cancer ACC-2 cells via up-regulation of Bim and down-regulation of Bcl-2 expression, *Can J Physiol Pharmacol* 89 (2011) 875–883.
- [275] Y.-C. Hseu, M.-S. Lee, C.-R. Wu, H.-J. Cho, K.-Y. Lin, G.-H. Lai, S.-Y. Wang, Y.-H. Kuo, K.J. Senthil Kumar, H.-L. Yang, The chalcone flavokawain B induces G₂/M cell-cycle arrest and apoptosis in human oral carcinoma HSC-3 cells through the intracellular ROS generation and downregulation of the Akt/p38 MAPK signaling pathway, *J Agric Food Chem* 60 (2012) 2385–2397.
- [276] E. Lin, W.-H. Lin, S.-Y. Wang, C.-S. Chen, J.-W. Liao, H.-W. Chang, S.-C. Chen, K.-Y. Lin, L. Wang, H.-L. Yang, Y.-C. Hseu, Flavokawain B inhibits growth of human squamous carcinoma cells: Involvement of apoptosis and cell cycle dysregulation in vitro and in vivo, *J Nutr Biochem* 23 (2012) 368–378.
- [277] Y.-F. Kuo, Y.-Z. Su, Y.-H. Tseng, S.-Y. Wang, H.-M. Wang, P.J. Chueh, Flavokawain B, a novel chalcone from *Alpinia pricei* Hayata with potent apoptotic activity: Involvement of ROS and GADD153 upstream of mitochondria-dependent apoptosis in HCT116 cells, *Free Radic Biol Med* 49 (2010) 214–226.
- [278] J. An, Y. Gao, J. Wang, Q. Zhu, Y. Ma, J. Wu, J. Sun, Y. Tang, Flavokawain B induces apoptosis of non-small cell lung cancer H460 cells via Bax-initiated mitochondrial and JNK pathway, *Biotechnol Lett* 34 (2012) 1781–1788.
- [279] C.-T. Lin, K.J. Senthil Kumar, Y.-H. Tseng, Z.-J. Wang, M.-Y. Pan, J.-H. Xiao, S.-C. Chien, S.-Y. Wang, Anti-inflammatory activity of flavokawain B from *Alpinia pricei* Hayata, *J Agric Food Chem* 57 (2009) 6060–6065.
- [280] N. Li, J.-H. Liu, J. Zhang, B.-Y. Yu, Comparative Evaluation of cytotoxicity and antioxidative activity of 20 flavonoids, *J Agric Food Chem* 56 (2008) 3876–3883.
- [281] C. Dorn, B. Kraus, M. Motyl, T.S. Weiss, M. Gehrig, J. Schölmerich, J. Heilmann, C. Hellerbrand, Xanthohumol, a chalcone derived from hops, inhibits hepatic inflammation and fibrosis, *Mol Nutr Food Res* 54 (2010) 205–213.
- [282] C. Dorn, F. Bataille, E. Gaebele, J. Heilmann, C. Hellerbrand, Xanthohumol feeding does not impair organ function and homeostasis in mice, *Food Chem Toxicol* 48 (2010) 1890–1897.

- [283] J.-H. Lee, H.S. Jung, P.M. Giang, X. Jin, S. Lee, P.T. Son, D. Lee, Y.-S. Hong, K. Lee, J.J. Lee, Blockade of nuclear factor-kappaB signaling pathway and anti-inflammatory activity of cardamomin, a chalcone analog from *Alpinia conchigera*, *J Pharmacol Exp Ther* 316 (2006) 271–278.
- [284] D.A. Israf, T.A. Khaizurin, A. Syahida, N.H. Lajis, S. Khozirah, Cardamonin inhibits COX and iNOS expression via inhibition of p65NF-kappaB nuclear translocation and Ikappa-B phosphorylation in RAW 264.7 macrophage cells, *Mol Immunol* 44 (2007) 673–679.
- [285] Y.-L. Chow, K.-H. Lee, S. Vidyadaran, N.H. Lajis, M.N. Akhtar, D.A. Israf, A. Syahida, Cardamonin from *Alpinia rafflesiana* inhibits inflammatory responses in IFN- γ /LPS-stimulated BV2 microglia via NF- κ B signalling pathway, *Int Immunopharmacol* 12 (2012) 657–665.
- [286] A. Takahashi, N. Yamamoto, A. Murakami, Cardamonin suppresses nitric oxide production via blocking the IFN- γ /STAT pathway in endotoxin-challenged peritoneal macrophages of ICR mice, *Life Sci* 89 (2011) 337–342.
- [287] Y. Qin, C.-Y. Sun, F.-R. Lu, X.-R. Shu, D. Yang, L. Chen, X.-M. She, N.M. Gregg, T. Guo, Y. Hu, Cardamonin exerts potent activity against multiple myeloma through blockade of NF- κ B pathway in vitro, *Leuk Res* 36 (2012) 514–520.
- [288] S. Ahmad, D.A. Israf, N.H. Lajis, K. Shaari, H. Mohamed, A.A. Wahab, K.T. Ariffin, W.Y. Hoo, N.A. Aziz, A.A. Kadir, M.R. Sulaiman, M.N. Somchit, Cardamonin, inhibits pro-inflammatory mediators in activated RAW 264.7 cells and whole blood, *Eur J Pharmacol* 538 (2006) 188–194.
- [289] S. Hatzieremia, A.I. Gray, V.A. Ferro, A. Paul, R. Plevin, The effects of cardamonin on lipopolysaccharide-induced inflammatory protein production and MAP kinase and NFkappaB signalling pathways in monocytes/macrophages, *Br J Pharmacol* 149 (2006) 188–198.
- [290] T. Ohtsuki, H. Kikuchi, T. Koyano, T. Kowithayakorn, T. Sakai, M. Ishibashi, Death receptor 5 promoter-enhancing compounds isolated from *Catimbum speciosum* and their enhancement effect on TRAIL-induced apoptosis, *Bioorg Med Chem* 17 (2009) 6748–6754.
- [291] V.R. Yadav, S. Prasad, B.B. Aggarwal, Cardamonin sensitizes tumour cells to TRAIL through ROS- and CHOP-mediated up-regulation of death receptors and down-regulation of survival proteins, *Br J Pharmacol* 165 (2012) 741–753.
- [292] M.K. Park, S.H. Jo, H.J. Lee, J.H. Kang, Y.R. Kim, H.J. Kim, E.J. Lee, J.Y. Koh, K.O. Ahn, K.C. Jung, S.H. Oh, S.Y. Kim, C.H. Lee, Novel suppressive effects of cardamonin on the activity and expression of transglutaminase-2 lead to blocking the migration and invasion of cancer cells, *Life Sci* 92 (2013) 154–160.

- [293] X.-D. Cao, Z.-S. Ding, F.-S. Jiang, X.-H. Ding, J.-Z. Chen, S.-H. Chen, G.-Y. Lv, Antitumor constituents from the leaves of *Carya cathayensis*, *Nat Prod Res* 26 (2012) 2089–2094.
- [294] S. Vogel, J. Heilmann, Synthesis, cytotoxicity, and antioxidative activity of minor prenylated chalcones from *Humulus lupulus*, *J Nat Prod* 71 (2008) 1237–1241.
- [295] Y. Zhang, J. Guo, H. Dong, X. Zhao, L. Zhou, X. Li, J. Liu, Y. Niu, Hydroxysafflor yellow A protects against chronic carbon tetrachloride-induced liver fibrosis, *Eur J Pharmacol* 660 (2011) 438–444.
- [296] Y.-B. Zhang, H.-Y. Dong, X.-M. Zhao, L. Fan, Y. Zou, C. Zhang, G. Li, J.-C. Liu, Y.-C. Niu, Hydroxysafflor yellow A attenuates carbon tetrachloride-induced hepatic fibrosis in rats by inhibiting ERK5 signaling, *Am J Chin Med* 40 (2012) 481–494.
- [297] C.-C. Li, C.-Z. Yang, X.-M. Li, X.-M. Zhao, Y. Zou, L. Fan, L. Zhou, J.-C. Liu, Y.-C. Niu, Hydroxysafflor yellow A induces apoptosis in activated hepatic stellate cells through ERK1/2 pathway in vitro, *Eur J Pharm Sci* 46 (2012) 397–404.
- [298] S.W. Woo, S.H. Lee, H.-C. Kang, E.-J. Park, Y.-Z. Zhao, Y.-C. Kim, D.H. Sohn, Butein suppresses myofibroblastic differentiation of rat hepatic stellate cells in primary culture, *J Pharm Pharmacol* 55 (2003) 347–352.
- [299] A. Szuster-Ciesielska, K. Plewka, M. Kandefer-Szerszeń, Betulin, betulinic acid and butein are inhibitors of acetaldehyde-induced activation of liver stellate cells, *Pharmacol Rep* 63 (2011) 1109–1123.
- [300] S.H. Lee, G.S. Seo, H.S. Kim, S.W. Woo, G. Ko, D.H. Sohn, 2',4',6'-Tris(methoxymethoxy) chalcone attenuates hepatic stellate cell proliferation by a heme oxygenase-dependent pathway, *Biochem Pharmacol* 72 (2006) 1322–1333.
- [301] S.H. Lee, Y.-Z. Zhao, E.-J. Park, X.-H. Che, G.S. Seo, D.H. Sohn, 2',4',6'-Tris(methoxymethoxy) chalcone induces apoptosis by enhancing Fas-ligand in activated hepatic stellate cells, *Eur J Pharmacol* 658 (2011) 9–15.
- [302] S.W. Woo, S.H. Lee, G. Ko, Y.-C. Kim, D.H. Sohn, Isoliquiritigenin inhibits cell proliferation by a heme oxygenase-dependent pathway in rat hepatic stellate cells, *Planta Med* 74 (2008) 834–839.
- [303] M. Zhang, J.P. Zhang, H.T. Ji, J.S. Wang, D.H. Qian, Effect of six flavonoids on proliferation of hepatic stellate cells in vitro, *Acta Pharmacol Sin* 21 (2000) 253–256.
- [304] C. Dorn, J. Heilmann, C. Hellerbrand, Protective effect of xanthohumol on toxin-induced liver inflammation and fibrosis, *Int J Clin Exp Pathol* 5 (2012) 29–36.

- [305] F. Jin, X.Y. Jin, Y.L. Jin, D.W. Sohn, S.-A. Kim, D.H. Sohn, Y.C. Kim, H.S. Kim, Structural requirements of 2',4',6'-tris(methoxymethoxy) chalcone derivatives for anti-inflammatory activity: the importance of a 2'-hydroxy moiety, *Arch Pharm Res* 30 (2007) 1359–1367.
- [306] J. Loa, P. Chow, K. Zhang, Studies of structure-activity relationship on plant polyphenol-induced suppression of human liver cancer cells, *Cancer Chemother Pharmacol* 63 (2009) 1007–1016.
- [307] F. Li, S. Awale, Y. Tezuka, S. Kadota, Cytotoxic constituents from Brazilian red propolis and their structure-activity relationship, *Bioorg Med Chem* 16 (2008) 5434–5440.
- [308] C. Echeverria, J.F. Santibañez, O. Donoso-Tauda, C.A. Escobar, R. Ramirez-Tagle, Structural antitumoral activity relationships of synthetic chalcones, *Int J Mol Sci* 10 (2009) 221–231.
- [309] Y.-Z. Cai, Mei Sun, Jie Xing, Q. Luo, H. Corke, Structure-radical scavenging activity relationships of phenolic compounds from traditional Chinese medicinal plants, *Life Sci* 78 (2006) 2872–2888.
- [310] J.-C. Lee, K.-T. Lim, Y.-S. Jang, Identification of *Rhus verniciflua* Stokes compounds that exhibit free radical scavenging and anti-apoptotic properties, *Biochim Biophys Acta* 1570 (2002) 181–191.
- [311] B. Srinivasan, T.E. Johnson, R. Lad, C. Xing, Structure-activity relationship studies of chalcone leading to 3-hydroxy-4,3',4',5'-tetramethoxychalcone and its analogues as potent nuclear factor kappaB inhibitors and their anticancer activities, *J Med Chem* 52 (2009) 7228–7235.
- [312] R.J. Rodriguez, C.L. Miranda, J.F. Stevens, M.L. Deinzer, D.R. Buhler, Influence of prenylated and non-prenylated flavonoids on liver microsomal lipid peroxidation and oxidative injury in rat hepatocytes, *Food Chem Toxicol* 39 (2001) 437–445.
- [313] G.V. Rao, B.N. Swamy, V. Chandregowda, G.C. Reddy, Synthesis of (±)abyssinone I and related compounds: Their anti-oxidant and cytotoxic activities, *Eur J Med Chem* 44 (2009) 2239–2245.
- [314] F. Cottiglia, L. Casu, L. Bonsignore, M. Casu, C. Floris, M. Leonti, J. Gertsch, J. Heilmann, New cytotoxic prenylated isoflavonoids from *Bituminaria morisiana*, *Planta Med* 71 (2005) 254–260.
- [315] W. Wätjen, N. Weber, Y.-j. Lou, Z.-q. Wang, Y. Chovolou, A. Kampkötter, R. Kahl, P. Proksch, Prenylation enhances cytotoxicity of apigenin and liquiritigenin in rat H4IIE hepatoma and C6 glioma cells, *Food Chem Toxicol* 45 (2007) 119–124.

- [316] H. Forejtníková, K. Lunerová, R. Kubínová, D. Jankovská, R. Marek, R. Kares, V. Suchý, J. Vondráček, M. Machala, Chemoprotective and toxic potentials of synthetic and natural chalcones and dihydrochalcones in vitro, *Toxicology* 208 (2005) 81–93.
- [317] F. Zhao, H. Nozawa, A. Daikonnya, K. Kondo, S. Kitanaka, Inhibitors of nitric oxide production from hops (*Humulus lupulus* L.), *Biol Pharm Bull* 26 (2003) 61–65.
- [318] P.J. O'Brien, W. Irwin, D. Diaz, E. Howard-Cofield, C.M. Krejsa, M.R. Slaughter, B. Gao, N. Kaludercic, A. Angeline, P. Bernardi, P. Brain, C. Hougham, High concordance of drug-induced human hepatotoxicity with in vitro cytotoxicity measured in a novel cell-based model using high content screening, *Arch Toxicol* 80 (2006) 580–604.
- [319] O. Ndozangue-Touriguine, J. Hamelin, J. Bréard, Cytoskeleton and apoptosis, *Biochem Pharmacol* 76 (2008) 11–18.
- [320] S.-Y. Jeong, D.-W. Seol, The role of mitochondria in apoptosis, *BMB Rep* 41 (2008) 11–22.
- [321] A. Rasola, P. Bernardi, The mitochondrial permeability transition pore and its involvement in cell death and in disease pathogenesis, *Apoptosis* 12 (2007) 815–833.
- [322] G. Kroemer, Mitochondrial control of apoptosis: an overview, *Biochem Soc Symp* 66 (1999) 1–15.
- [323] R. Kachadourian, B.J. Day, Flavonoid-induced glutathione depletion: potential implications for cancer treatment, *Free Radic Biol Med* 41 (2006) 65–76.
- [324] O. Sabzevari, G. Galati, M.Y. Moridani, A. Siraki, P.J. O'Brien, Molecular cytotoxic mechanisms of anticancer hydroxychalcones, *Chem Biol Interact* 148 (2004) 57–67.
- [325] Z. Jin, W.S. El-Deiry, Overview of cell death signaling pathways, *Cancer Biol Ther* 4 (2005) 139–163.
- [326] D. Brenner, T.W. Mak, Mitochondrial cell death effectors, *Curr Opin Cell Biol* 21 (2009) 871–877.
- [327] N. Mohamad, A. Gutiérrez, M. Núñez, C. Cocca, G. Martín, G. Cricco, V. Medina, E. Rivera, R. Bergoc, Mitochondrial apoptotic pathways, *Biocell* 29 (2005) 149–161.
- [328] P.C. Ashe, M.D. Berry, Apoptotic signaling cascades, *Prog Neuropsychopharmacol Biol Psychiatry* 27 (2003) 199–214.
- [329] J. Strathmann, K. Klimo, S.W. Sauer, J.G. Okun, J.H.M. Prehn, C. Gerhäuser, Xanthohumol-induced transient superoxide anion radical formation triggers cancer cells into apoptosis via a mitochondria-mediated mechanism, *FASEB J* 24 (2010) 2938–2950.

- [330] J.-Y. Yang, M.A. Della-Fera, S. Rayalam, C.A. Baile, Effect of xanthohumol and isoxanthohumol on 3T3-L1 cell apoptosis and adipogenesis, *Apoptosis* 12 (2007) 1953–1963.
- [331] M. Festa, A. Capasso, C.W. D'Acunto, M. Masullo, A.G. Rossi, C. Pizza, S. Piacente, Xanthohumol induces apoptosis in human malignant glioblastoma cells by increasing reactive oxygen species and activating MAPK pathways, *J Nat Prod* 74 (2011) 2505–2513.
- [332] L. Pan, H. Becker, C. Gerhäuser, Xanthohumol induces apoptosis in cultured 40-16 human colon cancer cells by activation of the death receptor- and mitochondrial pathway, *Mol Nutr Food Res* 49 (2005) 837–843.
- [333] D. Deeb, X. Gao, H. Jiang, A.S. Arbab, S.A. Dulchavsky, S.C. Gautam, Growth inhibitory and apoptosis-inducing effects of xanthohumol, a prenylated chalone present in hops, in human prostate cancer cells, *Anticancer Res* 30 (2010) 3333–3339.
- [334] A. Boumendjel, X. Ronot, J. Boutonnat, Chalcones derivatives acting as cell cycle blockers: potential anti cancer drugs?, *Curr Drug Targets* 10 (2009) 363–371.
- [335] M.L. Edwards, D.M. Stemerick, P.S. Sunkara, Chalcones: a new class of antimitotic agents, *J Med Chem* 33 (1990) 1948–1954.
- [336] Y.K. Rao, S.-H. Fang, Y.-M. Tzeng, Differential effects of synthesized 2'-oxygenated chalcone derivatives: modulation of human cell cycle phase distribution, *Bioorg Med Chem* 12 (2004) 2679–2686.
- [337] A. Boumendjel, J. Boccard, P.-A. Carrupt, E. Nicolle, M. Blanc, A. Geze, L. Choisnard, D. Wouessidjewe, E.-L. Matera, C. Dumontet, Antimitotic and antiproliferative activities of chalcones: forward structure-activity relationship, *J Med Chem* 51 (2008) 2307–2310.
- [338] C. Gerhauser, A. Alt, E. Heiss, A. Gamal-Eldeen, K. Klimo, J. Knauft, I. Neumann, H.-R. Scherf, N. Frank, H. Bartsch, H. Becker, Cancer chemopreventive activity of Xanthohumol, a natural product derived from hop, *Mol Cancer Ther* 1 (2002) 959–969.
- [339] J.G. Drenzek, N.L. Seiler, R. Jaskula-Sztul, M.M. Rausch, S.L. Rose, Xanthohumol decreases Notch1 expression and cell growth by cell cycle arrest and induction of apoptosis in epithelial ovarian cancer cell lines, *Gynecologic Oncology* 122 (2011) 396–401.
- [340] B. Ernst, *Moderne Pharmakokinetik: Transport durch Membranen*, Wiley-VCH, Weinheim, 2010.
- [341] H. Wolff, M. Motyl, C. Hellerbrand, J. Heilmann, B. Kraus, Xanthohumol uptake and intracellular kinetics in hepatocytes, hepatic stellate cells, and intestinal cells, *J Agric Food Chem* 59 (2011) 12893–12901.

- [342] A.P. Li, Preclinical in vitro screening assays for drug-like properties, *Drug DiscToday: Technol* 2 (2005) 179–185.
- [343] J.R. Gillette, Factors affecting drug metabolism, *Ann NY Acad Sci* 179 (1971) 43–66.
- [344] U.A. Meyer, Overview of enzymes of drug metabolism, *J Pharmacokinet Biopharm* 24 (1996) 449–459.
- [345] A. Dudda, G.U. Kürzel, Metabolism studies in vitro and in vivo, *Drug Disc Eval* (2004) 493–520.
- [346] D.F. Lewis, On the recognition of mammalian microsomal cytochrome P450 substrates and their characteristics: towards the prediction of human p450 substrate specificity and metabolism, *Biochem Pharmacol* 60 (2000) 293–306.
- [347] L. Jia, X. Liu, The conduct of drug metabolism studies considered good practice (II): in vitro experiments, *Cur Drug Metab* 8 (2007) 822–829.
- [348] S.C. Khojasteh, S. Prabhu, J.R. Kenny, J.S. Halladay, A.Y.H. Lu, Chemical inhibitors of cytochrome P450 isoforms in human liver microsomes: a re-evaluation of P450 isoform selectivity, *Eur J Drug Metab Pharmacokinet* 36 (2011) 1–16.
- [349] E.F.A. Brandon, C.D. Raap, I. Meijerman, J.H. Beijnen, J.H.M. Schellens, An update on in vitro test methods in human hepatic drug biotransformation research: pros and cons, *Toxicol Appl Pharmacol* 189 (2003) 233–246.
- [350] D. Lang, A. Kalgutkar, Drug metabolizing enzymes: Non-P450 mediated oxidative metabolism of xenobiotics, *Informa Healthcare* (2003) 483–539.
- [351] J.A. Williams, Drug-drug interactions for UDP-glucuronosyltransferase substrates: a pharmacokinetic explanation for typically observed low exposure (AUCI/AUC) ratios, *Drug Metab Dispos* 32 (2004) 1201–1208.
- [352] M. Coughtrie, M. Fisher, Drug metabolizing enzymes: The role of sulfotransferases (SULTs) and UDP-glucuronosyltransferases (UGTs) in human drug clearance and bioactivation, *Informa Healthcare* (2003) 541–575.
- [353] S. Asha, M. Vidyavathi, Role of human liver microsomes in in Vitro metabolism of drugs—a review, *Appl Biochem Biotechnol* 160 (2010) 1699–1722.
- [354] R. Hänsel, *Pharmakognosie - Phytopharmazie: Mit 120 Tabellen*, Springer, Berlin, 2004.
- [355] E. Hijova, Bioavailability of chalcones, *Bratisl Lek Listy* 107 (2006) 80–84.
- [356] T. Walle, Absorption and metabolism of flavonoids, *Free Radic Biol Med* 36 (2004) 829–837.

- [357] P.C. Hollman, Absorption, bioavailability, and metabolism of flavonoids, *Pharm Biol* 42 (2004) 74–83.
- [358] J.A. Ross, C.M. Kasum, Dietary flavonoids: bioavailability, metabolic effects, and safety, *Annu Rev Nutr* 22 (2002) 19–34.
- [359] J.K. Prasain, S. Barnes, Metabolism and bioavailability of flavonoids in chemoprevention: current analytical strategies and future prospectus, *Mol Pharmaceutics* 4 (2007) 846–864.
- [360] P.C. Hollman, J.M. van Trijp, M.N. Buysman, M.S. van der Gaag, M.J. Mengelers, J.H. de Vries, M.B. Katan, Relative bioavailability of the antioxidant flavonoid quercetin from various foods in man, *FEBS Lett* 418 (1997) 152–156.
- [361] A.L.A. Sesink, I.C.W. Arts, M. Faassen-Peters, P.C.H. Hollman, Intestinal uptake of quercetin-3-glucoside in rats involves hydrolysis by lactase phlorizin hydrolase, *J Nutr* 133 (2003) 773–776.
- [362] P.C. Hollman, M.N. Buijsman, Y. van Gameren, E.P. Cnossen, J.H. de Vries, M.B. Katan, The sugar moiety is a major determinant of the absorption of dietary flavonoid glycosides in man, *Free Radic Res* 31 (1999) 569–573.
- [363] R.A. Walgren, K.J. Karnaky, G.E. Lindenmayer, T. Walle, Efflux of dietary flavonoid quercetin 4'-beta-glucoside across human intestinal Caco-2 cell monolayers by apical multidrug resistance-associated protein-2, *J Pharmacol Exp Ther* 294 (2000) 830–836.
- [364] A. Rechner, G. Kuhnle, P. Bremner, G. Hubbard, K. Moor, C. Rice-Evans, The metabolic fate of dietary polyphenols in humans, *Free Radic Biol Med* 33 (2002) 220–235.
- [365] T. Walle, U.K. Walle, P.V. Halushka, Carbon dioxide is the major metabolite of quercetin in humans, *J Nutr* 131 (2001) 2648–2652.
- [366] T. Walle, Y. Otake, J.A. Brubaker, U.K. Walle, P.V. Halushka, Disposition and metabolism of the flavonoid chrysin in normal volunteers, *Br J Clin Pharmacol* 51 (2001) 143–146.
- [367] E.U. Graefe, J. Wittig, S. Mueller, A.K. Riethling, B. Uehleke, B. Drewelow, H. Pforte, G. Jacobasch, H. Derendorf, M. Veit, Pharmacokinetics and bioavailability of quercetin glycosides in humans, *J Clin Pharmacol* 41 (2001) 492–499.
- [368] Y. Otake, T. Walle, Oxidation of the flavonoids galangin and kaempferide by human liver microsomes and CYP1A1, CYP1A2, and CYP2C9, *Drug Metab Dispos* 30 (2002) 103–105.
- [369] Y. Otake, F. Hsieh, T. Walle, Glucuronidation versus oxidation of the flavonoid galangin by human liver microsomes and hepatocytes, *Drug Metab Dispos* 30 (2002) 576–581.

- [370] M.C. Henderson, C.L. Miranda, J.F. Stevens, M.L. Deinzer, D.R. Buhler, In vitro inhibition of human P450 enzymes by prenylated flavonoids from hops, *Humulus lupulus*, *Xenobiotica* 30 (2000) 235–251.
- [371] M. Yilmazer, J.F. Stevens, M.L. Deinzer, D.R. Buhler, In vitro biotransformation of xanthohumol, a flavonoid from hops (*Humulus lupulus*), by rat liver microsomes, *Drug Metab Dispos* 29 (2001) 223–231.
- [372] M. Yilmazer, J.F. Stevens, D.R. Buhler, In vitro glucuronidation of xanthohumol, a flavonoid in hop and beer, by rat and human liver microsomes, *FEBS Lett* 491 (2001) 252–256.
- [373] D. Nikolic, Y. Li, L.R. Chadwick, G.F. Pauli, R.B. van Breemen, Metabolism of xanthohumol and isoxanthohumol, prenylated flavonoids from hops (*Humulus lupulus* L.), by human liver microsomes, *J Mass Spectrom* 40 (2005) 289–299.
- [374] C.E. Ruefer, C. Gerhäuser, N. Frank, H. Becker, S.E. Kulling, In vitro phase II metabolism of xanthohumol by human UDP-glucuronosyltransferases and sulfotransferases, *Mol Nutr Food Res* 49 (2005) 851–856.
- [375] L. Hanske, G. Loh, S. Sczesny, M. Blaut, A. Braune, Recovery and metabolism of xanthohumol in germ-free and human microbiota-associated rats, *Mol Nutr Food Res* 54 (2010) 1405–1413.
- [376] R. Jirásko, M. Holčapek, E. Vrublová, J. Ulrichová, V. Šimánek, Identification of new phase II metabolites of xanthohumol in rat in vivo biotransformation of hop extracts using high-performance liquid chromatography electrospray ionization tandem mass spectrometry, *J Chromatogr A* 1217 (2010) 4100–4108.
- [377] L. Legette, L. Ma, R.L. Reed, C.L. Miranda, J.M. Christensen, R. Rodriguez-Proteau, J.F. Stevens, Pharmacokinetics of xanthohumol and metabolites in rats after oral and intravenous administration, *Mol Nutr Food Res* 56 (2012) 466–474.
- [378] J. Guo, D. Liu, D. Nikolic, D. Zhu, J.M. Pezzuto, R.B. van Breemen, In vitro metabolism of isoliquiritigenin by human liver microsomes, *Drug Metab Dispos* 36 (2008) 461–468.
- [379] J. Guo, A. Liu, H. Cao, Y. Luo, J.M. Pezzuto, R.B. van Breemen, Biotransformation of the chemopreventive agent 2',4',4'-trihydroxychalcone (isoliquiritigenin) by UDP-glucuronosyltransferases, *Drug Metab Dispos* 36 (2008) 2104–2112.
- [380] Y.-Q. He, L. Yang, Y. Liu, J.-W. Zhang, J. Tang, J. Su, Y.-Y. Li, Y.-L. Lu, C.-H. Wang, L. Yang, Z.-T. Wang, Characterization of cardamonin metabolism by P450 in different species via HPLC-ESI-ion trap and UPLC-ESI-quadrupole mass spectrometry, *Acta Pharmacol Sin* 30 (2009) 1462–1470.

- [381] Y. Kohno, S. Kitamura, S. Sanoh, K. Sugihara, N. Fujimoto, S. Ohta, Metabolism of the alpha,beta-unsaturated ketones, chalcone and trans-4-phenyl-3-buten-2-one, by rat liver microsomes and estrogenic activity of the metabolites, *Drug Metab Dispos* 33 (2005) 1115–1123.
- [382] J.D. van der Merwe, E. Joubert, M. Manley, D. de Beer, C.J. Malherbe, W.C.A. Gelderblom, In vitro hepatic biotransformation of aspalathin and nothofagin, dihydrochalcones of rooibos (*Aspalathus linearis*), and assessment of metabolite antioxidant activity, *J Agric Food Chem* 58 (2010) 2214–2220.
- [383] Y. Zhang, X. Guo, E.T. Lin, L.Z. Benet, In vitro biotransformation of a novel antimalarial cysteine protease inhibitor in human liver microsomes, *Pharmacology* 58 (1999) 147–159.
- [384] C.E. Gutteridge, D.S. Thota, S.M. Curtis, M.P. Kozar, Q. Li, L. Xie, J. Zhang, V. Melendez, C.O. Asher, T.T. Luong, L. Gerena, D.A. Nichols, G. Montip, In vitro biotransformation, in vivo efficacy and pharmacokinetics of antimalarial chalcones, *Pharmacology* 87 (2011) 96–104.
- [385] M. Yoshimura, A. Sano, J.-I. Kamei, A. Obata, Identification and quantification of metabolites of orally administered naringenin chalcone in rats, *J Agric Food Chem* 57 (2009) 6432–6437.
- [386] M.B. Fisher, D. Jackson, A. Kaerner, S.A. Wrighton, A.G. Borel, Characterization by liquid chromatography-nuclear magnetic resonance spectroscopy and liquid chromatography-mass spectrometry of two coupled oxidative-conjugative metabolic pathways for 7-ethoxycoumarin in human liver microsomes treated with alamethicin, *Drug Metab Dispos* 30 (2002) 270–275.
- [387] H. Yamazaki, K. Inoue, M. Mimura, Y. Oda, F.P. Guengerich, T. Shimada, 7-Ethoxycoumarin O-deethylation catalyzed by cytochromes P450 1A2 and 2E1 in human liver microsomes, *Biochem Pharmacol* 51 (1996) 313–319.
- [388] J.H. Fentem, J.R. Fry, Metabolism of coumarin by rat, gerbil and human liver microsomes, *Xenobiotica* 22 (1992) 357–367.
- [389] C. Ballard, S. Gauthier, A. Corbett, C. Brayne, D. Aarsland, E. Jones, Alzheimer's disease, *Lancet* 377 (2011) 1019–1031.
- [390] W.G. Blackard, JR, G.K. Sood, D.R. Crowe, M.B. Fallon, Tacrine. A cause of fatal hepatotoxicity?, *J Clin Gastroenterol* 26 (1998) 57–59.
- [391] M.J. Knapp, D.S. Knopman, P.R. Solomon, W.W. Pendlebury, C.S. Davis, S.I. Gracon, A 30-week randomized controlled trial of high-dose tacrine in patients with Alzheimer's disease. The Tacrine Study Group, *JAMA* 271 (1994) 985–991.

- [392] P.B. Watkins, H.J. Zimmerman, M.J. Knapp, S.I. Gracon, K.W. Lewis, Hepatotoxic effects of tacrine administration in patients with Alzheimer's disease, *JAMA* 271 (1994) 992–998.
- [393] S.I. Gracon, M.J. Knapp, W.G. Berghoff, M. Pierce, R. DeJong, S.J. Lobbestael, J. Symons, S.L. Dombey, F.A. Luscombe, D. Kraemer, Safety of tacrine: clinical trials, treatment IND, and postmarketing experience, *Alzheimer Dis Assoc Disord* 12 (1998) 93–101.
- [394] L. Fang, B. Kraus, J. Lehmann, J. Heilmann, Y. Zhang, M. Decker, Design and synthesis of tacrine-ferulic acid hybrids as multi-potent anti-Alzheimer drug candidates, *Bioorg Med Chem Lett* 18 (2008) 2905–2909.
- [395] A. Lupp, D. Appenroth, L. Fang, M. Decker, J. Lehmann, C. Fleck, Tacrine-NO donor and tacrine-ferulic acid hybrid molecules as new anti-Alzheimer agents: hepatotoxicity and influence on the cytochrome P450 system in comparison to tacrine, *Arzneimittelforschung* 60 (2010) 229–237.
- [396] J.H.M. Lange, H.K.A.C. Coolen, M.A.W. van der Neut, A.J.M. Borst, B. Stork, P.C. Verveer, C.G. Kruse, Design, synthesis, biological properties, and molecular modeling investigations of novel tacrine derivatives with a combination of acetylcholinesterase inhibition and cannabinoid CB1 receptor antagonism, *J Med Chem* 53 (2010) 1338–1346.
- [397] L. Fang, S. Jumpertz, Y. Zhang, D. Appenroth, C. Fleck, K. Mohr, C. Tränkle, M. Decker, Hybrid molecules from xanomeline and tacrine: enhanced tacrine actions on cholinesterases and muscarinic M1 receptors, *J Med Chem* 53 (2010) 2094–2103.
- [398] S. Madden, V. Spaldin, B.K. Park, Clinical pharmacokinetics of tacrine, *Clin Pharmacokinet* 28 (1995) 449–457.
- [399] J.-W. Wu, L.-C. Lin, T.-H. Tsai, Drug–drug interactions of silymarin on the perspective of pharmacokinetics, *J Ethnopharmacol* 121 (2009) 185–193.
- [400] V. Spaldin, S. Madden, W.F. Pool, T.F. Woolf, B.K. Park, The effect of enzyme inhibition on the metabolism and activation of tacrine by human liver microsomes, *Br J Clin Pharmacol* 38 (1994) 15–22.
- [401] S. Madden, V. Spaldin, R.N. Hayes, T.F. Woolf, W.F. Pool, B.K. Park, Species variation in the bioactivation of tacrine by hepatic microsomes, *Xenobiotica* 25 (1995) 103–116.
- [402] L. Becquemont, M.A. Le Bot, C. Riche, P. Beaune, Influence of fluvoxamine on tacrine metabolism in vitro: potential implication for the hepatotoxicity in vivo, *Fundam Clin Pharmacol* 10 (1996) 156–157.

- [403] J.T. Larsen, L.L. Hansen, O. Spigset, K. Brøsen, Fluvoxamine is a potent inhibitor of tacrine metabolism in vivo, *Eur J Clin Pharmacol* 55 (1999) 375–382.
- [404] Y.H. Han, H.X. Lou, D.M. Ren, L.R. Sun, B. Ma, M. Ji, Stereoselective metabolism of silybin diastereoisomers in the glucuronidation process, *J Pharm Biomed Anal* 34 (2004) 1071–1078.
- [405] T. Woolf, W. Pool, R. Walker, D. Monteith, Liver reactions to tacrine, *Handbook Experim Pharmacol* 121 (1996) 395–410.
- [406] G.G. Benoit, C.F. Naud, M.A. Simard, A.L. Astier, Noninterference of cytochrome P4501A2 in the cytotoxicity of tacrine using genetically engineered V79 Chinese hamster cells for stable expression of the human or rat isoform and two human hepatocyte cell lines, *Biochem Pharmacol* 53 (1997) 423–427.
- [407] Q. Meng, J. Ru, G. Zhang, C. Shen, S. Schmitmeier, A. Bader, Re-evaluation of tacrine hepatotoxicity using gel entrapped hepatocytes, *Toxicol Lett* 168 (2007) 140–147.
- [408] M.-S. Lee, J.-I. Kim, T. Utsuki, N.-G. Park, H.-R. Kim, Cytoprotective effects of phlorofucofuroeckol A isolated from *Ecklonia stolonifera* against tacrine-treated HepG2 cells, *Fitoterapia* 83 (2012) 1060–1067.
- [409] M.-S. Lee, T. Shin, T. Utsuki, J.-S. Choi, D.-S. Byun, H.-R. Kim, Isolation and identification of phlorotannins from *Ecklonia stolonifera* with antioxidant and hepatoprotective properties in tacrine-treated HepG2 cells, *J Agric Food Chem* 60 (2012) 5340–5349.
- [410] E. Byun, G.-S. Jeong, R.-B. An, T.S. Min, Y.-C. Kim, Tribuli fructus constituents protect against tacrine-induced cytotoxicity in HepG2 cells, *Arch Pharm Res* 33 (2010) 67–70.
- [411] R.B. An, G.S. Jeong, J.-S. Beom, D.H. Sohn, Y.C. Kim, Chromone glycosides and hepatoprotective constituents of *Hypericum erectum*, *Arch Pharm Res* 32 (2009) 1393–1397.
- [412] H. Jaeschke, G.J. Gores, A.I. Cederbaum, J.A. Hinson, D. Pessayre, J.J. Lemasters, Mechanisms of hepatotoxicity, *Toxicol Sci* 65 (2002) 166–176.
- [413] A. Berson, S. Renault, P. Lettéron, M.A. Robin, B. Fromenty, D. Fau, M.A. Le Bot, C. Riché, A.M. Durand-Schneider, G. Feldmann, D. Pessayre, Uncoupling of rat and human mitochondria: a possible explanation for tacrine-induced liver dysfunction, *Gastroenterology* 110 (1996) 1878–1890.
- [414] J.J. Lemasters, T. Qian, C.A. Bradham, D.A. Brenner, W.E. Cascio, L.C. Trost, Y. Nishimura, A.L. Nieminen, B. Herman, Mitochondrial dysfunction in the pathogenesis of necrotic and apoptotic cell death, *J Bioenerg Biomembr* 31 (1999) 305–319.

- [415] H. Oh, J.-S. Kim, E.-K. Song, H. Cho, D.-H. Kim, S.-E. Park, H.-S. Lee, Y.-C. Kim, Sesquiterpenes with hepatoprotective activity from *Cnidium monnieri* on tacrine-induced cytotoxicity in Hep G2 cells, *Planta Med* 68 (2002) 748–749.
- [416] D.K. Monteith, J.C. Theiss, J.R. Haskins, F.A. de La Iglesia, Functional and subcellular organelle changes in isolated rat and human hepatocytes induced by tetrahydroaminoacridine, *Arch Toxicol* 72 (1998) 147–156.
- [417] R.A. Osseni, C. Debbasch, M.O. Christen, P. Rat, J.M. Warnet, Tacrine-induced reactive oxygen species in a human liver cell line: The role of anethole dithiolethione as a scavenger, *Toxicol In Vitro* 13 (1999) 683–688.
- [418] D.G. Robertson, T.K. Braden, E.R. Urda, N.D. Lalwani, F.A. de La Iglesia, Elucidation of mitochondrial effects by tetrahydroaminoacridine (tacrine) in rat, dog, monkey and human hepatic parenchymal cells, *Arch Toxicol* 72 (1998) 362–371.
- [419] T. Melo, R.A. Videira, S. André, E. Maciel, C.S. Francisco, A.M. Oliveira-Campos, L.M. Rodrigues, M.R. Domingues, F. Peixoto, M. Manuel Oliveira, Tacrine and its analogues impair mitochondrial function and bioenergetics: a lipidomic analysis in rat brain, *J Neurochem* 120 (2012) 998-1013.

9 Abbreviations

| | |
|------------------|---|
| 3OHHeli | 3-hydroxyhelichrysetin |
| 3OHXANH | 3-hydroxyxanthohumol H |
| 3OMeXANH | 3-methoxyxanthohumol H |
| 4'MeXAN | 4'-methylxanthohumol |
| 4AcXAN | 4-acetyl xanthohumol |
| 4MeXAN | 4-methylxanthohumol |
| 5-HT | 5-hydroxytryptamine (serotonin) |
| 7-EC | 7-ethoxycoumarin |
| 7-HC | 7-hydroxycoumarin |
| A | alpinetin chalcone |
| AA | anisaldehyde |
| AChE | acetylcholinesterase |
| AD | Alzheimer's disease |
| Ala | alamethicin |
| ALP | alkaline phosphatase |
| ALT | alanine amino transferase |
| AP-1 | activator protein 1 |
| Apaf-1 | apoptotic protease-activating factor 1 |
| ASI | Anxiety Status Inventory |
| AST | aspartate amino transferase |
| ATCC | American Type Culture Collection |
| ATP | adenosine triphosphate |
| BChE | butyrylcholinesterase |
| Bcl-2 | B-cell lymphoma 2 protein family |
| BfArM | Bundesinstitut für Arzneimittel und Medizinprodukte |
| BSβG | broad-specific β-glucosidase |
| C | tacrine-silibinin codrug |
| CB | cannabinoid |
| CDK/Cdk | cyclin-dependent kinase |
| Ch | channel |
| CHOP | CCAAT/enhancer binding protein homologous protein |
| CM | culture medium |
| C _{max} | maximum (peak) concentration |
| CNS | central nervous system |

| | |
|------------------|---------------------------------------|
| cof | cofactors |
| COMT | catechol-O-methyltransferase |
| conc. | concentrated |
| COSY | correlation spectroscopy |
| COX | cyclooxygenase |
| ctl | control |
| CV | crystal violet |
| CYP(450) | cytochrome P450 enzyme |
| DAC | Deutscher Arzneimittel Codex |
| DAD | diode array detector |
| dhFKC | dihydroflavokawain C |
| dhHeli | dihydrohelichrysetin |
| DHK | dihydrokawain |
| DHM | dihydromethysticin |
| dhXANC | dihydroxanthohumol C |
| DILI | drug induced liver injury |
| DMEM | Dulbecco's Modified Eagle Medium |
| DMSO | dimethyl sulfoxide |
| DMY | desmethoxyyangonin |
| DNA | deoxyribonucleic acid |
| DPPH | 2,2-diphenyl-1-picrylhydrazyl |
| DR | death receptor |
| EC ₅₀ | half maximal effective concentration |
| ECM | extracellular matrix |
| EDTA | ethylenediaminetetraacetic acid |
| ER | endoplasmic reticulum |
| ERK | extracellular signal-regulated kinase |
| ESI | electrospray ionization |
| ET-1 | endothelin-1 |
| EtOAc | ethyl acetate |
| EtOH | ethanol |
| ex/em | excitation/emission |
| FA | formic acid |
| FasL | Fas-ligand |
| FCS | fetal calf serum |
| FDA | Food and Drug Administration |
| FKA | flavokawain A |

| | |
|------------------|---|
| FKB | flavokawain B |
| FKC | flavokawain C |
| FMO | flavin monooxygenase |
| G-6-P | glucose-6-phosphate |
| G-6-P-DH | glucose-6-phosphate dehydrogenase |
| GABA | γ -aminobutyric acid |
| GADD | growth arrest and DNA-damage-inducible proteins |
| GF | germ-free |
| GGT | glutamyl transpeptidase |
| GIT | gastrointestinal tract |
| Glu | glucuronic acid |
| GSH | glutathione |
| GST | glutathione-S-transferase |
| HAM-A | Hamilton Anxiety Scale |
| HAV | hepatitis A virus |
| HBsAg | hepatitis B surface antigen |
| HBV | hepatitis B virus |
| HCA | high content analysis |
| HCC | hepatocellular carcinoma |
| HCV | hepatitis C virus |
| HDAC | histone deacetylase |
| Heli | helichrysetin |
| hi | heat inactivated |
| HLM | human liver microsomes |
| HMA | human microbiota-associated |
| HMBC | heteronuclear multiple bond correlation |
| HO-1 | heme oxygenase 1 |
| HPLC | high pressure liquid chromatography |
| HPLC–NMR | high pressure liquid chromatography–nuclear magnetic resonance spectroscopy |
| HPTLC | high performance thin layer chromatography |
| HSC | hepatic stellate cells |
| HSQC | heteronuclear single quantum coherence |
| HSRRB | Health Science Research Resources Bank |
| HSYA | hydroxysafflor yellow A |
| IC ₅₀ | half maximal inhibitory concentration |
| ICAM | intercellular adhesion molecule |

| | |
|----------------|---|
| IgG | immunglobuline G |
| IKK | I κ B kinase |
| IL | interleukin |
| INF | interferon |
| iNOS | inducible NO synthase |
| I κ B | inhibitor of NF-kappaB |
| JHSF | Japan Health Science Research Resources Bank |
| JNK | c-Jun N-terminal kinase |
| K | kawain |
| LC–HRESIMS | liquid chromatography–high resolution electrospray ionization mass spectrometry |
| LC–MS | liquid chromatography–mass spectrometry |
| LDH | lactate dehydrogenase |
| LPH | lactase phlorizidin hydrolase |
| LPS | lipopolysaccharide |
| M | methysticin |
| MAO | monoamine oxidase |
| MAPK | mitogen-activated kinase |
| matrix | blank control |
| MeCN | acetonitrile |
| MEF | myocyte enhancer factor |
| MeOH | methanol |
| micr | microsomes |
| MMP | matrix metalloproteinase |
| MPLC | middle pressure liquid chromatography |
| mRNA | messenger ribonucleic acid |
| MRP2 | multidrug resistance-associated protein 2 |
| MTT | 3-(4,5-dimethylthiazol-2-yl)-2,5-diphenyltetrazolium bromide |
| NA | noradrenaline |
| NADP(H) | (reduced) nicotinamide adenine dinucleotide phosphate |
| NAFLD | non-alcoholic fatty liver disease |
| NASH | non-alcoholic steatohepatitis |
| NAT | <i>N</i> -acetyltransferase |
| NEA | non-essential amino acids |
| NF- κ B | nuclear factor κ B |
| NMDA | <i>N</i> -methyl-D-aspartate |
| NMR | nuclear magnetic resonance (spectroscopy) |

| | |
|----------------|---|
| Nrf2 | nuclear factor (erythroid-derived 2)-like 2 |
| NSAID | non-steroidal anti-inflammatory drug |
| ORAC | oxygen radical absorbance capacity |
| P | pinostrobin chalcone |
| p.a. | pro analysi |
| PA | pyrrolizidine alkaloids |
| PARP | poly(ADP-ribose)polymerase |
| PBO | trans-4-phenyl-3-buten-2-one |
| PBS | Dulbecco's Phosphate Buffered Saline |
| PDGF | platelet derived growth factor |
| PFA | paraformaldehyde |
| PGE2 | prostaglandin E2 |
| Pgp | P-glycoprotein |
| PHH | primary human hepatocytes |
| PhI | phase I |
| PhII | phase II |
| PT | prothrombin time |
| R _f | retention factor |
| ROS | reactive oxygen species |
| R _t | retention time |
| S | silibinin |
| SAR | structure activity relationship |
| SD | standard deviation |
| SDS | sodium dodecyl sulfate |
| SE | standard error |
| SGLT1 | sodium-dependent glucose transporter 1 |
| SNMC | stronger neo-minophagen C |
| SP | sodium pyruvate |
| stabi | stability control |
| stock | stock solution |
| SULT | sulfotransferase |
| T | tacrine |
| T ₃ | triiodothyronine |
| T ₄ | thyroxine |
| TCM | Traditional Chinese Medicine |
| TFA | trifluoroacetic acid |
| TGF-β | transforming growth factor β |

| | |
|---------------|---|
| THSA | tacrine hemi succinamide |
| thXANC | tetrahydroxanthohumol C |
| TIMP | tissue inhibitor of metalloproteinases |
| TLC | thin layer chromatography |
| t_{\max} | time to peak concentration |
| TMMC | 2',4',6'-tris(methoxymethoxy)chalcone |
| TMS | tetramethylsilane |
| TNF | tumor necrosis factor |
| TOF | time of flight |
| TRAIL | TNF-related apoptosis inducing ligand |
| TxB2 | thromboxane B2 |
| UDPGA | uridine 5'-diphosphoglucuronic acid |
| UGT | UDP-glucuronosyl transferase |
| UHPLC | ultra high pressure liquid chromatography |
| US | United States |
| UV | ultraviolet |
| VOD | venoocclusive disease |
| WHO | World Health Organization |
| XAN | xanthohumol |
| XANC | xanthohumol C |
| XANH | xanthohumol H |
| Y | yangonin |
| α -SMA | alpha smooth muscle actin |

10 Appendix

10.1 Supplementary HCA data of the chalcones

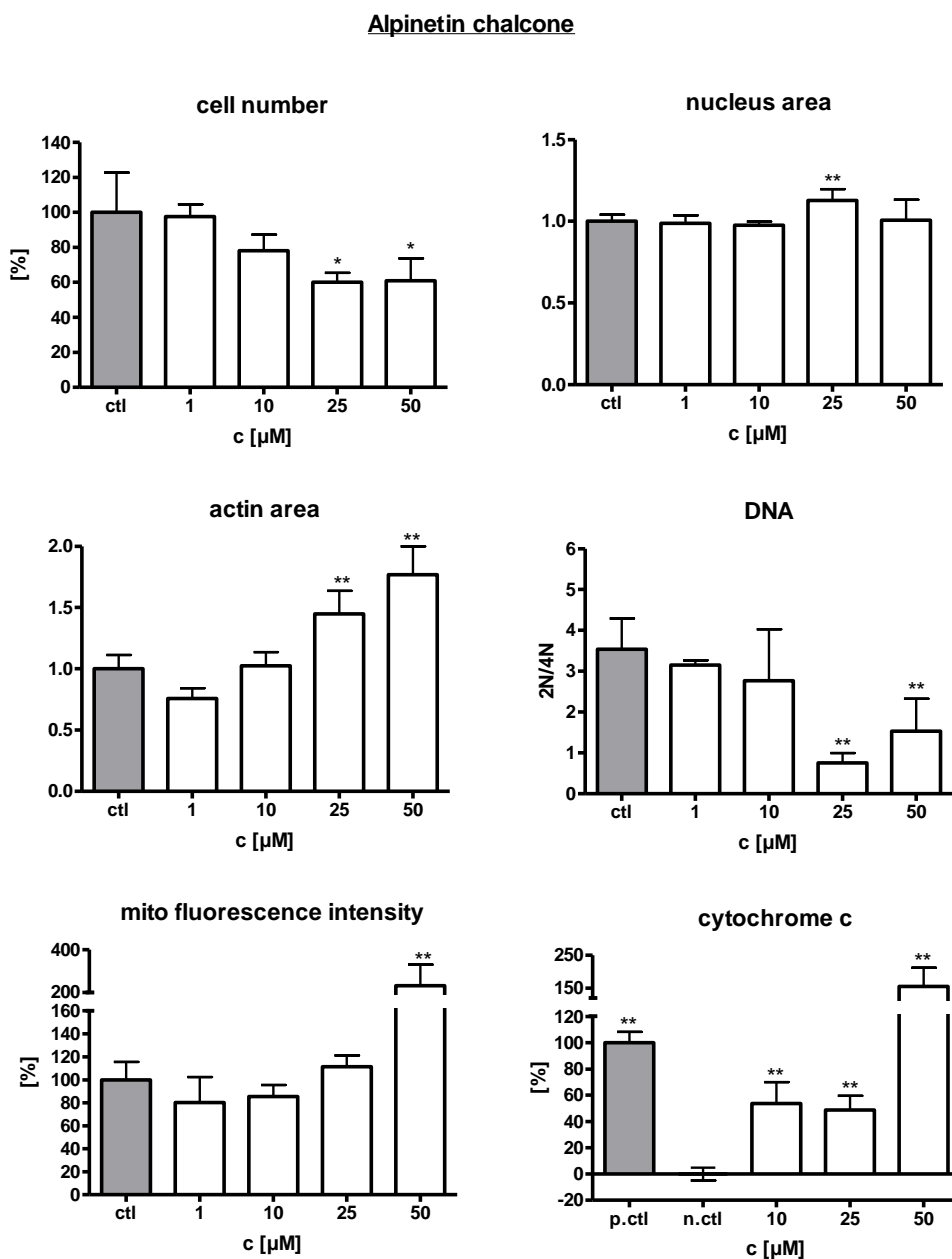


Figure 10.1: Supplementary HCA data of alpinetin chalcone (A) (1-50 μM). Cell number [%], nucleus area, actin area, and mitochondrial fluorescence intensity [%] were determined by fluorescence microscopy (see chapter 2.2.6.1). Cytochrome c release [%] was analyzed by fluorescence microscopy (see chapter 2.2.6.2). Hoechst33342 staining of cell nuclei was used to determine the DNA content (see chapter 2.2.6.3) and to calculate the ratio 2N/4N. Values are presented as mean ± SD and refer to untreated control cells (ctl/nctl). Statistical analysis (one-way ANOVA following Dunnett's multi-comparison post-hoc test) was performed using GraphPad Prism 4 software. Levels of significance *p < 0.05, **p < 0.01 vs ctl/nctl.

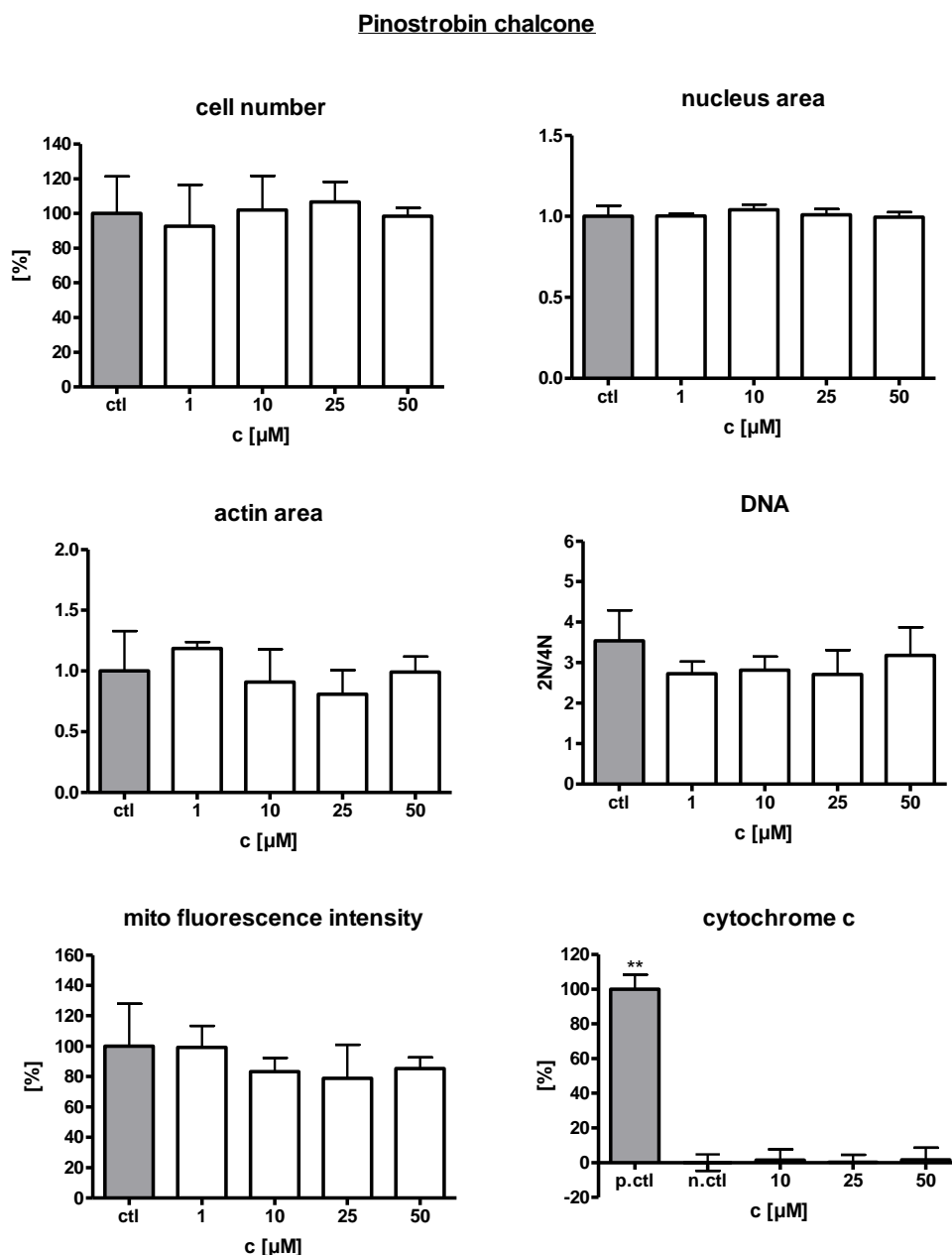


Figure 10.2: Supplementary HCA data of pinostrobin chalcone (P) (1-50 μM). Cell number [%], nucleus area, actin area, and mitochondrial fluorescence intensity [%] were determined by fluorescence microscopy (see chapter 2.2.6.1). Cytochrome c release [%] was analyzed by fluorescence microscopy (see chapter 2.2.6.2). Hoechst33342 staining of cell nuclei was used to determine the DNA content (see chapter 2.2.6.3) and to calculate the ratio 2N/4N. Values are presented as mean ± SD and refer to untreated control cells (ctl/n.ctl). Statistical analysis (one-way ANOVA following Dunnett's multi-comparison post-hoc test) was performed using GraphPad Prism 4 software. Levels of significance * $p < 0.05$, ** $p < 0.01$ vs ctl/n.ctl.

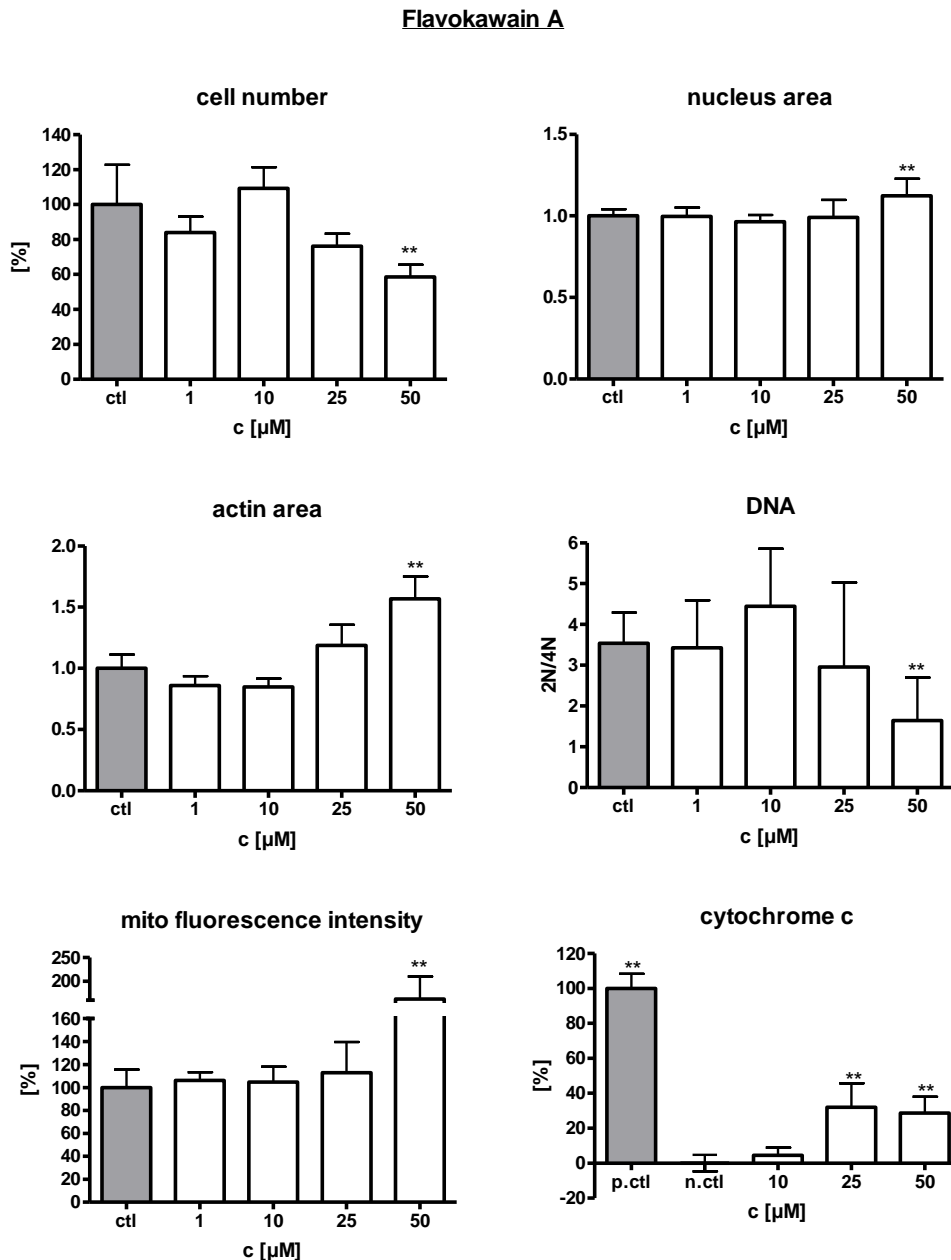


Figure 10.3: Supplementary HCA data of flavokawain A (FKA) (1-50 μM). Cell number [%], nucleus area, actin area, and mitochondrial fluorescence intensity [%] were determined by fluorescence microscopy (see chapter 2.2.6.1). Cytochrome c release [%] was analyzed by fluorescence microscopy (see chapter 2.2.6.2). Hoechst33342 staining of cell nuclei was used to determine the DNA content (see chapter 2.2.6.3) and to calculate the ratio 2N/4N. Values are presented as mean ± SD and refer to untreated control cells (ctl/n.ctl). Statistical analysis (one-way ANOVA following Dunnett's multi-comparison post-hoc test) was performed using GraphPad Prism 4 software. Levels of significance *p < 0.05, **p < 0.01 vs ctl/n.ctl.

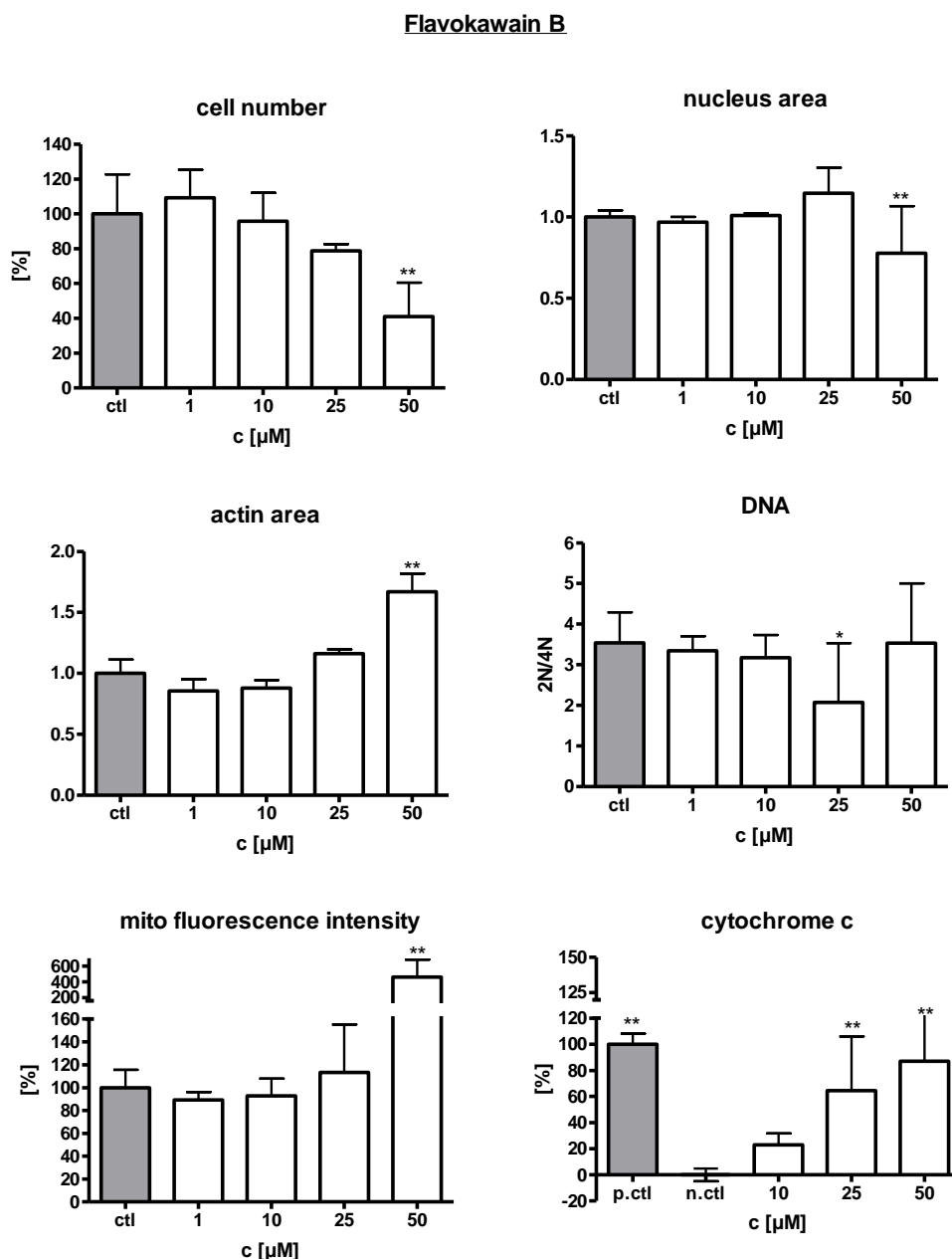


Figure 10.4: Supplementary HCA data of flavokawain B (FKB) (1-50 μM). Cell number [%], nucleus area, actin area, and mitochondrial fluorescence intensity [%] were determined by fluorescence microscopy (see chapter 2.2.6.1). Cytochrome c release [%] was analyzed by fluorescence microscopy (see chapter 2.2.6.2). Hoechst33342 staining of cell nuclei was used to determine the DNA content (see chapter 2.2.6.3) and to calculate the ratio 2N/4N. Values are presented as mean ± SD and refer to untreated control cells (ctl/n.ctl). Statistical analysis (one-way ANOVA following Dunnett's multi-comparison post-hoc test) was performed using GraphPad Prism 4 software. Levels of significance *p < 0.05, **p < 0.01 vs ctl/n.ctl.

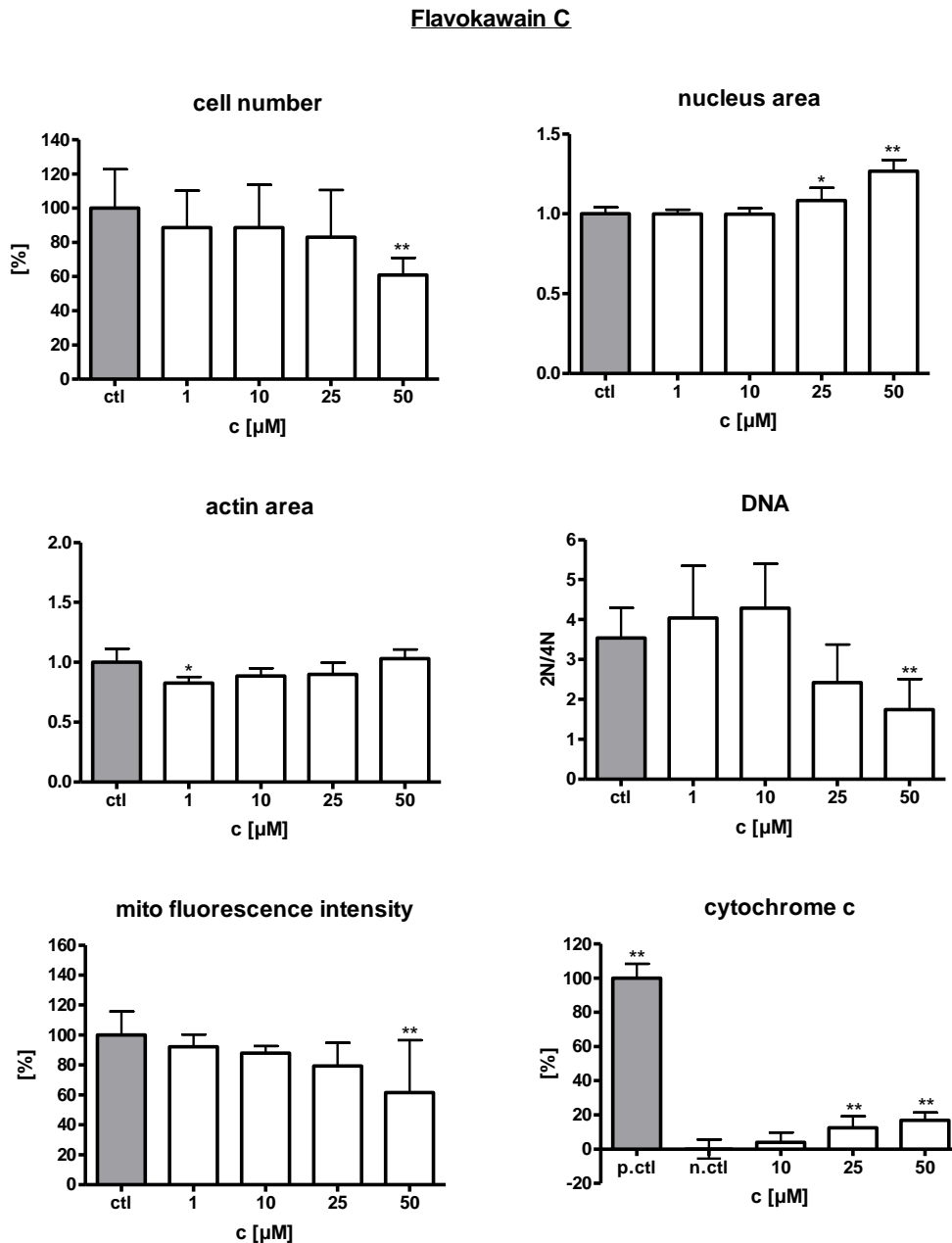


Figure 10.5:Supplementary HCA data of flavokawain C (FKC) (1-50 μM). Cell number [%], nucleus area, actin area, and mitochondrial fluorescence intensity [%] were determined by fluorescence microscopy (see chapter 2.2.6.1). Cytochrome c release [%] was analyzed by fluorescence microscopy (see chapter 2.2.6.2). Hoechst33342 staining of cell nuclei was used to determine the DNA content (see chapter 2.2.6.3) and to calculate the ratio 2N/4N. Values are presented as mean \pm SD and refer to untreated control cells (ctl/n.ctl). Statistical analysis (one-way ANOVA following Dunnett's multi-comparison post-hoc test) was performed using GraphPad Prism 4 software. Levels of significance * $p < 0.05$, ** $p < 0.01$ vs ctl/n.ctl.

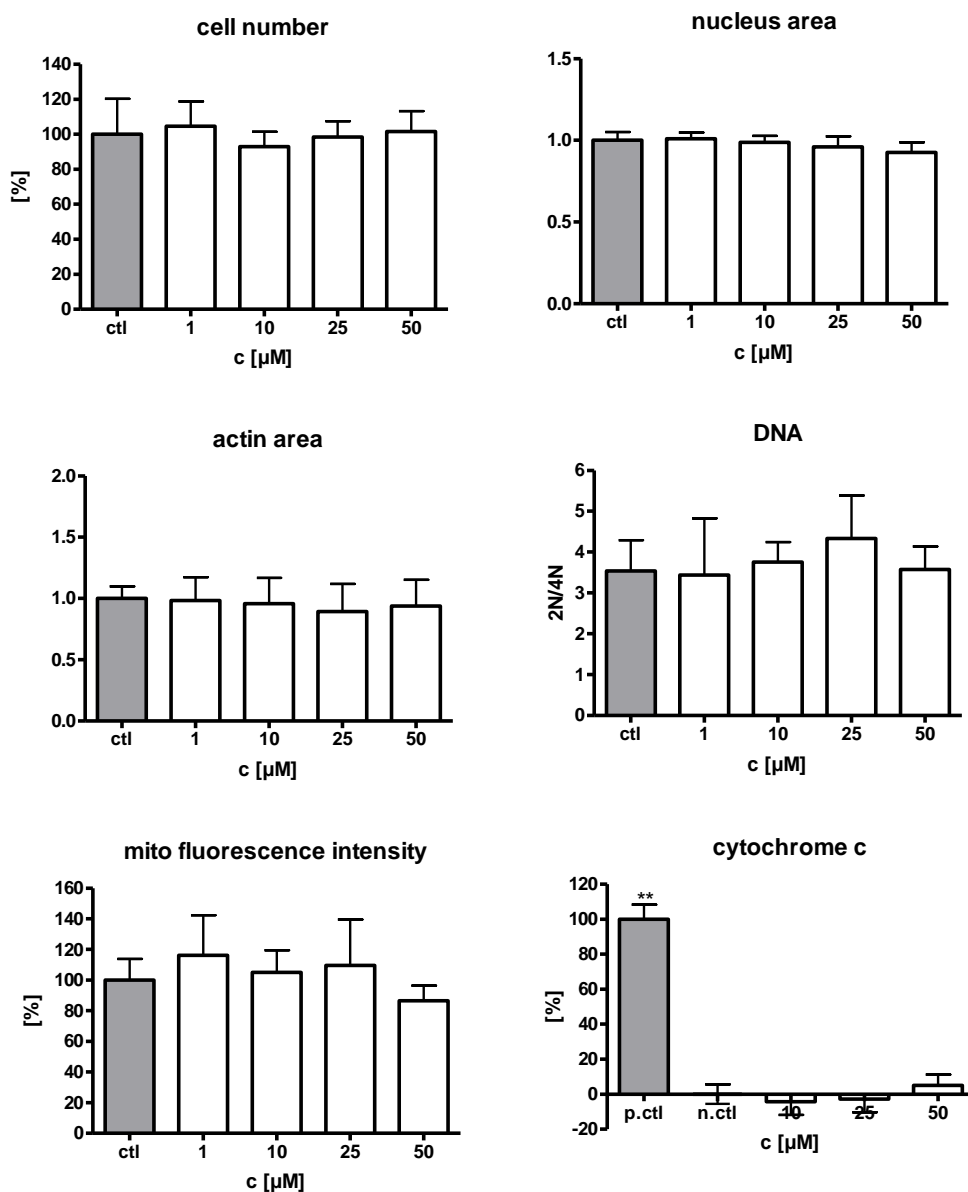
Dihydroflavokawain C

Figure 10.6: Supplementary HCA data of dihydroflavokawain C (dhFKC) (1-50 μM). Cell number [%], nucleus area, actin area, and mitochondrial fluorescence intensity [%] were determined by fluorescence microscopy (see chapter 2.2.6.1). Cytochrome c release [%] was analyzed by fluorescence microscopy (see chapter 2.2.6.2). Hoechst33342 staining of cell nuclei was used to determine the DNA content (see chapter 2.2.6.3) and to calculate the ratio 2N/4N. Values are presented as mean \pm SD and refer to untreated control cells (ctl/n.ctl). Statistical analysis (one-way ANOVA following Dunnett's multi-comparison post-hoc test) was performed using GraphPad Prism 4 software. Levels of significance * $p < 0.05$, ** $p < 0.01$ vs ctl/n.ctl.

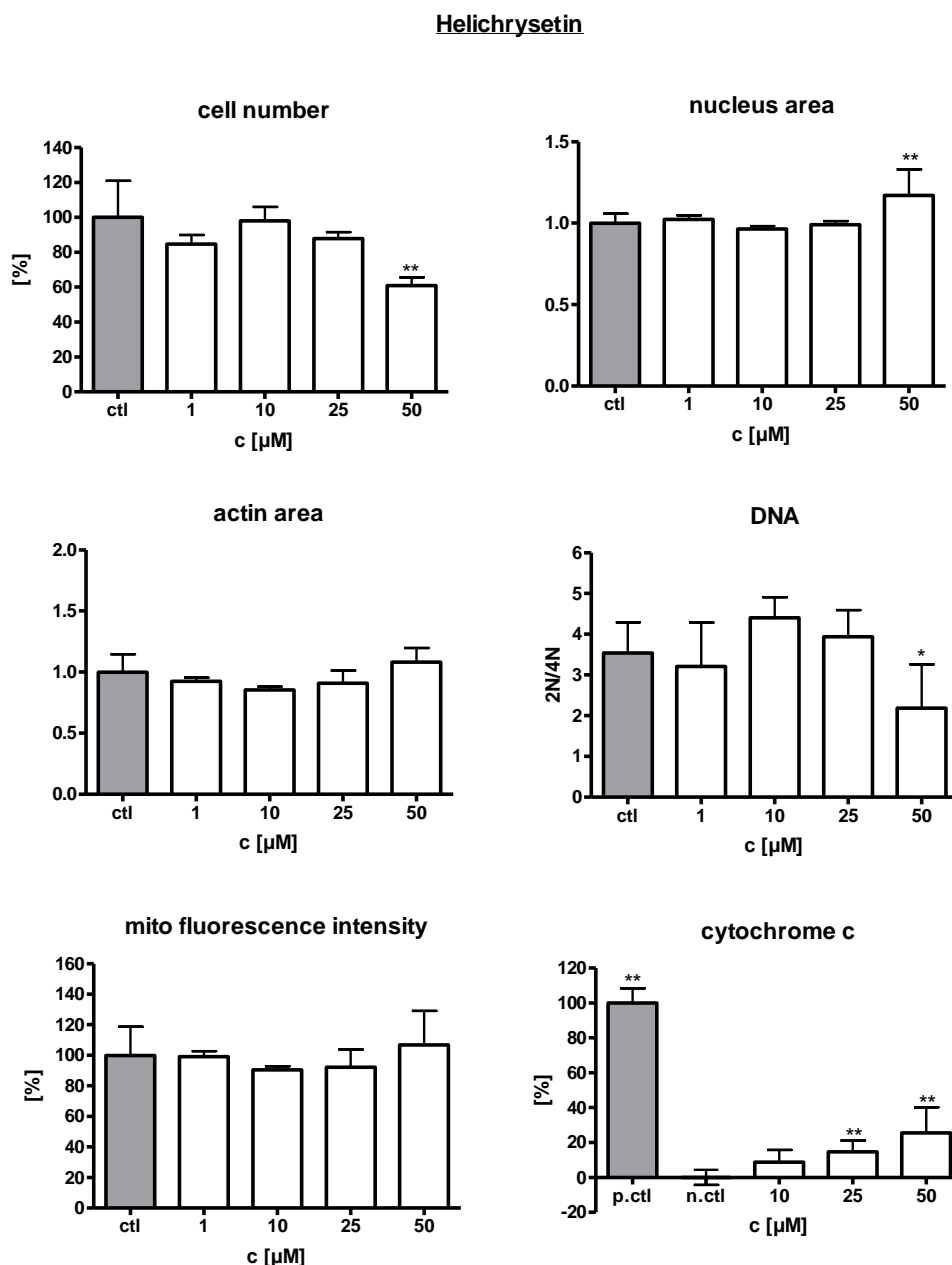


Figure 10.7: Supplementary HCA data of helichrysetin (Heli) (1-50 μM). Cell number [%], nucleus area, actin area, and mitochondrial fluorescence intensity [%] were determined by fluorescence microscopy (see chapter 2.2.6.1). Cytochrome c release [%] was analyzed by fluorescence microscopy (see chapter 2.2.6.2). Hoechst33342 staining of cell nuclei was used to determine the DNA content (see chapter 2.2.6.3) and to calculate the ratio 2N/4N. Values are presented as mean ± SD and refer to untreated control cells (ctl/n.ctl). Statistical analysis (one-way ANOVA following Dunnett's multi-comparison post-hoc test) was performed using GraphPad Prism 4 software. Levels of significance *p < 0.05, **p < 0.01 vs ctl/n.ctl.

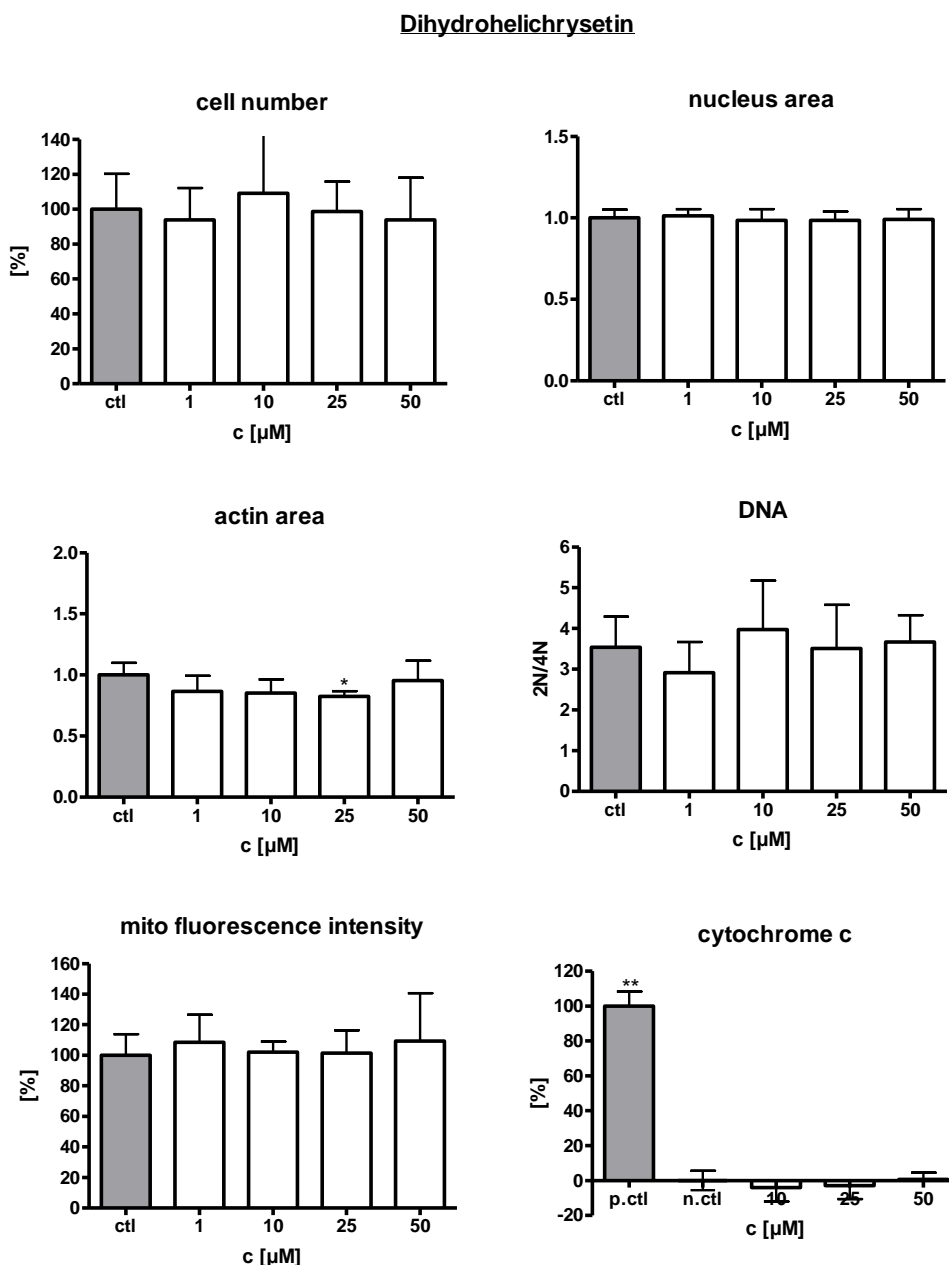


Figure 10.8: Supplementary HCA data of dihydrohelichrysetin (dhHeli) (1-50 μM). Cell number [%], nucleus area, actin area, and mitochondrial fluorescence intensity [%] were determined by fluorescence microscopy (see chapter 2.2.6.1). Cytochrome c release [%] was analyzed by fluorescence microscopy (see chapter 2.2.6.2). Hoechst33342 staining of cell nuclei was used to determine the DNA content (see chapter 2.2.6.3) and to calculate the ratio 2N/4N. Values are presented as mean ± SD and refer to untreated control cells (ctl/n.ctl). Statistical analysis (one-way ANOVA following Dunnett's multi-comparison post-hoc test) was performed using GraphPad Prism 4 software. Levels of significance *p < 0.05, **p < 0.01 vs ctl/n.ctl.

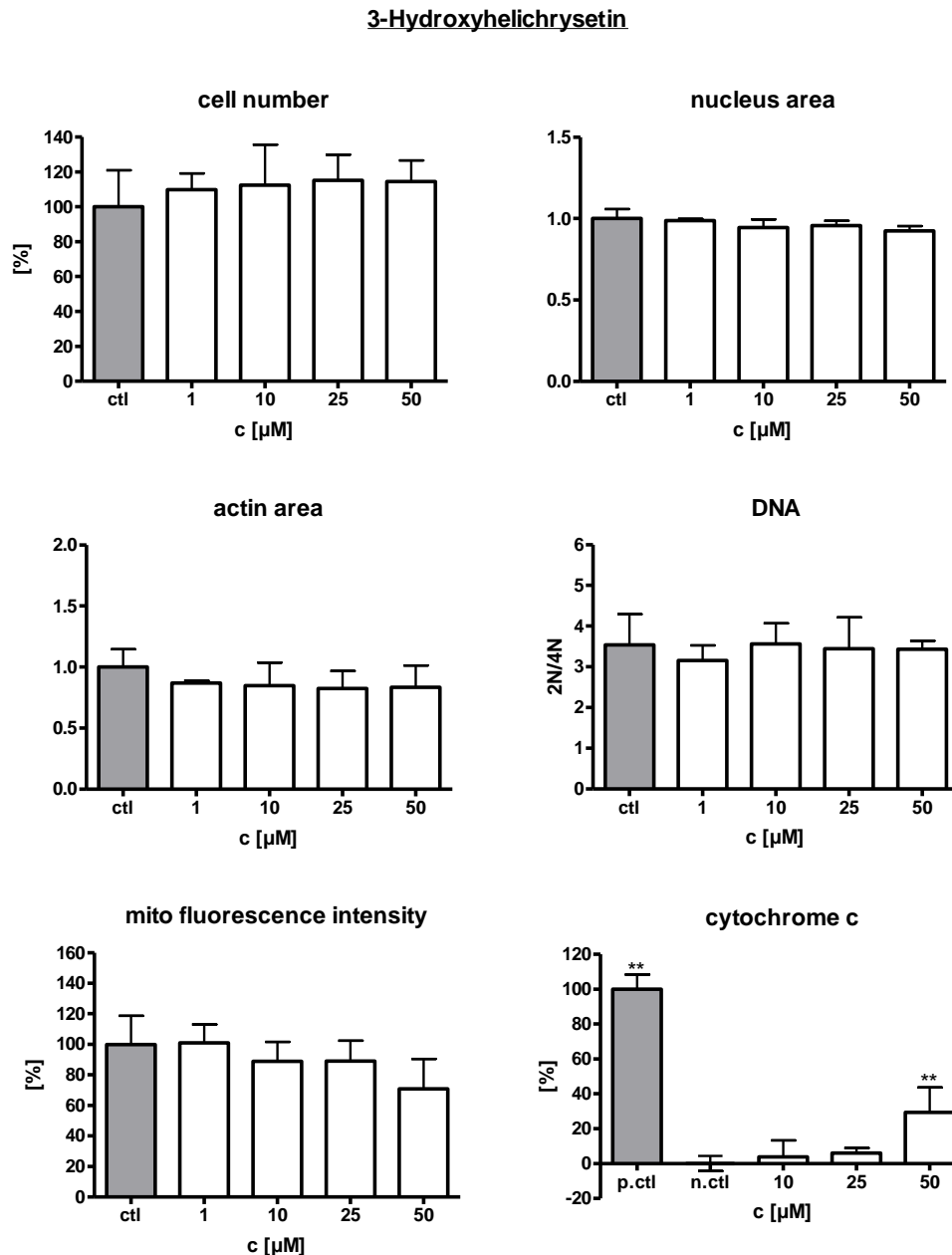


Figure 10.9: Supplementary HCA data of 3-hydroxyhelichrysetin (3OHHeli) (1-50 μM). Cell number [%], nucleus area, actin area, and mitochondrial fluorescence intensity [%] were determined by fluorescence microscopy (see chapter 2.2.6.1). Cytochrome c release [%] was analyzed by fluorescence microscopy (see chapter 2.2.6.2). Hoechst33342 staining of cell nuclei was used to determine the DNA content (see chapter 2.2.6.3) and to calculate the ratio 2N/4N. Values are presented as mean ± SD and refer to untreated control cells (ctl/n.ctl). Statistical analysis (one-way ANOVA following Dunnett's multi-comparison post-hoc test) was performed using GraphPad Prism 4 software. Levels of significance *p < 0.05, **p < 0.01 vs ctl/n.ctl.

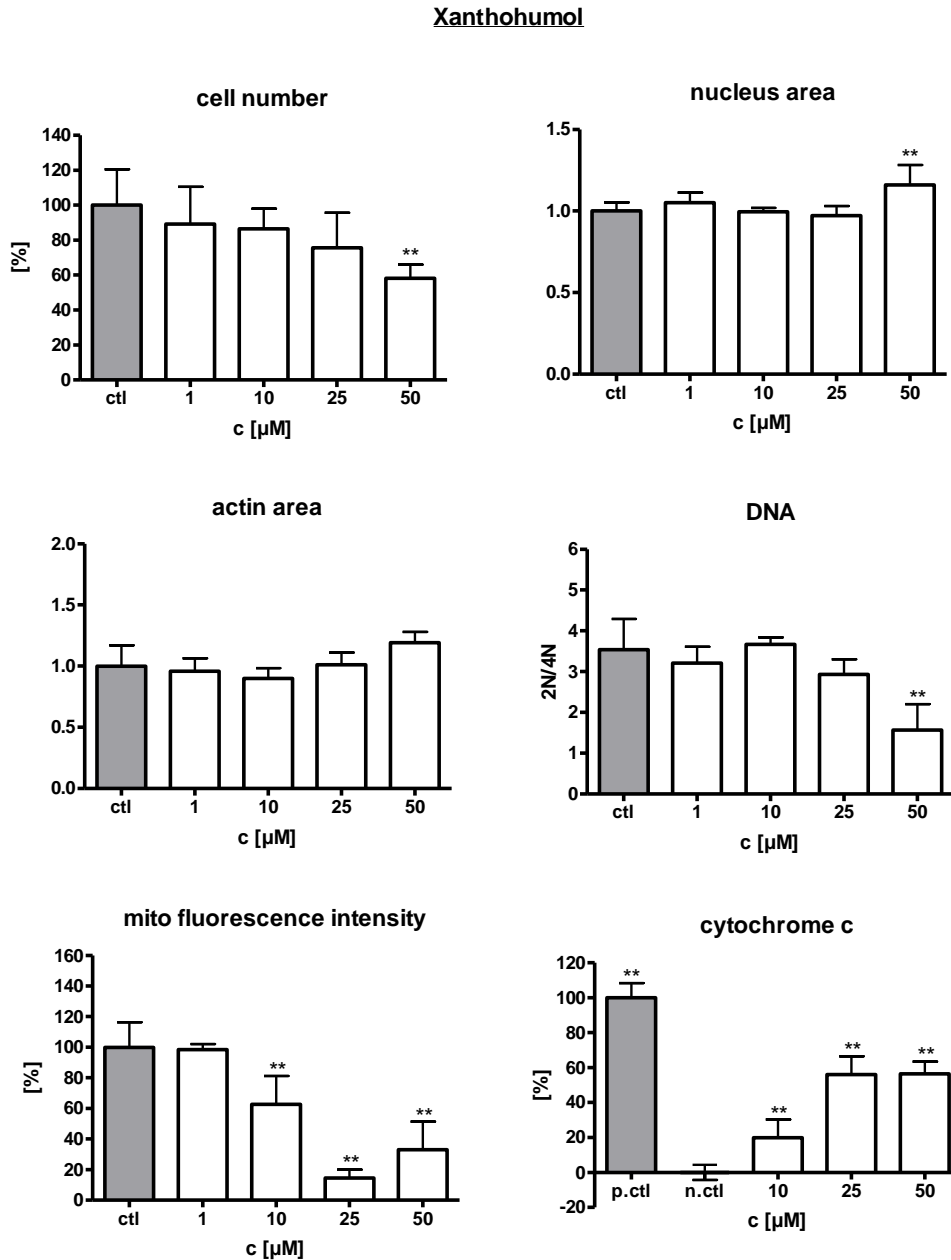


Figure 10.10: Supplementary HCA data of xanthohumol (XAN) (1-50 μM). Cell number [%], nucleus area, actin area, and mitochondrial fluorescence intensity [%] were determined by fluorescence microscopy (see chapter 2.2.6.1). Cytochrome c release [%] was analyzed by fluorescence microscopy (see chapter 2.2.6.2). Hoechst33342 staining of cell nuclei was used to determine the DNA content (see chapter 2.2.6.3) and to calculate the ratio 2N/4N. Values are presented as mean ± SD and refer to untreated control cells (ctl/n.ctl). Statistical analysis (one-way ANOVA following Dunnett's multi-comparison post-hoc test) was performed using GraphPad Prism 4 software. Levels of significance *p < 0.05, **p < 0.01 vs ctl/n.ctl.

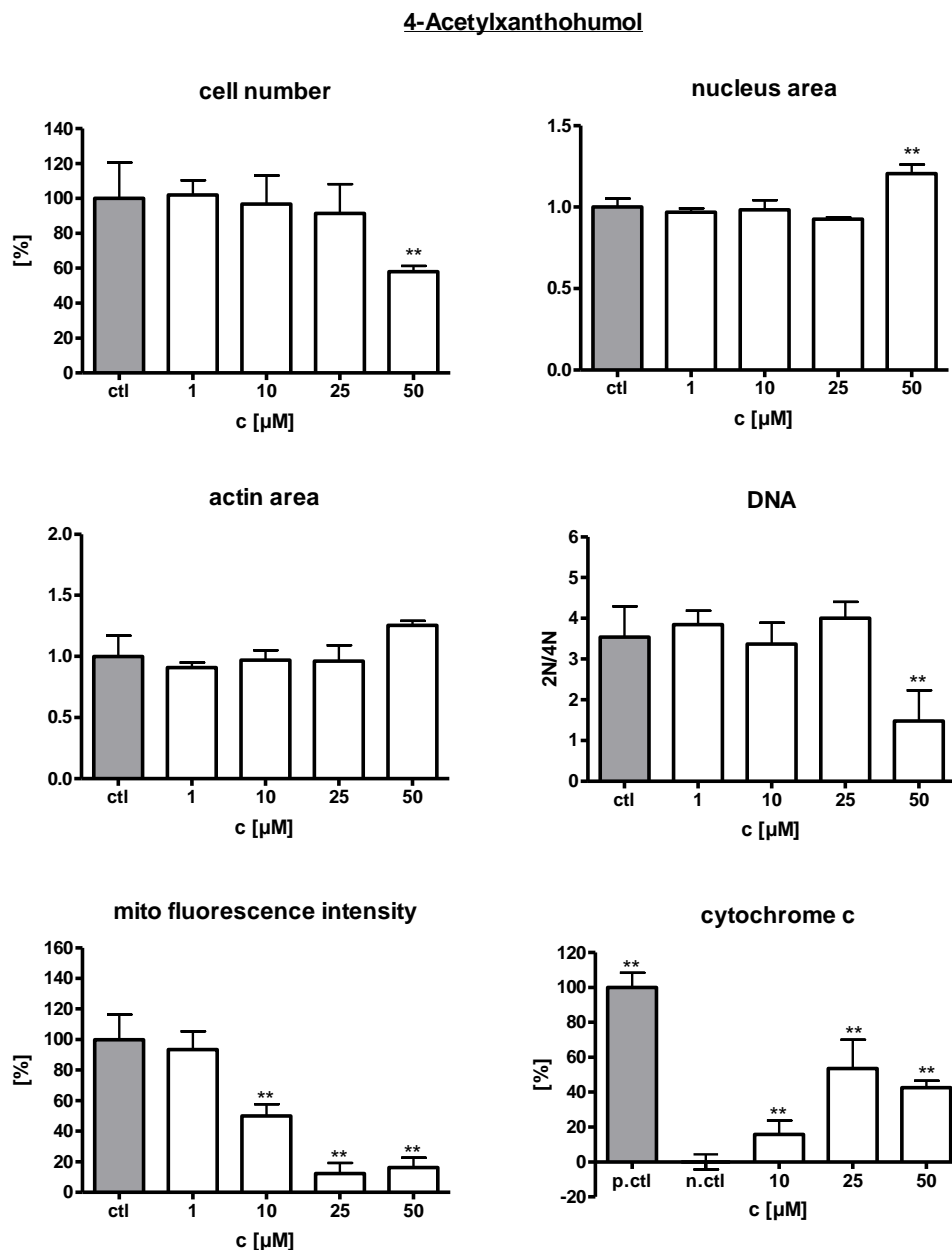


Figure 10.11: Supplementary HCA data of 4-acetyl-xanthohumol (4AcXAN) (1-50 μM). Cell number [%], nucleus area, actin area, and mitochondrial fluorescence intensity [%] were determined by fluorescence microscopy (see chapter 2.2.6.1). Cytochrome c release [%] was analyzed by fluorescence microscopy (see chapter 2.2.6.2). Hoechst33342 staining of cell nuclei was used to determine the DNA content (see chapter 2.2.6.3) and to calculate the ratio 2N/4N. Values are presented as mean ± SD and refer to untreated control cells (ctl/n.ctl). Statistical analysis (one-way ANOVA following Dunnett's multi-comparison post-hoc test) was performed using GraphPad Prism 4 software. Levels of significance *p < 0.05, **p < 0.01 vs ctl/n.ctl.

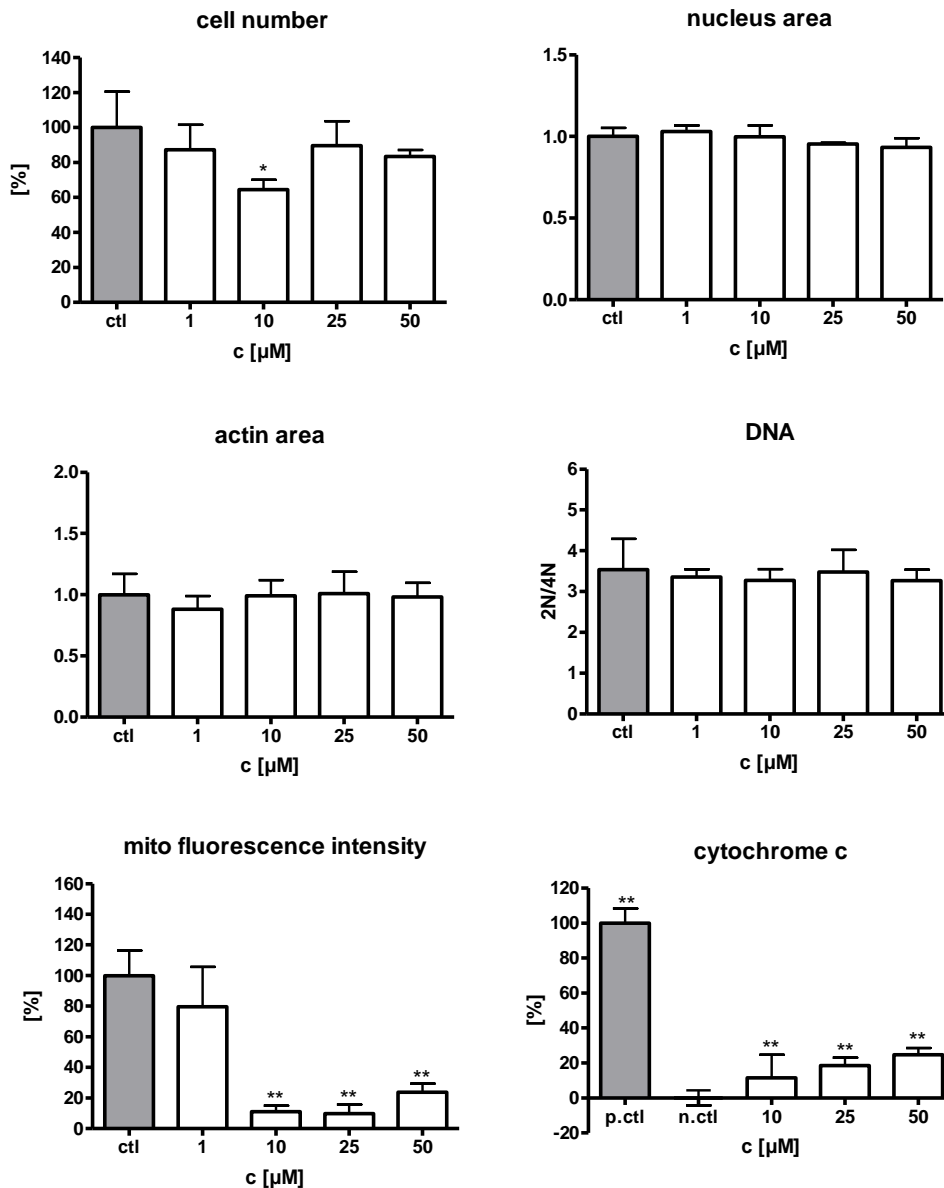
4-Methylxanthohumol

Figure 10.12: Supplementary HCA data of 4-methylxanthohumol (4MeXAN) (1-50 μM). Cell number [%], nucleus area, actin area, and mitochondrial fluorescence intensity [%] were determined by fluorescence microscopy (see chapter 2.2.6.1). Cytochrome c release [%] was analyzed by fluorescence microscopy (see chapter 2.2.6.2). Hoechst33342 staining of cell nuclei was used to determine the DNA content (see chapter 2.2.6.3) and to calculate the ratio 2N/4N. Values are presented as mean ± SD and refer to untreated control cells (ctl/n.ctl). Statistical analysis (one-way ANOVA following Dunnett's multi-comparison post-hoc test) was performed using GraphPad Prism 4 software. Levels of significance *p < 0.05, **p < 0.01 vs ctl/n.ctl.

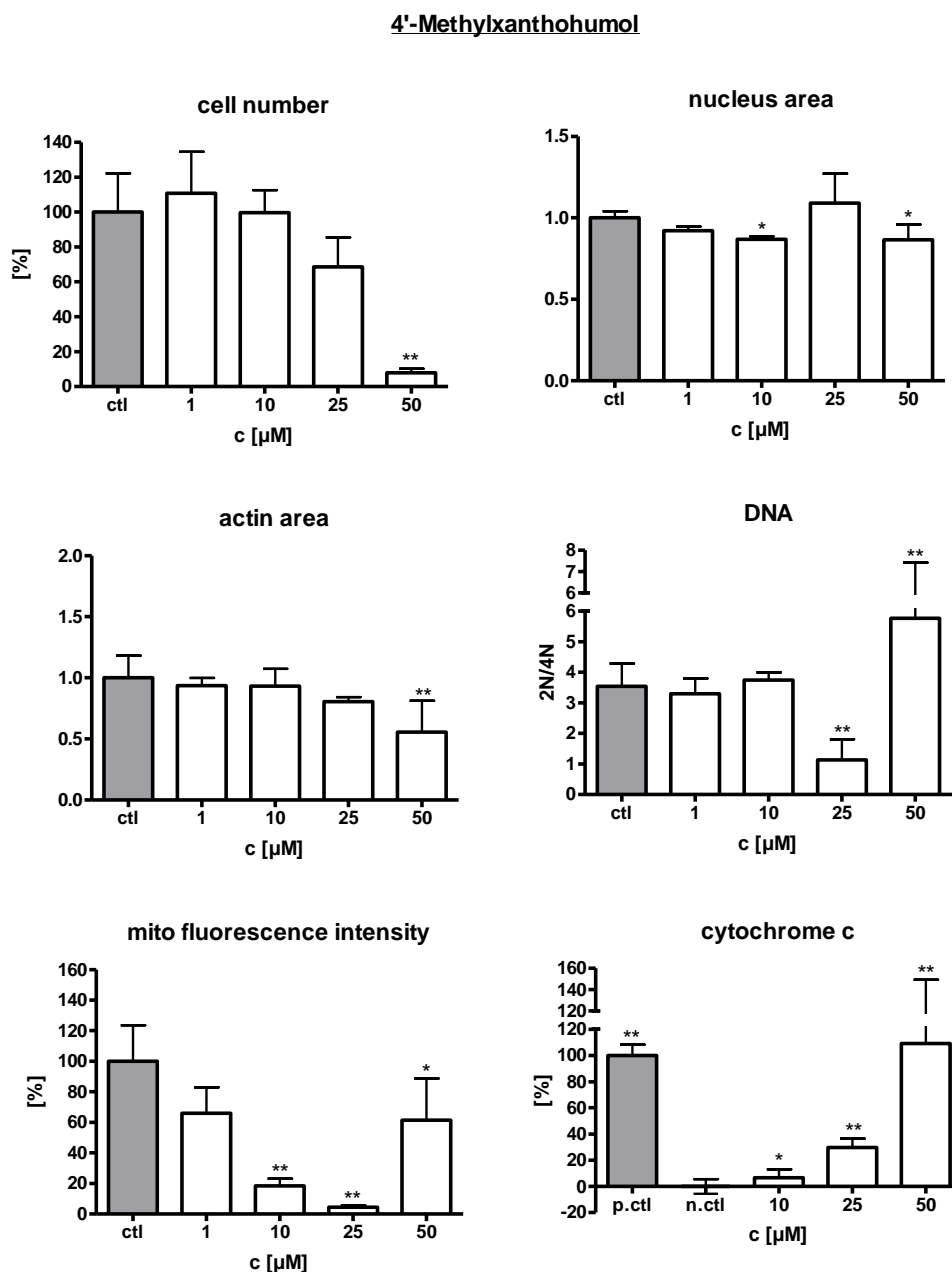


Figure 10.13: Supplementary HCA data of 4'-methylxanthohumol (4'MeXAN) (1-50 μM). Cell number [%], nucleus area, actin area, and mitochondrial fluorescence intensity [%] were determined by fluorescence microscopy (see chapter 2.2.6.1). Cytochrome c release [%] was analyzed by fluorescence microscopy (see chapter 2.2.6.2). Hoechst33342 staining of cell nuclei was used to determine the DNA content (see chapter 2.2.6.3) and to calculate the ratio 2N/4N. Values are presented as mean ± SD and refer to untreated control cells (ctl/n.ctl). Statistical analysis (one-way ANOVA following Dunnett's multi-comparison post-hoc test) was performed using GraphPad Prism 4 software. Levels of significance *p < 0.05, **p < 0.01 vs ctl/n.ctl.

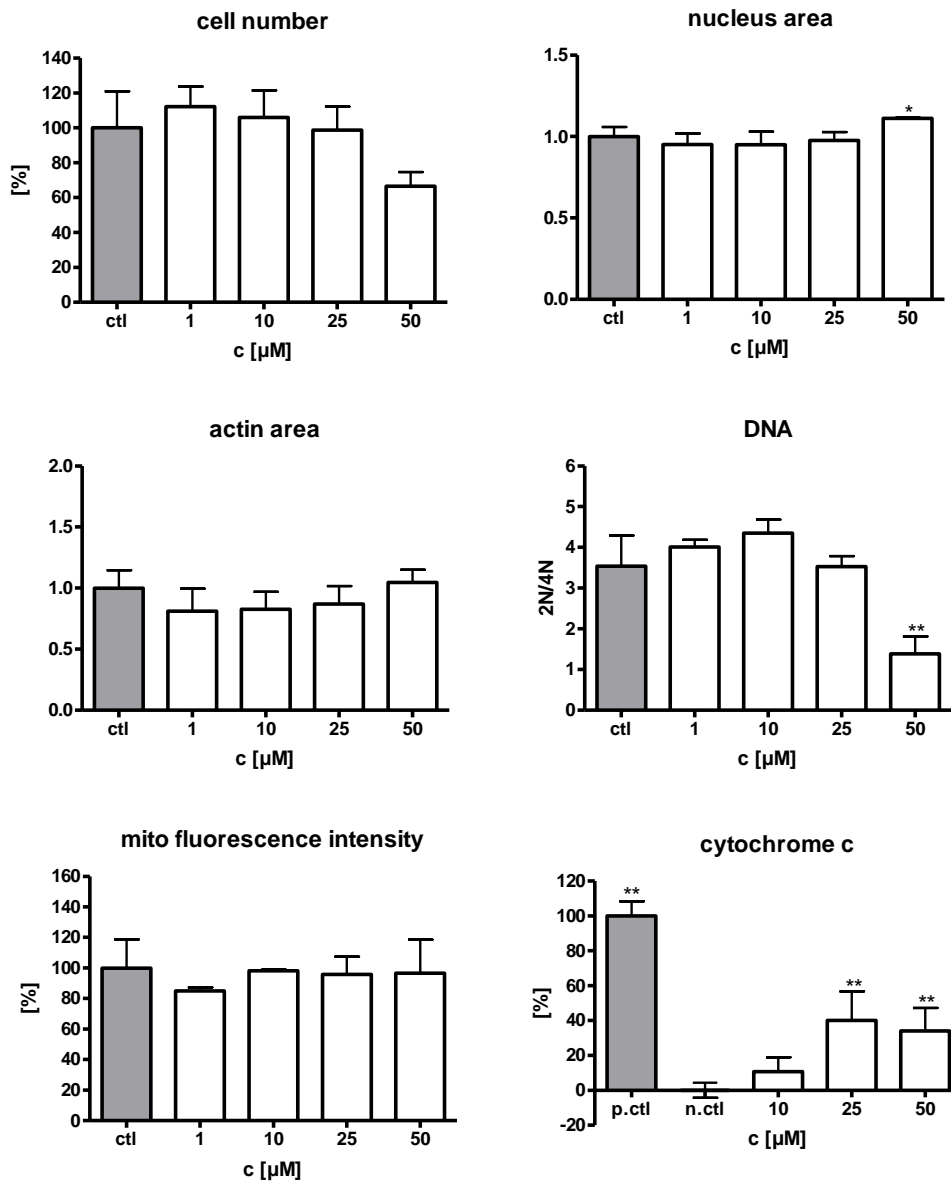
Xanthohumol H

Figure 10.14: Supplementary HCA data of xanthohumol H (XANH) (1-50 μM). Cell number [%], nucleus area, actin area, and mitochondrial fluorescence intensity [%] were determined by fluorescence microscopy (see chapter 2.2.6.1). Cytochrome c release [%] was analyzed by fluorescence microscopy (see chapter 2.2.6.2). Hoechst33342 staining of cell nuclei was used to determine the DNA content (see chapter 2.2.6.3) and to calculate the ratio 2N/4N. Values are presented as mean \pm SD and refer to untreated control cells (ctl/n.ctl). Statistical analysis (one-way ANOVA following Dunnett's multi-comparison post-hoc test) was performed using GraphPad Prism 4 software. Levels of significance * $p < 0.05$, ** $p < 0.01$ vs ctl/n.ctl.

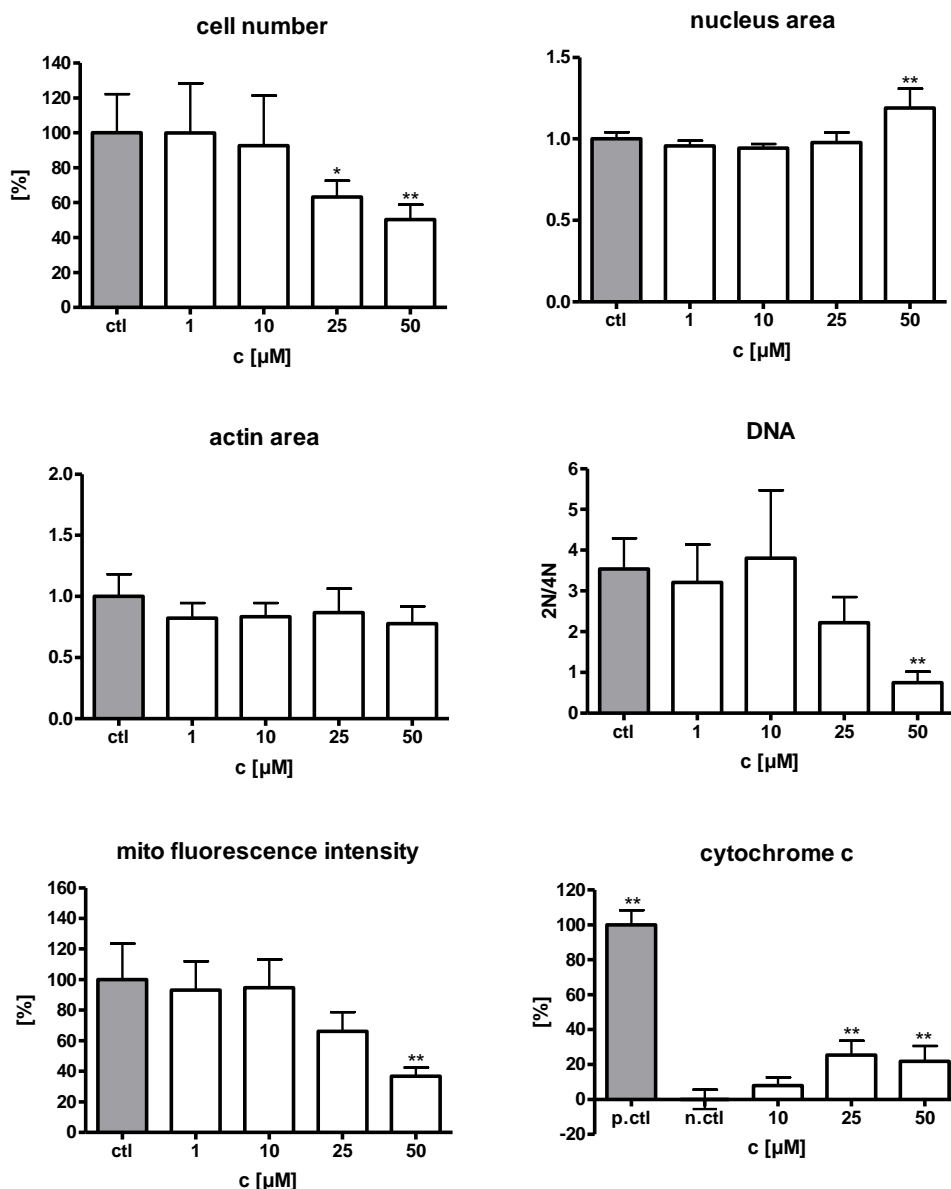
3-Hydroxyxanthohumol H

Figure 10.15: Supplementary HCA data of 3-hydroxyxanthohumol H (3OHXANH) (1-50 μM). Cell number [%], nucleus area, actin area, and mitochondrial fluorescence intensity [%] were determined by fluorescence microscopy (see chapter 2.2.6.1). Cytochrome c release [%] was analyzed by fluorescence microscopy (see chapter 2.2.6.2). Hoechst33342 staining of cell nuclei was used to determine the DNA content (see chapter 2.2.6.3) and to calculate the ratio 2N/4N. Values are presented as mean ± SD and refer to untreated control cells (ctl/nctl). Statistical analysis (one-way ANOVA following Dunnett's multi-comparison post-hoc test) was performed using GraphPad Prism 4 software. Levels of significance *p < 0.05, **p < 0.01 vs ctl/nctl.

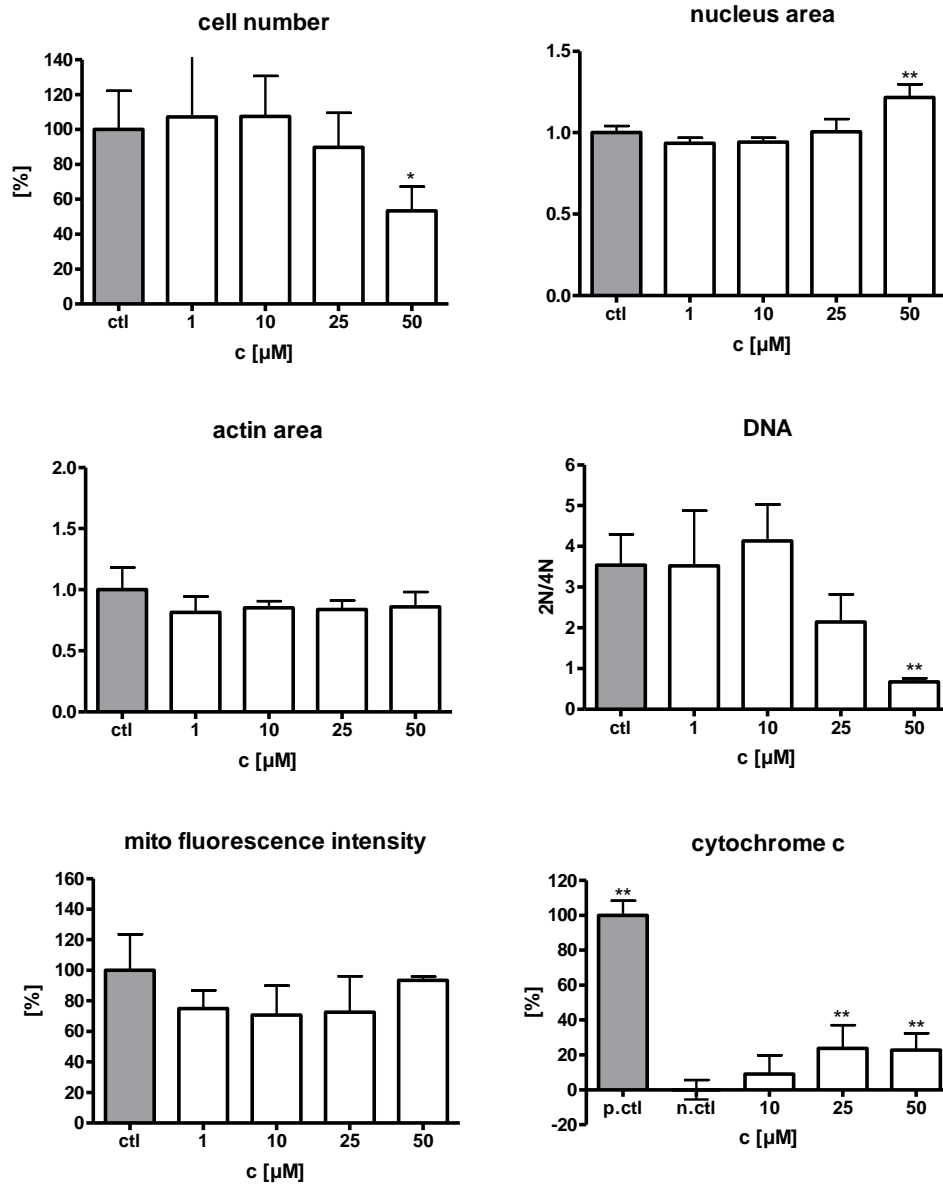
3-Methoxyxanthohumol H

Figure 10.16: Supplementary HCA data of 3-methoxyxanthohumol H (3OMeXANH) (1-50 μM). Cell number [%], nucleus area, actin area, and mitochondrial fluorescence intensity [%] were determined by fluorescence microscopy (see chapter 2.2.6.1). Cytochrome c release [%] was analyzed by fluorescence microscopy (see chapter 2.2.6.2). Hoechst33342 staining of cell nuclei was used to determine the DNA content (see chapter 2.2.6.3) and to calculate the ratio 2N/4N. Values are presented as mean ± SD and refer to untreated control cells (ctl/n.ctl). Statistical analysis (one-way ANOVA following Dunnett's multi-comparison post-hoc test) was performed using GraphPad Prism 4 software. Levels of significance *p < 0.05, **p < 0.01 vs ctl/n.ctl.

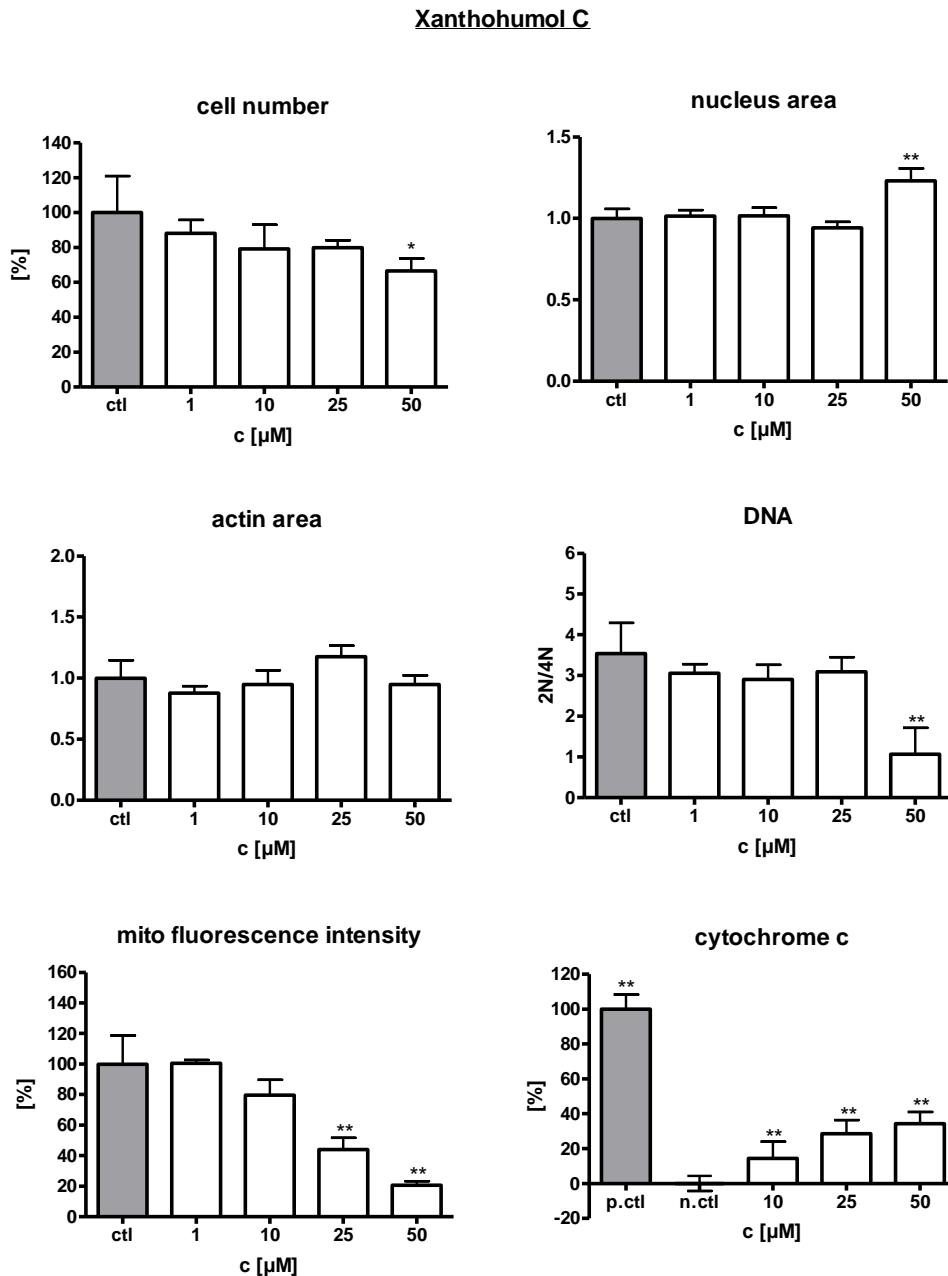


Figure 10.17: Supplementary HCA data of xanthohumol C (XANC) (1-50 μM). Cell number [%], nucleus area, actin area, and mitochondrial fluorescence intensity [%] were determined by fluorescence microscopy (see chapter 2.2.6.1). Cytochrome c release [%] was analyzed by fluorescence microscopy (see chapter 2.2.6.2). Hoechst33342 staining of cell nuclei was used to determine the DNA content (see chapter 2.2.6.3) and to calculate the ratio 2N/4N. Values are presented as mean ± SD and refer to untreated control cells (ctl/n.ctl). Statistical analysis (one-way ANOVA following Dunnett's multi-comparison post-hoc test) was performed using GraphPad Prism 4 software. Levels of significance *p < 0.05, **p < 0.01 vs ct/n.ctl.

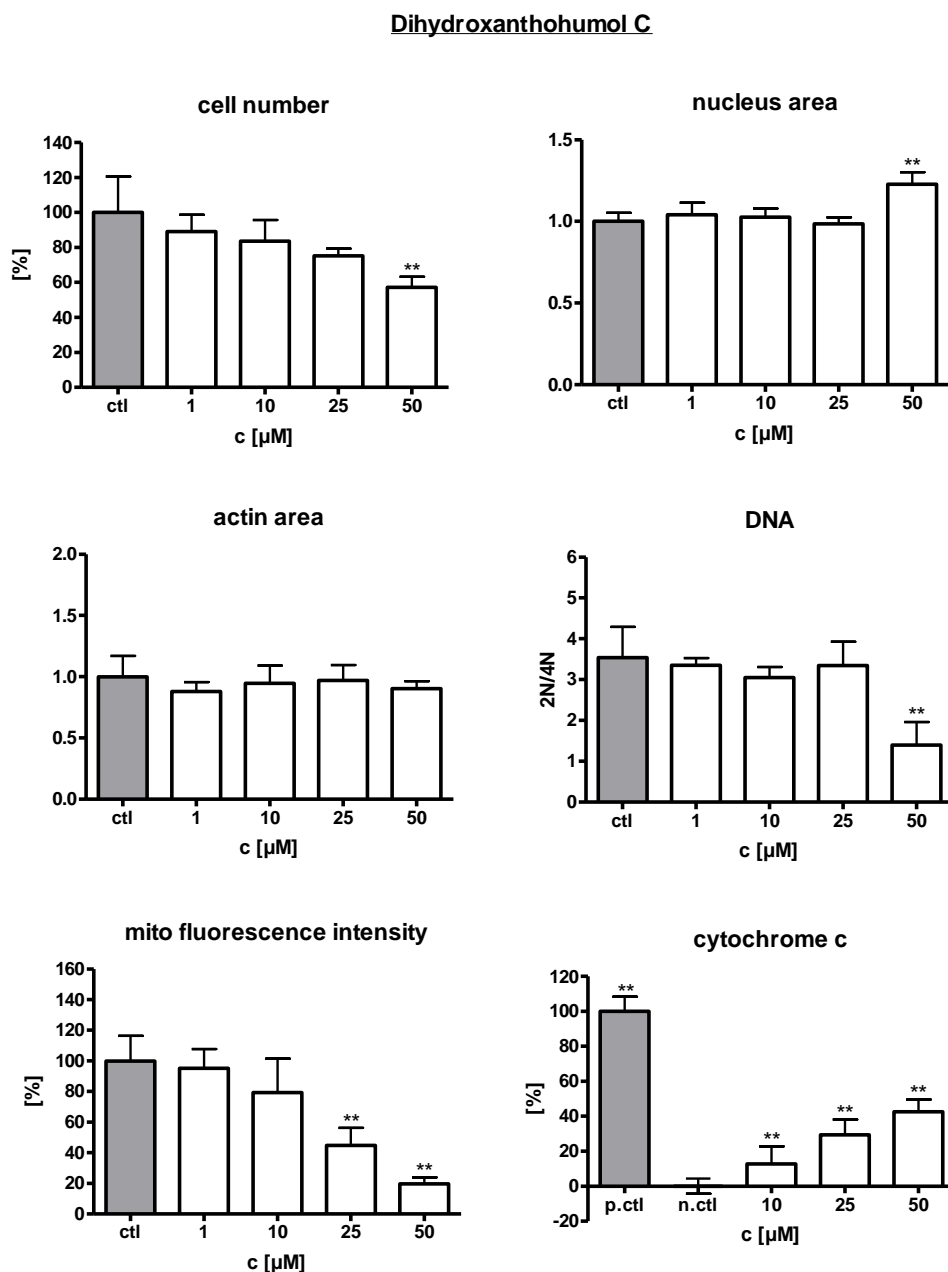


Figure 10.18: Supplementary HCA data of dihydroxanthohumol C (dhXANC) (1-50 μM). Cell number [%], nucleus area, actin area, and mitochondrial fluorescence intensity [%] were determined by fluorescence microscopy (see chapter 2.2.6.1). Cytochrome c release [%] was analyzed by fluorescence microscopy (see chapter 2.2.6.2). Hoechst33342 staining of cell nuclei was used to determine the DNA content (see chapter 2.2.6.3) and to calculate the ratio 2N/4N. Values are presented as mean ± SD and refer to untreated control cells (ctl/n.ctl). Statistical analysis (one-way ANOVA following Dunnett's multi-comparison post-hoc test) was performed using GraphPad Prism 4 software. Levels of significance *p < 0.05, **p < 0.01 vs ctl/n.ctl.

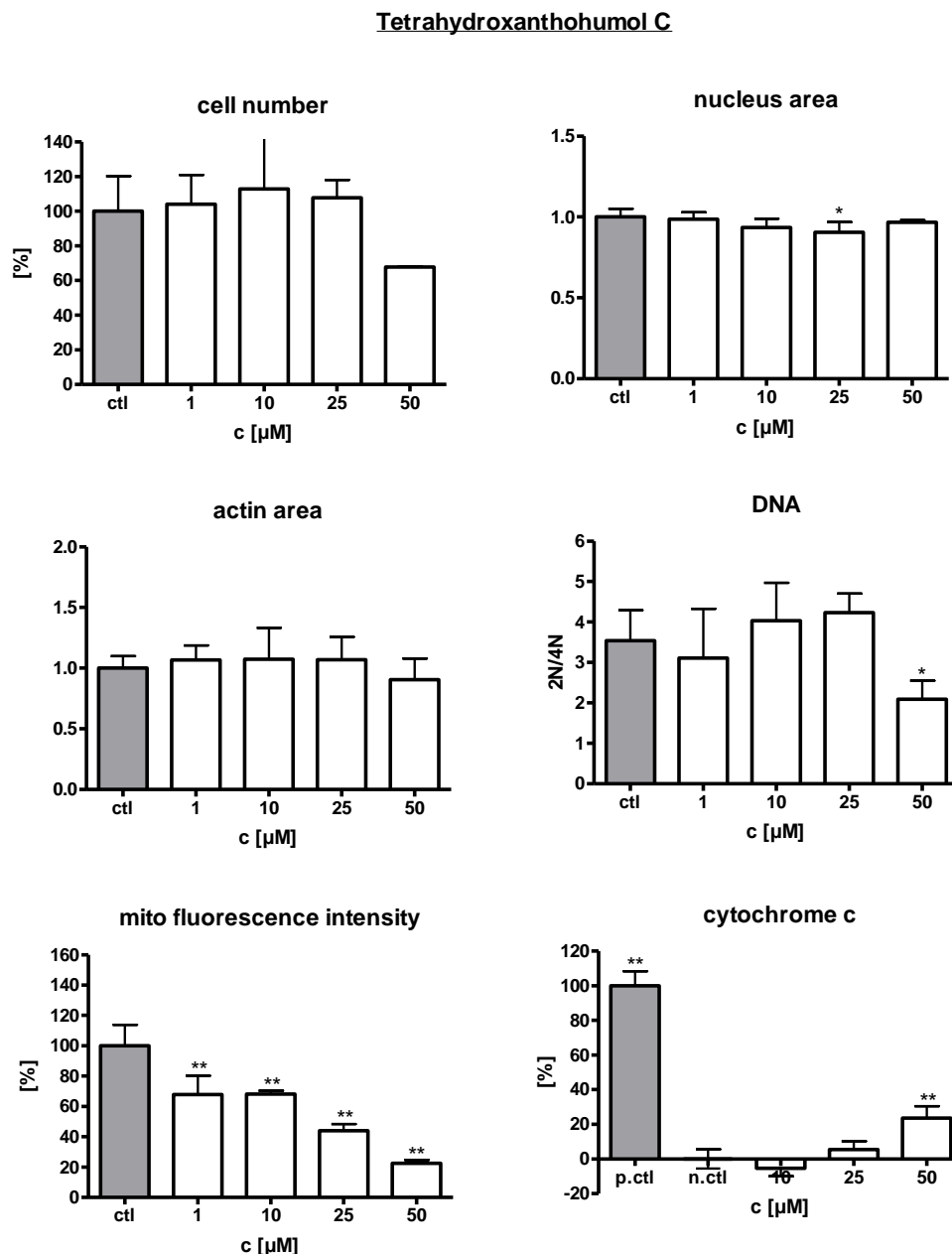
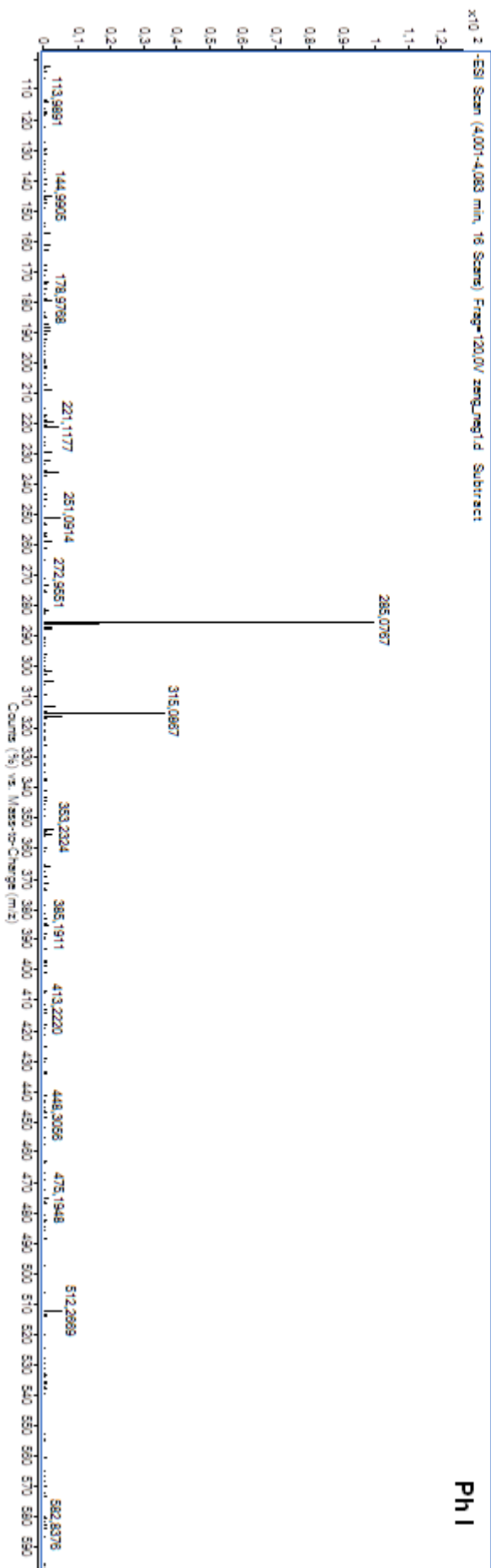
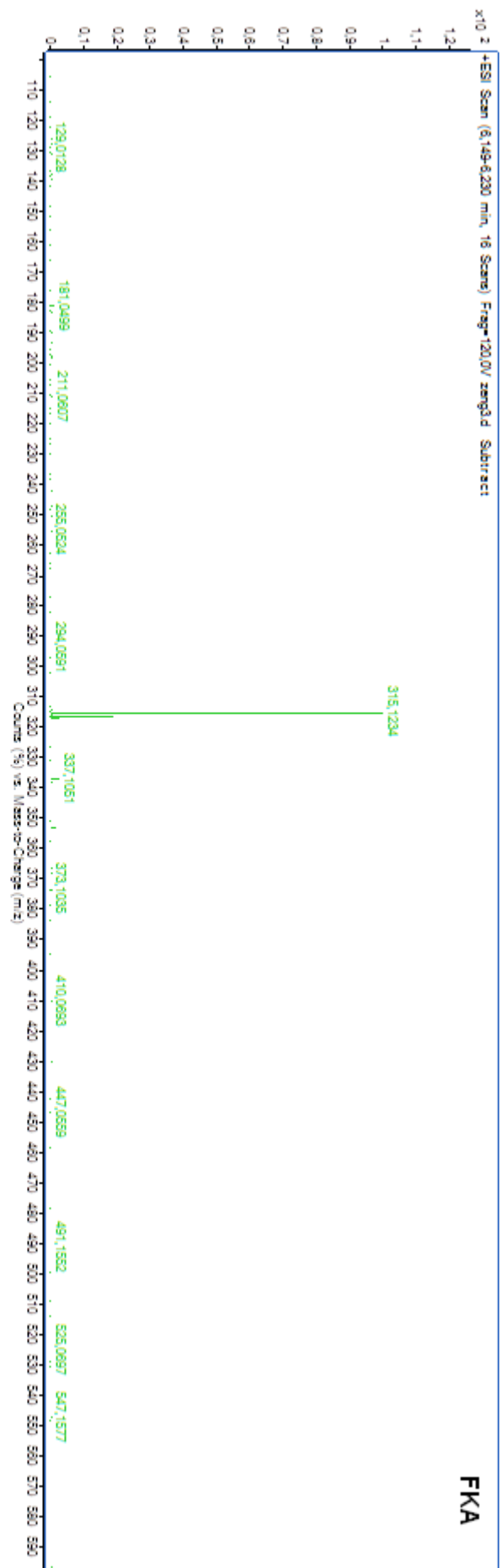
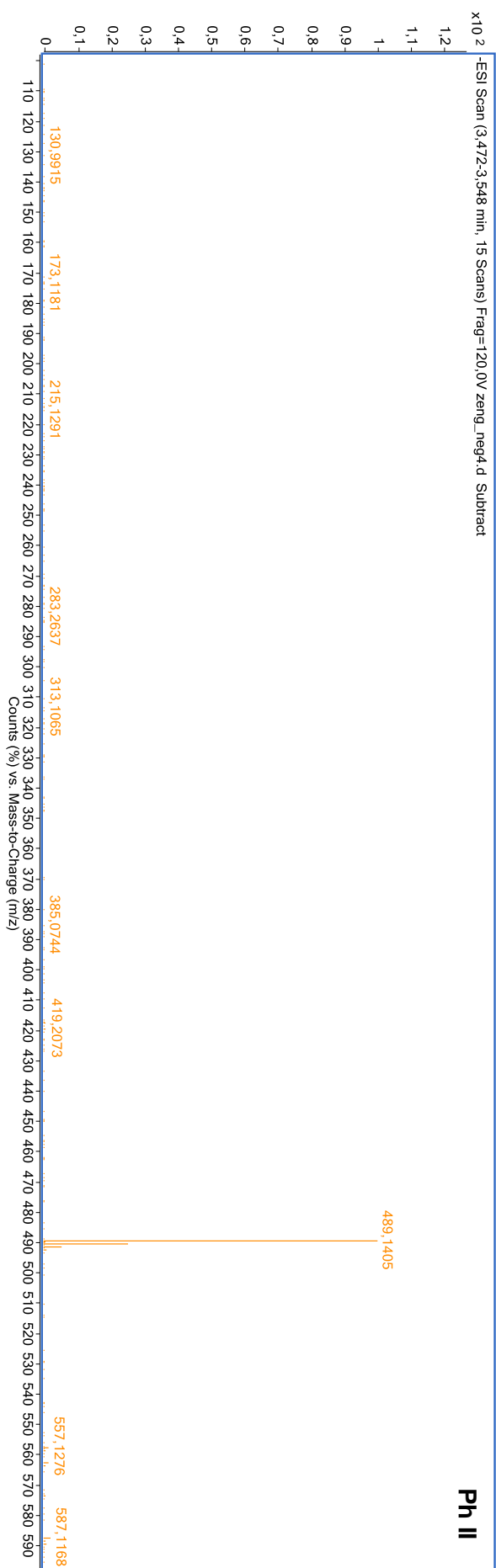
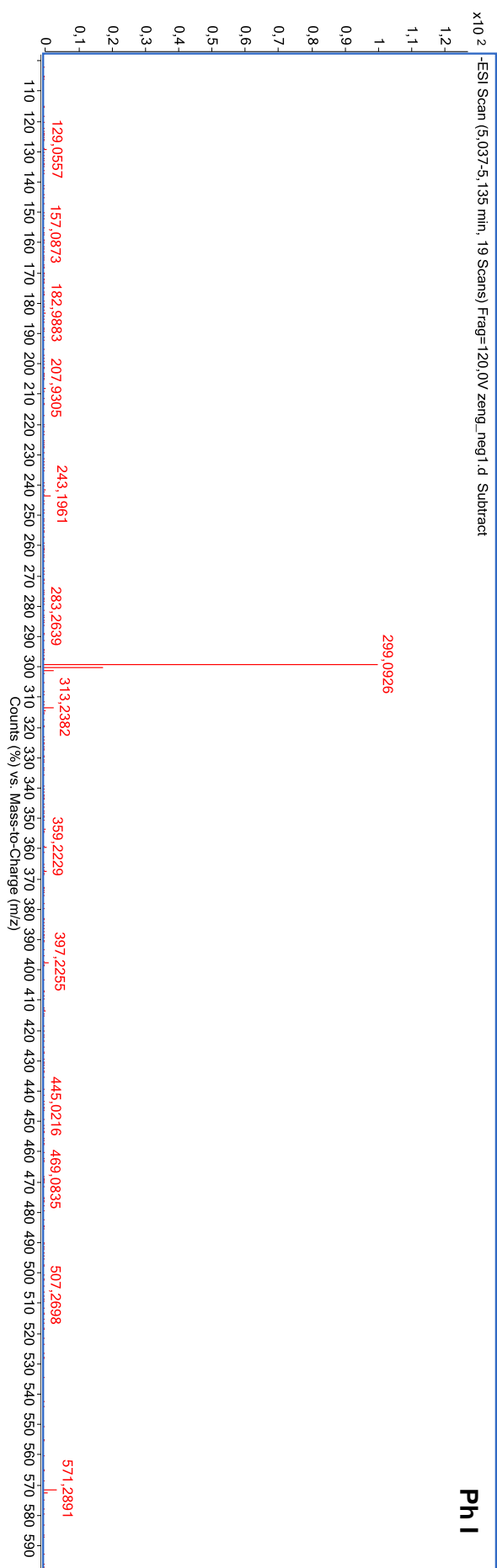
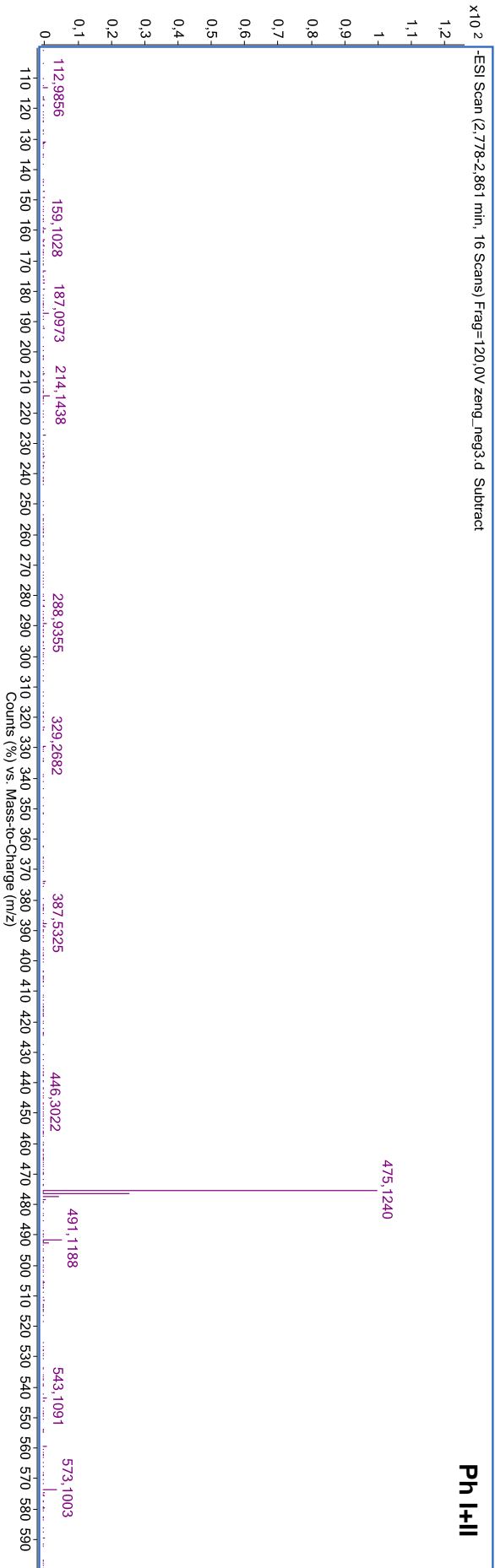
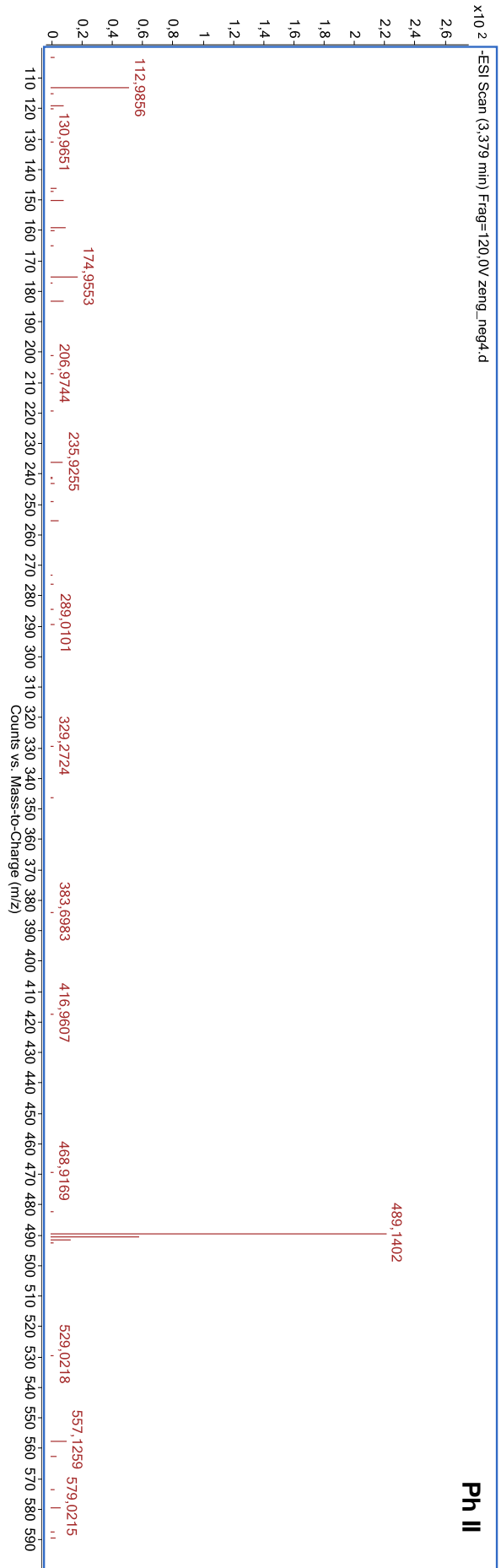


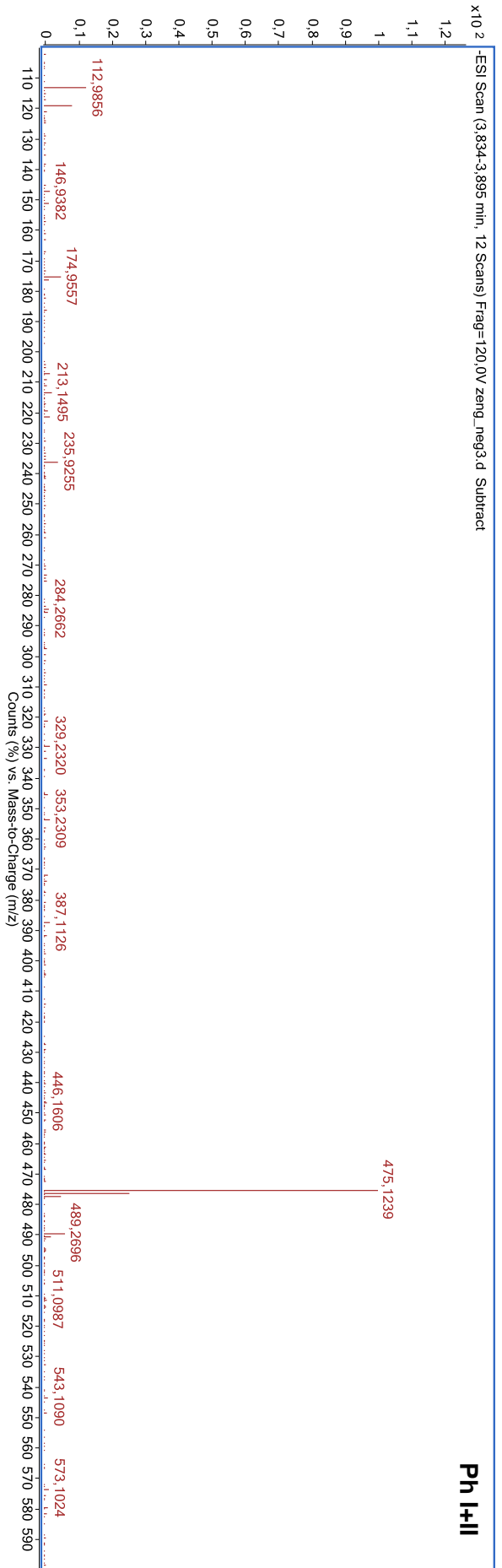
Figure 10.19: Supplementary HCA data of tetrahydroxanthohumol C (thXANC) (1-50 μM). Cell number [%], nucleus area, actin area, and mitochondrial fluorescence intensity [%] were determined by fluorescence microscopy (see chapter 2.2.6.1). Cytochrome c release [%] was analyzed by fluorescence microscopy (see chapter 2.2.6.2). Hoechst33342 staining of cell nuclei was used to determine the DNA content (see chapter 2.2.6.3) and to calculate the ratio 2N/4N. Values are presented as mean ± SD and refer to untreated control cells (ctl/n.ctl). Statistical analysis (one-way ANOVA following Dunnett's multi-comparison post-hoc test) was performed using GraphPad Prism 4 software. Levels of significance *p < 0.05, **p < 0.01 vs ctl/n.ctl.

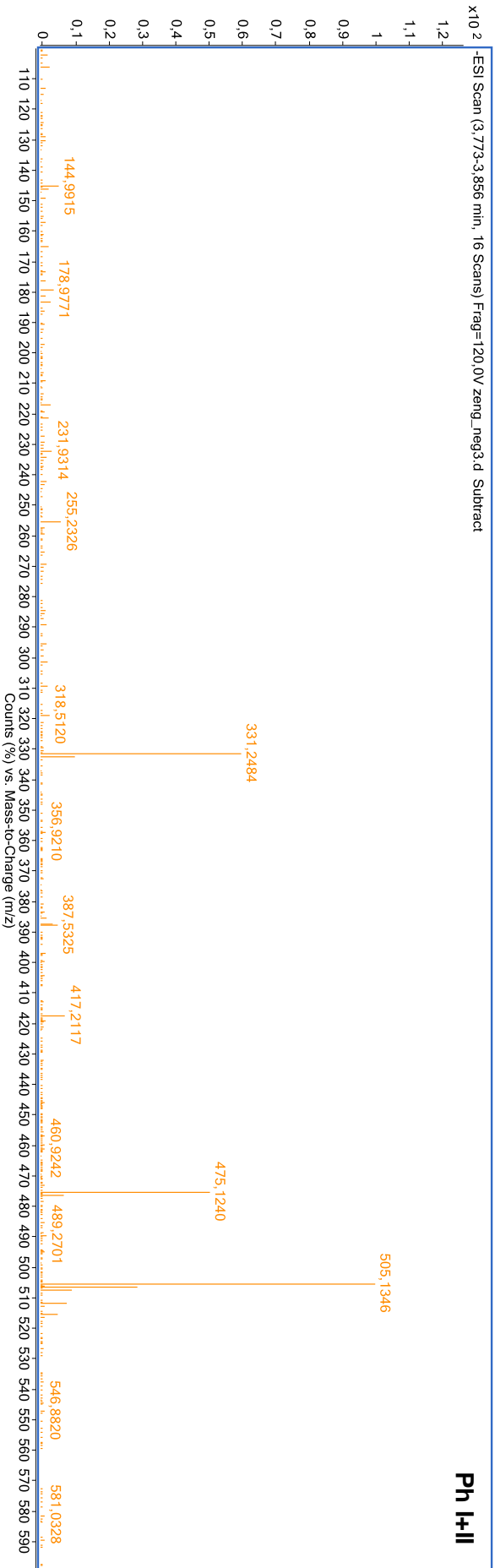
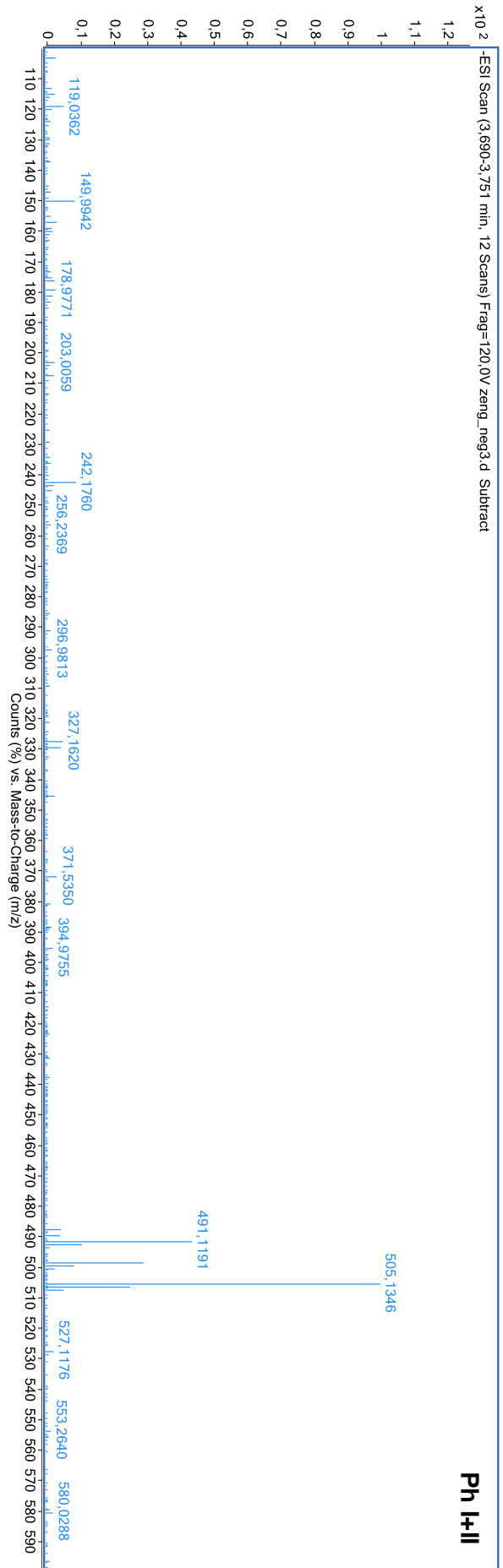
10.2 Mass spectra of chalcone metabolites











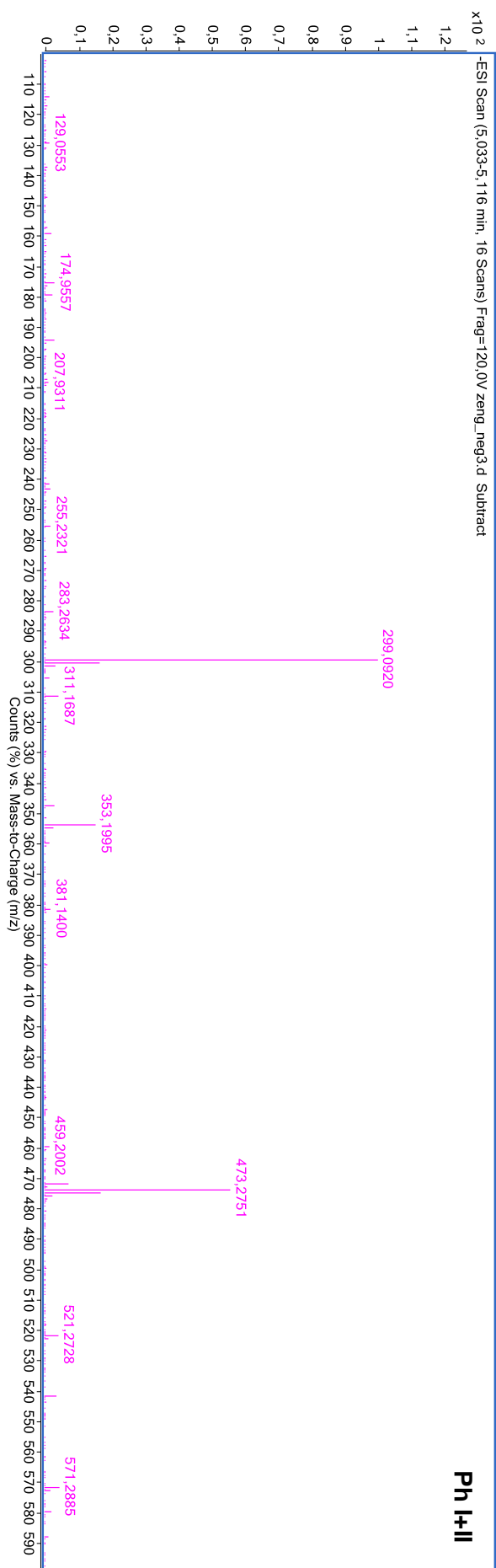
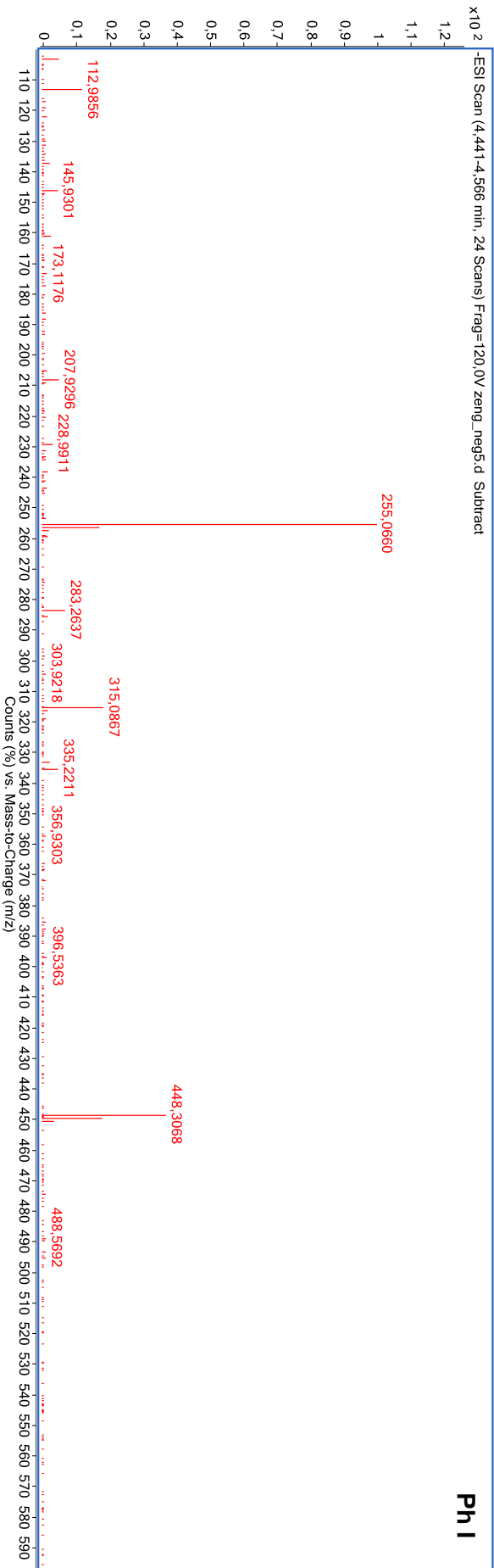
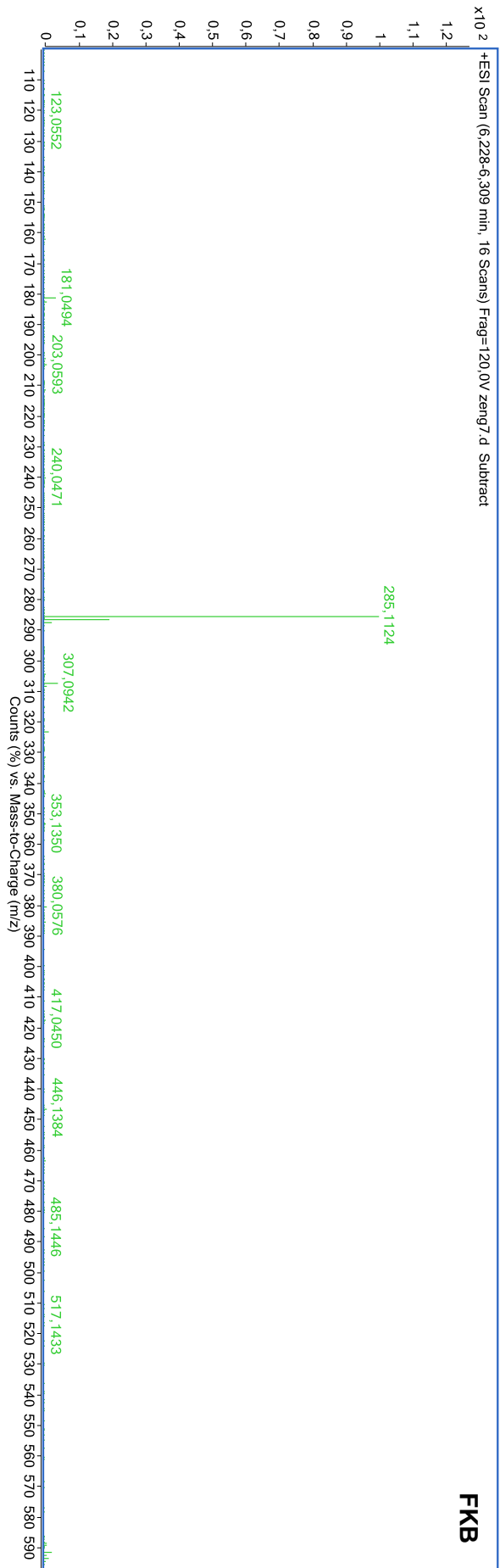
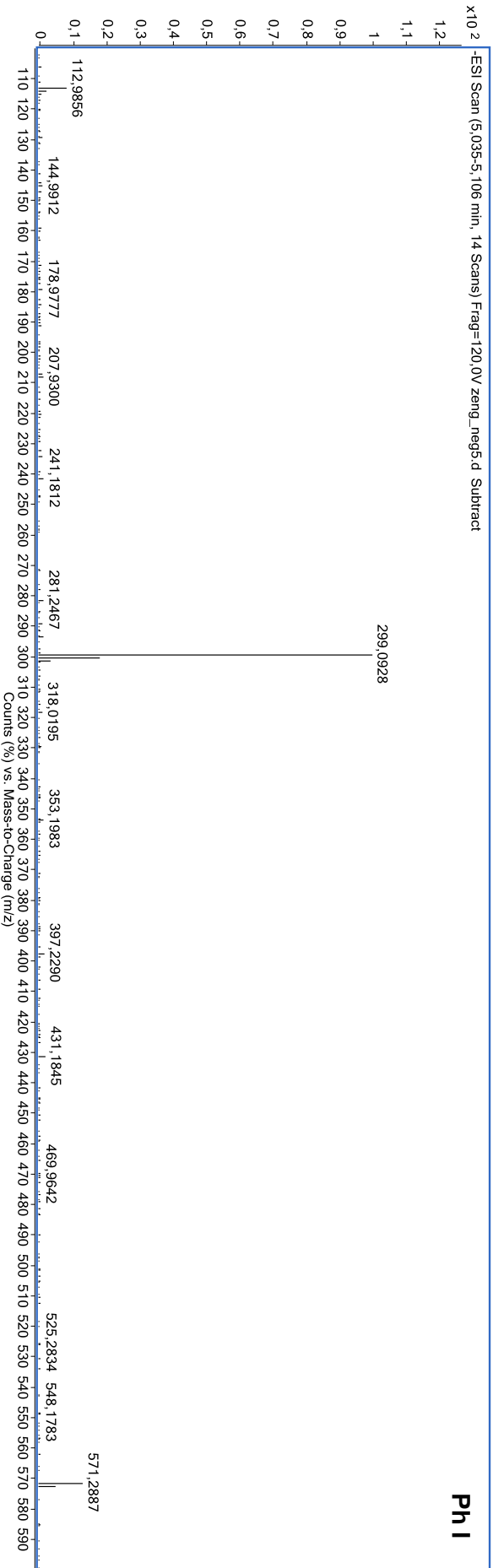
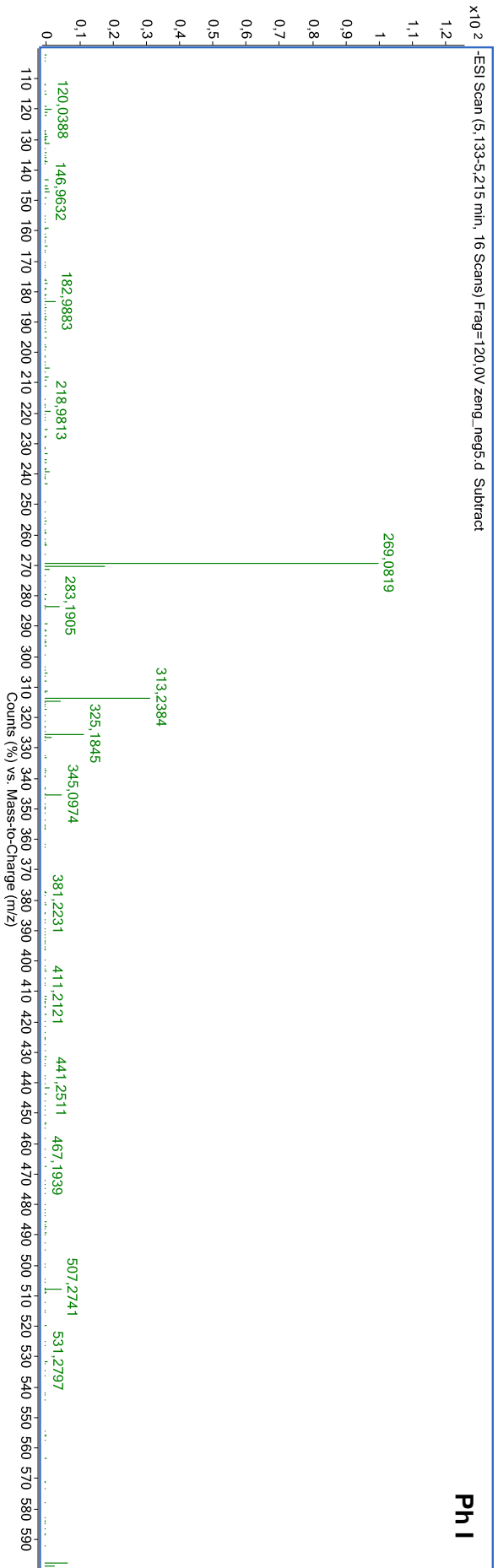
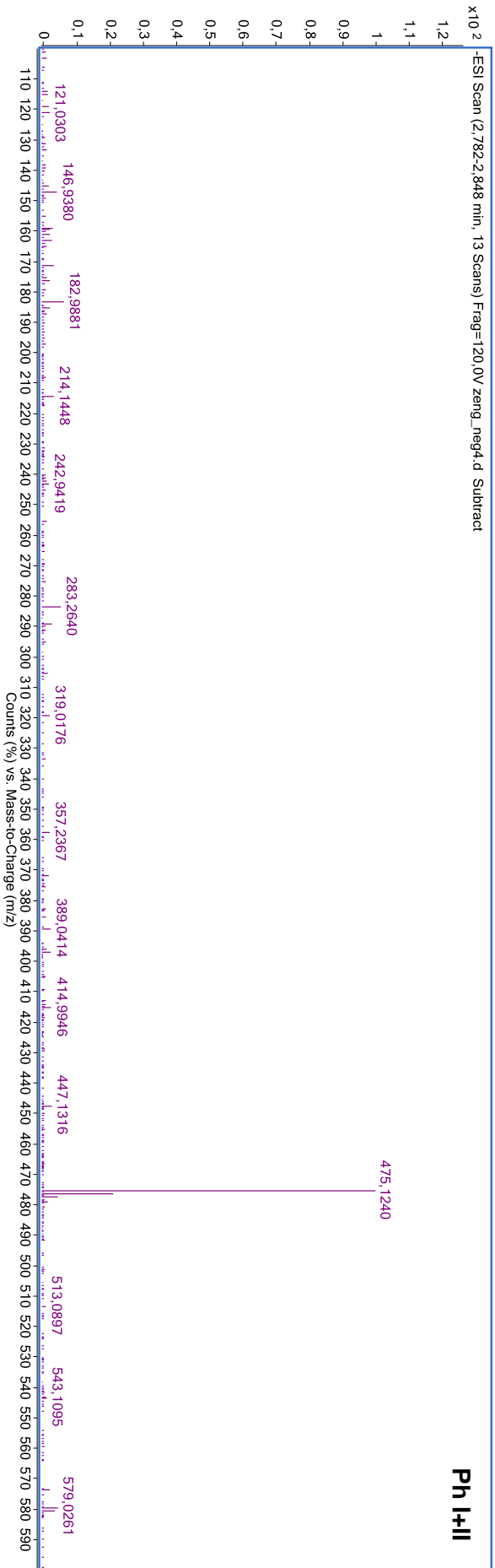
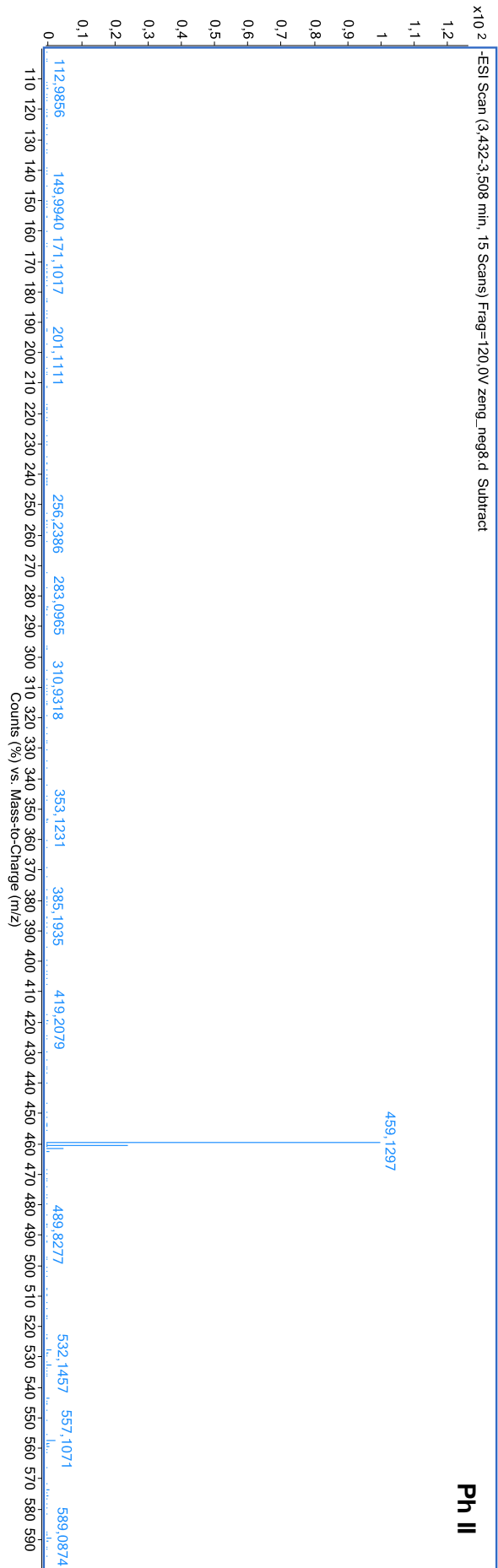
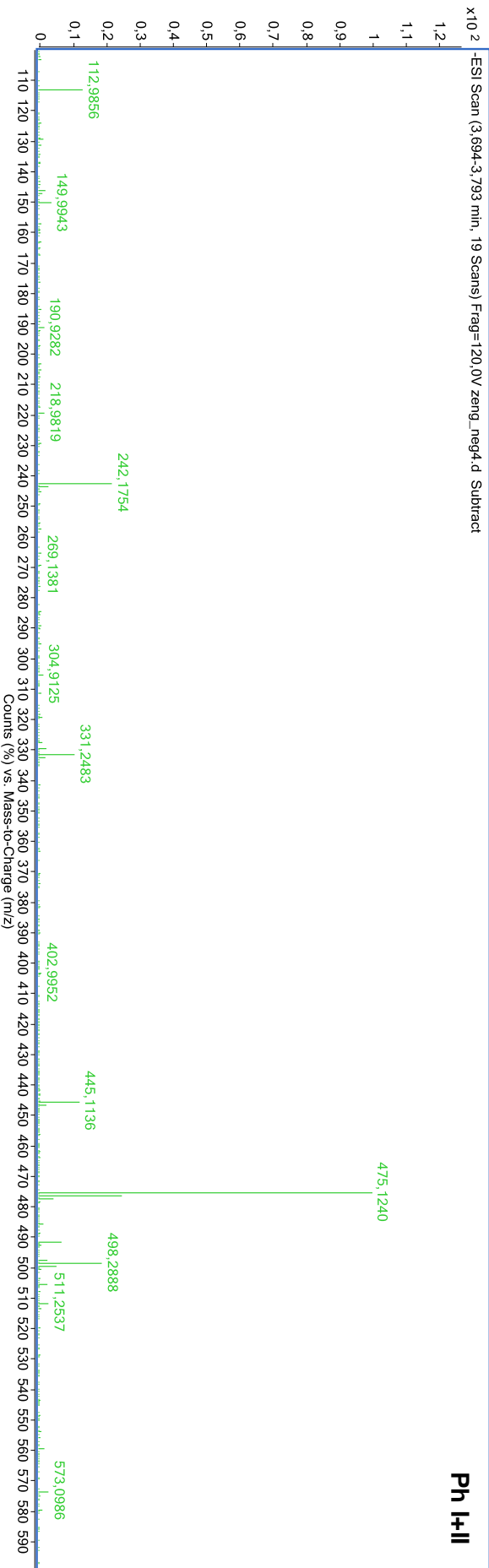
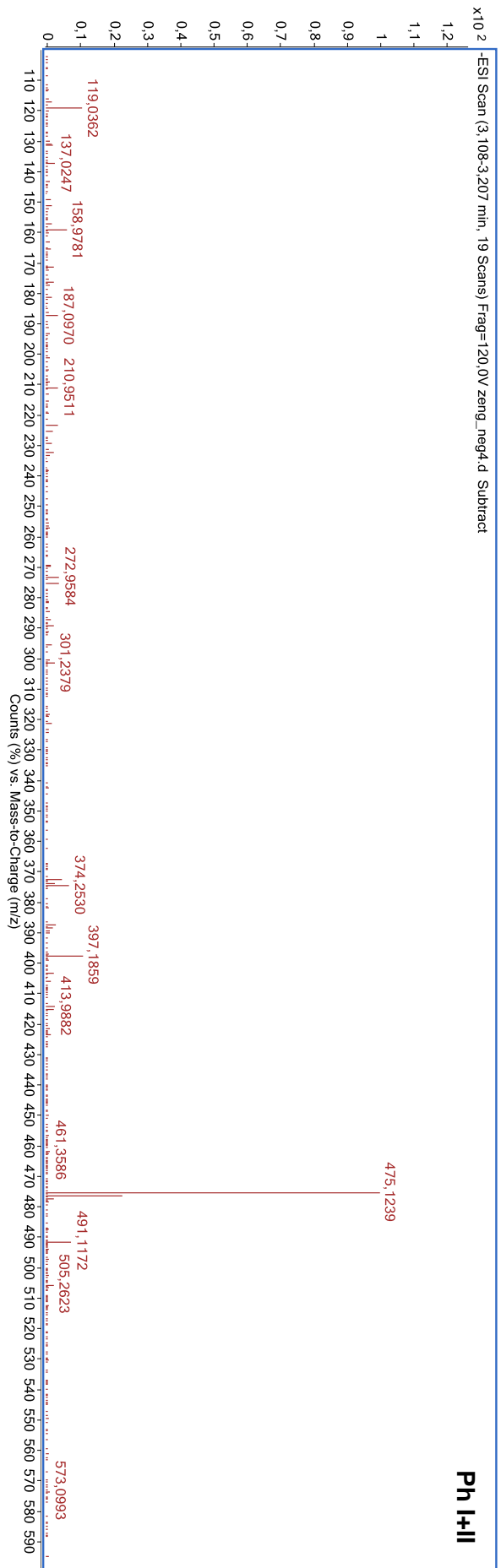


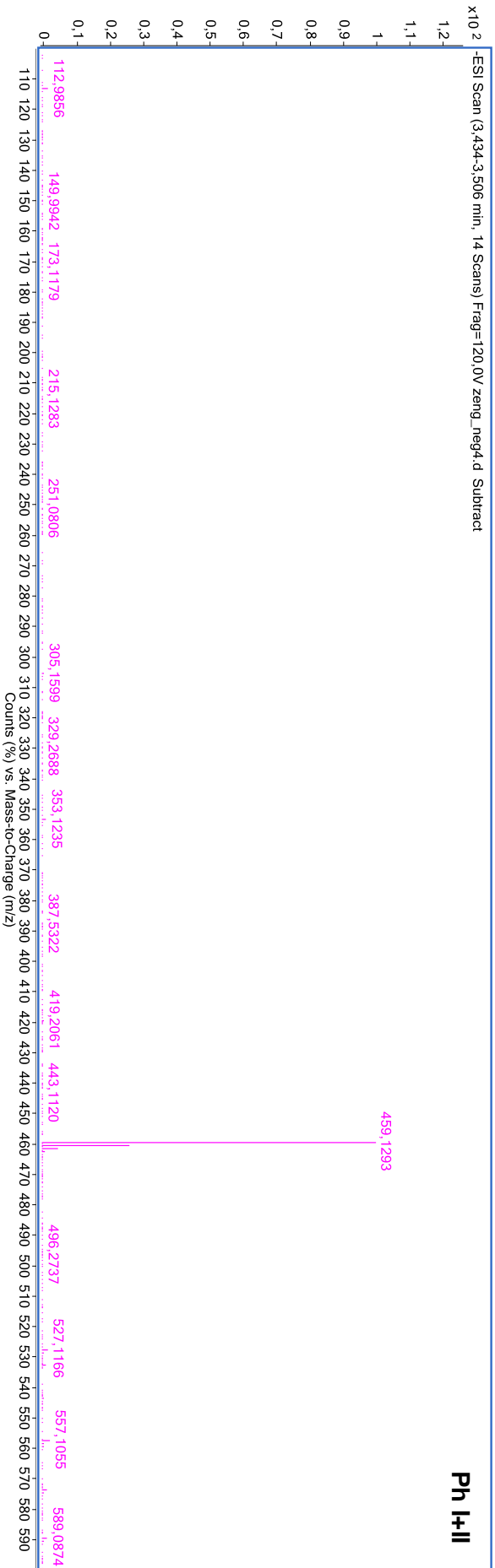
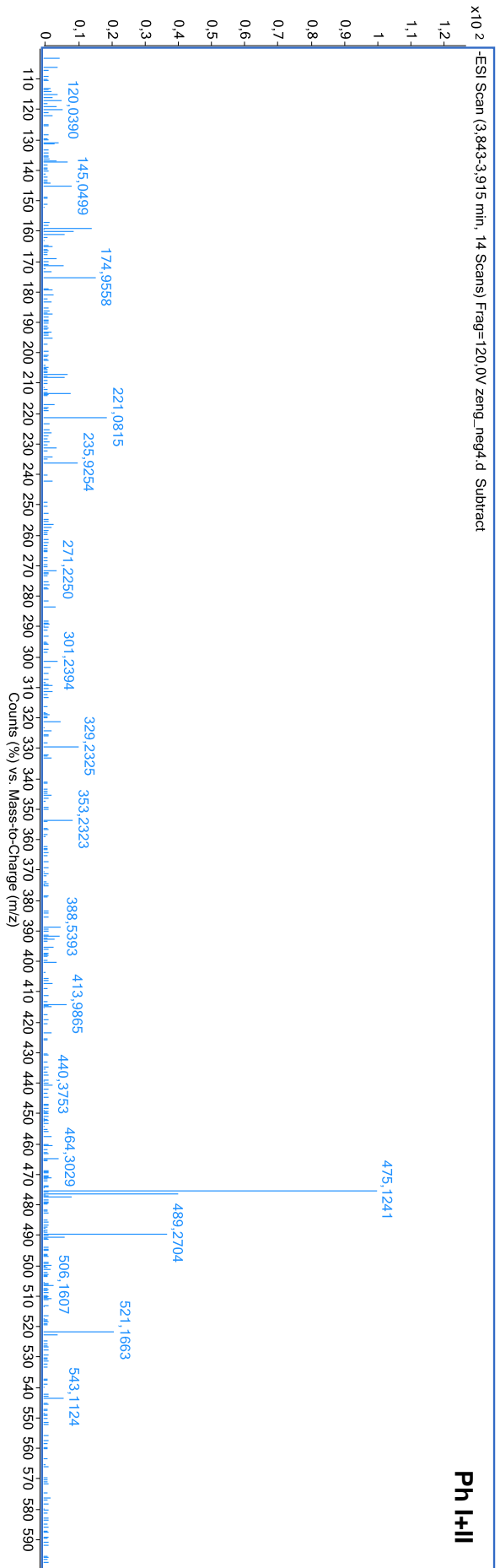
Figure 10.20: Mass spectra of FKA and FKA metabolites corresponding to Table 5.4.











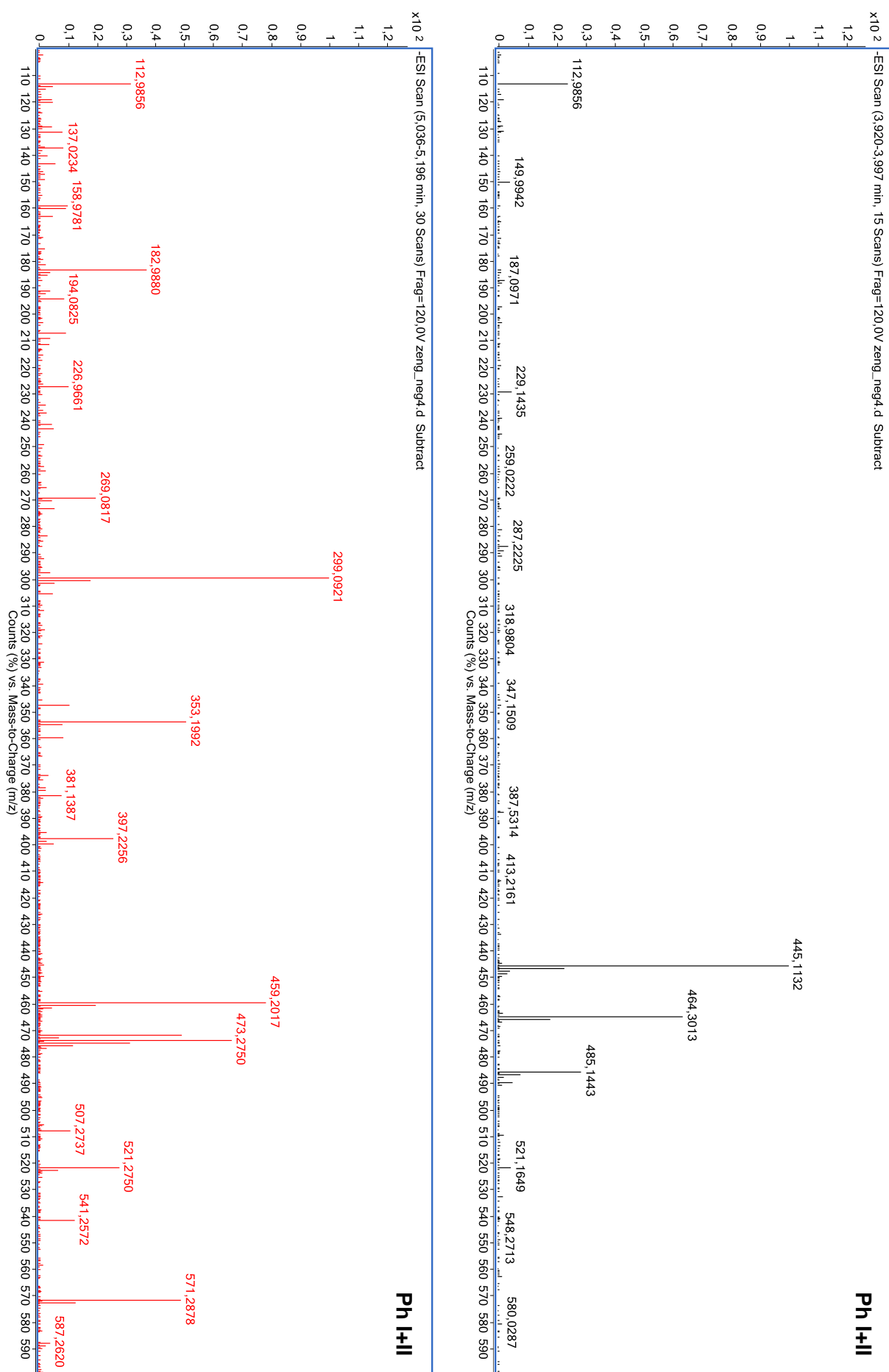
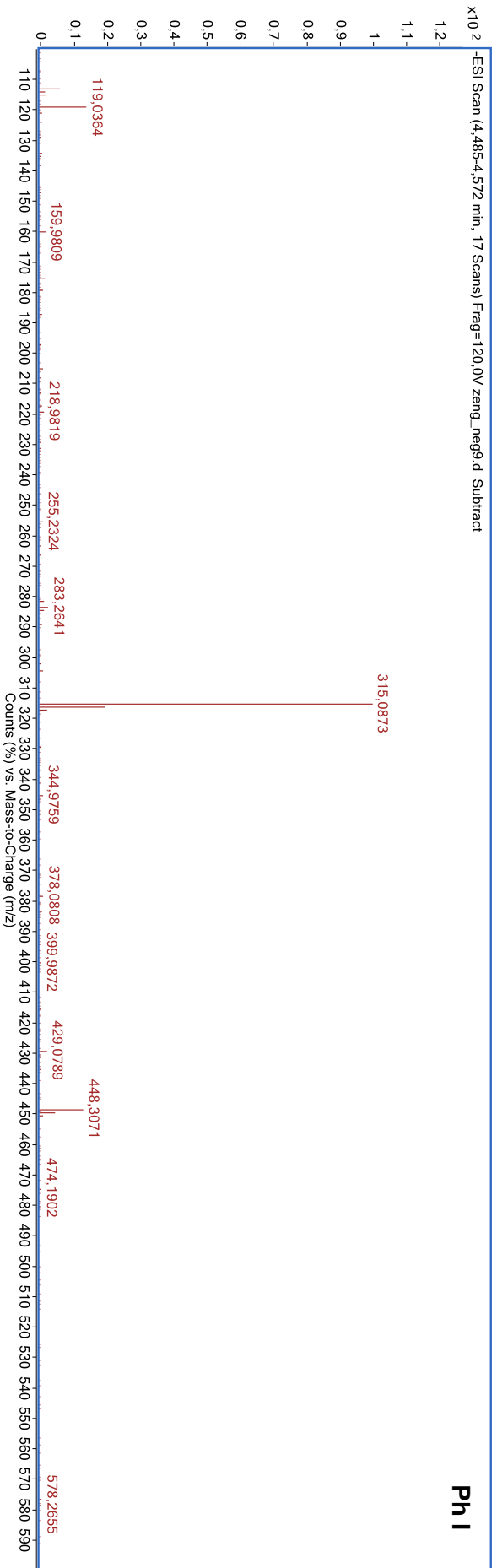
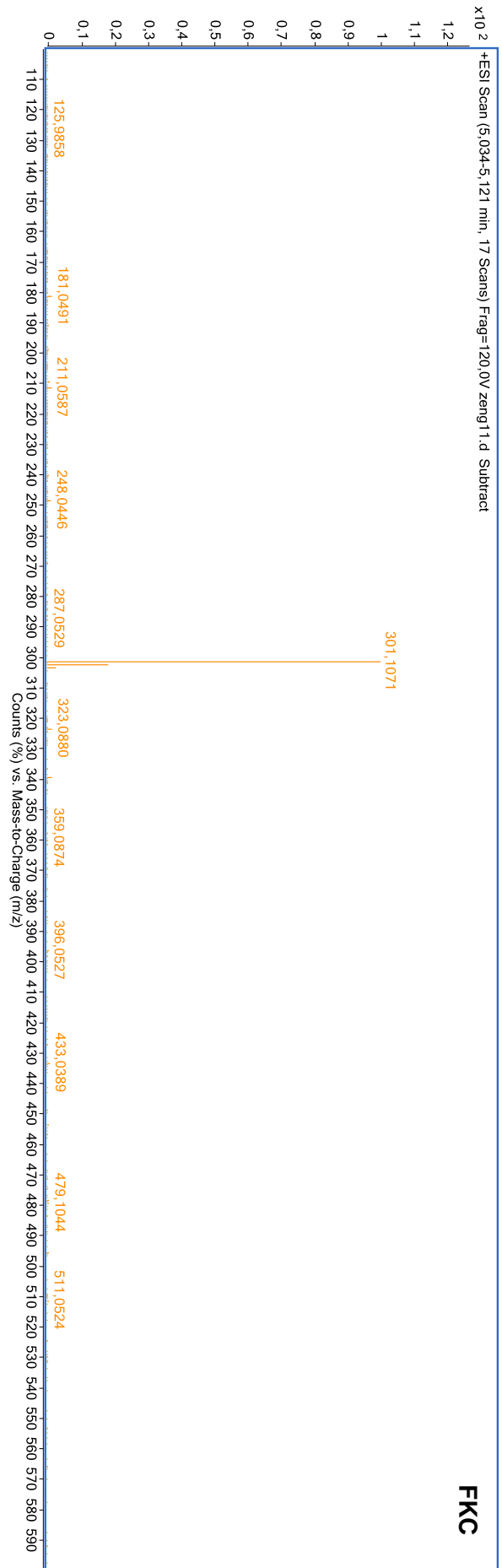
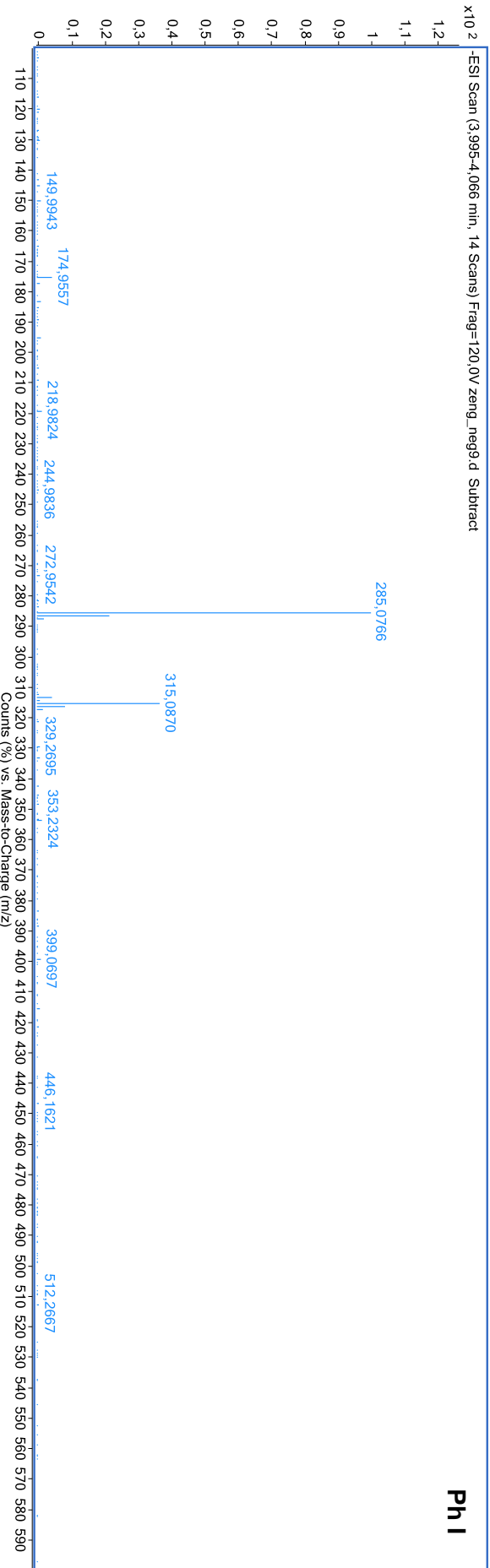
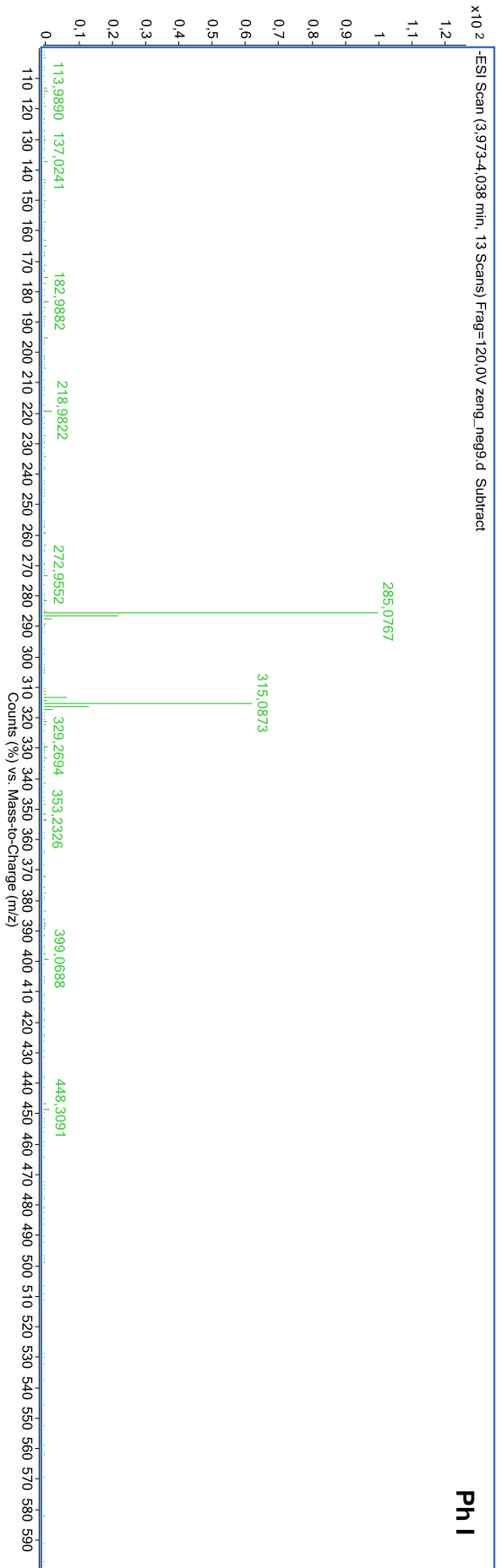
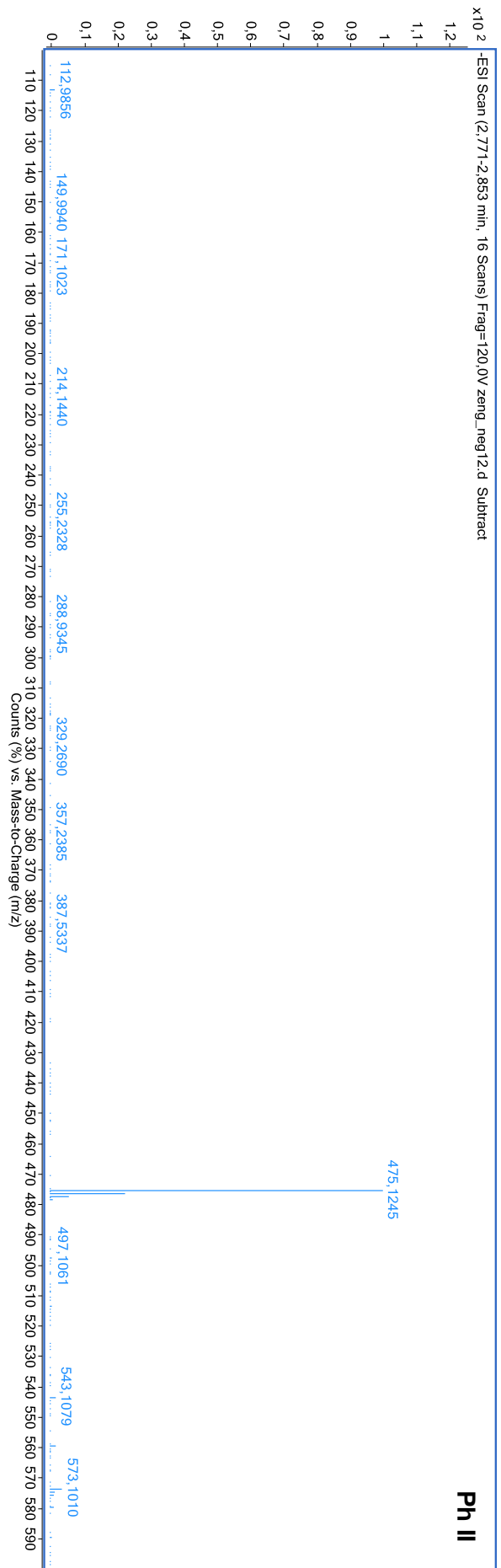
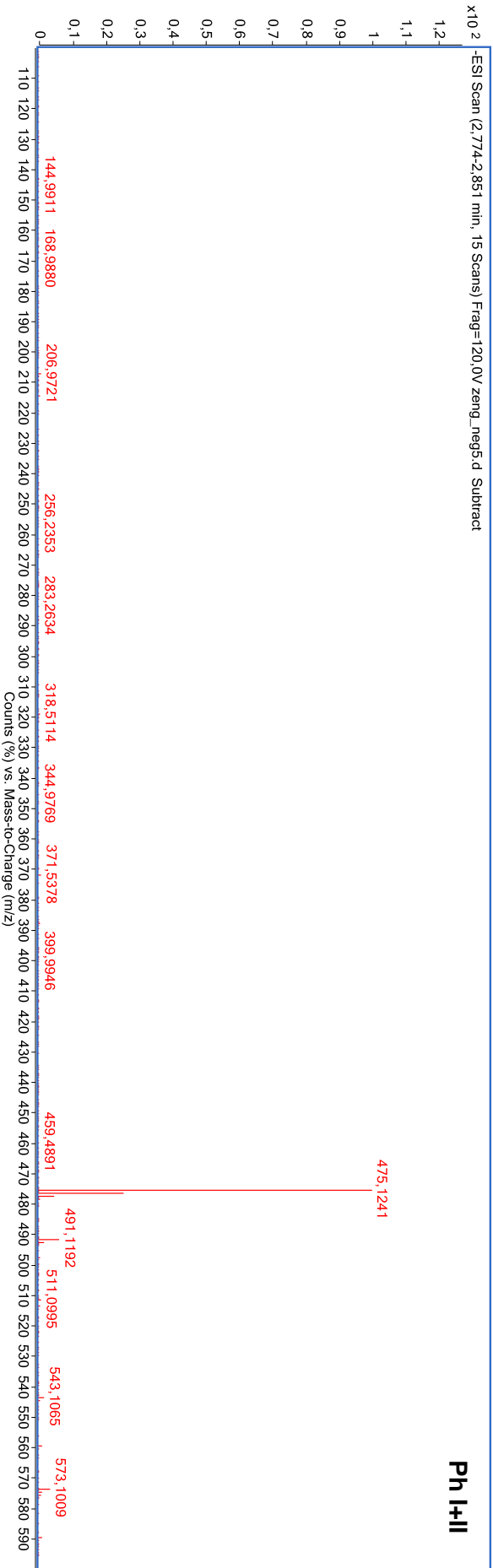


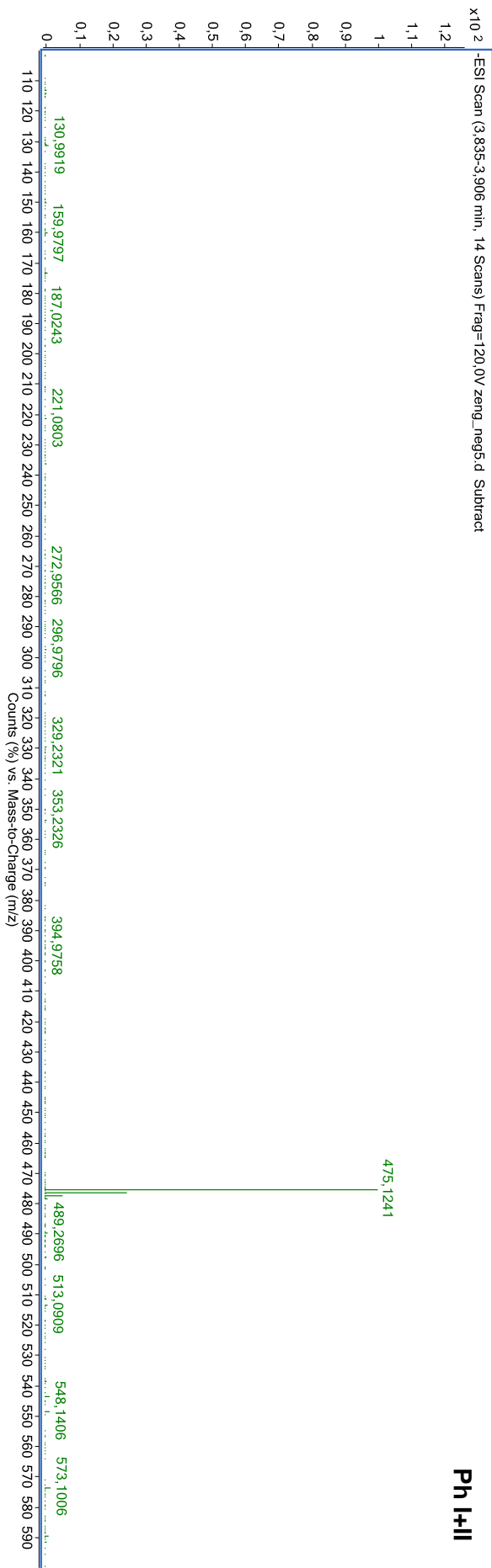
Figure 10.21: Mass spectra of FKB and FKB metabolites corresponding to Table 5.5.

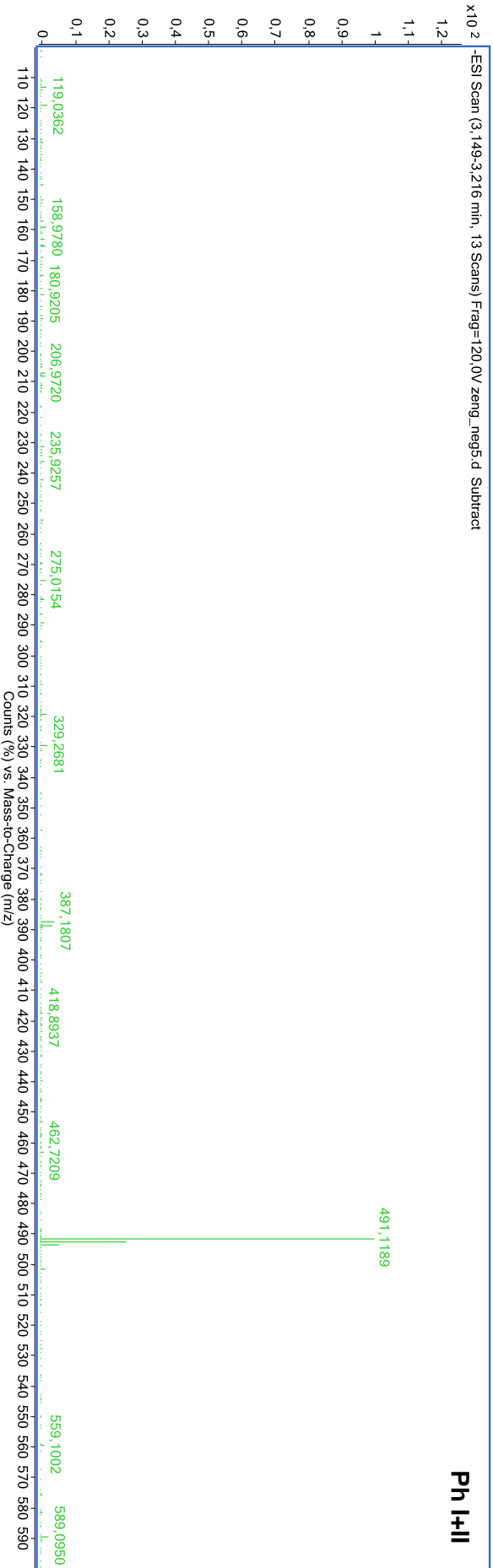
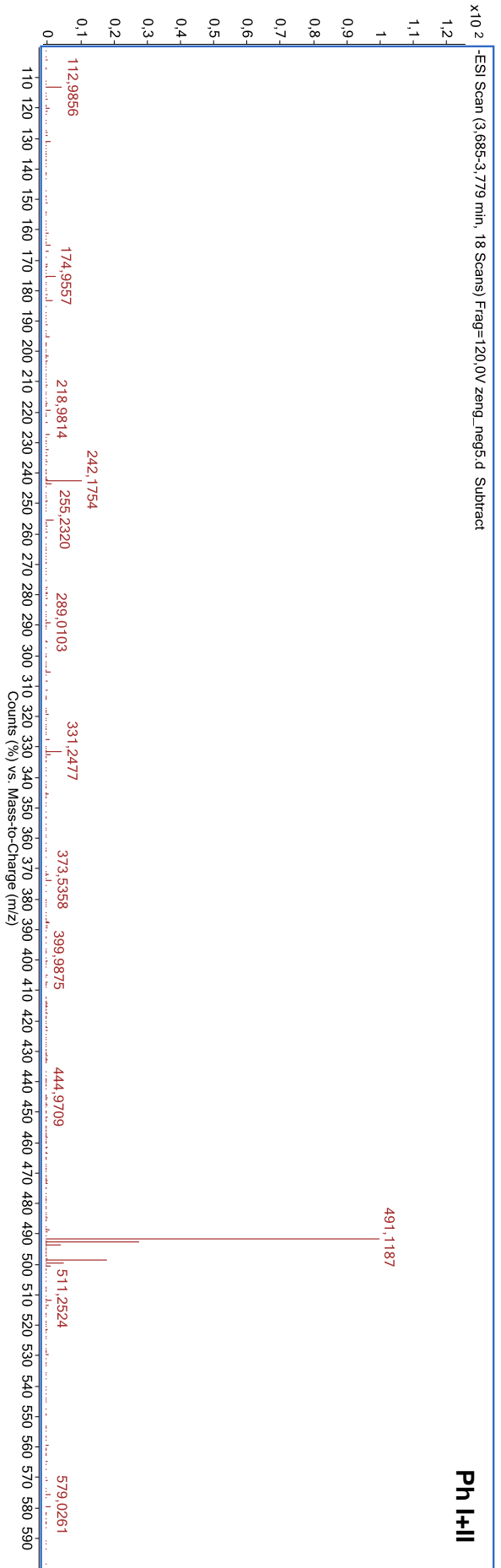












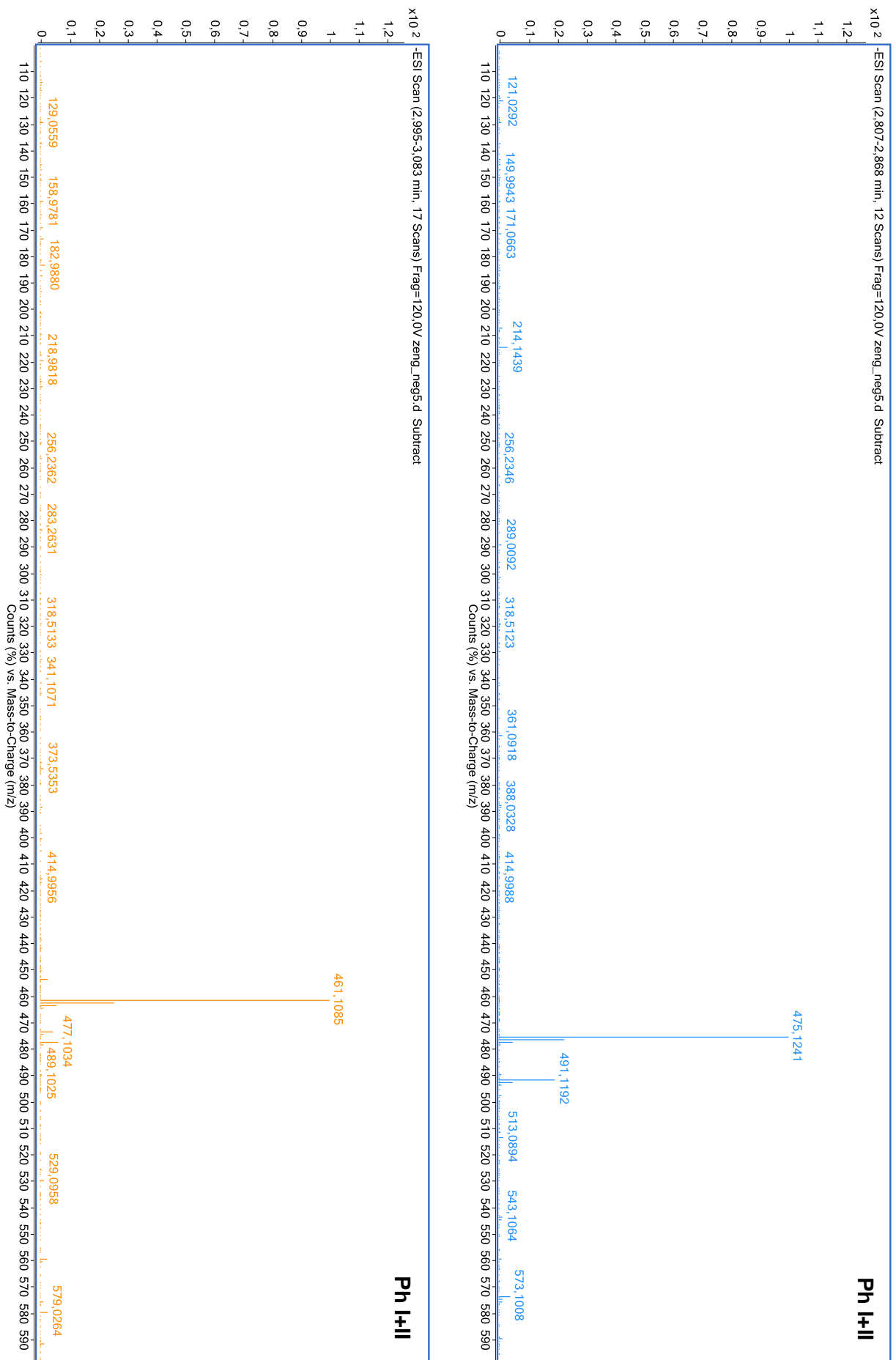
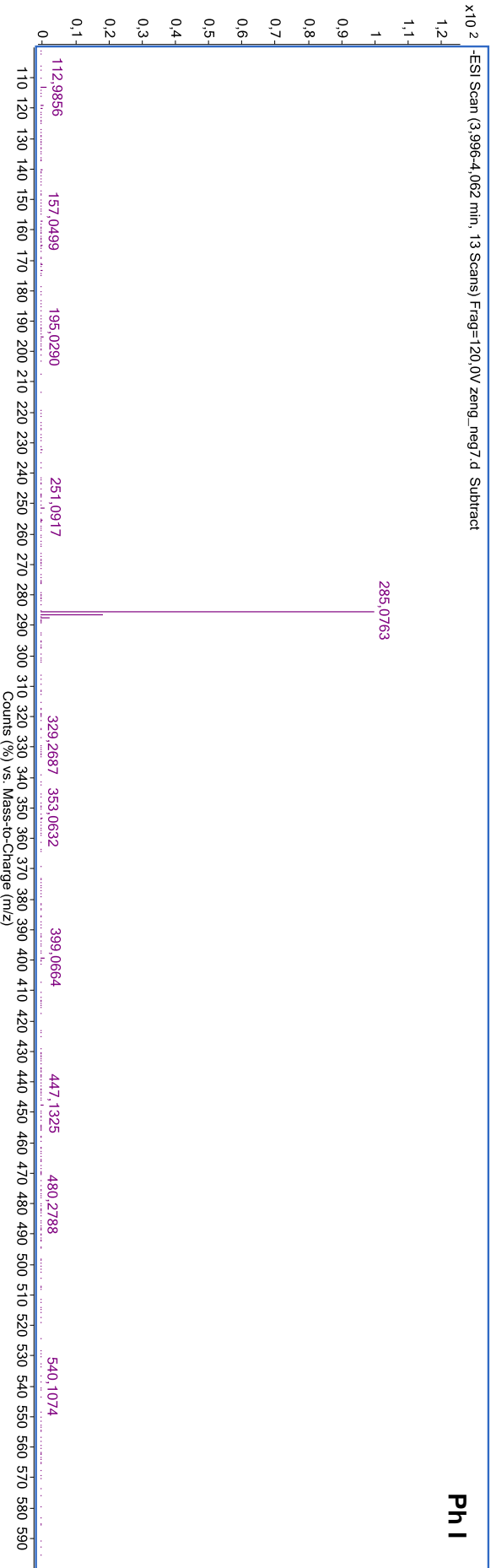
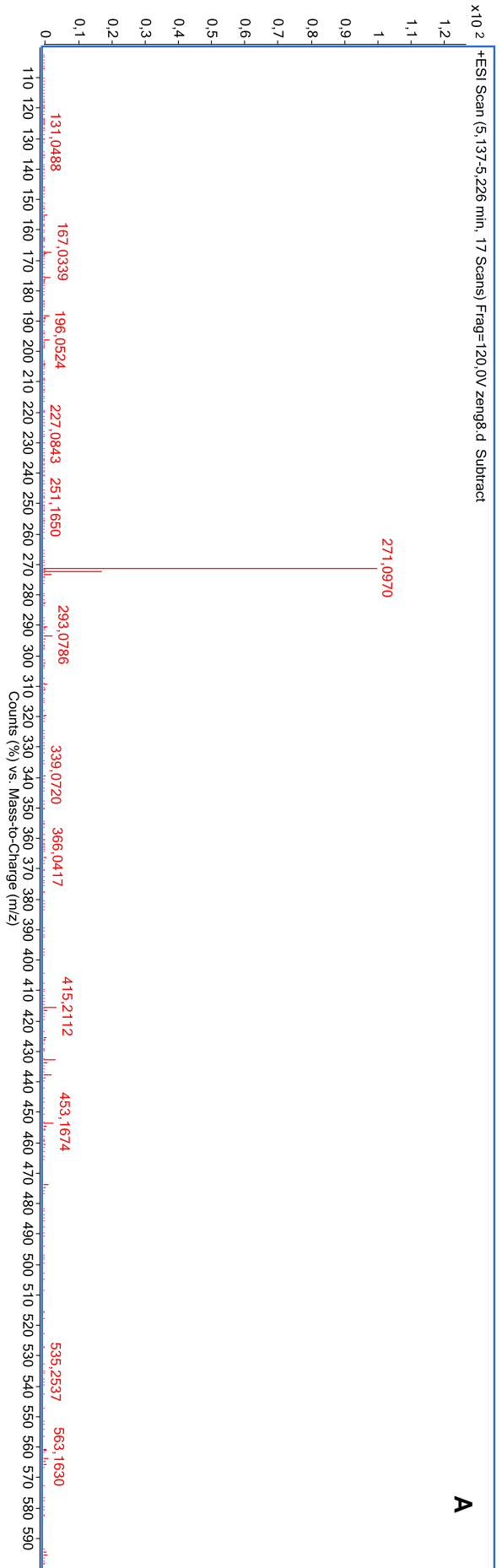
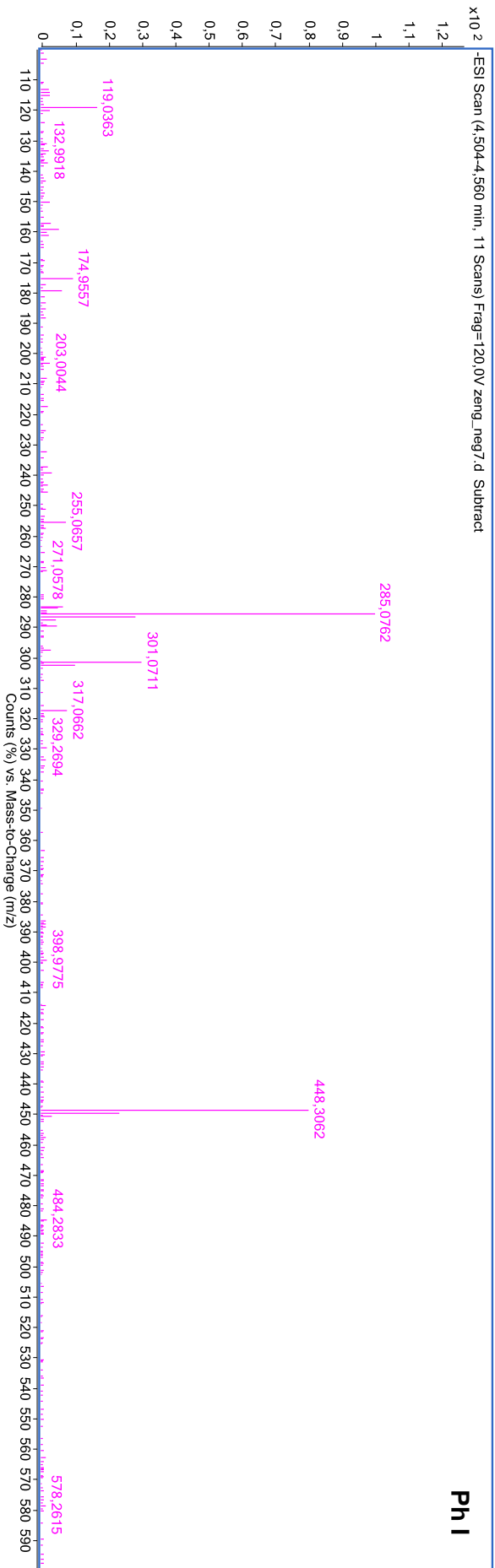
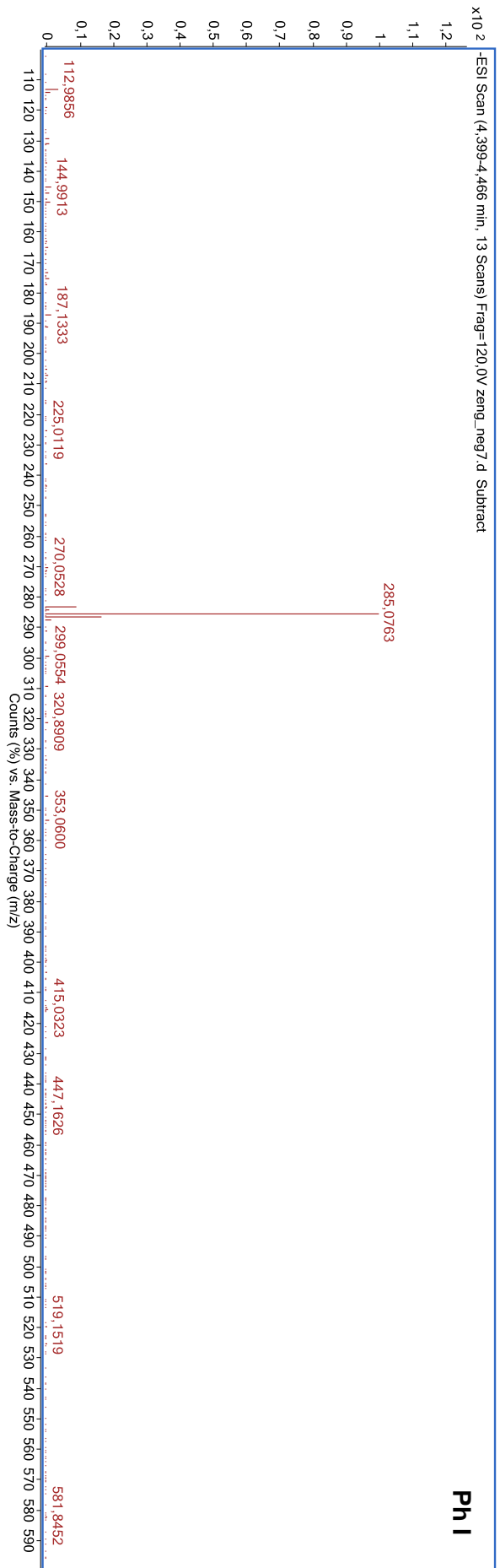
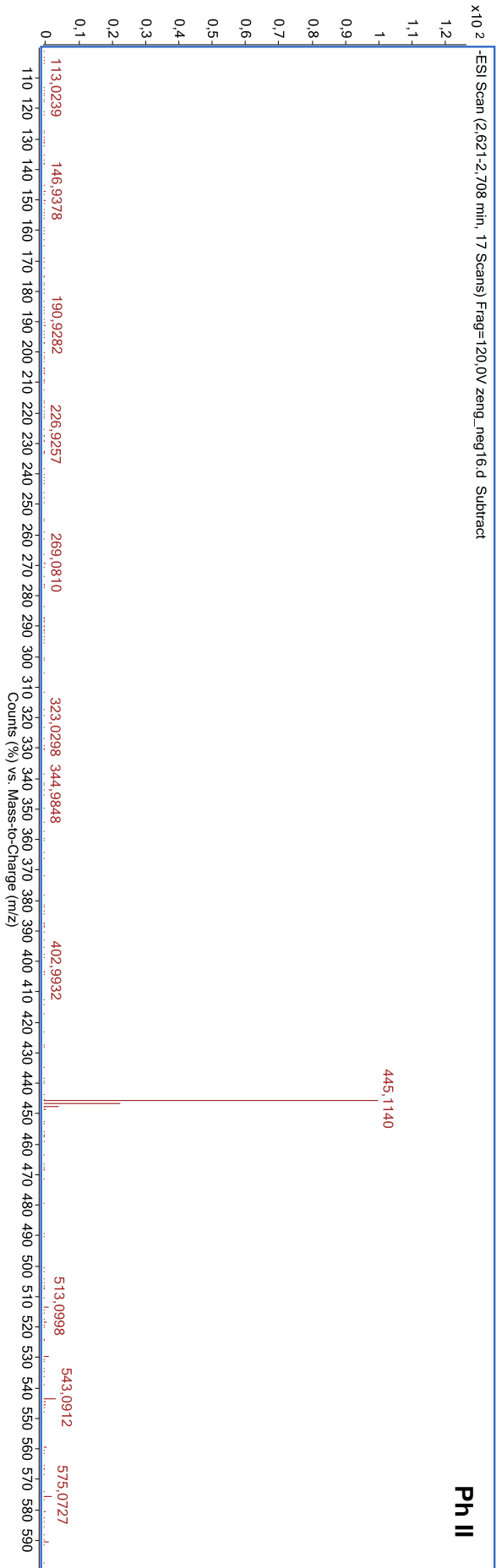
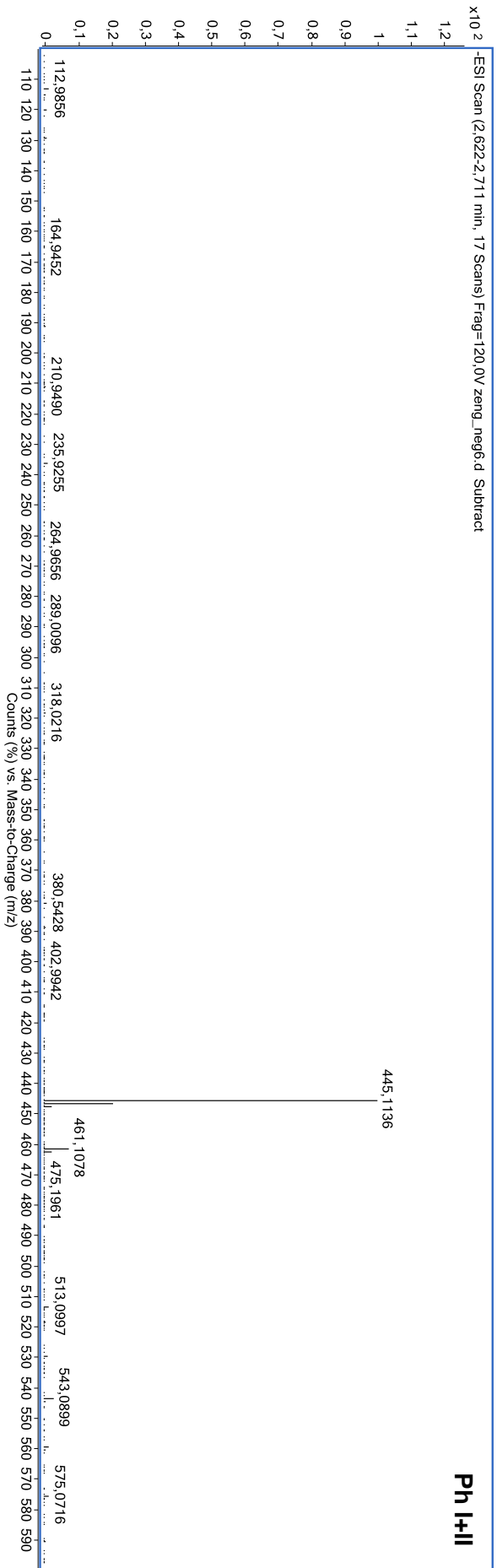
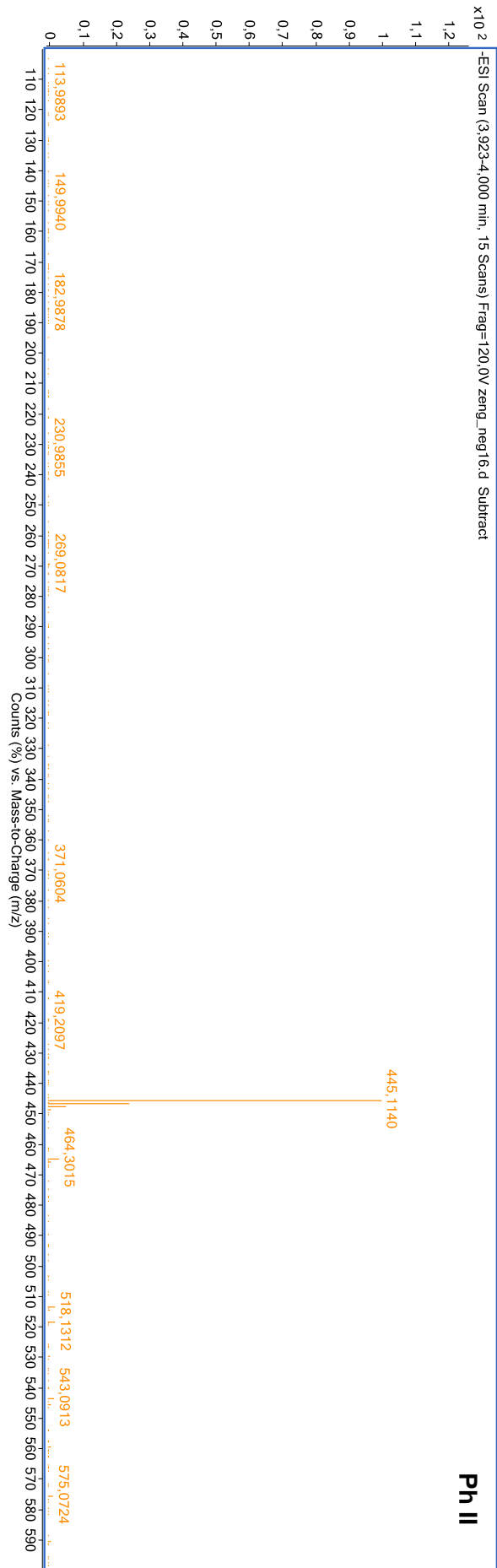


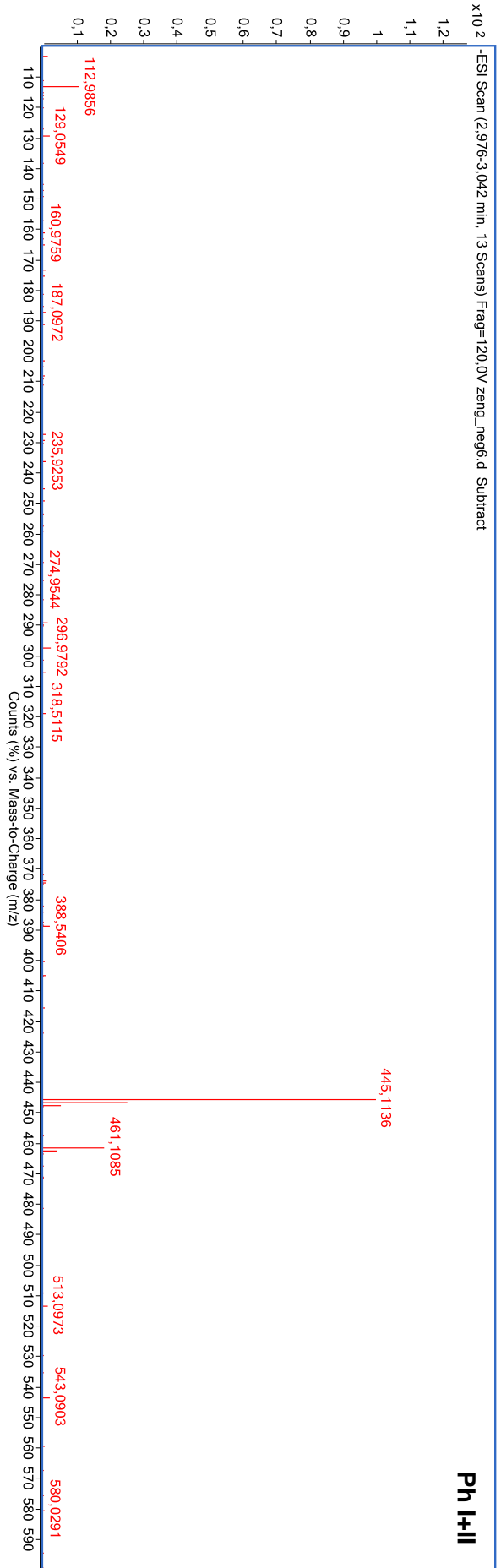
Figure 10.22: Mass spectra of FKC and FKC metabolites corresponding to Table 5.6.











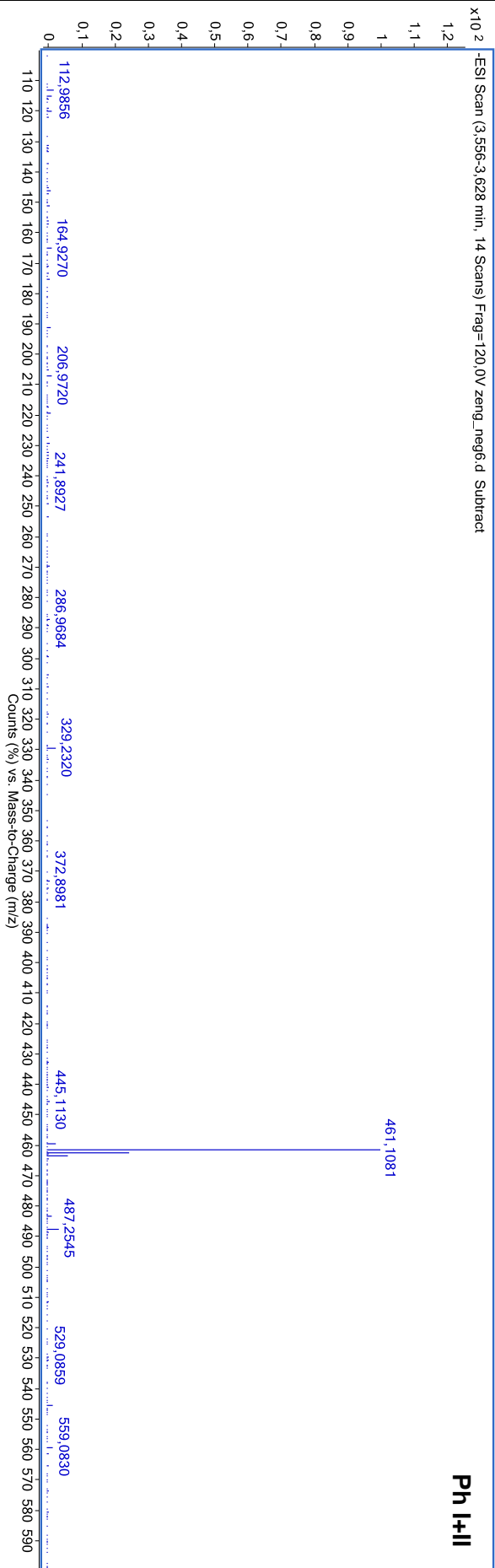


Figure 10.23: Mass spectra of A and A metabolites corresponding to Table 5.7.

10.3 Supplementary table of the codrug metabolites

Table 10.1: Detailed information about calculated (calc m/z [M-H]⁻) and actual found (m/z [M-H]⁻) substance and metabolite masses in the different incubation systems. Data in the table complement HPLC chromatograms of Figure 6.5.

| incubation system | m/z [M-H] ⁻ | base formula [M] | calc m/z [M-H] ⁻ | compounds/ metabolites |
|--------------------|--------------------------|--|-------------------------------|--------------------------|
| a) w/o micr | 860.3404 | C ₄₈ H ₅₁ N ₃ O ₁₂ | 860.3400 | codrug |
| b) w/o cof | 860.3402 | C ₄₈ H ₅₁ N ₃ O ₁₂ | 860.3400 | codrug |
| | 481.1144 | C ₂₅ H ₂₂ O ₁₀ | 481.1140 | silibinin |
| | 396.2295 | C ₂₃ H ₃₁ N ₃ O ₃ | 396.2293 | tacrine hemi succinamide |
| c) Ph I | 860.3401 | C ₄₈ H ₅₁ N ₃ O ₁₂ | 860.3400 | codrug |
| | 481.1143 | C ₂₅ H ₂₂ O ₁₀ | 481.1140 | silibinin |
| | 396.2295 | C ₂₃ H ₃₁ N ₃ O ₃ | 396.2293 | tacrine hemi succinamide |
| d) Ph II | 860.3404 | C ₄₈ H ₅₁ N ₃ O ₁₂ | 860.3400 | codrug |
| | 1036.3720 | C ₅₄ H ₅₉ N ₃ O ₁₈ | 1036.3721 | codrug glucuronide |
| | 1036.3721 | C ₅₄ H ₅₉ N ₃ O ₁₈ | 1036.3721 | codrug glucuronide |
| | 481.1142 | C ₂₅ H ₂₂ O ₁₀ | 481.1140 | silibinin |
| | 1212.4029 | C ₆₀ H ₆₇ N ₃ O ₂₄ | 1212.4042 | codrug diglucuronide |
| | 396.2296 | C ₂₃ H ₃₁ N ₃ O ₃ | 396.2293 | tacrine hemi succinamide |
| | 657.1465 | C ₃₁ H ₃₀ O ₁₆ | 657.1461 | silibinin glucuronide |
| | 657.1463 | C ₃₁ H ₃₀ O ₁₆ | 657.1461 | silibinin glucuronide |
| e) Ph I+II | 1036.3716 | C ₅₄ H ₅₉ N ₃ O ₁₈ | 1036.3721 | codrug glucuronide |
| | 1036.3722 | C ₅₄ H ₅₉ N ₃ O ₁₈ | 1036.3721 | codrug glucuronide |
| | 481.1141 | C ₂₅ H ₂₂ O ₁₀ | 481.1140 | silibinin |
| | 1212.403 | C ₆₀ H ₆₇ N ₃ O ₂₄ | 1212.4042 | codrug diglucuronide |
| | 396.2295 | C ₂₃ H ₃₁ N ₃ O ₃ | 396.2293 | tacrine hemi succinamide |
| | 657.1463 | C ₃₁ H ₃₀ O ₁₆ | 657.1461 | silibinin glucuronide |
| | 657.1467 | C ₃₁ H ₃₀ O ₁₆ | 657.1461 | silibinin glucuronide |

10.4 List of publications

Poster presentations and conference abstracts

Zenger, K., Kraus, B., Untersuchung der zyto- und mitotoxischen Wirkung von Xanthohumol und Strukturderivaten auf hepatische Sternzellen, 2012, Phytotherapeutika, May 17-19, Wien (Austria)

Hild, W., **Zenger, K.**, Rose, C., Hezinger, A., Tessmar, J., Goepferich, A., 2008, Towards the optimization of quantum dot preparation for use in biological systems, 2008, NaNaX 3, May 21-23, Lecce (Italy)

Hild, W., **Zenger, K.**, Caporale, A., Cabrele, C., Breunig, M., Teßmar, J., und Göpferich, A., 2008, Towards peptide-modified nanocrystals for drug targeting applications, Controlled Release Society, Local Chapter, Braunschweig (Germany)

Publications

Wolff, H., **Zenger, K.**, Kraus, B., Progress in live-cell imaging and screening applications using Definite Focus, 2009, BioTechniques, 47 (5), pp. 976–978

Chen, X., **Zenger, K.**, Lupp, A., Kling, B., Heilmann, J., Fleck, C., Kraus, B., Decker, M., Tacrine-silibinin codrug shows neuro- and hepatoprotective effects in vitro and pro-cognitive and hepatoprotective effects in vivo, 2012, Journal of Medicinal Chemistry, 55 (11), pp. 5231–5242

Zenger, K., Chen, X., Decker, M., Kraus, B., *In vitro* stability and metabolism of a tacrine-silibinin codrug, 2013, Journal of Pharmacy and Pharmacology, accepted

10.5 Curriculum Vitae

| | |
|--------------------|--|
| Name | Katharina Julia Zenger |
| Geburtsdatum | 7. März 1983 |
| Geburtsort | Heidenheim a. d. Brenz |
| Saatsangehörigkeit | deutsch |
| 09/89 bis 08/93 | Volksschule Duggendorf |
| 09/93 bis 06/02 | Johann-Michael-Fischer Gymnasium, Burglengenfeld |
| 06/02 | Erwerb der allgemeinen Hochschulreife |
| 10/02 bis 04/07 | Studium der Pharmazie an der Universität Regensburg |
| 04/05 | Erster Abschnitt der Pharmazeutischen Prüfung |
| 09/05 bis 02/06 | Forschungsaufenthalt am Lehrstuhl Pharmacotechnie Industrielle, Université de Lille 2 (Frankreich) |
| 04/07 | Zweiter Abschnitt der Pharmazeutischen Prüfung |
| 05/07 bis 10/07 | Pharmaziepraktikantin in der Wolfgang Apotheke, Regensburg |
| 11/07 bis 04/08 | Pharmaziepraktikantin am Lehrstuhl Pharmazeutische Technologie, Universität Regensburg |
| | Dritter Abschnitt der Pharmazeutischen Prüfung |
| | Approbation als Apothekerin |
| 08/08 bis 01/09 | Anstellung als Apothekerin in der Wolfgang Apotheke, Regensburg |
| 02/09 bis 02/13 | Promotion am Lehrstuhl Pharmazeutische Biologie, Universität Regensburg |